UQAC
Université du Québec
à Chicoutimi

Fabrication of Durable Self-healing Superhydrophobic Coating to Improve the Performance of High Voltage Insulators During Winter Conditions

By

Anahita Allahdini Hesarouyeeh

Under supervision of Prof. Gelareh Momen and co-supervision of Prof. Reza Jafari

Manuscript-Based Thesis Presented to Université du Québec à Chicoutimi in Partial fulfillment of the Requirements for the Degree of Doctor of Philosophy (Ph.D.) in Engineering

BOARD OF EXAMINERS:

Professor Yasar Kocaefe, Department of Applied Sciences at UQAC, President of the Board

Professor Sylvain G. Cloutier, École de technologie supérieure (ETS), External Member of the Board

Doctor Ehsan Bakhshandeh, Department of Applied Sciences at UQAC, Internal Member of the Board

Professor Gelareh Momen, Department of Applied Sciences at UQAC, Internal Member of the Board

Professor Reza Jafari, Department of Applied Sciences at UQAC, Internal Member of the Board

Québec, Canada

RÉSUMÉ

Avec l'émergence dans plusieurs domaines de nouveaux types de matériaux, polymères et technologies qui ont révolutionné les infrastructures sociales et industriels, la demande pour des matériaux de nouvelle génération multifonctionnels à propriétés spécifiques enregistre une forte croissance. Notamment, les matériaux superhydrophobes et autoréparant ont connu une ascension fulgurante, au cours des dernières décennies.

Dans des applications pour la vie quotidienne, les revêtements et les surfaces subissent de sévères contraintes mécaniques qui affectent l'intégrité des structures à long terme. Pourtant, il existe très peu de méthodes disponibles pour maintenir l'efficacité et leur durabilité lorsque les surfaces polymériques sont abimées. Ainsi, s'inspirant de mère nature et du potentiel auto-régénérassions des systèmes biologiques, des matériaux composites autoréparant ont été développé pour apporter une solution auto-réparatrice avec très peu voire aucune intervention humaine.

Ici, la conception d'un revêtement superhydrophobe multifonctionnel capable d'augmenter la durée de vie effective des isolateurs à haute tension est au cœur de notre préoccupation. Ce dernier vise à prévenir voire retarder les éventuels dommages mécaniques causés par les arcs électriques et les contournements résultant de problèmes de mouillabilité et de ces dommages.

Dans un premier temps, un polydiméthylsiloxane doté d'une terminaison en silanol téléchélique (DMS-S12) et un catalyseur (dilaurate de Dibutylétain, DBTL) ont été encapsulés séparément dans membrane de poly (mélamine-urée-formaldéhyde) via la technique de polymérisation en émulsion. L'encapsulation des matériaux du noyau ainsi que la morphologie de surface, la distribution de leur taille et la stabilité thermique des microcapsules ont été étudiées. Les microcapsules synthétisées présentaient un diamètre compris entre 10-110 µm avec une morphologie sphérique et uniforme, et une stabilité thermique jusqu'à des températures élevées. Celles ont été incorporées par la suite à l'intérieur d'une matrice élastomérique de polydiméthylsiloxane (PDMS), dénommée SILGARD 184 pour former le revêtement composite. Le potentiel de cicatrisation du composite de silicone ainsi obtenu a été évalué en surveillant une réparation de fissure par microscopie électronique à balayage (MEB) et en mesurant l'ampleur de la récupération des propriétés mécaniques par des essais de traction.

Dans un second temps, le revêtement développé a été appliqué par pulvérisation sur une variété de substrats notamment le verre, la porcelaine, l'aluminum et l'acier. Le revêtement présent un angle de contact de 163° et une hystérésis d'angle de contact de 2.3° avec d'excellentes propriétés autonettoyantes (évalué en pollution sèche et humide) et glaciophobes (faible adhérence à la glace et retard élevé du temps de congélation). La robustesse et la durabilité représentent généralement le talon d'Achille des matériaux superhydrophobes. C'est pourquoi un ensemble des essais mécaniques et chimiques ont été effectués pour évaluer la robustesse du revêtement final vis à vis des conditions réels. Les résultats recueillis ont confirmé la stabilité des propriétés du revêtement développé soumis à conditions extrêmes.

Troisièmement, la performance du revêtement superhydrophobe final (SHP) sous contrainte électrique a été évaluée à l'aide de diverses méthodes tels que la spectroscopie diélectrique, des tests de mesure de tension d'amorçage, de condensation et des tests de plan incliné. Le revêtement SHP offrait une permittivité diélectrique et un facteur de perte inférieurs à ceux d'un échantillon vierge dans la plage de fréquences est comprise entre 10^{-4} et 10^{3} Hz. De plus, les résultats portant sur le courant de fuite ont montré que le revêtement réduisait avec succès le courant de fuite à sa surface dans des environnements à forte humidité. En plus, une augmentation de la tension de contournement dans différentes conditions qu'il s'agisse d'un état sec, humide ou pollué a été observée.

Enfin, les microcapsules autoréparants obtenues ont été adaptées/ redimensionnées pour être incorporées dans des revêtements de surface de manière à obtenir une couche mince grâce à certaines modifications des paramètres du procédé. Les observations MEB ont révélé des diamètres moyens de 18 et 16 µm pour les microcapsules. Concernant l'évaluation de la capacité d'auto-guérissons, les revêtements ont été rayés et inspectés visuellement en utilisant l'imagerie par microscopie. La spectroscopie d'impédance électrochimique (EIS) a été également utilisée pour étudier quantitativement la fonction d'auto-guérissons du revêtement tel que préparé. L'efficacité d'auto-guérissons et l'indice de délaminage du revêtement ont été calculés à l'aide des données obtenues à partir des mesures EIS (résistance de transfert de charge (R_{ct}) et impédance ($Z_{0.01}$ Hz)). Les données ont montré des efficacités d'auto-guérissons allant jusqu'à 96% par rapport au revêtement superhydrophobe vierge. L'indice de délaminage des échantillons a également confirmé que la cicatrisation de la microfissure a lieu après 48 heures.

Mots clés: Auto-réparation extrinsèque; Microencapsulation; Efficacité d'auto-réparation; Revêtement superhydrophobe; Auto-nettoyant; Glaciophobicité; Durabilité mécanique; Polydiméthylsiloxane; Isolateurs en porcelaine; Performances diélectriques; Essai sur plan incliné; Haute tension.

ABSTRACT

With the emerging advancements in different fields of new materials, polymers, and technologies which have been revolutionary in industries, the demand for new generation of multi-functional materials with specific properties is highly growing. Superhydrophobic and self-healing materials are among these developments and have arisen as an unstoppable demand in the recent decades.

In real world applications, coatings and surfaces are subjected to mechanical damages that are severe threat to the integrity of the structures. Once polymeric structures are damaged, there might be few limited methods available to sustain their functional lifetime. By the inspirations from mother nature and biological systems, the self-healing composite materials are designed to trigger a self-repair response without any or slight external human intervention.

Herein, we aimed at designing a multifunctional superhydrophobic coating in order to increase the effective life-span of high-voltage insulators by preventing and/or delaying the possible arcing and flashover driven damages that originated from wettability issues and mechanical damages.

Firstly, a telechelic silanol terminated polydimethylsiloxane (DMS-S12) and catalyst (Dibutyl tin dilaurate, DBTL) were encapsulated inside poly (melamine-urea-formaldehyde) shells separately via emulsion polymerization technique. The encapsulation of core materials, surface morphology and size distribution of microcapsules, and thermal stability of microcapsules were investigated. The synthesized microcapsules were obtained within a size range of 10-110 μm showing a spherical and uniform morphology, and thermal stability up to elevated temperatures. The microcapsules were incorporated inside a polydimethylsiloxane (PDMS) elastomer matrix, namely SILGARD 184, and the healing performance of the silicone composite was evaluated by monitoring a crack repair via scanning electron microscopy (SEM) and measuring the extent of recovery in mechanical properties via tensile and tear tests. The composites containing microcapsules depicted self-healing efficiencies of 67% and 55% calculated based on the recovered toughness and tearing energy of the healed samples.

Secondly, a silicone-based superhydrophobic (SHP) coating was developed using spray coating method which was applicable to a variety of substrates including glass, porcelain, aluminum, and steel. The developed coating exhibited contact angle of 163° and contact angle hysteresis of 2.3° with excellent self-cleaning (in both dry and wet pollution scenarios) and icephobic (low ice adhesion and high delay in freezing time) properties. Robustness and durability which are the Achilles heel of superhydrophobic materials were assessed via a set of mechanical and chemical testing techniques in which the great non-wetting properties of the as-prepared coating was shown to be maintained even after various extreme treatments, i.e., waterjet impacting, immersing in pollutants and acid/base solutions for 24 h, tape peeling test, and sandpaper abrasion.

Thirdly, the performance of superhydrophobic coating under electrical stress was evaluated employing a variety of methods including dielectric spectroscopy analyses, flashover voltage measurements tests, condensation, and inclined plane tests. The SHP coating represented lower dielectric permittivity and loss factor compared to a pristine sample within the frequency range of 10^{-4} – 10^{3} Hz. Also, the leakage current results showed that the coating successfully reduced the leakage current on its surface in environments with high humidity. Moreover, the developed coating was able to increase flashover voltage in different conditions including dry, wet, and polluted states.

Lastly, the obtained self-healing microcapsules were adapted for incorporation in thin layer surface coatings by some modifications in the process parameters. The SEM observations illustrated mean diameters of 18 and 16 μm for microcapsules. For the evaluation of self-healing ability, the scratched coatings were visually inspected using microscopy imaging. Electrochemical Impedance Spectroscopy (EIS) was employed to quantitatively investigate the self-healing function of the as-prepared coating. The self-healing efficiency and delamination index of the coating were calculated using the obtained data from EIS measurements (charge transfer resistance (R_{ct}) and impedance ($Z_{0.01\ Hz}$)). The data showed self-healing efficiencies up to 96% compared to the blank superhydrophobic coating. The delamination index of the samples also confirmed the healing of the microcrack after 48 hours.

Keywords: Extrinsic self-healing; Microencapsulation; Self-healing efficiency; Superhydrophobic coating; Water-repellency; Self-cleaning; Icephobicity; Mechanical durability; Polydimethylsiloxane; Porcelain insulators; Dielectric performance; Inclined plane test; Flashover voltage.

TABLE OF CONTENTS

LIST OF FIGURES

LIST OF TABLES

LIST OF ABBREVIATIONS

AC	Alternating Current
AFM	Atomic Force Microscopy
Al	Aluminum
AMIL	Anti-Icing Materials International Laboratory
ARF	Adhesion Reduction Factor
ATH	Aluminum Trihydrate
ATR	Attenuated Total Reflection
CA	Contact Angle
CAH	Contact Angle Hysteresis
CAT	Centrifuge Adhesion Test
CB	Cassie-Baxter
CVD	Chemical Vapor Deposition
D_4 units	Octamethylcyclotetrasiloxane monomers
DA	Diels–Alder
DBTL	Dibutyltin Dilaurate
DBTL-MUF	Microcapsules containing DBTL core
DC	Direct Current
DCPD	Dicyclopentadiene
DI Water	Deionized Water
DI%	Delamination Index
DSC	Differential Scanning Calorimetry
EDS	Energy Dispersive Spectroscopy
EE%	Encapsulation Efficiency
EEC	Electrical Equivalent Circuit
EIS	Electrochemical Impedance Spectroscopy
EMA	Ethylene-Maleic Anhydride

FoV	Flashover Voltage
FS	Fumed Silica
FTIR	Fourier-Transform Infrared Spectrometry
H_2	Hydrogen
HCl	Hydrochloric Acid
HMDS	Hexamethyldisilazane
HNO_3	Nitric Acid
HPP	Hard Elastic Polypropylene
IE%	Inhibition Efficiency
IPT	Inclined Plane Test
LBL	Layer-By-Layer Deposition
MCs	Microcapsules
MTES	Methyltriethoxysilane
N_2	Nitrogen
NaCl	Sodium Chloride
NH_4Cl	Ammonium Chloride
NPs	Nanoparticles
NSERC	Natural Science and Engineering Research Council of Canada
O/W	Oil-in-Water
O_2	Oxygen
OCP	Open Circuit Potential
OH	Hydroxyl
OP	Optical Microscopy
PC	Polycarbonate
PDMS	Polydimethylsiloxane
PDMS-MUF	Microcapsules containing DMS-S12 core
PLA	Poly (Lactic Acid)

PMMA	Poly (methyl methacrylate)
PMUF	Poly (melamine-urea-formaldehyde) shell
PS	Polystyrene
PTFE	Poly (tetrafluoroethylene)
PU	Polyurethane
PUF	Poly (Urea-Formaldehyde)
PVA	Poly (vinyl Alcohol)
PVC	Poly (vinyl Chloride)
PVDF	Poly (Vinylidene Fluoride)
RMS	Root Mean Square
RTV	Room Temperature Vulcanized
SA	Sliding Angle
SDBS	Sodium Dodecyl Benzene Sulfonate
SEM	Scanning Electron Microscopy
SHE%	Self-Healing Efficiency
SHP/SHPS/SHPC	Superhydrophobic/ Superhydrophobic surface/ Coating
SiO_2	Silicon Oxide
SLIPS	Slippery Liquid Infused Porous Surfaces
SMA	Styrene-Maleic Anhydride
SMPs	Shape Memory Polymers
TDCB	Tapered Double Cantilever Beam geometry
TEOS	Tetraethoxysilane
T_g	Glass Transition Temperature
TGA	Thermogravimetric Analysis
TiO_2	Titanium Oxide
UV	Ultra-Violet
ZnO	Zinc Oxide

LIST OF SYMBOLS

A	Area
C_s	Capacitance
CPE_f	Film Capacitance
CPE_{dl}	Double Layer Capacitance
ε_0	Permittivity of Free Space
ε'	Real part of Dielectric Permittivity
ε''	Imaginary part of Dielectric Permittivity
f	Frequency
R_{ct}	Charge Transfer Resistance
R_f	Film Resistance
r	Roughness Factor
S_a	Arithmetic Mean Height of Area Roughness
S_p	Maximum Peak Height
S_v	Maximum Pit Height
S_{sk}	Skewness Coefficient of Area Roughness
S_q	Root-Mean-Square Height of Area Roughness
tan δ	Loss Factor
τ	Adhesion Shear Stress
θ	Contact Angle
Z	Impedance

ACKNOWLEDGMENT

I would like to express my appreciation to my research supervisor, Prof. Gelareh Momen, for her continuous support, kindness, and care during my Ph.D.

I would like to warmly thank my co-supervisor, Prof. Reza Jafari, for his support, guidance, and continuous involvement in my project.

I am deeply grateful to the members of my committee, Prof. Yasar Kocaefe, Prof. Sylvain G. Cloutier, Dr. Ehsan Bakhshandeh for their worthwhile guidance and supports.

I would like to express my gratitude to Ms. Helene Gauthier, Chercheuse Métallurgie et génie des Matériaux, IREQ, Hydro Québec, for her feedback and support during this academy-industry collaboration.

I would like to thank Prof. Stephan Brettschneider, professor of electrical engineering department at the Université du Québec à Chicoutimi, and M. Fredric Munger, graduate student at the Université du Québec à Chicoutimi, for their time, collaborations, and involvement in performing the electrical analyses.

I would like to thank all the professionals and technicians for their assistance in this project, M. Luc Chatigny, technician of Laboratoire Revêtements glaciophobes et ingénierie des surfaces (LARGIS), Ms. Caroline Potvin, the laboratory assistant of the chemistry department, Prof. Issof Fofana, professor of electrical engineering department at the Université du Québec à Chicoutimi, for his time, and valuable collaboration in the electrical investigations, Ms. Kouba Marie Lucia Yapi for the dielectric spectroscopy analyses, Ms. Shamim Roshan, guest researcher of the Laboratoire Revêtements glaciophobes et ingénierie des surfaces (LARGIS), for performing the Electrochemical Impedance Spectroscopy tests, and Ms. Pauline Moniot, graduate student at the Université du Québec à Chicoutimi, for her generous contributions to the self-healing experiments.

I would like to express my appreciation for the financial support of the Hydro-Québec, Québec, Canada; Natural Sciences and Engineering Research Council of Canada (NSERC); and le Pôle Recherche

Innovation en Matériaux avancés du Québec (PRIMA Québec), Canada without which completion of this research would not have been possible.

Last but not least, I would like to sincerely thank my family and friends in my country, Iran, and my great friends in LARGIS (Samaneh Heydarian Dolatabadi, Elham Vazirinasab, Mohammadreza Shamshiri, and Khosrow Maghsoudi) for all the supports they provided me throughout my studies, and all the good memories we made together.

INTRODUCTION

Definition of Problem

Outdoor insulators are of the main components in the high-voltage sectors, and their accurate function will guarantee the operational safety and efficiency of the electrical power in the transmission system; therefore these components must fulfil particularly high demands in terms of electrical, mechanical and chemical reliability for several years [1], [2]. Insulators are used to mechanically support high-voltage conductors and electrically separate them from each other or ground and should resist normal operating electrical stresses without flashover failure.

The main dielectric materials used for outdoor high voltage insulation are glass, porcelain, and composite polymeric materials. Ceramic insulators, made of porcelain and glass, have been used in the power utilities for over one century. These types of insulators demonstrate great mechanical performance and weathering resistance. Furthermore, they have outstanding resistance against electrical stresses degradation and discharge activities [3]. Due to their high surface energy, porcelain and glass insulators have always suffered from high degrees of wettability by water which leads to the formation of conductive films along the creepage way, resulting in higher values of surface leakage currents to stream on the wet surface [3]–[6]. In cold regions of North America, Europe and Asia, transmission towers, conductors and high voltage insulators are every year exposed to ice accumulation causing severe damages, deformations, power outages, flashovers, compromising the reliability of power lines and telecommunication services, black outs and losses of millions of dollars [7]–[10]. When ice and snow accumulate on exposed equipment and surfaces, the increased weight can deform or even make the structure collapse. The formation of ice along the insulators can cause flashovers due to bridging the shed spacing (distance between convolutions in the insulator surface) or creating a conductive film on the surface in which current passes through and facilitates short circuit [11], [12].

The contamination flashover is also a major problem especially in industrial, coastal, and polluted regions and involves the propagation of arc across the surface of an electrolyte created by chemical residues, dust, or salts. The pollution not only affects the appearance and efficiency of the

power equipment, but also can increase the conductivity of the insulator surface and decrease the performance of insulators against leakage, arc, and discharge. The pollutants are usually inactive while staying dry, being active as they are exposed to different types of water (fog, dew, rain, snow, frost, condensation, etc.) and form a conductive layer on the surface [10].

A coating layer is known as a universal solution to endow desired functions and properties to diverse substrate materials. Therefore, by properly designing an appropriate coating applicable on porcelain insulators, one can benefit from the outstanding characteristics of porcelain while its surface properties are governed by the coating layer.

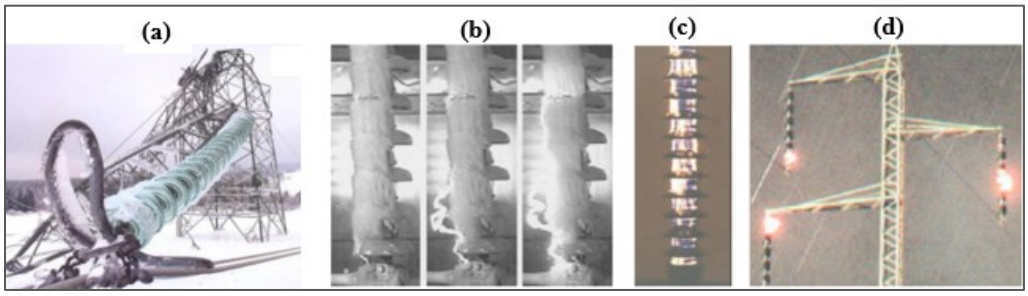

a) Collapse of transmission tower due to ice storm in Slovenia 2014 [13]*; b) A flashover process by ice* [14]*; c) Discharges and dry bands on long rod insulators by pollution* [15]*; d) Discharges on 110-kV line insulators in Israel* [15] *(Reprinted with permission).*

Currently, room temperature vulcanized (RTV) silicone rubber coatings are employed to prevent contamination-related outages of power networks. Polydimethylsiloxane (PDMS) is one of the main components of RTV silicone rubber coatings, the molecular chains of which contain CH_3– groups providing a certain degree of hydrophobicity. Water contact angles on the surface of RTV silicone rubber coatings are around 110°, and such a low hydrophobic level cannot effectively prevent pollution accumulation on substrates. RTV insulator coatings, firstly developed for improving contamination flashover performance, have also been applied to enhance the performance of insulators against ice and snow [16]. However, the performed research has shown that at lower temperatures the effectiveness of these coatings reduce and they cannot effectively reduce ice accumulation on the insulator surface and prevent insulator icing flashovers [7], [8]. Over the past few decades, artificial nanocomposite superhydrophobic surfaces have been developed inspired by nature, and it has been shown that there is generally a good correlation between self-cleaning properties and superhydrophobicity. Also, a wide

range of studies in the literature correlated non-wettability and water repellency to icephobicity [17]–[19].

Therefore, to optimize the maintenance and efficiency of outdoor insulation, application of superhydrophobic coatings to prevent icing and contamination-related concerns was proposed [9]. Some investigation on comparing performance of porcelain insulators with and without nano-coatings in the laboratory has shown that nano-coated distribution 33 kV post-insulators increased the flashover voltage up to 18% under artificial rain tests as per IEC 60060-1 [20], [21].

Though there are numerous reports for fabricating superhydrophobic coatings, durability of such coatings (SHPCs) in operational conditions is still bottlenecking the transfer of this technology from laboratory to industrial applications. Hence, fabrication of a robust superhydrophobic coating against harsh chemical and mechanical conditions is of great importance.

On the other hand, the coatings and surfaces are always subjected to mechanical damages, and microcracking can likely occur through normal usage, ultimately failing. The way to a system failure might begin with tiny, microscopic cracks as they propagate and coalesce, eventually ending in catastrophic and irreversible failures in terms of corrosion, electrical insulation, etc. These understandings and in-depth investigations have resulted to mechanisms of retard or repair of the freshly formed microscopic damages prior to failure or soliciting complicated and time-consuming conventional methods of surface repair [22]–[24].

Therefore, we employed two bio-inspired methodologies to develop a durable coating with self-cleaning, icephobic, and self-healing properties for preventing/retarding the occurrence of severe damages in the insulation parts of the power system that originated from wettability issues and mechanical damages.

For these purposes, in the first place, we designed a simple but robust superhydrophobic coating from silicone-based materials which is applicable via spraying on various substrates and more importantly porcelain and glass. The durability of the coating was thoroughly investigated using vigorous mechanical and chemical testing. Moreover, the dielectric properties of the coating, as well as

dry and wet flashover voltages (FoV), leakage currents, and resistance against tracking and erosion were also evaluated employing various test methods.

Furthermore, we used the microencapsulation technique to synthesize microcapsules as the reservoirs for self-healing materials to introduce self-healing ability into the coatings thereby extending their working life as well as enhancing the safety and accuracy of the whole system.

There are various methods to assess the self-healing performance of the system. The characterization methods are chosen based on the final application. In this thesis, we have used the self-healing microcapsules inside two different systems. Firstly, in Chapter 3, we have developed a silicone composite, and the self-healing efficiency was evaluated via mechanical tests in which we could assess its performance after mechanical damages and healing process. In chapter 6, we used the self-healing microcapsules inside a superhydrophobic coating which is designed for insulator surfaces to prevent wetting driven flashovers. So, the performance of coating in a water bath could be a good indication of its function. Therefore, we chose the EIS measurements to quantify the self-healing efficiency of the developed self-healing superhydrophobic coating.

This project is defined as an academic-industry collaboration to develop a durable self-healing superhydrophobic coating for high voltage outdoor insulators for Hydro Québec porcelain insulator sector.

Overview

With the impressive discoveries and advancements of new materials obtained between the 20th and the 21st century which have been revolutionary in social structures and industries, the demand for new generation of materials with specific properties is highly growing. Superhydrophobic and self-healing materials are among these developments and have arisen as an unstoppable demand in the recent decades.

In real-world applications, all surfaces are subjected to mechanical damages. Once polymeric materials used as structural components are damaged, there might be only limited methods available to extend the functional lifetime of the material. An ideal repair method should be executed quickly and effectively on site, to eliminate the need for removing or replacing the component for repair. The idea of self-healing materials was originally inspired by living organisms and became possible after observations and technological developments of polymers. Currently, multiple methods exist for introducing self-healing ability to polymeric materials, while most of these methods require complicated structural designs on the backbone of polymeric materials. Owing to the existence of various materials and methods for preparation of microcapsules, and the possibility of incorporating them into diverse matrices, microencapsulation approach was chosen to impart self-healing capability into the coatings in this thesis.

Wettability which is quantified by the contact angle value of a liquid droplet is one of the basic characteristics of solid surfaces. Since water is the most abundant liquid on earth and presents in different forms in the environment as rain, snow, and fog, the degree of wettability of solid surfaces by water is of great importance. Therefore, designing surfaces with different wettability has attracted tremendous attention in recent years, to achieve specific applications. Among these behaviors, superhydrophobic behavior, defined as the surfaces with contact angles larger than 150° and roll off angles of lower than 10°, which leads to a non-wettable regime has shown promises in many fields of applications such as self-cleaning (washing down of pollutants under the natural forces of wind, rain), anti-icing (by prevent/delay ice formation and reduce ice adhesion strength), anti-corrosion, oil-water separation, etc. [25], [26]. Considering the insulation parts of the power equipment, water spreading, accumulation of

pollutants, and ice accretion on the surface is not favorable and therefore, application of superhydrophobic coatings on the surface of glass and porcelain insulators would be promising to prevent the wetting driven flashovers and their consequences [27].

For superhydrophobicity, two criterions must be satisfied, namely lowering surface energy, and increasing surface roughness, in order to minimize the contact between water and the solid surface [18], [28]–[31]. Among low surface energy polymers, silicone resins are preferable for developing superhydrophobic coatings due to numerous advantages in all aspects of thermal, chemical, and electrical resistance [32]. Also, surface roughness could be easily achieved via incorporating micro/nano particles into the polymeric matrix. The superhydrophobic coatings are fabricated by numerous methods, however, the main challenges bottlenecking their large-scale and industrial execution are complicated fabrication procedures, laboratory-scale application methods, and low mechanical durability [33].

This thesis aims to develop a robust self-healing and superhydrophobic coating, via a simple procedure, and using spraying method for its application on high-voltage porcelain insulators. The developed coating must not have any adverse effect on the dielectric properties of the system. Therefore, it is necessary to precisely investigate the effect of coating on electrical performance.

Objectives

The main objective of this project is to develop a durable superhydrophobic coating which contains self-healing microcapsules and can heal the mechanical damages and microcracks. The developed superhydrophobic coating can be applied on the glass and porcelain high voltage insulators to reduce the harmful consequences of pollution accumulation and ice accretion.

To achieve the main goal, some secondary objectives should be met as presented:

- Designing a suitable self-healing system (materials, processes, equipment).
- Investigation of the healing ability of the microcapsules inside a silicone matrix through SEM observations of microcracks, and mechanical analysis methods.
- Optimization of microcapsules to be used inside a thin silicone coating.
- Selection of materials and processes to develop a superhydrophobic coating.
- Investigation of the healing efficiency of microcracks in the superhydrophobic coating by incorporating appropriate healing agents.
- Investigation of the self-cleaning and icephobic properties and durability of the coating.
- Evaluation of electrical behavior of the developed coating by conducting different electrical analyses.

Originality Statement

We live in an era of striking advancements in various domains of science and technology, where separate fields and specializations are overlapping into new horizons. This cooperative approach is emerging rapidly in polymer science, by employing the organic and physical chemistry, materials science, and biochemistry, as well as electrical and mechanical engineering, to collaborate and develop uniquely innovative materials. Here, we aimed at designing a multifunctional superhydrophobic coating in order to increase the effective life-span of high-voltage insulators by preventing and/or delaying the possible arcing and flashover driven damages. The originality of this work is classified in the subsequent paragraphs from various aspects.

Firstly, most of the research efforts to enhance the pollution performance of insulators have been devoted to RTV silicone rubber coatings to treat the inherent hydrophilic characteristics of porcelain and glass with some degrees of hydrophobicity. In recent years, superhydrophobic materials with intrinsic self-cleaning properties, and enhanced icephobic performance have been introduced as promising alternatives to silicone [21]. Yet, the current research on the superhydrophobic surfaces in high voltage fields are primarily focused on bulk materials, while there are fewer reports on thin layer coatings. In the present thesis, we focused on the development of a coating for applications in the high-voltage porcelain insulator sector to enhance their performance in harsh environmental circumstances including extremely cold and polluted conditions.

Secondly, as the coatings are prone to mechanical damages, by introducing self-healing microcapsules inside the matrix, the coating is capable of repairing the micro-scale damages which are likely to happen during its service life.

Thirdly, all the structural components of the coating including healing agents, matrixes, and nano particles are silicone-based materials. The importance of this point is highlighted since fluorinated compounds are yet one of the integral components for robust non-wettable coatings, while the global concerns have risen on their application due to their environmental hazards.

Fourthly, the utilized materials and method in the current research work, emboss the developed coating with an enhancement in robustness by increasing the potential interactions and crosslinking sites between the nanoparticles and the matrix via a non-complicated approach in order to reduce the coatings delamination due to abrasion or erosion.

To conclude, to the best of our knowledge, as a multifunctional coating, there are not much comprehensive research conducted on the development of simple but robust superhydrophobic coatings for porcelain insulators in which the icephobic, self-cleaning, and mechanical durability of the coating are investigated in parallel to precisely assessing its performance in terms of leakage current, flashover voltage, resistivity, and tracking and erosion resistance.

Thesis Outline

In this context, a brief outline of the subsequent 5 body chapters composing this Ph.D. thesis is provided.

Chapter 1. For the readers to get familiar with the general idea behind this study, a literature review is presented. The main materials used in high-voltage outdoor insulators and their pros and cons are firstly introduced. The fundamentals of wetting and superhydrophobicity are represented, and the various materials and methods for fabrication of superhydrophobic coatings are briefly discussed. To mention the most important characteristics of superhydrophobic materials, some of the main applications of superhydrophobic coatings are later introduced. The current commercial status of such coatings is stated following the major shortcomings of the superhydrophobic coatings which has led to this limited real-world application. As the main drawback of these coatings, the durability issue is discussed with more details and some of the new approaches for overcoming this challenge are represented.

In the second part of the literature review, self-healing phenomena is introduced and the three general concepts for imparting self-healing ability into polymeric materials are presented, while the microencapsulation approach, as utilized in this work, is discussed more carefully. The common methods for characterizing self-healing ability are further explained in the final section of this chapter.

Chapter 2. Microencapsulation method is the most reported mechanism to impart self-healing ability to a material. In this method, the microcracks could be repaired via releasing the active materials that are stored inside the reservoirs. The type of healing agent and its solidification mechanism could be varied based on the nature of the utilized materials, the environmental condition, and the final application. In this chapter, self-healing microcapsules containing a OH-PDMS and the DBTL catalyst were synthesized via an emulsion polymerization technique. The microcapsules were characterized using various analyses including SEM, DSC, and FTIR, and incorporated inside a silicone matrix to observe the self-healing ability of the system. The self-healing process of the silicone composite was investigated using SEM observation of the crack filling, as well as tensile and tear tests to quantify its healing efficiency. The acquired results were published as "*Development of a Dual Capsule Self-healing*

Silicone Composite Using Silicone Chemistry and Poly(Melamine-Urea-Formaldehyde) Shells" published in *Journal of Applied Polymer Science* [34].

Chapter 3. In recent years, superhydrophobic coatings have gained extensive attention and are potentially applied in self-cleaning, anti-icing, anti-corrosion, anti-fogging, and oil-water separation applications. Here, an all-silicone superhydrophobic coating was developed using a silicone resin, fumed silica nanoparticles, and methyltriethoxysilane (MTES), that was applicable by spray on a variety of substrates. The wettability of coating was evaluated by contact angle goniometer, showing WCA of 163° and CAH of 2.3°. The self-cleaning of the coating was investigated using dry and wet pollution conditions. Both anti-icing (delay in ice formation) and de-icing (reduction of ice adhesion strength) performance of the coating were assessed, and the coating showed excellent icephobic properties. The existence of active functional groups on the incorporated materials in addition to the introduction of MTES could lead to the enhanced robustness of the coating through increasing the crosslink sites between the components. An extensive series of experiments were conducted to vigorously evaluate the resilience of the prepared coating and the results confirm the formation of a highly robust superhydrophobic coating. Furthermore, the coating showed high transparency that makes the developed method promising for a variety of applications. The obtained results were published as an article "*Transparent Non-Fluorinated Superhydrophobic Coating with Enhanced Anti-icing Performance*" in the *Progress in Organic Coating* journal [35].

Chapter 4. Based on the literature reviews on the investigation of electrical performance of the coatings and more specifically superhydrophobic coatings, some test methods and set-ups were designed to assess the function of the developed coating in terms of flashover voltage, leakage current, and tracking and erosion resistance. The dielectric properties of the coating were investigated via a broadband dielectric spectroscopy instrument to obtain the dielectric permittivity and tanδ values. Also, an accelerated weathering test was performed to evaluate the effect of environmental conditions on the wettability of the coating. The obtained results are published as an article "*Performance of a Nanotextured Superhydrophobic Coating Developed for High-voltage Outdoor Porcelain Insulators*" in the *Colloids and Surfaces A: Physicochemical and Engineering Aspects* journal [36].

Chapter 5. Based on the obtained results in the previous chapters, the self-healing ability was introduced into the developed superhydrophobic coating by dispersing the as-prepared microcapsules inside the silicone matrix of the coating. In this chapter, the microcapsules were adapted for well-dispersion in thin layer coatings (around 150-200 μm film thickness). For assessing the self-healing ability microscopic imaging of a microcrack as well as electrochemical impedance spectroscopy (EIS) were utilized. The self-healing efficiency and delamination index of the coating were calculated using the obtained EIS data.

Conclusions. An overview of the important findings of this project is presented in the conclusion section. The most important results obtained in the papers are firstly presented in the same order as their presentation in this thesis. The general conclusions are provided afterwards.

Recommendations. The thesis purpose was to develop a self-healing superhydrophobic coating for high voltage insulator sectors. Within the body chapters, the results, and discussions on the main objectives of the thesis were presented. In this section, specific measures or directions that can be taken for the future works are recommended based on the obtained results and literature reviews.

CHAPTER 1: LITERATURE REVIEW

1.1 Introduction

Porcelain is defined as a traditional ceramic made by heating raw materials based on clay, feldspathic materials and silica or alumina, and have been evolved in terms of design, manufacturing process and raw materials in order to fulfill the requirements of the electrical market [37]–[39]. Electrical grade porcelain has been used in power lines for outdoor insulating for more than 150 years, owing to high hardness and mechanical strength, chemical, thermal and corrosion resistance, as well as great dielectric performance [40]. Other materials considered to produce electrical insulators were wood, mica, ebonite and glass, however, only porcelain and glass continued as raw materials for manufacturing outdoor insulators [38], [41]. Decades of in-service performance of porcelain insulators have demonstrated appropriate environmental aging in addition to excellent degradation resistance against electrical stress and discharge activities [42]. Critically, porcelain insulators have hydrophilic surface characteristics that can lead to being easily wetted by water and forming of a continuous conductive film along the creepage path, thus allowing high surface leakage currents to flow. To overcome these issues, polymeric insulators have been introduced and utilized at distribution voltage levels since the 1960's owing to better hydrophobic characteristics. Although several advantages of polymeric insulators, more specifically silicone rubber, such as great hydrophobic surface properties, resistance against vandalism, and reduced maintenance costs, the polymeric insulators have some deficiencies, which must be considered. For example, the life expectancy of composite insulators is sometimes difficult to estimate specifically in harsh environments, and the reliability of the polymer materials is unknown. The polymeric materials are susceptible to degradation under electric field stress, which may lead to failure. Hence, the performance of polymeric materials in electric fields must be analyzed and the electric field distribution along the overhead insulator must be studied [3]–[5], [38], [43], [44].

As the range of transmission voltage increases, the severity of pollution and icing becomes crucial in determining the insulation level of porcelain insulators and the reliability of the network might

be compromised. The formation of a conductive layer by water or pollution on the surface of porcelain insulators results in the flow of a leakage current causing the formation of dry band arcing and a strong arcing or discharge can cause flashover across its surface [45]. The amount of leakage current through the insulator surface determines its performance. The insulation capability of the materials to withstand damage might diminish gradually by erosion. Higher magnitudes of leakage current could accelerate these conditions leading to the insulation failure [46], [47]. Therefore, imparting a hydrophobic characteristic to the surface by applying a hydrophobic coating, shows promises regarding easier removal of water and contaminations from the surface of insulators [48], [49]. RTV silicone rubber coatings, are the mostly used coatings for ceramic insulators due to their good dielectric properties, low thermal conductivities and high thermal stability over a wide temperature range, low chemical reactivity, good resistance against oxygen, UV and ozone and capability to be used under energized conditions making them a great alternative compared to greasing [50]–[56]. However, the performance of RTV insulator coatings in harsh conditions is still far from ideal due to the low hydrophobic level that cannot effectively prevent ice and pollution accumulation [7], [8], [16].

Superhydrophobic materials have been endorsed as research hotspots in recent years. These surfaces are recognized via their ultra-nonwetting behavior exhibiting a static water contact angle of more than 150˚ and dynamic contact angle (contact angle hysteresis and sliding angle) of less than 10˚ which can be achieved by a combination of low surface energy materials and micro-nanostructures. Superhydrophobic surfaces are shown to be promising candidates for numerous applications due to their significant water repellency and self-cleaning behavior such as anti-icing, water-oil separation, anti-bio-fouling, anti-corrosion, solar panels, windows and anti-fogging surfaces, etc., [25], [57], [58]. Therefore, to optimize the maintenance and efficiency of outdoor insulation in cold and polluted conditions, the surface of porcelain could be coated by a superhydrophobic coating layer to impart non-wettable character thereby mitigate surface leakage current, surface discharges and flashover occurrence [9].

While there are numerous studies on the fabrication of superhydrophobic coatings, yet durability of superhydrophobic surfaces (SHPSs) in operational conditions has restricted their industrial

and large-scale applications and most of the current endeavor in the field of superhydrophobicity, is dedicated to the methods and mechanisms to overcome this challenge.

Furthermore, the polymeric materials are prone to microscale mechanical damages leading to big failures of the whole system over time [59]. This concern has led to comprehensive research on the mechanisms to decelerate and/or repair these microscopic defects before catastrophic damages.

Smart self-healing materials could be able to address these issues, either intrinsically, or extrinsically via a pre-added healing agent. The incorporation of microcapsules was the first self-healing methodology and overall experimental results are yet suggesting this approach as the one with the highest potential of being used in real applications [60], [61].

In this chapter, firstly we have an introduction on wetting theories. The criterions for fabricating superhydrophobic coatings are explained after a quick look into the superhydrophobic surfaces in nature. We have a short glance on the commercial status of superhydrophobic coatings and their shortcomings. As the main challenge of superhydrophobic coatings, durability issues are surveyed more extensively and the methods to overcome this issue are provided. This chapter proceeds with the self-healing phenomenon, its timeline and development in polymeric material. The microencapsulation technique as the method employed within this work is introduced particularly in more detail. The characterization methods of self-healing are further represented in the final section of the chapter.

1.2 Wettability and Superhydrophobicity

Wettability is an important property for many surfaces in different industries and is governed by the intermolecular interactions between the contacting liquid and the solid surface. To quantify the degree of wettability of a solid by a specific liquid, contact angle (CA) of a given volume droplet is measured on the solid surface. Contact angle is defined as “The angle between the tangent to the solid surface and the tangent to the liquid−air interface at the contact line separating the three phases” (as shown in **Figure 1-1a**) [33]. Surfaces could be categorized into superhydrophilic, hydrophilic, hydrophobic and superhydrophobic based on their water CA values. A superhydrophobic surface is a surface on which the WCA is higher than 150° and roll-off angle is less than 10° under ambient

conditions. The roll-off angle is referred to the inclination angle of the plane at which the droplet starts rolling. A small value of the roll-off angle could indicate a small contact angle hysteresis, CAH [33]. In order to better clarify the definition and criterions of superhydrophobicity, a brief introduction to wetting, contact angle, and contact angle hysteresis is presented in the following subsections.

1.2.1 Wetting Regimes

The wettability of a surface is characterized by the contact angle (CA) of a water droplet on the solid surface. Once the perimeter of a liquid droplet encounters a solid, three separated interfaces form among solid, liquid, and gas. Each of these interfaces have a specific energy, called the interfacial energy (**Figure 1-1a**), and is proportionate to their interfacial areas. Different wetting regimes and proposed equations are represented in **Table 1-1**.

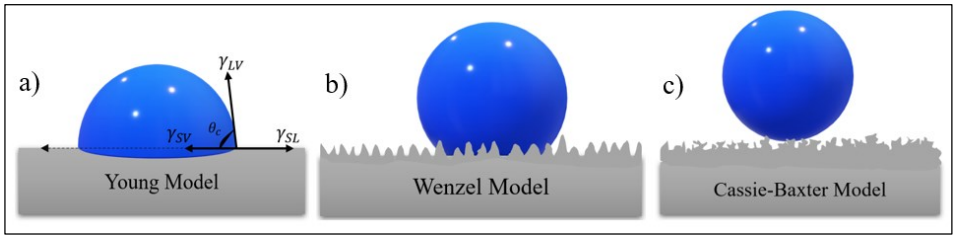

Figure 1-1. CA of water droplet on (a) flat surface with interfacial energies, (b) surface with roughness in Wenzel state, (c) surface with roughness in Cassie-Baxter state.

Young's equation defines the static WCA on an ideal surface (**Figure 1-1a**) [62], whereas most actual surfaces are not perfectly smooth. There are several models to determine the wetting state of a liquid droplet on a rough surface. Among the classical models, the Wenzel, and the Cassie–Baxter models are the mostly known models. Wenzel model predicts the WCA of a droplet where the liquid penetrates the interstices between protrusions and touches the base of the protrusions (**Figure 1-1b**) [63]. Mathematically, this equation states that roughening the surface leads to an increase in the WCA if the material is already hydrophobic ($\theta_c > 90°$), whereas increasing the roughness for a hydrophilic material will tend to make the surface more hydrophilic.

Table 1-1. Different wetting regimes, equations and the conditions applied for wetting states.

Model	Equation	Parameters	Conditions
Young [62]	$\cos\theta_c = \frac{\gamma_{SV} - \gamma_{SL}}{\gamma_{LV}}$ (Eq. 1-1)	γ_{SV}, γ_{SL}, and γ_{LV} interfacial energies of the s-v, s-l, and l-v interfaces, θ_c the equilibrium CA	Ideal surface (chemically and physically homogeneous)
Wenzel [63]	$cos\theta_w = rcos\theta_c$ (Eq. 1-2)	$r = \frac{A_{real}}{A_{projected}}$	Liquid penetrates the interstices between protrusions and touches the base of the protrusions
Cassie-Baxter [64]	$cos\theta_{CB} = f_{SL}cos\theta_c + f_{SL} - 1$ (Eq. 1-3)	f_{SL} fraction of solid-liquid interface	Composite interface of solid and air
Modified Cassie-Baxter [65]	$\cos\theta_{CB}^{W} = rf_{SL}cos\theta_c + f_{SL} - 1$ (Eq. 1-4)	$r = \frac{A_{real}}{A_{projected}}$	Microstructured or hierarchically rough surfaces, lower/macro-Cassie–Baxter and upper/micro-Wenzel

Cassie-Baxter model is related to an equilibrium state in which the liquid sits on top of the asperities and the air pockets, producing a composite interface (**Figure 1-1c**) [66]. In the heterogenous wetting regimes, increasing the surface roughness results in an increase in the amount of trapped air in the structures and a smaller f_{SL} which is responsible for increasing the WCA value. However, the fully Cassie-Baxter equation is only an approximation of the real WCA and is only reliable for specific geometries [67], [68]. For microstructured or hierarchically rough surfaces, the Cassie-Baxter equation could be modified according to Wenzel equation [65]. This equation can also predict a mixed wetting state (lower/macro-Cassie–Baxter and upper/micro-Wenzel). Interestingly, a hydrophobic behavior of the structured surface ($\theta_{CB}^{W} > 90°$) even if the pristine material is hydrophilic (i.e., $\theta_c < 90°$), would be achievable if the following condition is satisfied [65], [69].

$$f_{LA} \geq r\cos\theta_c/[1 + r\cos\theta_c] \quad \text{(Eq. 1-5)}$$

1.2.2 Contact Angle Hysteresis

Ideal surface in the Young`s equation is rigid, flat on an atomic scale, and chemically homogeneous which is not affected by vapor or liquid adsorption or any chemical interaction while most practical systems are far from the ideal surface conditions [62], [70]. Contact angle hysteresis (CAH) is an important parameter for studying surface wettability and is generally due to the deviation of the surface from being ideal. CAH has two aspects of thermodynamic and dynamic [71]–[73]. The more important sources of CAH`s thermodynamic aspect is either the presence of surface roughness or chemical heterogeneity of the substrates. The presence of any contamination on the surface by foreign materials as well as the drop size effect are the remaining sources of deviation [74]–[76]. This phenomena is responsible for the formation of different metastable states for the liquid droplet and leads to the discrepancies in CA measurements [77]. Therefore, CAH is defined as the difference between the advancing and receding CAs of a water droplet and represents the ability of a droplet to move or roll on a surface [78], [79].

Advancing CA, θ_a , could be represented by the angle when the volume of the droplet is increased through an attached needle and the three-phase contact line advances on a fresh solid surface; whereas θ_a is a measure of solid–liquid cohesion [80]. Receding CA, θ_r, is the minimum value of the CA before the three-phase line is broken while the volume of a previously formed droplet on the substrate is reduced by suction through the needle. θ_r is always smaller than or equal to the advancing CA and is mostly connected with the strength of liquid-solid adhesion [28], [76], [81]. Given an ideal, atomically smooth, and chemically homogeneous surface, $\theta_a = \theta_r$ and CAH = 0°; however, on real surfaces, CAH can be quite large [33].

Since the CAH, i.e., θ_a and θ_r, depends on the surface roughness (shapes, sizes, and configurations of the pillars) as well as the chemical heterogeneity of the surface it should be noted that a single apparent θ is not sufficient and reporting of the advancing and receding angles are mandatory for characterizing a solid surface [33], [82].

The dynamic component of the CAH is time-dependent and is mainly due to chemical interactions between the liquid and solid, penetration of the liquid into the solid's pores, and reorientations on the surface [77]. For some polymers with extensive polar groups or hydrogen bonding in their structures, CA might be changed by time due to some chain reorientations of functional groups. As an example, in a polymer backbone chain, the hydroxyl groups are re-oriented in a way to locate at the farthest possible distance from the hydrophobic air phase at the interface of solid and air. Though, by placing a water droplet on its surface, the hydroxyl groups revolve to form hydrogen bonding with the liquid water, in which, the time-dependent kinetic change in CA could be reported by measuring the extent of the reorientation of the chains on the polymer surface [33], [83].

1.3 Fabrication of Superhydrophobic Coatings

1.3.1 Inspiration from Nature

With the advent of nanotechnology and nanomaterials, numerous investigations have been devoted to simulating the natural phenomenon for practical applications. Artificial superhydrophobic surfaces are fabricated inspiring from nature, more commonly lotus leaf (Nelumbo nucifera plant) which has been the symbol of purity in ancient religions for thousands of years, and is a species that typically grows in swamps and shallow waters in eastern Asia and eastern North America [84], [85].

The surface of the lotus leaves are mainly covered with a range of different epicuticular wax crystalloids made from a mixture of large hydrocarbon molecules with –C–O and –C–H bonds, having a strong phobia of being wet [86]. On the other hand, their surface is highly roughened owing to the papillose epidermal cells, forming microscale asperities or papillae. In addition, the surface of each papilla is also covered with submicron asperities leading to hierarchical micro- and nano-sized structures. When water droplets reach to the surface of a lotus leaf, it readily sits on the peaks of the nanostructures, while air bubbles fill in the valleys under the droplet, leading to the considerable superhydrophobic behavior. The water droplets on the leaves could remove the contaminant particles when rolling off, resulting in the so-called self-cleaning ability, also referred to as the lotus effect. Other examples of non-wettable surfaces in nature include rice leaves, planthopper insects, duck feathers, and

butterfly wings. Their corrugated surfaces provide the presence of air pockets in the structures that prevent water from completely wetting the surface. Study and simulation of biological objects with desired properties is referred to as “biomimetics”, which comes from the Greek word biomimesis meaning to mimic life [85], [87]. **Figure 1-2** shows SEM pictures of some natural superhydrophobic surfaces. The SEM observation of the lotus leaf clearly shows that the surface is covered with 3-10 µm protrusions, decorated with 70-100 nm particles of the wax, and a lot of nano-sticks with the average diameter of about 50 nm randomly distributed on the subsurface layer (**Figure 1-2b, c**) [88].

A similar non-wetting behavior is also observed on the rice leaf (**Figure 1-2 d-f**). The rice leaf surface is covered with papillae, measuring diameter of about 5–8 µm, arranged in parallel order (**Figure 1-2e**), which is the main difference from the surface structure of lotus leaf. However, the sub-layer of the surface is much more similar to the lotus structure with innumerable pins with nanometric scales distributed evenly to enhance the amount of air trapped in the structures. [89]. We can also mention the planthopper among the insects with the same hierarchical patterns in its hindwings showing superhydrophobic properties as shown in **Figure 1-2 g-i** [90]. These pillars, and non-wettable property on insects in general, serve a variety of purposes, including prevention of water (and thus weight) accumulation, exhibiting low adhesion to external particles, promoting the rolling of droplet and remove sticking contaminants, and discouraging bacterial growth [90], [91].

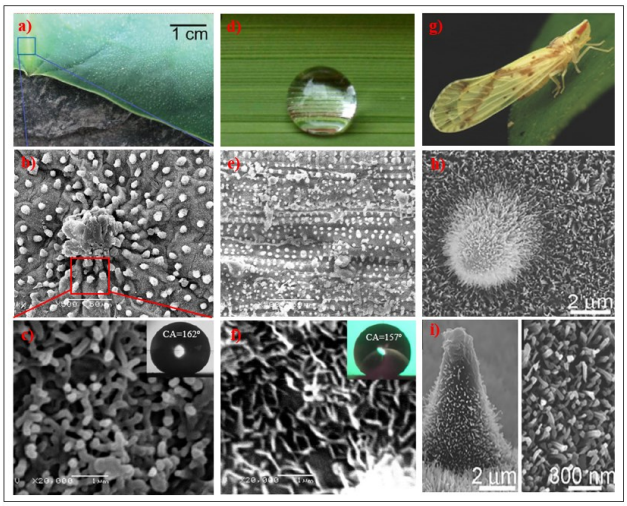

Figure 1-2. A-c) SEM images of lotus leaf [88]*; d-f) SEM images of rice leaf* [89]*; g-i) SEM images of hindwings of the planthopper insect* [90] *(Reprinted with permission).*

1.3.2 Criterions for Superhydrophobicity

The in-depth research on natural superhydrophobic surfaces led to a comprehensive conclusion for mimicking the ultra-nonwetting behavior, as synthetic superhydrophobic surfaces were developed after the 1990s. For achieving superhydrophobicity, two criterions are required to be satisfied, namely a low surface energy chemistry, and existence of physical roughness. The maximum CA obtained for water on a flat surface by reducing the surface energy is reported to be about 120° and was achieved for n-Perfluoroeicosan ($C_{20}F_{42}$)-coated glass. The researchers stated that the closest hexagonal packed -CF_3 groups provide the lowest possible surface energy of 6.7 mJ/m^2 which is much smaller than that of PTFE (22 mJ/m^2) [92]. Though it is possible to fabricate roughened surfaces with low surface energy and wettability angles of up to 170° [93]–[95].

Based on the field of application and feasibility, we can benefit from the superhydrophobic characteristics in two ways; we can fabricate a superhydrophobic bulk material, and/or we can apply a superhydrophobic coating on any used surface. Applying a coating layer is a universal solution to endow specific characteristics to a prefabricated surface. In this thesis we mainly focus on the development of superhydrophobic coatings, considering both criterions. Firstly, we introduce the prevailing materials and then we have a brief discussion on the conventional fabrication and application methods for achieving a superhydrophobic coating.

1.3.3 Materials for Fabricating Superhydrophobic Coatings

Materials that can be employed for chemical modifications should possess intrinsically low surface energy. Polysiloxanes (−Si–O–Si– groups), fluorocarbons (CF_2/CF_3), and nonpolar materials (containing bulky CH_2/CH_3 groups) are great examples of low surface energy materials due to their nonpolar chemistry, and closely packed stable atomic structures [28]. Superhydrophobic composite coatings are usually fabricated using a film-former and micro/nanoparticles. The roughness could be achieved either by incorporation of variety of micro and/or nanoparticles, and transition metal and their oxides that are able to grow nano-morphologies on the surface by creating various oxide complexes and forming coordination bonds with ligands, such as water, ammonia, and chloride ions [96], [97]. Cross-

linkable polymers such as epoxy [98]–[100], polyurethane [101], [102], polydimethylsiloxane [103], acrylic resin [102], [104], etc., are used as the film-formers to bond nanoparticles, and offer intended properties for the application.

It is possible to fine-tune the superhydrophobicity of a coating by changing its surface functionality, which intrinsically depended on its synthesis methods. In addition, orientation ordering and packing density of the functional groups could also imperatively affect the surface energy [28].

1.3.3.1 Fluorinated Compounds

Fluorinated compounds including fluorocarbons and fluorosilicones have been proved to show the lowest surface energy among various organic materials (16-18 mN/m), which has made them superior for fabrication of superhydrophobic and oleophobic surfaces. Since surface energy is associated with the formation or failure of adhesive bonds [105], these extraordinary properties are driven by the high bonding energy of fluor atoms along with the dispersive intermolecular force of the C-F bonds [106]–[108]. In addition to their extremely low surface energy, fluorinated compounds show anti-biofouling properties and excellent oxidative, thermal, and chemical resistance, as well as barrier and corrosion resistance [109], [110].

Pan et.al, fabricated a smart superhydrophobic surface composed of an array of shape memory micropillars, which were coated by pH-responsive microcapsules of fluoroalkylsilane. The low surface energy of the surface could be restored after acid stimuli and breakage of microcapsules, while the shape memory array was repaired by heat treatment and thus the superhydrophobicity of the surface could be regenerated [111].

Despite extraordinary characteristics of fluorinated compounds, their application is under global debate because in spite of their high costs, they have shown adverse consequences for the biological species and biomagnification in food webs [112], [113]. These compounds could be degraded into smaller molecules of perfluorooctanoic acid and perfluorooctane sulfonate, making them easily bio-accumulate in the living organisms [114], [115].

The increasing global awareness of the environmental effects of fluorinated compounds, has prompted researchers to develop non-fluorinated superhydrophobic materials using other low surface energy materials and more specifically silicone-based materials, fatty acids and long chain alkanes, waxes, carbon nanomaterials, etc. [116].

1.3.3.2 Silicones

The second group of materials which is well-established in the fabrication of non-wettable surfaces is silicone containing compounds. The classification of silicones is very wide [117] and beyond the scope of this thesis. Silanes and silicones are utilized in the fabrication of superhydrophobic in three main categories including nanoparticles for constructing micro-/nanostructures, alkyl silanes as coupling agents for surface treatment to decrease the surface energy, and organosilicone polymers as binders.

Incorporation of micro and nanoparticles are one of the easiest ways to impart hierarchical structure for developing superhydrophobic coatings and surfaces. Silica particles are attractive options for this purpose thanks to their low toxicity, optical transparency, and low environmental impacts [25]. Their roles and applications are discussed later in **section 1.3.3.3**.

Silanes containing hydrolysable groups (e.g., Si-Cl, Si-NH-Si, Si-OCH_3 and Si-OCH_2CH_3), are able to form silanols via reacting with water, that could be grafted to the hydroxyl groups at the interface of substrates. Also, the alkyl groups of silanes decrease the surface tension and could be used as active sites for surface treatment. Due to the high variety of these compounds, there are numerous possibilities to tailor the coatings properties by altering the reactive groups of silanes, the alkyl groups and reaction conditions [118].

Among silicone polymers, those containing highly stable Si-O bonds, with two monovalent organic radicals attached to each silicon atom, namely as polydimethylsiloxanes (PDMS) have been widely used in many protective coatings due to owing unique characteristics such as biocompatibility, great thermal, chemical and weathering stability, dielectric resistance, high air permeability, and low surface energy (surface tension of PDMS is shown to be around 20 mN/m [119]). Besides, PDMS-type silicones are normally flexible polymers with relatively low T_g (around -120°C). These outstanding

properties have made them a promising matrix in automobile industry, outdoor insulation, aerospace, and medical devices [120], [121]. Structural modification of the organosiloxanes is quite simple as their end-groups could be substituted with various reactive organofunctional groups, thereby offering more flexible tailor-designed chemistries and reactions for the resultant polymers along with controlling molecular weight yielding and varying physicochemical properties. These substituents could be inert, such as methyl, phenyl and 3,3,3-trifluoropropyl, or reactive such as vinyl, epoxy, alkoxy, hydroxyl, alkylamino groups, etc. For constructing silicones containing block copolymers, inert backbones are favorable while for crosslinked networks backbones with reactive groups could be preferred [32], [122].

Besides, PDMS are usually easy to process and multi-scale structures with high stability can be fabricated using various methods of templating [123], lithography [124], or pulsed laser etching [125]. Moreover, PDMS superhydrophobic thin films containing nanoparticles can be coated onto diverse substrates by either spray-coating, dip-coating or grafting, etc. Though PDMSs are more cost effective compared to fluorinated compounds they are yet more expensive than some other organic compounds. These higher costs in addition to their low cohesive strength are among factors that might limit their applications in certain fields (Average costs for PDMS are about $6 per kilogram, $30 per kilogram for PTFE emulsion with solid content of 60%, and $36.5 per kilogram for PVDF powder) [116]. Most PDMS are commercially available as block reactive and non-reactive copolymers from Dow Corning, GELEST, Sigma Aldrich and Fluorochem, etc.

1.3.3.3 Nanoparticles

Deposition of nanoparticles (NPs) on the substrate is a feasible way to govern the wettability of surface and impart superhydrophobic property by the formation of micro-/nanostructures to maintain air pockets underneath water droplets, forming a stable non-wetting Cassie-Baxter state. NPs could be introduced to the surface prior to the low surface energy binder application, or being well dispersed in a mixture of binder and solvent in order to spontaneously self-assemble during solvent evaporation [116]. The role of inorganic particles such as silicon oxide (SiO_2) [126], titanium oxide (TiO_2) [127], zinc oxide (ZnO) [128], etc. are investigated and exhibited in numerous studies on the superhydrophobic properties of coatings. These particles not only introduce roughness as one criterion of superhydrophobicity but

impart multiple physical and chemical characteristics to the coatings. Surface roughness can be enhanced by incorporating particles of different size ranges, which will further improve the robustness of the structures and water repellency.

Silica NPs are the most used nanoparticles in the preparation of superhydrophobic coatings due to their low toxicity, optical transparency, and low environmental impacts [25]. Silica NPs are often formed by hydrolytic condensation of a silica precursor, mainly tetraethyl orthosilicate (TEOS), via the Stöber method [129]. Since these particles are naturally hydrophilic, they can be functionalized with different silanes [130]–[137] and fluorosilanes [138]–[142] to insert hydrophobicity to their nature in order to be incorporated in superhydrophobic applications.

Kenig et.al, [137] developed a superhydrophobic coating on glass through a one-step dip coating process. They immersed glass slides into the reaction vessel and added different molar ratios of TEOS:alkyl trimethoxysilane (ATMS) obtaining a WCA of 150°. They found that the simultaneous addition of TEOS and a long chain low surface energy co-precursor in appropriate concentrations could lead to the formation of spherical superhydrophobic silica NPs, making the process favorable for being directly taken place in-situ and on any compatibilized substrate.

In another study, Wang and coworkers reported the preparation of superhydrophobic coating based on a fluorosilicone resin as the matrix and silica NPs. The developed coating was cured at room temperature and obtained by dispersing 1H, 1H, 2H, 2H perfluorooctyltriethoxysilane modified silica NPs in fluorosilicone resin. They also studied the effect of nano silica concentration and its dispersion on the non-wettability properties of the coating and figured out that silica content and dispersion time highly influence on the morphology and topography of the nanocomposite coating by reuniting configuration of NPs on the surface. **Figure 1-3** shows the surface morphology and wetting behavior of coatings based on the silica content and dispersion time [143].

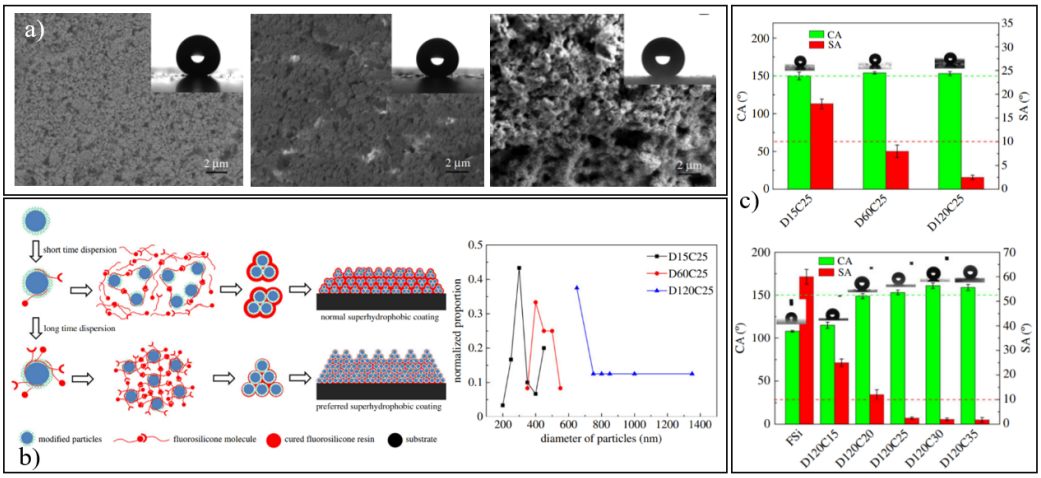

Figure 1-3. Fabrication of superhydrophobic coating using silica NPs with different dispersion times (in DnCm, n represents the dispersion time and m is silica percentage in formulation); a) SEM images of D15C25, D60C25 and D120C25; b) Formation of the nanocomposite coating in short (15 minutes) and long dispersion (120 minutes) times and the final diameter of particles; c) CA and SA values for different conditions [143] *(Reprinted from Open Access).*

NPs of transition metals oxides possess unique physical, chemical, and electrical properties originating from loosely bound electrons of d-orbitals in their valence shell are also utilized in the fabrication of superhydrophobic surfaces. Among these particles are titanium, manganese, tungsten, zinc, copper, vanadium, cobalt, rhodium, and molybdenum oxides, that have attracted more attention. Owing to variable oxidation states of transition metals, these materials can form different transition oxide complexes by coordinate bonds with water, ammonia and chloride ions making them unique engineered materials in many industrial fields [96].

1.3.3.4 Paraffins, Fatty Acids and Green Chemicals

In addition to the silicones and fluorocarbon, other organic materials containing long hydrocarbon chains, termed as paraffin in many fields, have been used to prepare superhydrophobic surfaces as it has been employed widely in nature [144]. In a recent study, Li et al. [145] demonstrated a simple method to create adhesive superhydrophobic coatings by dispersing silica NPs (50 nm) and paraffin wax in ethanol to form a network via covalent bonding. They sprayed the obtained mixture followed by solvent evaporation. The resultant superhydrophobic coating exhibited a WCA of 157.8° with enhanced resistance against tape peeling and linear abrasion.

Fatty acids are another group of biological macromolecules consisting of long hydrocarbon chains terminating with carboxylic acid groups that are the primary components of lipids. Their physical and chemical properties could be varied based on their chain lengths and degree of saturation. Fatty acids are mostly insoluble in water and hydrophobic in nature. Among the common fatty acids, stearic acid has been frequently used in the preparation of superhydrophobic coatings and hydrophobic surface treatments [146]–[148].

There are also other various organic materials used for the fabrication of superhydrophobic surfaces including polyvinyl alcohol (PVA), polyvinyl chloride (PVC), polymethylmethacrylate (PMMA), poly (lactic acid) (PLA), and polystyrene (PS).

In the recent years, the demand for bio-safe, eco-friendly, and sustainable processes with lower potential environmental footprint has been aroused and superhydrophobic materials are not excluded within this global approach. In case of process, these approaches are mainly focusing on the processing methods that could help to conserve resources like water and energy (e.g., The curing steps do not consume excess heat or radiation, or release pollutants) [149], [150]. In case of materials, the term ecofriendly could be used for the ingredients which are biocompatible, biodegradable, and are not considered as pollutants for the environment. On the other hand, it should be considered that using special compounds are sometimes inevitable to achieve specific characteristics, e.g., long-chain fluorocarbons for superhydrophobicity and oleophobicity. Since there is no known green alternative for them yet, it would be recommended to replace those long-chain persistent polymers with that of low chain length (C_6 chemistry) which are dispersed in waterborne carriers in order to reduce the environmental hazards [150]. Naderizadeh and coworkers [151] developed superhydrophobic coatings for reducing bacterial adhesion and utilized fluorinated acrylic copolymer having environmentally approved C-6 chemistry in which the coatings were shown to be biocompatible based on human HeLa cells viability tests.

Another safety concern is brought up by inorganic oxide particles, as they are not biodegradable and have been found to be toxic when produced at small length scales and aspect ratios [152]. The recent investigations on natural compounds that do not release toxic by-products would be helpful for future

applications (e.g., biological monomers, macromolecular polymers from biomass, cellulose, natural proteins and waxes, cellulosic fillers, plant compounds or components, such as Lycopodium spores, which are ideal to create texture due to hydrophobic nature and high surface area) [113], [115], [144], [146], [152], [153]. However, these investigations still need to be improved significantly but can certainly open new avenues for technological advancement in water-repellent coatings with small adverse environmental consequences.

1.3.4 Fabrication and Synthesis Methods

Different physical and chemical deposition methods are used for producing superhydrophobic surfaces via depositing a thin layer of a low surface energy mixture on the substrates. Representative chemical deposition methods include sol-gel, chemical vapor deposition (CVD), layer-by-layer deposition (LBL), and electrophoretic deposition, which are the most reported methods in the literature. The synthesized coatings could also be applied on different types of substrates via spraying, spin coating and dip coating methods. The most common synthesis and application methods for achieving superhydrophobic coatings are introduced and discussed in this section.

1.3.4.1 Sol-gel Method

Sol-gel method is one of the most popular and well-established techniques to synthesize superhydrophobic coatings. The sol–gel method is based on solution hydrolysis and condensation reactions in which a macromolecular network is obtained [154]. In this method, a precursor (chemically active compound) undergoes a rapid hydrolysis, and an active hydroxyl is generated, leading to the formation of a colloidal solution (sol) and a three-dimensional network (gel). The gel is formed due to the impregnation of the sol onto the solvent, followed by aging, drying, and thermal curing based on the reaction condition. The precursor is converted into a glassy material when undergoing hydrolysis and polycondensation reactions, forming a layer on the substrate and could show superhydrophobic properties due to the presence of several nano-pore structures produced by the removal of the solvent. The composition of the coating can be adjusted by controlling the sol–gel chemistry. Alkoxides or organically modified alkoxides and organosilanes are employed as the reactive precursors in the sol-gel

systems and can be used alone or in combination. Sol–gel method has also been employed for producing nanomaterials, micro and nanoparticles with the possibility of controlling particle size, distribution, morphology, and surface porosity. SiO_2 and TiO_2 NPs have been frequently used in developing superhydrophobic surfaces via the sol–gel method [25], [95], [149], [155]. Following this method, Ke et al. [156] developed a highly transparent superhydrophobic coating via sol-gel method using TEOS as the silica precursor to prepare the $Si(OH)_4$ sol, and added different amounts of SiO_2 nano-particles, showing optical transparency of 91% and a haze of 2.4% that was only <1% lower than the bare substrate. The as-prepared coating showed a WCA of 154° in the optimum condition. Also, due to the surface decoration with fluorosilane, the coating showed oleophobicity with an oleic acid CA of 130°. However, one of the key disadvantages of the sol-gel method is the high cost of used raw materials [157].

1.3.4.2 Chemical Vapor Deposition (CVD)

The Chemical Vapor Deposition (CVD) is a technique used for depositing a film on a substrate from a gas-phase precursor in which, the materials and substrate are placed in a chamber that is filled with the gaseous precursors in order to let them react and deposit on the surface. The major drawbacks of CVD are low deposition rate and high film-forming temperatures. Also, this method is not suitable for the preparation of large sized superhydrophobic surfaces [158].

1.3.4.3 Electrochemical Processes

Another deposition-base technique to fabricate superhydrophobic coatings, is based on using electric fields to deposit the layers of solid metal or its compound on electrically conductive substrates and is called electrochemical method in general [159]. There are four types of electrochemical processes used in the fabrication of superhydrophobic surfaces, namely, anodization, electrodeposition of conducting polymers, electrodeposition of metals and metal oxides, and electroless galvanic deposition [97], [158], [160], [161].

1.3.4.4 Layer-by-Layer Assembly (LBL)

The LBL deposition is another advanced technique to produce multilayered superhydrophobic surfaces and is a substrate-independence method using a solution-dipping process and a multilayered film is prepared by dipping the charged substrate into a solution containing an opposite charged material [162]. This process leads to building up multiple layers of coating which is responsible for the formation of a rough surface through multiple weak interactions (such as charge-transfer interactions, electrostatic interactions, hydrogen-bonding, cation–dipole interactions) [25], [163]. The addition of nano or microparticles could also be used to improve the wettability and surface roughness of the fabricated films. This method offers the advantage of a precise control over the thickness, thereby being used to fabricate transparent coatings [95].

1.3.4.5 Spin Coating

Spin-coating is a common application method for applying uniform and high-quality superhydrophobic coatings on surfaces. The typical spin-coating process normally begins with the deposition of a small quantity of the coating mixture on the substrate which is fixed via vacuuming. The entire system then rotates with a controlled speed and time until the excess liquid flies off through the edges of the substrate, and a coating with desired thickness is obtained [149], [164]. Spin coating is applicable on planar substrates using different mixtures of NPs, solvents and binders, or even without NPs [116]. Following this method, an organic/inorganic hybrid coating consisting of long-fluorine groups and hydrophobic silica NPs was fabricated. The hybrid coating synthesized via sol-gel method using a glycidyl organosilane, inherited the advantages of their self-designed resin (hardness and transparency) as well as the hydrophobic NPs showing WCA of 160.1° and SA of 7°. The coating exhibited outstanding mechanical properties and WCA of 140° after 200 tape peeling cycles, and high transparency of average of 93.6% [165], [166].

1.3.4.6 Dip Coating

Another technique used to apply a superhydrophobic coating on a substrate is using the dip coating method and is mostly used on textile and meshes [167]–[169]. This method also offers

controllability and uniformity of thickness, as well as being waste-free and easy to scale-up. In this method, the substrate is immersed in a bath containing the superhydrophobic mixture, lifted out with a constant velocity, and cured at optimal condition. Dip-coating method is applicable for a variety of substrates including planar, and 3D structural objects [116], [170]–[172].

In order to obtain superhydrophobic films with robust mechanical property, Hu et al. [173] used hydroxy acrylic resin and commercial SiO_2 NPs. The organic-inorganic superhydrophobic composite films were obtained by dip-coating an obtained dispersion of above materials on substrates with a withdrawal rate of 2.5 cm/min on various substrates such as glass, paper, cloth and aluminum. The WCA and SA of the dip-coated films reached ~170° and about 2°, respectively.

1.3.4.7 Spray Coating

Spray coating which involves an atomizer nozzle to spray a desired mixture on a surface, is an attractive application method in industries and large scale productions as it does not require sophisticated equipment and can be utilized to treat a variety of objects with different geometries and sizes [174]. There are several reports of superhydrophobic coatings in the literature applied via spray coating [175]–[179]. It is noteworthy that for achieving a desirable surface wettability it is essential to delicately design the formula in different aspects including the solvent type and ratio, dispersion of the filler, viscosity, and rheology of the mixture, etc. [116].

Spraying method was utilized to fabricate superhydrophobic coating on a variety of substrates such as glass, filter paper, copper sheets, polyethylene terephthalate (PET) films, using silica particles in micron and nano sizes to obtain a dual scale roughness morphology inside an epoxy-PDMS hybrid matrix [180]. The developed coating showed desirable non-wettability properties (CA: 161°, SA: 3.5°, advancing CA: 150.7°, and receding CA: 148.2°), that could withstand 75 sandpaper abrasion cycles, hand kneading, tape peeling and knife scraping. Also, in the buoyancy test, a coated filter paper could bear 39 times its own gravity.

The assembly of particles and surface morphology can be controlled through tuning of the evaporation rate of solvents, in a way that slower evaporation might lead to the formation of

larger concavities on the substrate surface. For example, Elzaabalawy et al. [181] fabricated a superhydrophobic epoxy-silicone hybrid coating and showed 28 wt.% of nano silica provided appropriate balance of durability and non-wettability. They used ethanol and acetone to investigate the effect of solvent volatility on the hierarchical structure, and it was found that a spray mixture of ethanol with lower solvent volatility compared to acetone could result in an enhanced surface microstructure, consequently improving the water repellency characteristics.

Li et.al. [174] utilized spray coating method to prepare superhydrophobic coating using silane functionalized silica particles and different binders including Polymethylmethacrylate, polystyrene, Siloxane-based materials (SYLGARD 184 Silicone Elastomer, hydrogen silsesquioxane resin (HSQ), DOWSIL OE-6370 M Optical Encapsulant, DOWSIL OE-6630 Optical Encapsulant) and Polyurethane to investigate the effect of binder-filler interactions on the morphology and non-wetting properties of the surface. The researchers used the Hansen solubility parameter to estimate the aggregation of a filler in a binder due to partial phase separations. This theory is based on the idea of ‘’like dissolves like’’ and the materials with similar polar, dispersive and hydrogen bond energies are considered similar within this theory. Regardless of the used binder, superhydrophobic coatings were prepared by tuning the binder-filler ratio and the solvent (**Figure 1-4**). Their results confirmed that the length of silane used for surface treatment of NPs effects on the silica solubility parameters resulting in the alteration of the microstructure of a spray-coated PDMS-silica composite. They showed that for hydrophobic polymers, the load of filler required to achieve superhydrophobicity is correlated with the relative energy difference between the binder and filler; while higher filler loads are necessary for intrinsically hydrophilic binders to achieve superhydrophobicity.

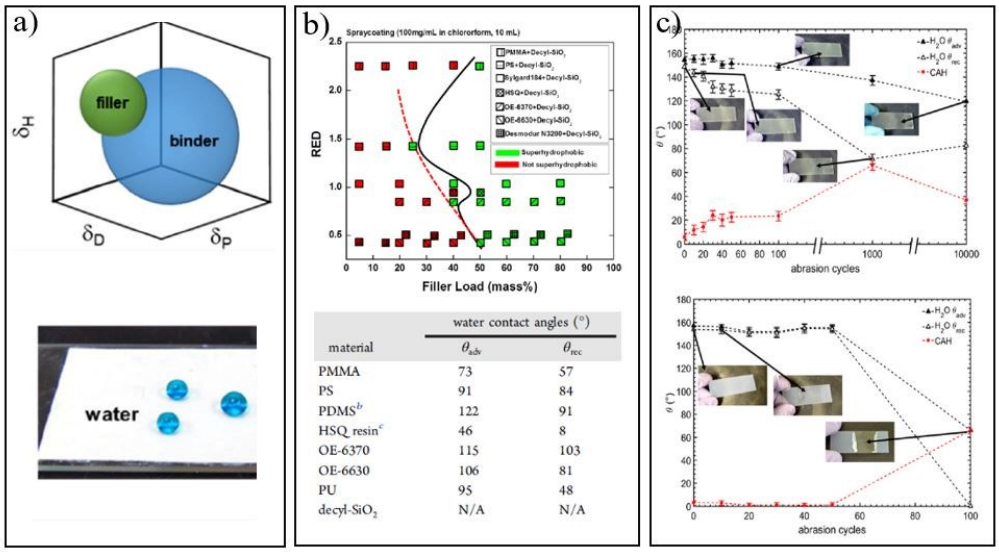

material	water contact angles (°) θ_{adv}	θ_{rec}
PMMA	73	57
PS	91	84
PDMS[b]	122	91
HSQ resin[c]	46	8
OE-6370	115	103
OE-6630	106	81
PU	95	48
decyl-SiO_2	N/A	N/A

Figure 1-4. a) Developing superhydrophobic coating with different binders and silica NPs by Hansen solubility theory; b) Superhydrophobicity phase diagram (plotted as red) vs. filler load. Green markers indicate the conditions that give superhydrophobicity. The black solid line depicts the boundary between the superhydrophobic and the not superhydrophobic coatings. The red dashed line shows the trend of red vs filler load with the outlier conditions (i.e., the two hydrophilic binders) excluded; WCA on the utilized binders d) Abrasion test on the DOWSIL OE-6370 M Optical Encapsulant/decyl-SiO_2 coating with 30% filler load and NeverWet [174]*, (Reprinted with permission).*

It is also possible to pre-fabricate surface roughness through etching techniques while an ultra-thin layer of a low surface energy material is applied on the surface structures in order to achieve a superhydrophobic surface without the incorporation of NPs [182].

Owing to the great advantages of the spray coating method, especially in industrial applications, in this thesis spray coating is employed to fabricate the superhydrophobic coating.

1.4 Application of Superhydrophobic Coatings

Superhydrophobic coatings have shown to be promising candidates as multifunctional coatings in different fields. The main applications of these surfaces are shown in **Figure 1-5**, and briefly explained in the following subsections.

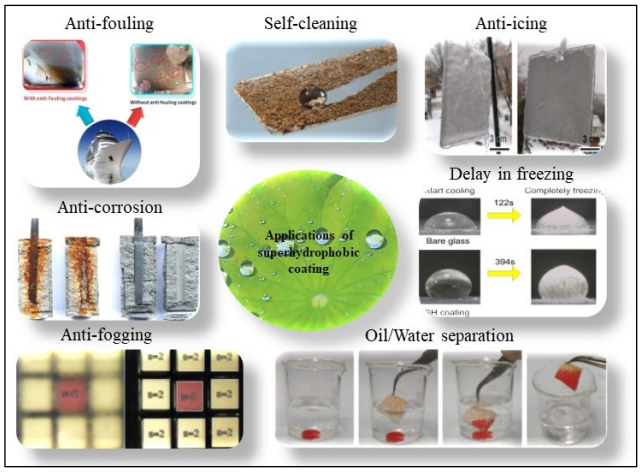

Figure 1-5. Most important applications of superhydrophobic coatings.

1.4.1 Self-cleaning

Self-cleaning has gained remarkable attention due to its distinct features and inclusive range of applications in different fields. Self-cleaning behavior is defined as the ability of a surface to keep itself clean without any external force which is stable under severe environmental conditions over an intended period.

Self-cleaning coatings are generally classified into two major categories: hydrophilic and superhydrophobic. In a hydrophilic coating, the water carries away the dirt and other impurities through spreading over the surface. Also, some inorganic oxides, such as TiO_2, can chemically decompose the organic pollutant due to their photocatalytic activity and are helpful in this self-cleaning mechanism. In the superhydrophobic self-cleaning technique, inspired by the lotus plant, the water droplets can slide and roll over the surfaces consequently cleaning them by scrolling down and picking up the pollutants on their way down [183]. The self-cleaning property of the lotus leaves is caused by its extraordinary surface structure which can reduce the adhesion of water droplets to the surface, and the rolling water droplets can remove dirt particles [184], [185]. For electrical insulation sectors, as the formation of water film on the surface could increase the chance of arcing and flashover, the superhydrophobic self-cleaning mechanism is more favorable.

1.4.2 Icephobicity

Literature reviews of common strategies to encounter icing problems can be categorized into two main groups; liquid trapping surfaces and air-trapping surfaces [186]. The first strategy is inspired by Nepenthe's pitcher plants and is fabricated by infusing a non-freezing lubricating liquid into micro/nano-porous substrate, in which a thin, ultra-smooth lubricating layer is produced that enhances the surface mobility of liquid drops and facilitates the elimination of the ice. The second strategy "air trapping" is the mechanism based on superhydrophobic behavior and is utilized in this thesis.

There are at least three different approaches to characterize icephobicity of a surface. First, low adhesion force between ice and a solid surface which is mostly quantified by measuring the critical shear stress; where, the critical shear stress is referred to the magnitude of shear stress which is required to move a given amount of ice on the surface [187]–[189]. Second, the ability of a surface to prevent or delay ice formation characterized by time delay of heterogeneous ice nucleation [190]–[192]. Third, repelling small bouncing-off droplets at subfreezing temperatures signifying the condition of rain, fog, etc. in order to prevent enough contact time and condition for ice formation [193].

Regarding to these three approaches, an icephobic surface is a surface which 1) can decrease the heterogeneous nucleation temperature, 2) prevents or delay freezing of incoming water, and 3) shows small ice adhesion strength if any ice is formed on the surface so that it can be easily removed [186].

Icephobic-superhydrophobic mechanism is mostly based on the rapid removal of water prior to freezing. This strategy functions by preventing the nucleation of ice and helps rapidly eliminate water droplets arriving on the surface. It has been shown that superhydrophobic surfaces can potentially retard ice nucleation on the solid surface by decreasing both contact time and contact area and also increasing droplet roll-off [194], [195]. It has been found that a CAH less than 10°, a micro/nano surface structure with nanospikes and surface roughness in the range of 10–80 nm, are appropriate for automatic ice sliding at −20°C at a tilting angle of 30° [196]. A minimized water-solid contact area which is resulted by the formation of rough superhydrophobic structures leads to reduced heat transfer paths in such

surfaces. In another word, compared to the hydrophilic surfaces, the interface of SHP surface and water droplets are endowed with higher temperature lowering the probability of droplet freezing [197].

On the contrary, some investigations have raised questions concerning the use of SHPSs for icephobic applications [198]–[200]. Condensation frosting is one of the major concerns of SHPSs because condensed microdroplets can penetrate into the pores and structures of the surface causing a sticky Wenzel state [199], [200].

1.4.3 Corrosion Resistance

Metal is an important type of engineering material for industries and equipment, however, corrosion has been always one of their most related challenging concerns, by bringing about large damages and monetary loss. Therefore, anti-corrosion mechanisms should be considered as of the top priorities requiring special care in their application. Long-term exposure to pollutants and moisture may increase the corrosion of the metals, resulting in considerable reduction of its service life or even safety hazards [120]. Numerous methods including chemical conversion coatings, sacrificial anodic coatings or metal painting, and cathodic protection have been proposed and utilized to prevent or reduce the corrosion rate of surfaces [201]. Recently application of a layer of superhydrophobic coatings on the material surface has shown promise in this area by decreasing corrosion rate on various metals such as aluminum [202], steel [203], copper [204], etc. When the surface of the metal which is in contact with a corrosive solution is coated with a superhydrophobic coating, the reduction in corrosion rate could be observed owing to the trapped air in the surface grooves acting as an inherent isolator hindering the direct contact between the surface and the media and inhibiting the corrosive ions movement [201], [205], [206]. Besides, Wang et al. [207] claimed that the presence of long-chain hydrocarbons can also play a key role in the anticorrosion performance of superhydrophobic coatings.

1.5 Commercial Status of Superhydrophobic Coatings

The global demand for superhydrophobic coatings in the practical fields has noticeably grown in the recent years yet expects to grow further in the upcoming years. It is anticipated that the global market may rise to an impressive value of around 37 million USD by 2024 while being 2.9 million USD

in 2015 [208]. **Table 1-2** presents some of the companies producing superhydrophobic coatings with the largest market shares.

Table 1-2. Examples of some prominent companies that are commercially manufacturing superhydrophobic products in the market [149]*, (Reprinted with permission).*

Company	Trade name	Product features	Potential substrates
NeverWet LLC (USA)	NeverWet®	Durable, drying in 30 minutes Spray application	Metal, wood, Plastics, concrete, asphalt, fiberglass, canvas
Lotus Leaf Coatings, Inc. (USA)	HydroFoe™	Stable under ambient condition, ultraviolet, lotus-like structure, 6 months shelf life at room temperature and applicable using dip, spin, spray, or blade coating	Paper, steel, wood
Aculon® Technology (USA)	Aculon®	Repels water, dust, oil, and dirt	Optical and display devices and smartphones, stainless steel, and aluminum cans
Xiamen Hehoo Tech. Co., Ltd. (China)	TUORMAT®	Fluorine-free and silicone-based; Spray application, shelf life of 3 years	Fiber and garment, footwear, and leather
NICCA Chemical Co., Ltd. (Japan)	NEOSEED®	Spray application, fluorine-free and biodegradable, retaining breathability	Textile and fabric surfaces
Daikin Chemical Europe GmbH (Germany)	Unidyne®	PFOS-free and PFOA-free, water and oil repellency, stain release, resistance to liquid chemicals	Surgical gowns, medical drapes, packs, face masks, and sterilization wipes

Though the future prospect of the superhydrophobic coating market seems to be promising, on one hand, most of the current commercially available products are still suffering from very low durability compared to the minimum standards of the conventional coatings, as well as being intolerant against high temperatures and corrosive mediums.

On the other hand, there are a small number of companies currently manufacturing superhydrophobic coatings and specifically fluorine-free coatings. Fluorinated polymers such as Teflon,

polyvinyl fluoride, or polyvinylidene fluoride are still used in industries on large scales. However, it is expected that fluorinated compounds will be replaced by silicone-based materials in the near future.

1.6 Shortcomings of Current Superhydrophobic Coatings

Unless the outstanding function of the superhydrophobic coatings in various fields, there are still many concerns that need to be fully addressed in order to transfer these technologies into the real-world applications within acceptable functionality.

Generally speaking, the starting materials which are used in the fabrication and synthesis of superhydrophobic coatings and surfaces are quite costly. In many cases, the fabrication techniques involve tedious multistep processes and require complicated facilities that are only applicable for small surfaces [209]. In addition, the application of nano and microparticles in the process of fabrication of these coatings, oblige the industries to facilitate the working environments with appropriate ventilation systems, as well as powerful mixing utilities. Therefore, it is necessary to develop some simple and cost-effective methods that can be used to form superhydrophobic coatings on various substrates. Among the application methods, spray coating and dip coating methods have shown to be very promising. In addition, as mentioned in **Section 1.3.3.4**, it is better to find natural and ecofriendly building blocks for the fabrication of SHP coatings.

Durability issues have always been the Achill's heel of large-scale application of superhydrophobic coatings. Mechanical robustness of superhydrophobic coatings is highly dependent on the robustness of the micro- and nano-structures on the surface, while these structures could be easily damaged via abrasion, erosion, impact, etc. [128], [210]. This mechanical fragility is the main reason for an irreversible loss in the SH properties of the coating indicated by a decrease in WCA and an increase in CAH and sticking of water droplets on such locations. For this purpose, it is crucial to wisely select the utilized matrix and nanomaterials and precisely control the formulation and ratios, in order to have the highest interaction between the materials [33].

Another challenge in the SHP coatings, is related to the condensation of water droplets inside the coating's structures. Most of the as-prepared SHP coatings do not show superhydrophobic behavior

in sub-zero temperatures, as they are not water vapor repellent, as well. When the temperature is well below the dew point, water condensation occurs on the surface of superhydrophobic coating and a significant transition in the non-wetting behavior of the coating is observed [211], [212]. Active strategies to encounter condensation frosting on SHP surfaces include the use of electric heating, oscillation, and antifreeze chemical substances [197], [213], [214]. The application of electric heating is considered as the most widely used approach to prevent frost formation or to melt the formed frost but it is costly due to the huge consumption of energy [197].

The impacting water droplets such as heavy rains could also have a similar detrimental effect on the non-wetting behavior of SH coatings by impregnation of water droplets into the surface structures and occurrence of Cassie to Wenzel transitions [215].

Considering the self-cleaning and anti-icing applications of superhydrophobic coatings, glass windows, solar cells, windows of surveillance cameras, and mirrors are examples of the target markets of these coatings. For a superhydrophobic coating to be an appropriate candidate for such surfaces, the optical transparency is of great importance. As discussed earlier, roughening is favorable to induce nonwetting characteristics to chemically functionalized surfaces and coatings, via introducing trapped air pockets within the peak-and-valley topography. However, the size of hierarchical micro- and nano-roughness must be finely controlled to restrain the intrusion of water and maintain essential volume of air pockets for a stable Cassie-Baxter regime [216]. The formation of roughness, increases the light scattering in a media because of Mie scattering specially if the roughness size exceeds the wavelength of light [217], [218]. Consequently, from the perspective of surface roughness, superhydrophobicity and transparency are generally in conflict. The other factor affecting on the amount of scattered light from a surface is related to its refractive index. Therefore, to guarantee the formation of a simultaneous transparent and robust superhydrophobic coating, the precise manipulation of roughness size and the material selection are extremely crucial [219]. It is shown for superhydrophobic coating to become optically transparent, adjusting the mean size of the rough particles on the surface below 100 nm is optimal as the refraction intensity at the interface of air and coating is reduced [220].

Within an investigation for developing transparent superhydrophobic coating, impact and the waterjet resistance were evaluated for a coating composed of silica particles and bis-phenol A epoxy resin on glass plates [221]. The NPs were deposited and self-assembled on the surface of semi-cured epoxy films and were then placed in the oven for accomplishing the curing process. The obtained transparent superhydrophobic coating was able to resist water drops released at a speed of 4.47 m/s and water jet impact at a speed of 8.6 m/s (with a Weber number of ~ 2500), thereby satisfying the conditions of a heavy rain.

1.7 Durability of Superhydrophobic Coatings

Owing to the undeniable durability drawbacks of the superhydrophobic coatings, it is crucial to have a more comprehensive survey on the origin and characterization methods in order to invent methods and mechanisms for its enhancement. For this purpose, in the subsequent sections, we have discussed the mentioned headlines in more detail.

1.7.1 Definition and Importance

Robust and durable are alternatively used in the literature referring to the stability of superhydrophobic properties against harsh conditions such as wear, abrasion, impact, UV, chemicals, etc. Robust superhydrophobicity is a must to meet industrial criteria for commercial products. Nowadays, thanks to the numerous fabrication techniques and new materials, endowing superhydrophobic characteristic to a surface is not challenging anymore; therefore, in the recent years, major effort has been made in elucidating the mechanisms of wetting transitions, design strategies and fabrication techniques of superhydrophobicity to enhance the durability of superhydrophobic coatings. However, in the majority of reports, as the abrasion, either physical or chemical, surpasses a certain value, the non-wettability is permanently lost [222].

The existence of a hierarchical surface topography creates a large extent of trapped air in the interface of water/SH surface. Therefore, only a small portion of the overall area is in contact with water, and even small mechanical loads generate high local pressures to the structures, thereby leading to deterioration in the surface patterns altering its superhydrophobicity [223].

A loss in the superhydrophobic behavior could be explained by considering a Cassie to Wenzel transition, and for a surface to become superhydrophobic again, this transition must go in the reverse direction. Thermodynamically speaking, it is shown that the corresponding equilibrium point of the Wenzel state is much lower compared to the Cassie state. Also, the energetic barrier for a transition from Wenzel to Cassie is much larger than the opposite direction. This point of view can explain why the reverse transition from Wenzel to Cassie (i.e., recovering superhydrophobicity once it is lost) is very challenging and requires excess energy to be triggered [224], [225]. Due to this matter of fact, the importance of robustness and durability is extremely highlighted in the literature when speaking about superhydrophobic surfaces and coatings.

1.7.2 Durability Assessment

Depending on the sought-after application, the durability of the coating is characterized by means of mechanical, physical, and chemical analysis. One of the biggest challenges for robustness evaluation of superhydrophobic coatings is the lack of standard and universal methods for this purpose, making it extremely difficult to have a meaningful comparison on the obtained data.

For investigating mechanical durability, the effect of abrasion, wear or impact on the chemistry and topography of the coating could be evaluated. Researchers have employed different apparatus and test conditions, while the most commonly used methods include sandpaper abrasion, bending, drop impinging, knife-scratch, pencil hardness, finger pressing, tape-peeling test, and falling sand grains test [226], [227]. Among these tests, the sandpaper abrasion test is more widely used for evaluating mechanical robustness as it seems straightforward to visualize the robustness of superhydrophobicity. However, there is not any defined standard for superhydrophobic coatings in order to unify the test conditions like the grit size of the sandpaper, the direction and distance of drag, speed, applied force, the size of the contact area, etc., causing the interpretation and repeatability of the data to be in question and more importantly vague from the perspective of quantitative characterization.

Chemical stability of superhydrophobic coatings is usually assessed via exposing the superhydrophobic coating to corrosive media with different pH levels or salt concentration, and UV light

irradiation. The wettability of the coatings after these tests could exhibit the chemical robustness of the coating. The superhydrophobic coatings are supposed to show acceptable performance in corrosion tests as mentioned in **Section 1.4.3** owing to the presence of air cavities and reduced contact area. The UV-resistance of superhydrophobic coatings is mostly investigated via an accelerated QUV weathering test while monitoring its degradation process in time. As a matter of fact, the superhydrophobicity of the coating is lost once the coating is decomposed, which is basically more related to the inherent characteristics of the incorporated materials, and could be fine-tuned by the proper selection of the coating composition [228]–[230].

Tiwari`s group developed an all-organic superhydrophobic nanocomposite coating with high mechanical robustness that could be applied by spraying or brushing. Firstly, they synthesized a fluorinated amine curing agent to graft fluor groups to an epoxy backbone. Then, a perfluoropolyether was blended with the fluorinated-epoxy resin to further enhance the hydrophobicity and enhance the mechanical flexibility of the epoxy matrix. Finally, polytetrafluoroethylene (PTFE) NPs were incorporated into the resin to obtain the superhydrophobic nanocomposite coating. The developed coating (as shown in **Figure 1-6**) with WCA of ~158° showed mechanical robustness under cyclic tape peeling and Taber abrasion, as well as sustaining highly corrosive media [231].

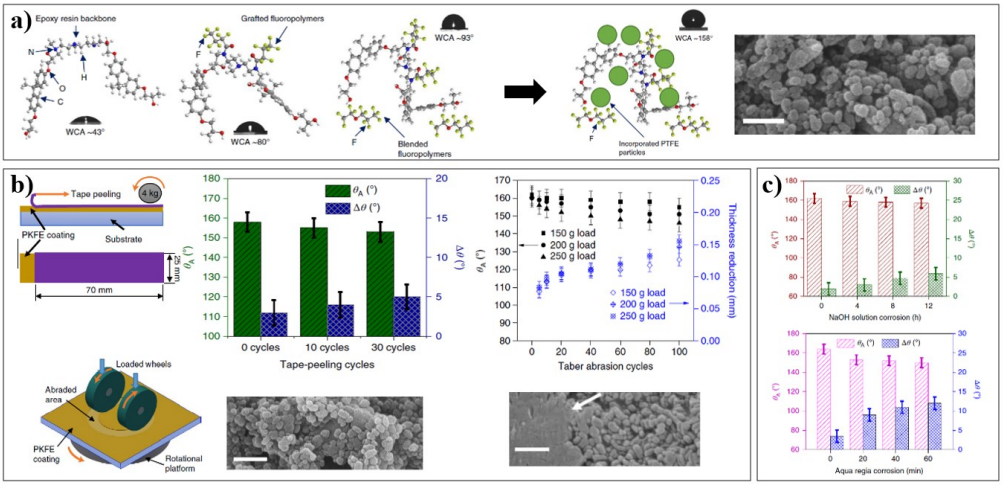

Figure 1-6. a) Multiple steps of the fabrication of a robust perfluorinated epoxy nanocomposite coating and the SEM image of the coating; b)Tape peeling and abrasion tests for evaluation of mechanical durability of coating via contact angle goniometry and SEM observations after test cycles; c) Assessment of chemical durability of coating [231]*, (Reprinted with permission).*

It should be considered that the robustness of superhydrophobic coatings should be mostly evaluated based on the meaningfulness of a test method for a specific end-use application. For example, when a coating is used for indoor applications, the exhausting cycles of sand grain test or long-term UV exposures might not be applicable to assess its overall performance. Also, it is well known that robustness results obtained via various tests are governed by different characteristics of the coatings and these results could not be alternatively used without considering their main functions. In particular, stability of a coating against tape peeling test is more related to the adhesion and cohesion interactions between the coating/substrate or coating`s composition itself; while the data from scratching or indentation-based methods are mainly dominated by the hardness and stiffness of the material [232], [233].

1.7.3 Durability Enhancement

The most common methodologies for enhancing the robustness of superhydrophobic coatings could be categorized in two active and passive strategies. The passive strategies mainly focus on the retention and strengthening the superhydrophobic properties against wear or harsh conditions and include those intrinsically employing abrasion resistive and stable materials, increasing the crosslinking sites and interactions between the components, or adding elastic compositions to soften the applied stress. While the active strategies attempt to induce regeneration of the superhydrophobicity after its loss via self-repair strategies [234]. However, using multiple strategies in a coating could be helpful to insure different aspects of robustness.

From a theoretical point of view, mechanical robustness and superhydrophobicity are conflicting and nanostructures having high aspect ratios are severely sensitive to impact forces [235]. For a surface to be superhydrophobic, high aspect ratio and thereby less contact area is required leading to high contact pressure. Increasing these local contact pressures will be responsible for the abrasion of the surface protrusions by surpassing the materials yield stress, and an irretrievable loss in ultra-non wettability will occur. It has been shown that crater-like structures consisting of a network of pores would withstand the mechanical shear forces up to an extremely large amounts compared to a surface with needle-like structure [235]–[237]. Recalling the hierarchical micro/nano Cassie state argument

from previous sections, designing surface patterns with dual scales roughness is a common strategy for enhancing the mechanical stability of superhydrophobic surfaces in which the microscale structures could bear the mechanical load and protect the much more fragile nanoscale structures from being abraded [238]–[240].

It is well known that one of the initial principles of applying a coating on a surface, is related to the proper adhesion between the coating layer and the substrate, highly influencing the mechanical properties. A defect in the adhesion or cohesion properties of a coating, will lead to the failure of the whole system, whether it is superhydrophobic or not. A strong adhesion is generally a means of forming strong interactions at the interface. Hence, increasing the possible interaction sites and crosslinking between the existing functional groups could significantly enhance the mechanical stability of superhydrophobic coatings applied on their desired substrates. Among the possible interactions, the chemical bonding is able to provide higher stability compared to physical adsorption or deposition, leading to much more strengthened superhydrophobic coating [241], [242]. This strategy is of high potential in the fabrics and textile industries via the incorporation of silanes containing hydrolysable groups that can form silanol thereby covalently bond to hydroxyl groups on the fabrics [243]–[245]. Glass is another substantial substrate which could be treated with silanes to induce superhydrophobic character on its surface. The glass surface is covered by Si-OH groups making glass to be hydrophilic in its common form. When using such alkyl silanes or fluoroalkyl silanes with the proper reaction condition, the generated siloxane groups from the hydrolysis reaction of the alkyl silane can undergo a reaction with the Si-OH of the glass surface, resulting in the attachment of long alkyl chain groups to the glass surface and transformation of Si-OH into the Si-O-Si bonds, thus inducing hydrophobic properties to glass [246], [247].

Zhang et al. [248] proposed a strategy to increase the interfacial adhesion of an epoxy based superhydrophobic coating (WCA = 160°, SA ≤ 2°) with polycarbonate (PC) substrates, via solvent induced crystallization of PC in the presence of acetone. It was found that the acetone-induced crystallization and roughening of PC leads to a firm bonding of superhydrophobic coating onto the surface of PC substrates. Epoxy resin was utilized as the matrix to bond the fluorinated silica NPs (F-

SiO_2 NPs) onto the roughened polycarbonate. The fabrication procedure consisted of fluorination of silica particles and preparation of F-SiO_2 NP/Epoxy dispersions in acetone, followed by submerging of PC sheets, dripping off and curing. They also compared the as-prepared coating with commercial NeverWet® coatings, and their results showed enhanced interfacial adhesion, excellent chemical/mechanical stability, and anti-icing property, implying its potential for outdoor applications.

The interaction between the particles and the matrix is another crucial factor affecting the robustness of superhydrophobic coatings. A weak interaction will be responsible for the nanostructures to be removed easily via abrasion or erosion leading to superhydrophobic failure. The mechanical properties of the nanomaterials, resistance of the matrix against wearing and adhesion of the coating to the substrate are other factors which should be considered to design such coatings to enhance their life-time and efficiency in order to obtain a mechanical durable superhydrophobic surface [249]. Compared to brittle and hard materials, elastomeric materials can buffer the peak stress via elastic deformation, thereby avoiding irreversible damage, and making them favorable options to design mechanically robust superhydrophobic coatings, while the adhesion with the substrate can also be improved through dispersing energy with deformation [250]. Among elastic polymers, PDMS and related elastic components are the most reported candidates and incorporation of suitable amounts of NPs would enhance their resistance against mechanical wear [251], [252].

Ming et al. [253] reported a procedure in order to increase the possible crosslinking sites in a hierarchically roughened superhydrophobic coating using raspberry-like silica particles and an epoxy-amine matrix. For the synthesis of raspberry-like particles, monodisperse silica particles and amine-functionalized silica particles (particle size of about 700 nm and 70 nm, respectively) were covalently bonded through the epoxy and amine group's reaction. Then, these amine-functionalized particles were deposited onto the semi-cured epoxy. They also coated the particles with a thin layer of mono epoxy-end-capped polydimethylsiloxane to chemically treat the surface energy of the coating, resulted in a superhydrophobic coating with WCA of 165° and CAH of 2° (**Figure 1-7a**). In another study, Yang et al. [254] used a mixture of TEOS, heptadecafluoro-1,1,2,2-tetrahydrodecyl triethoxysilane, and nano silica in an ethanol solution to formulate a bridged NPs/sol solution for spray coating, leading to a

transparent superamphiphobic coating. The coating showed enhanced robustness against sand abrasion, heating, and water jetting (**Figure 1-7b**).

Despite great progress and efforts in the fabrication of robust superhydrophobic coatings, the loss of superhydrophobicity is almost inevitable once the wear is beyond certain critical values.

Therefore, in recent years, alternative active strategies are proposed as promising strategies to prolong the life-span of these coatings via regenerating the lost characteristics within a healable manner in which healable superhydrophobicity means that the loss of non-wetting property can be recovered mainly by releasing low surface energy agents and/or reparable topography and chemistry [234], [249]. Biological organisms can retain their superhydrophobicity over their lifetime through biological renewal of the surface [255]. Surfaces with the ability to regenerate their roughness or/and restore the hydrophobic components are called self-healing superhydrophobic surfaces in the literature, while in this thesis the term ‘’self-healing’’ is used for the mechanical healing.

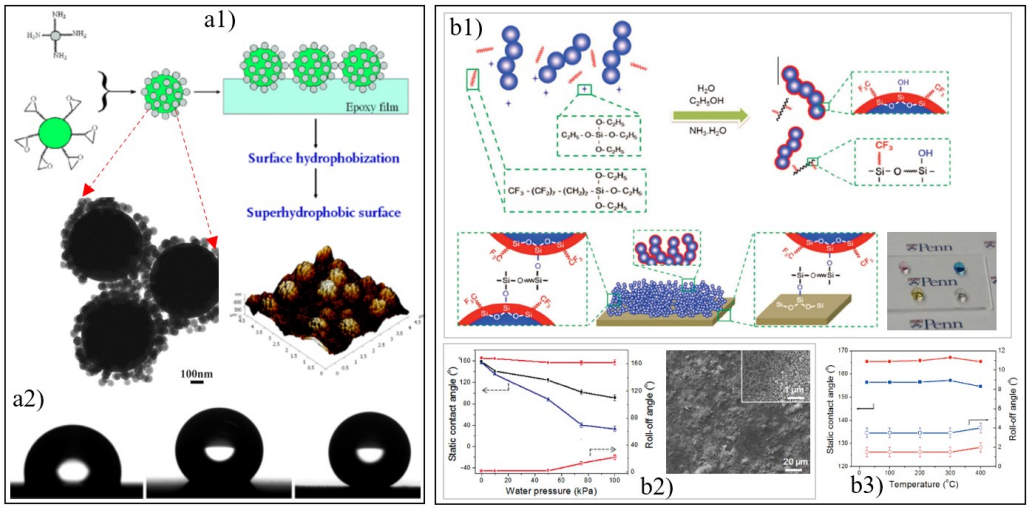

Figure 1-7. a1) Synthesis of raspberry like silica particles and crosslinking of particles to the epoxy matrix via epoxy/amin reactions, TEM images of particles and AFM analysis of the surface showing multiscale roughness; a2) CA of water on PDMS-covered epoxy with no particles, large particles and raspberry particles, respectively; [253] *b1) Preparation of functionalized NPs and spray coating of the mixture on glass to obtain a transparent superhydrophobic coating; b2) Water jet test and SEM image after water jet; b3) Evaluating thermal durability of coatings* [254]*, (Reprinted with permission).*

To chemically regenerate superhydrophobicity, storage of low surface energy materials inside the matrix or in reservoirs in a roughened structure is the more common used method; by decomposing

the hydrophobic chemicals on the surface, the ones inside the coating would migrate toward the surface, regenerating the surface chemical composition like a living organism does [256]–[258]. PDMSs have shown great promise regarding recovering surface hydrophobicity [10], [259]–[263]. The driving force of the hydrophobic recovery is a thermodynamic aspect to minimize the surface free energy. This phenomenon and the kinetics of the recovery are studied by many researchers and can be summarized into 1) Reorientation of polar groups into the bulk, 2) Condensation of the surface silanol groups, 3) Changes in surface roughness, 4) Migration of low molecular weight species from the bulk toward the surface, while migration of low molecular weight PDMS is found to be the dominant mechanism for this phenomenon by most researchers [262].

Also, self-repairing topography would be beneficial to retain superhydrophobicity by regenerating rough structures. There are only a few reports regarding this matter because growing rough structures as happens in living organisms is a great challenge for man-made surfaces. However, studies have shown that rearranging the top layer of some coatings is somehow possible with the aid of external stimulus or using shape memory polymers [264], [265].

As mentioned earlier, polymeric coatings are prone to mechanical damages during their service life, and even the formation of tiny micro-scale defects might provoke structural damages leading to catastrophic consequences. In order to prevent such undesirable occurrences, and more specifically in this thesis that the end-use application is the high-voltage sector, the introduction of self-repair mechanisms without human intervention is advantageous in different aspects of time, safety, human resources, and energy. Therefore, in the developed superhydrophobic coating, self-healing mechanism is imparted via the incorporation of microcapsules containing a silicone healing agent.

The following section is an introduction on the self-healing phenomena, the main mechanisms, and its characterization methods.

1.8 Self-healing Materials

Biological organisms possess inherent repair mechanisms helping them prevent losing their functions. Human skin has the ability to self-heal through an inflammatory response of cells below the

dermis layer via increasing the production of collagen and regenerating epithelial cells and tissue [266]. This characteristic in plants is induced by oligopeptides, oligosaccharides or other molecules that indicate damage and establish a sequence of chemical events leading to the macroscopic repair [267].

The impressive advancements in new materials and processes attained since the 20th and the 21st century, the demand for new generations of materials with specific functionalities is highly emerging. Inspired by the natural healing ability in the living organisms, researchers have attempted to introduce the self-repair mechanism into the functional materials to extend their service life. Among them, self-healing polymers have been widely used in different fields of biomedicine, tissue engineering, and protective coatings [268]–[272].

Self-healing or self-repairing or autonomic-repairing mechanisms in materials first gained attention in the 1970s. it was observed that hard elastic polypropylene (HPP), as well as other viscoelastic polymers, consisting of a stacked lamellar morphology, perpendicular to the axis of polymer extrusion, are capable of healing interlamellar micro voids which formed by stretching (in the perpendicular direction). In these materials, upon polymer stretching, surface energies are converted to strain energy and, subsequently, mechanical work, which helps the crack closure [255], [273].

Self-healing ability is highly striking in the current environmental circumstances as-far-as the demand for prolonging the lifespan of products thereby reducing waste is irresistible. In this context, functional polymers and materials should become well-suited with the modern circular economy and sustainability models. One of the practicable approaches to fulfil these requirements is conferring these materials with self-healing potentials. The introduction of the self-healing polymeric concept as a means of healing invisible microcracks for extending the working life of the polymeric components occurred in the 1980s for the first time [22]. Dry and Sottos [23] in 1993 and White et al. [24] in 2001 were pioneered to inspire worldwide interest in these materials.

To classify the various generations of self-healing materials, four concepts could be defined including localization, temporality, mobility and mechanism [274], [275].

The concept of localization is mainly referred to the position or scale of the damage in the material, which plays an important role in the self-healing ability of a material. The occurrence of a damage could be in the molecular scale as the breakage of the material network, can be superficial, such as scratches or microcracks; or it can be deep, such as the propagation of surface damage and delamination.

Temporality is defined as the time gap between the incident of the damage and the repair, as observed in nature, i.e., self-healing is not instantaneous but time dependent. However, it is desired to minimize the time needed for the self-healing for example by increasing the mobility of the material to promote the diffusion of the healing agents toward the damaged area [275].

In terms of mechanism, the last key concept, one can classify the self-healing materials into two main categories of extrinsic and intrinsic [274]. Extrinsic self-healing is referred to those containing an external healing agent, usually in the form of dispersed capsules or vascular networks. In these methods, the reservoirs release their healing agent to fill the damaged area and do not specifically interact with or change the chemistry of the matrix [274], [276]. These approaches are mainly used in thermoset systems [277]–[280], for various applications such as coatings [281], instrument panels [282] and sponges [283].

Intrinsic self-healing materials are principally composed of reversible bonds present in the backbone of the material and can be restored after a damage happens; these mechanisms are dominant in elastomers, such as silicones [284], [285], polyurethanes [286], [287], and rubbers [288] in different fields of nanogenerators [289], sensors [290], and conductive elastomers [291]. Intrinsic self-healing properties are imparted to polymeric materials by incorporating either covalent or non-covalent reversible bonds/interactions. Different types of reversible covalent interactions are the Diels-Alder (DA) reaction [292], [293], disulfide bonds [294], and acylhydrazone bonds [295]. Among the reversible noncovalent interactions, hydrogen bonding [296], [297], metal−ligand interactions [298], [299], hydrophilic/hydrophobic interactions [300], and Ionic interactions [301] have been used in self-healing polymers. The dynamic covalent bonds having a reversible nature, offer them the ability to break and reform. However, compared to non-covalent bonds, large amounts of energies are required for breakage (e.x., bond strengths of 150–550 $kJ.mol^{-1}$, in comparison to physicochemical bonds, like hydrogen

bonding with strengths of a few kJ.mol^{-1}). Owing to this high bond strength, dynamic covalent self-healing polymers generally require energy provided by an external stimulus, usually in the form of heat or light to perform healing [302].

Shape memory polymers (SMPs) are also emerging in different fields of self-healing applications. SMPs have an extraordinary potential to change their original shape under certain conditions, fix different temporary shapes under another condition, and finally restore their initial shape by external stimuli such as heat, light, electricity, or chemical induction [303]. Shape memory is not restricted to a certain polymer, but it is a result of molecular structure, reversible mobility changes, conformational entropy, and programming [299], [304].

One of the most comprehensive assortments of different intrinsic and extrinsic methodologies to impart self-healing ability into the materials is shown in **Figure 1-8**, which is based on three categories of physical, chemical and physico-chemical approaches [305].

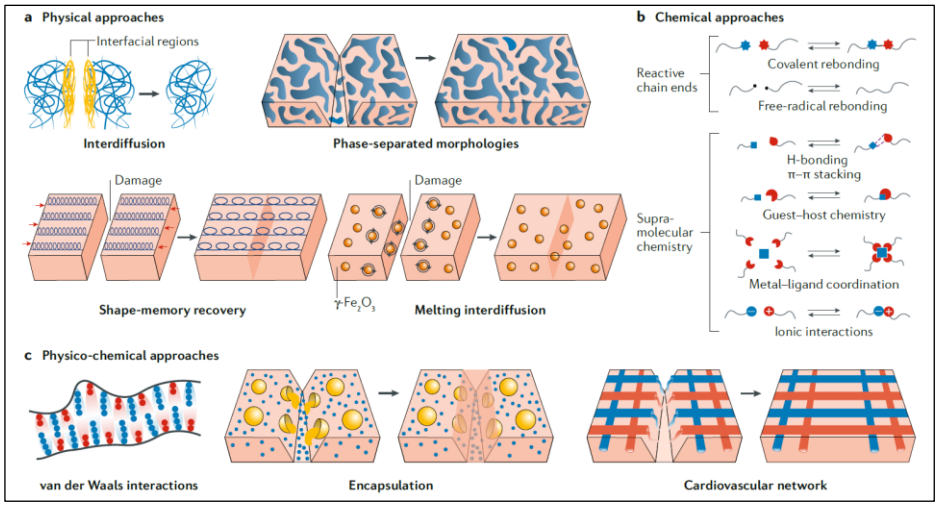

Figure 1-8. The most common approaches for imparting self-healing ability to a material; a) Physical processes to realize self-healing include interdiffusion of polymer chains, the introduction of phase-separated morphologies, shape-memory effects, and the introduction of active NPs into a polymer matrix. b) Chemical processes to facilitate self-healing involve either introducing reactive chain ends or supramolecular chemistries. c) Physical and chemical processes can be combined to realize self-healing. Self-healing is achieved by incorporating enhanced van der Waals interactions, or encapsulating nano capsules or microcapsules containing reactive liquids to heal a wound, or by mimicking cardiovascular architectures composed of hollow fibers filled with reactive chemicals to heal a polymer matrix [306]*, (Reprinted with permission).*

1.8.1 Timeline of Developing Self-healing Mechanisms

Microcapsule-based self-healing materials are the first generation of self-healing mechanisms as well as being by far the most studied concept in the literature. This method has been categorized within different aspects based on the arrangement of the healing agents and catalysts while the most extensive arrangement consists of five types: single-capsule, double-capsule, capsule and dispersed catalyst, phase-separated droplet and capsules, and all-in-one capsules [274].

The concept of autonomic self-healing, as it exists now, was established based on fiber-based healing by Dry et al. [23] firstly in cement and epoxy resins. However, the work of White et al. [24] is considered as the beginning of definitive inspiration for developing self-healing polymeric materials. They introduced the self-healing property to epoxy resin by the incorporation of dicyclopentadiene, DCPD, as the healing agent, embedded in urea-formaldehyde microcapsules and Grubbs catalyst, a platinum catalyst, dispersed in epoxy resin. Polymerization of the DCPD in the presence of a catalyst upon their crack-initiated release was responsible for sealing the crack. They could obtain efficiencies of up to 75% in the recovery of the maximum load in a fracture toughness test in their initial stage. However, the execution of this methodology in PDMS elastomers was carried out by Keller et al. [307] whom utilized two types of microcapsules for self-healing action (type1: containing a high molecular weight vinyl-PDMS and a platinum catalyst, and type 2: containing its curing agent composing a PDMS copolymer with active sites and initiator). The tear strength recovery showed efficiencies of up to 120% for their self-healing system.

The second generation of self-healing materials were based upon dynamic chemistry including supramolecular, and reversible covalent bonds. Chen et al. [308] formulated the first self-healing polymer based on Diels–Alder chemistry of furan/maleimide monomers; in which the fracture toughness tests exhibited a recovery efficiency of 57% at temperatures between 120 and 150°C. Their work reflected an important development in this field by proving multiple healing cycles whereafter subjecting the material to a third healing cycle the polymer allowed a recovery efficiency of 80%. Cordier et al. [309] was pioneer for introducing self-healing into elastomeric materials based on the supramolecular

assembly by designing molecules capable of forming chains and crosslinks through hydrogen bonding which was capable to self-heal at room temperature.

Inspired by the blood circulatory system, a somehow analogous concept was developed by Toohey et al. [310] as the third generation of self-healing materials termed as microvascular self-healing. In this concept, the composites contain hollow fibers that are filled with a reactive healing agent and serve as the delivery system of chemicals to the damaged area.

In this approach, self-healing microfibers with a core–shell geometry containing encapsulated healing agents would be formed by coaxial or emulsion electrospinning. Upon damage, the healing agent (and catalyst in many cases) are released from the broken fibers and repair the crack area. This approach would be conceptually exciting if the 'used' self-healing agents could be replenished after damage as it happens in nature [306].

Core-shell or core-sheath electro spun fibers can be produced by two different strategies: emulsion electrospinning and coaxial electrospinning. Coaxial electrospinning is the most common method to produce core-shell fibers involving multiple feed systems to simultaneously spin two or more polymer solutions through coaxial capillaries and was first demonstrated in 2002 by Loscertales [311]–[313]. In this procedure, two different solutions containing either core or shell materials are pumped by two separate nozzles. The inner and outer fluids should be delaminated and flow without mutual mixing. During the spinning, the shell layer act as a barrier to prevent or retard the evaporation of core material. Due to the encapsulation structure, the flow rates of both solutions should be matched; very small flow rates can cause an insufficient and discontinuous core phase however very large flow rates can cause very thick core phase or pendant droplets [312], [314]. Lee and coworkers [315], [316] used co-axial electrospinning to form networks of fibers with polyacrylonitrile (PAN) shell, and dimethylvinyl-terminated dimethylsiloxane healing agent as the core. They investigated the self-healing efficiency via anti-corrosive barrier properties.

Emulsion electrospinning methods utilize a single uniaxial process based on the immiscibility of the two phases while the surface tensions of two different polymeric solutions acts as the driving force

of separating materials into either a continuous phase or a disperse phase. The minor material exists as droplets in a suspension and they can agglomerate to form the core phase while pumping out and the continuous phase forms the shell [317], [318]. This method is less reported in elastomers due to the complexity of incorporating vascular networks in matrices.

1.8.2 Microencapsulation Method

Figure 1-9 shows the healing action via a microcapsule-based mechanism. There are three main steps in the fabrication of a capsule-based healing system, namely, encapsulation technique, material design for capsules, and the healing agent.

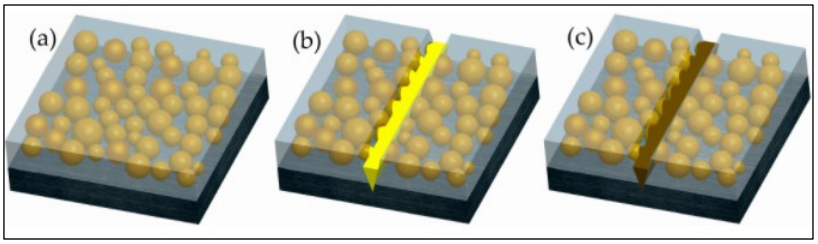

Figure 1-9. Schematic diagram of microencapsulated self-healing approach in a coating; a) Before crack; b) Formation of crack and releasing the healing agents; c) Solidification of the healing agent in the crack area [319]*, (Reprinted from Open Access).*

1.8.3 Encapsulation Techniques

Encapsulation is a process of enclosing solid, liquid or gases into an inert (no reactivity with core and surrounding) shell, which isolates and protects them from the environment. Microencapsulation process is an integration of different fields of material science, colloid chemistry and physical chemistry and a wide variety of techniques have been developed to synthesize microcapsules [320]. Generally, microcapsules consist of two parts; the core, the interior part, which is the functional material and needs to be protected, and the exterior part called the shell that plays a consistent role of protection for the healing agent.

Generally, fabrication techniques of microcapsules are divided into two main groups, chemical and physical methods, with the latter being further subdivided into physico-chemical and physico-mechanical techniques. Versatility of microencapsulation technologies offers unlimited combinations of

different core and shell materials based on the final applications. Some of the important processes used for microencapsulation are listed in **Table 1-3** [321]**.**

Table 1-3. Most common encapsulation techniques [321].

Chemical processes	***Physical processes***	
	Physico-chemical	***Physico-mechanical***
Suspension polymerization	Coacervation	Spray-drying
Emulsion polymerization	Layer-by-layer assembly	Fluid-bed coating
Interfacial polymerization	Sol-gel	Centrifugal techniques
In-situ polymerization	Supercritical CO_2 -assisted	Electrospraying

In the physical methods, the original chemical compositions of the shell materials, formed by physical processes such as dehydration and adhesion, are retained [322]. Chemical methods are based on polymerization processes and are divided into four types of: in situ polymerization, interfacial polymerization, suspension polymerization, and emulsion polymerization [321]. Different parameters affect the efficiency, size distribution and morphology of microcapsules which are varied based on the polymerization technique [323]. In the work of Koh et al. for developing a self-healing paint formulation, polyurethane microcapsules containing a water-borne polyurethane resin as core material were synthesized via interfacial polymerization of diol diisocyanate prepolymer and a chain extender in an emulsion solution. Capsules had an average diameter of 39-72 μm and shell thickness of 3.8-5.5 μm. These researchers showed that the efficiency of self-healing depends on the diameter of capsules, concentration of PU capsules and total content of core material [324].

In another approach, self-healing anticorrosive coatings were fabricated using urea-formaldehyde microcapsules containing functionalized polydimethylsiloxane. Urea formaldehyde microcapsules were synthesized through oil-in-water emulsion polymerization; PDMS reagents and surfactant solution were agitated to have a stabilized emulsion. Then, urea and resorcinol were added and after pH adjustment formaldehyde was added and temperature was raised to 60°C for 4 h to complete

the reaction. Finally, the mixture was neutralized, filtered, and washed with distilled water to have microcapsules [325].

1.8.4 Material Selection and Reaction Conditions

One of the main challenges for self-healing to be triggered, is the proper release of healing agent and polymerization in the crack area. For this purpose, appropriate selection of materials is significantly important. The properties of the shell and core materials should be considered in terms of solubility, viscosity, volatility, reactivity, and pH value. The healing agent is the main component affecting the properties of the healed system. Therefore, a suitable healing agent/pair is a key factor in designing the system based on the end-use application of the material. Different healing agents (core material) encapsulated within shells have been reported in the literature such as monomers, resin, diluted resins, catalyst, etc. [60], [326]–[328]. In most cases, the core and shell materials should not react with each other and with the main matrix. However, to achieve excellent adhesion between the healing agents and the matrix, a chemical reaction between the healing agent and the matrix could be advantageous. The physical and mechanical stability of the formed shell should be examined in order to bear the induced temperature and shear forces in the processing steps, while the capsule shell wall must break and release the core in the time of damage. The dimension of the capsules for integration is also an important factor affecting the final properties of the system; the matrix should not lose its mechanical strength due to the incorporation of capsules, triggering mechanism and the healing performance. However, it is well known that the mechanical properties of the self-healing material may be varied by capsule volume fraction, capsule shell wall stiffness, and capsule size [329]. The most familiar shell-forming materials for microencapsulation are urea, formaldehyde, ammonium chloride and resorcinol leading to the construction of a solid polymeric shell of poly(urea-formaldehyde), PUF. A copolymer such as ethylene-maleic anhydride (EMA) or styrene-maleic anhydride (SMA) is utilized as a surfactant to form an oil-in-water (O/W) emulsion, wherein the oil is the core material [330]–[333]. Ammonium chloride is also responsible for catalyzing the reaction between urea and formaldehyde, and resorcinol is used to enhance shell rigidity [334]. Replacing a part of urea with melamine will result in a melamine-modified urea-formaldehyde polymeric shell (PMUF), which is shown to have higher bond strength, enhanced

microcapsules properties and shell strength [335]. The other shell materials that have also been used include silica [336], polyurethane (PU) [337], [338], PMMA [339], etc. Also, recently, double-shelled systems have been also reported to enhance the mechanical stability of the microcapsules for in-process manipulations [340].

Zotiadis et al. [341] synthesized epoxy loaded microcapsules with a poly(urea-formaldehyde) shell via in situ polymerization. Microcapsules were colorless free-flowing powder within a diameter range of 37 to 66 μm and high encapsulation efficiency to induce self-healing ability to an alkyd-based coating. They examined process parameters, such as the core: wall mass ratio, pH adjustment, stirring method during the emulsification stage and emulsifier quantity with respect to microcapsules characteristics, i.e., morphology, particle size, encapsulation efficiency (EE), and thermal properties. Their results showed that the core: wall mass ratio affects the size of the microcapsules by determining the core droplets size under constant conditions of emulsification (stirring, emulsifier). Increasing the emulsifier resulted in more efficient restriction of the amount of precipitated PUF particles and roughening of the shells. The thermal properties of the microcapsules were also correlated to the existence of PUF particles and the shell crosslinking extent. **Figure 1-10**, shows the obtained microcapsules and effect of reaction conditions on the final properties of microcapsules.

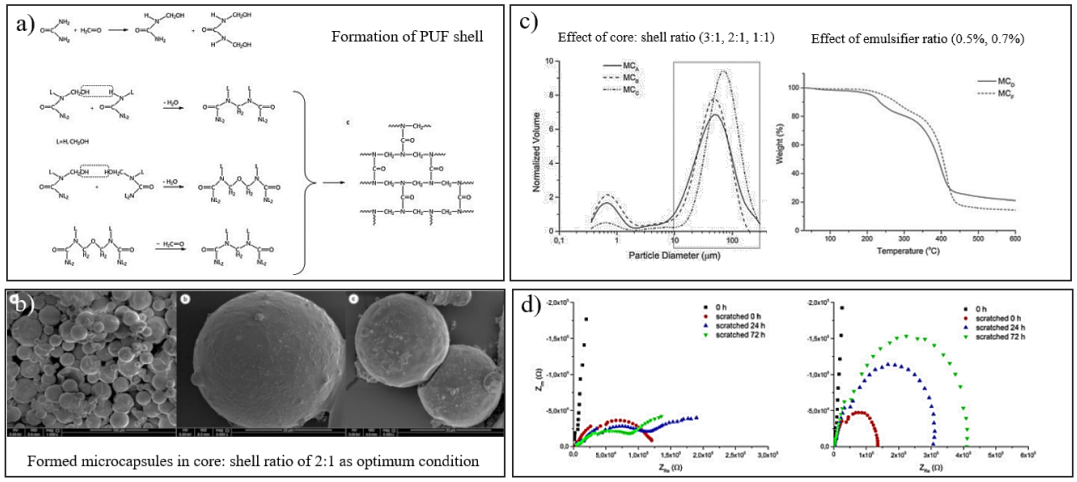

Figure 1-10. a) Formation of urea-formaldehyde shell; b) The microcapsules formed at core: shell mass ratio of 2:1; c) Effect of core: shell ratio on particle size and emulsifier ratio on thermal properties of the microcapsules; d) Nyquist diagrams of the coatings without microcapsules and self-healing coating showing desirable corrosion resistance of the microcapsules [341]*, (Reprinted with permission).*

1.8.5 Characterization of Microcapsules

Optical and electron microscopy can be used to measure microcapsule`s diameter with image analysis software [342]. Another method for measuring capsules diameter is employing a laser diffraction particle size analyzer [343].

Elemental analysis is a practical method to determine the amount of encapsulated healing liquid or encapsulation efficiency. Brown et. al, [334] used a CHN analyzer for freshly-made and dried PUF microcapsules containing DCPD healing agent, and microcapsule showed to contain 83−92 wt.% DCPD and 6−12 wt.% urea-formaldehyde. However, after 30 days, the average DCPD content was decreased by 2.3 wt.%. It has been found that dispersion of microcapsules within a polymeric matrix is effective to limit further leakage of the core from capsule shells. Extraction methods could be also exploited to measure the core content, microencapsulation efficiency and encapsulation yield [344], [345]. Differential scanning calorimetry (DSC) and thermogravimetric analysis (TGA) are deployed to characterize the thermal properties and stability of the microcapsules within a particular temperature range. Tian et al. [346] developed microcapsules to enhance the self-healing property of asphalt; since asphalt mixture must be mixed at high temperature, microcapsules need high thermal stability to ensure whether they can remain intact in the processing steps. Using TGA within a temperature range of up to 600°C, showed that their fabricated microcapsules had an appropriate heat resistance and could survive the process for asphalt construction without decomposition.

1.9 Characterization of Self-healing

In the previous section, different mechanisms of self-healing were discussed. However, regardless of the type of the mechanism, all self-healing polymers must have a common property that the damage is “healed” sometime after experiencing the damage, without manual intervention. This reduction in damage or healing leads to a partial or complete recovery of the mechanical or functional performance of the material. In designing a self-healing polymeric material, it is critical to demonstrate the extent of recovery for its functional properties. The appropriate test methods for the healing assessment must fit the nature of material, healing mechanism and the desired application. Although

scratch healing, imaging techniques and corrosion tests are adequate for coatings, tensile or tapered double cantilever beam geometry (TDCB) testing may be more appropriate for applications involving bulk samples [347]. It is noteworthy that the healing efficiency not only depends on the healing process but also on the nature and extent of damage and the conditions creating that damage. Therefore, in this section, the most common approaches for characterizing self-healing ability of the polymeric matrices are discussed briefly.

1.9.1 Imaging Techniques

Microscopy imaging techniques cover length scales higher than that for intrinsic healing in which the healing occurs mainly within the molecular scale. Considering the extrinsic healing mechanisms, the length scale of healing is well suited with these techniques and the release of healing agents from the capsules can be monitored [348]. Furthermore, a fluorescent dye can be mixed with or grafted to the encapsulated core material to better detect the release and filling process after crack formation [349], [350].

For monitoring the self-healing of a material, a micro-scratch is applied and the optical and microscopy imaging instruments (OP, SEM, AFM, profilometer) are mainly utilized to observe the crack area [351]–[353]. The imaging is conducted after a certain period of time based on the self-healing ability of the system to differentiate a crack and its repaired state. Although these imaging techniques could show the presence or absence of healing in a crack plane, they are qualitative methods offering rather poor quantitative information to measure the extent of materials recovery and its self-healing ability. Therefore mechanical tests such as tensile test, tear test, fatigue test and impact test are promising analysis methods for this purpose. By using a combination of scratching and electrochemical techniques, such as electrochemical impedance spectroscopy (EIS), the time dependence of healing based on the corrosion protective behavior of the coating under a range of conditions can also be determined [354]–[356]. **Figure 1-11** shows the self-healing ability of a coating via corrosion, morphological, and electrochemical evaluations [357].

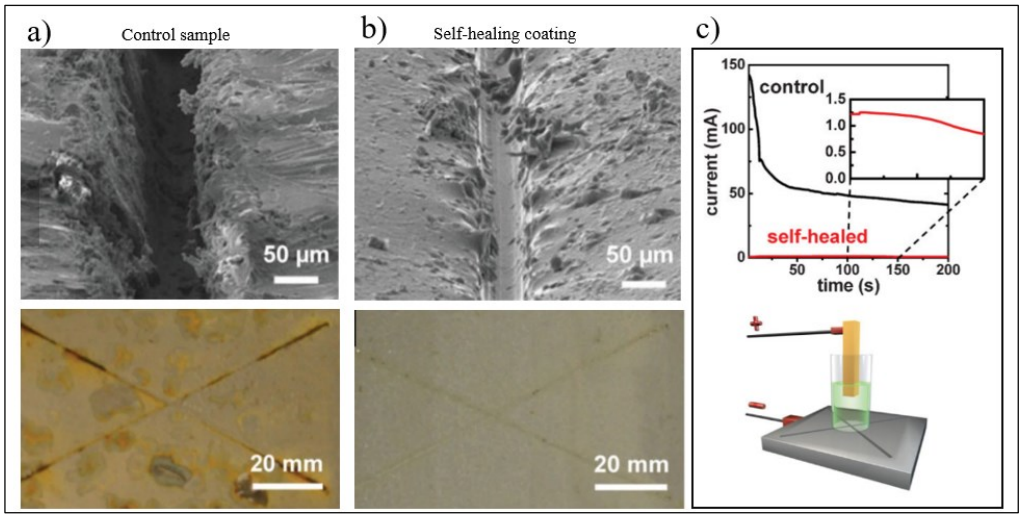

Figure 1-11. Self-healing evaluation via SEM imaging and corrosion tests; images of a,b) control epoxy vinyl ester coating and self-healing coating containing microencapsulated catalyst, and phase-separated PDMS healing agent after 120 h immersion in salt water; c) Schematic diagram of electrochemical test and current versus time for scribed control and self-healed sample [357]*, (Reprinted with permission).*

1.9.2 Tensile Test

Tensile testing is a standard method for determining the quasi-static mechanical properties of a material offering the possibility to measure various parameters namely tensile strength, elongation, Young´s modulus and yield strength [348]. For the tensile test, the samples are prepared in dumbbell or rectangular shapes and the original sample and the healed sample are tested under the same testing conditions until rupture occurs. The self-healing efficincy could be estimated through the resulting load-displacement or stress-strain curves by dividing the recovered toughness of the healed sample comparing to the non-defected self-healing composite. Tensile testing is also a common method for evaluating the effect of size and concentration of microcapsules in the self-healing matrix (**Figure 1-12b**). Ahangaran et al. [358] developed self-healing epoxy composites with poly(methyl methacrylate) (PMMA) microcapsules and the effect of microcapsule ratio on mechanical properties and self-healing behavior of the composites was investigated by embedding 2.5, 5, 7.5 and 10 wt.% of capsules into the epoxy. The results suggested almost 80% healing efficiency for 10 wt.% PMMA microcapsules at room temperature after 24 h. Besides, the tensile strength of the epoxy initially increased by addition of 2.5 wt.% microcapsules and then decreased gradually by increasing microcapsules content up to 10 wt.%.

1.9.3 Tapered Double Cantilever Beam (TDCB)

One of the most appropriate methods for self-healing investigations in brittle polymers is the tapered double cantilever beam geometry (TDCB) as represented in **Figure 1-12e**; while the healing efficiency is the quotient of the healed and the original fracture toughness. For brittle polymers, the fracture surface is more or less mirror-smooth and the crack surface is closely repositioned, thus this geometry allows a sensible quantification of the healing process as the fracture toughness is independent of the crack length [347], [348], [358], [359]. Kessler and coworkers [360] developed a self-healing fiber-reinforced structural polymer matrix composite containing a microencapsulated healing agent and a solid chemical catalyst dispersed within the matrix. They used the width-tapered double cantilever beam fracture specimens in which a mid-plane delamination was introduced and allowed to be healed. The results showed autonomic healing at room temperature by 45% recovery of virgin fracture toughness, and a recovery to over 80% at 80°C compared to that of neat epoxy resin.

Fatigue testing in which cyclic mechanical stress is applied to a material and a permanent damage occurs resulting in a crack after sufficient fluctuations is also used to measure the self-healing efficiency by the same TDCB geometry. Brown et al. [361] investigated the healing efficiency of a self-healing epoxy matrix containing DCPD-PUF microcapsules by injecting pre-catalysed mending agent into the crack region by no-load, constant load and cyclic load conditions using TDCB specimen. Researchers observed improved resistance to fatigue crack propagation, which was indicated by both reduced crack growth rates and improved cyclic stress intensity for the onset of unstable fatigue-crack growth. This behavior was attributed to the induced toughening mechanisms by incorporating microcapsules into the matrix as well as a crack shielding due to the release of healing agents.

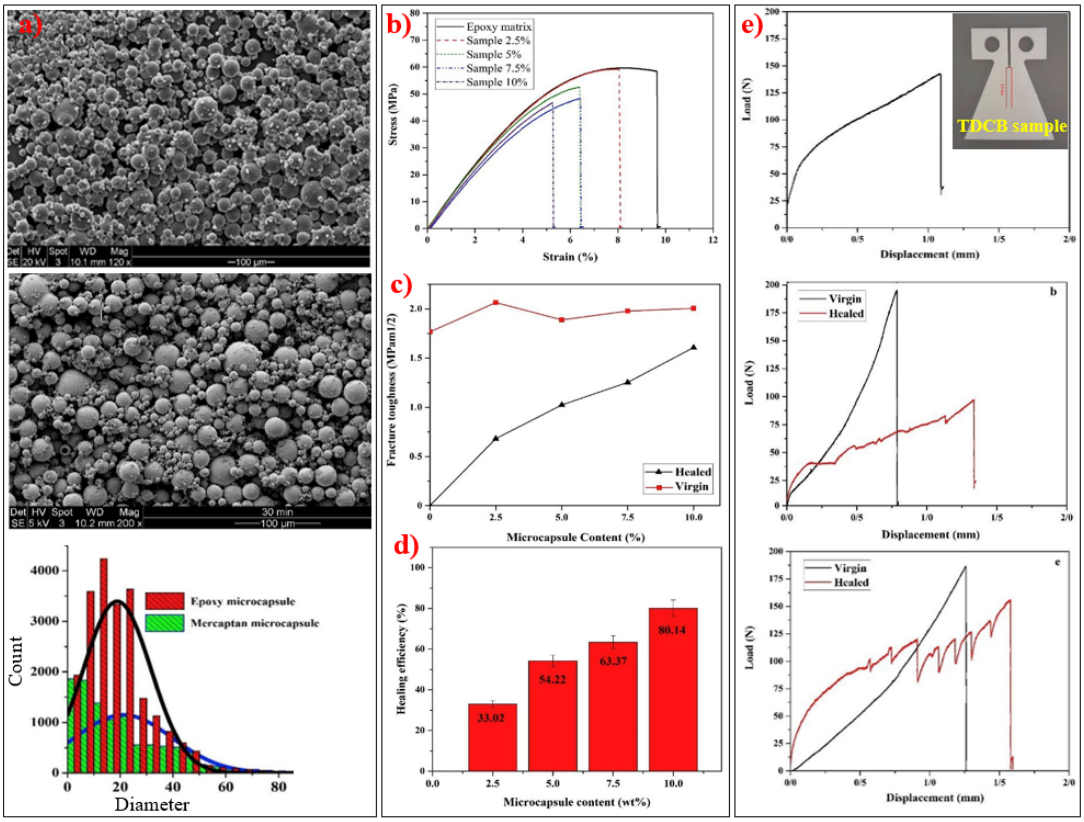

Figure 1-12. Preparation of a self-healing epoxy matrix; a)SEM images of synthesized microcapsules with two cores and the size distribution histogram; b) Effect of microcapsules concentration on tensile strength of the matrix; c) Fracture toughness of matrix versus microcapsule content; d) Healing efficiency of matrix versus microcapsule content; e)Typical TDCB specimen geometry and obtained load-displacement curves for the virgin and healed samples [358]*, (Reprinted with permission).*

1.9.4 Tear Test

A trouser tear test, based on ASTM D624 is also another method to measure the self-healing ability of composites, giving a load-displacement curve [362]. The healing efficiency could be calculated by dividing the tearing energy of the healed sample to the tearing energy of the virgin sample. Tearing energy is obtained from the area under the load versus displacement curves divided by the cross-sectional area of the fractured surface (the sample thickness, multiplied by the length of the fractured path) [363].

1.9.5 Impact Test

Impact test is also employed by several researchers to investigate the suitability of fiber-reinforced composites [364], [365]. Chowdhury et al. [366] fabricated microspheres to encapsulate a room-temperature curing epoxy resin and its amine hardener into UF shells to be embedded in an epoxy

matrix. They used low-velocity impact tests at 30 and 40 J for a pristine sample and a sample with 10% of microcapsules. Upon impact test, the sample absorbs energy and undergos an elastic deformation; while microcapsules release their cores and healing takes place at the damaged location. Healing efficiency was measured by conducting a second impact after 48 h at elevated energy levels of 40 and 55 J at the same location. Load and energy versus time plots were used to obtain quantitative information about the damage due to the impact. After the second impact test, samples containing microcapsules showed better impact resistance due to repairing. It was observed that samples without microcapsules exhibited higher peak loads for the first impact compared to those with microcapsules. However, after 48 h of the first impact, samples containing microcapsules showed higher impact resistance than the neat samples when subjecting to impact with an average of 6.16 kN and 7.52 kN peak loads for 40 J and 55 J impact energies, respectively compared to 5.36 kN and 6.67 kN for neat samples.

1.10 Conclusion

In this chapter, a literature review was presented to provide some general information on the idea of this thesis.

The most common wetting theories and superhydrophobicity were firstly discussed. Based on the two criterions that must be satisfied for superhydrophobicity (i.e., low surface energy, and presence of surface roughness), available materials and methods for fabricating superhydrophobic coatings were briefly introduced. Among these material and methods, a combination of silicone resin, NPs, and spray coating technique has shown to be favorable in terms of non-toxicity, ease of application and large-scale production.

The self-cleaning, anti-icing, anti-corrosion properties of these surfaces were mentioned as their main applications. A general overview of the current commercial status of superhydrophobic coatings was given to highlight the major shortcomings of the superhydrophobic coatings leading to the limited real-world application. As the main drawback of these coatings, the durability issue was discussed in more details and some of the new approaches for overcoming this challenge were represented.

Furthermore, self-healing materials, that are originally inspired by the wound healing in living organisms, were introduced as the promising solution for increasing the service-life of polymeric structures. Currently, multiple mechanisms exist for imparting self-healing ability to polymeric materials, while incorporation of self-healing microcapsules is still the most reported method. Here, microencapsulation method was introduced, the common methodologies for preparing microcapsules were presented, and the importance of selecting type and amount of materials as well as the processing parameters and microcapsules characteristics were then highlighted. Since the characterization of self-healing is of high importance, in the final section of this chapter the common methods for characterizing self-healing ability were also explained.

The results and disscusions on the objectives of this thesis are explained in detail within the subsequent chapters.

CHAPTER 2 - ARTICLE 1

DEVELOPMENT OF A DUAL CAPSULE SELF-HEALING SILICONE COMPOSITE USING SILICONE CHEMISTRY AND POLY (MELAMINE-UREA-FORMALDEHYDE) SHELLS

A. Allahdini *, R. Jafari, G. Momen

Department of Applied Sciences, University of Quebec in Chicoutimi (UQAC)
555, boul. de l'Université, Chicoutimi, Québec, G7H 2B1, Canada
E-mail: Anahita.Allahdini-Hesarouyeeh1@uqac.ca

2.1 Abstract

This study aims to develop microcapsules that can be used as room-temperature self-healing agents in silicone-based matrices. A telechelic reactive silanol-terminated polydimethylsiloxane (PDMS) as the healing agent, was selected to ensure the homogeneity of the polymeric matrix and encapsulated in poly(melamine-urea-formaldehyde) shells through an in-situ emulsion polymerization technique. To catalyze the polycondensation reaction of the healing agent, dibutyltin dilaurate (DBTL) was encapsulated within the same type of polymeric shell. The synthesized microcapsules were characterized using Fourier-transform infrared spectrometry, optical microscopy, scanning electron microscopy, and differential scanning calorimetry. The analyses confirmed that the spherical microcapsules with an average size of 56 μm for PDMS-MUF microcapsules and 42 μm for DBTL-MUF microcapsules, with a shell wall thickness of 100–200 nm, and good thermal stability were formed. Therefore, the two-component self-healing silicone composite was successfully developed using 10:1.2 wt.% PDMS: DBTL microcapsules within the silicone matrix. Scanning electron microscopy (SEM) showed the self-healing ability of the silicone matrix by observing the successful healing of microcracks at room temperature. Tensile and trouser tear tests were adopted to assess the self-healing performance of the elastomeric matrix, showing the self-healing efficiencies of 67% and 55%, respectively.

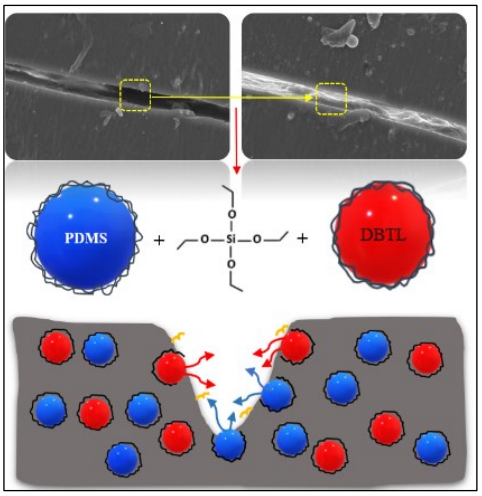

Figure 2-1. Graphical abstract.

2.2 Introduction

All surfaces are subjected to mechanical damage, and microcracking can likely occur during handling, use, etc. Since the 1980s, inspired by living organisms, demand for alternatives to surface reparation has led to the introduction and application of novel self-healing surfaces and the autonomous healing of microcracks to extend the life-span of polymeric components [22]–[24]. In the last decade, a growing number of research on the smart self-healing materials based on various approaches including encapsulation [367], [368], core-shell fibers [369], hollow fibers and microvascular networks [370]–[372] has been investigated. Microencapsulation technology—the action of enclosing a solid, liquid, or gas within an inert shell—was first developed in the 1950s and is by far the most-studied self-healing concept [373]. As microcapsules can be easily incorporated into various matrices through a range of available blending techniques, microencapsulated self-healing materials are favorable for commercialization [368], [374]. Healing occurs when the healing agent is released from the microcapsules and fills the microcracks through capillary action. The healing agent could be cured in situ by reacting to a catalyst phase dispersed within the matrix, a second type of microcapsule containing a catalyst or hardener, or a latent functionality in the matrix [305], [374].

The versatility of microencapsulation technologies offers an unlimited combination of core and shell materials for the self-healing of surfaces [321]. Encapsulation of dicyclopentadiene [24], [375], [376], epoxies [342], [343], [377]–[379], PDMS [282], [380]–[382], and isocyanates [383], inside

various polymeric shells such as urea-formaldehyde [325], [343], [384]–[386], melamine-formaldehyde [373], [387], melamine-urea-formaldehyde [387]–[389], polymethylmethacrylate [390]–[392], silica [393] , etc., are investigated for self-healing purposes. The fabrication of microcapsules can be divided into physical or chemical methods. In the physical methods, including electro-spraying [394] and coacervation [395], the shell is formed through physical processes, such as dehydration or adhesion, while the chemical composition of the shell materials remains unchanged [322]. Chemical methods are mainly based on the polymerization techniques while emulsion polymerization is by far the most widely reported [321]. Polymerization techniques are appealing for many purposes because of their large-scale productions, ability to control and scale-up to produce high-quality microcapsules having the desired mechanical and thermal properties. Various parameters can affect the efficacy, size distribution, and properties of the microcapsules [323], [368], [374], [396].

The design of a suitable self-healing system requires considering the ease of encapsulation, the stability of the components under various environmental conditions, and the system's reactivity over the service life of the polymeric components. Once triggered, a proper self-healing system should be able to respond quickly to damage. The microcapsules must disperse effectively within the polymeric matrix, rupture in the event of cracking, be capable of releasing the core material into the crack and have minimal adverse effects on the properties of the base matrix. The core material, as the key component of a self-healing system, is chosen mainly based on the desired properties of the final application. Almost all the other components and processes are designed and formulated to fulfill the proper encapsulation of the core material. However, the correct selection of the shell materials, emulsifiers, etc., strongly affects the properties and behavior of the microcapsules and, consequently, the self-healing ability.

Currently, silicones and specifically PDMS (polydimethylsiloxane)—considered as the simplest types of silicones—are widely used across a variety of fields. They are non-flammable, thermally and chemically stable, and they have low surface tension and a wide range of operating temperatures, making them suitable choices for common everyday uses [397], [398]. Nonetheless, the low rigidity and surface hardness of silicones makes them easily scratched or cracked, which can compromise the performance of these materials.

Using PDMS as a healing agent within a silicone matrix could therefore ensure the chemical homogeneity of the structure and maintain the bulk and surface properties; self-healing results are improved when using a self-healing PDMS chemistry within a PDMS matrix [399].

In this study, self-healing microcapsules containing a telechelic silanol-terminated PDMS—a group of polymeric chains with functional groups on both ends—that is curable even at temperatures as cold as −20°C [400], [401] were incorporated within a PDMS matrix. An organotin compound, DBTL, was selected to catalyze the polymerization reaction of the silicone resin. Microencapsulation offers various advantages to the proper functionality of the system and is used to enhance the effective service life of the self-healing material. In this work, both components of the healing system are encapsulated to prevent any possible side reaction inside the matrix within its service life. Also, if the materials are not encapsulated inside shells, they can migrate toward the surface of the composite/coating leading to the reduction in self-healing capability. The healing agent (DMS-S12) and the catalyst (DBTL) were encapsulated separately, using the same melamine-urea-formaldehyde shells. Urea-formaldehyde (UF) shells, the most widely used shell for various core materials, are modified by introducing small amounts of melamine into the synthesis procedure. This introduction of melamine greatly heightens the robustness and stability of the shell and enhances its flowability as a powder; as well, this approach is more cost-effective compared to melamine-formaldehyde (MF). These melamine-urea-formaldehyde (MUF) microcapsules are also much simpler to synthesize and handle than UF microcapsules [374], [387], [402]–[405]. The use of a similar chemical composition for both microcapsules as a self-healing pair within a single matrix is less common in the literature, despite this approach being able to increase compatibility within the system and reduce preparation costs. The effectiveness of these microcapsule-matrix combinations in the self-healing of microcracks at room temperature was evaluated inside the SYLGARD 184/TEOS elastomer. A polycondensation reaction of the healing agent with the present ethoxy groups in the presence of DBTL catalyst, is responsible to form an adhesive layer between the crack faces, which is quite the same chemistry as of the PDMS matrix. This combination leads to a self-healing composite with a unique feature in which the healed polymer in the crack plane is similar to the matrix.

2.3 Experimental Section

2.3.1 Materials and Equipment

The chemicals which were used in this paper and their functions are represented in **Table 2-1**.

The in-situ polymerizations were carried out inside a double-walled reactor (ACE Glass Inc., USA). To maintain a constant temperature for the polymerization, a circulating water bath was used. A digital overhead stirrer and an anchor type impeller were used to properly mix the emulsion bath.

Table 2-1. List of chemicals and their functions in this study.

Role of material	Material name	Company
Core healing agent	Silanol terminated polydimethylsiloxane (DMS-S12)	Gelest Company
Core catalyst	Dibutyltin dilaurate (DBLT)	Fisher Scientific
Shell forming components	Urea	Alfa Aesar
	Formaldehyde (37% solution)	Alfa Aesar
	Melamine 99%	Alfa Aesar
	Resorcinol 99%	Alfa Aesar
Electrolyte	Ammonium chloride 98%	Alfa Aesar
Emulsifiers	Poly (ethylene-alt-maleic anhydride) (EMA)	Sigma Aldrich
	Sodium dodecylbenzene sulfonate (SDBS)	Fisher Scientific
Anti-foam agent	1-octanol	Sigma Aldrich
Matrix	SYLGARD 184	Dow Silicones Corp.
	TEOS	Sigma Aldrich

2.3.2 Preparation of Microcapsules

PDMS-loaded microcapsules and catalyst-loaded microcapsules were both prepared separately through the in-situ polymerization of melamine, urea, and formaldehyde in oil-in-water emulsions. The

synthesis procedures are detailed in the following subsections and illustrated schematically in **Figure 2-2.**

2.3.2.1 Healing Agent Encapsulation: PDMS Encapsulated Inside MUF Shells

EMA (2.4 g) was dissolved in 170 mL of deionized (DI) water and then heated at 60°C for 2 h to obtain a transparent solution, which was then cooled to room temperature. 0.5 g melamine, 3 g urea, 0.3 g resorcinol, and 0.3 g ammonium chloride were added to the solution, and the solution was stirred to achieve a complete dissolution of all components. The pH of the solution was adjusted to a value of 5–6 by adding a few drops of ethylene diamine. Subsequently, 30 mL of DMS-S12 was added dropwise by a funnel and stirred at 600 rpm for 30 minutes to achieve a stable emulsion. A small amount of 1-octanol was added to remove the air bubbles from the solution. Eight milliliters of formaldehyde solution were then streamed into the reaction bath, and the temperature was raised to 70 ℃ using the programmable water bath. The polymerization lasted for three hours under reflux. The final slurry was then cooled to room temperature. The emulsion was filtered under vacuum using filter paper to separate microcapsules. A free-flowing powder of microcapsules was obtained after the slurry had been washed with ethanol and plenty of water, air-dried for 24 h, and vacuum-dried for another 24 h.

2.3.2.2 Catalyst Encapsulation: DBTL Encapsulated Inside MUF Shells

SDBS solution was prepared (100 mL of a 1 wt.%), 2 g melamine, 10 g urea, 0.4 g ammonium chloride, and 0.4 g resorcinol were also added to the solution, and the pH was adjusted using ethylene diamine. Using a funnel, 50 g of DBTL was introduced drop by drop to the solution, and then stirred for 30 min at 600 rpm to attain a stable emulsion. 1-octanol was added to remove the air bubbles. 20 mL of the formalin solution was streamed to the emulsion, and the temperature was increased to 70 ℃ and kept under reflux for 3 h. The filtration, washing, and drying steps were completed according to the procedures found in **Section 2.3.2.1**.

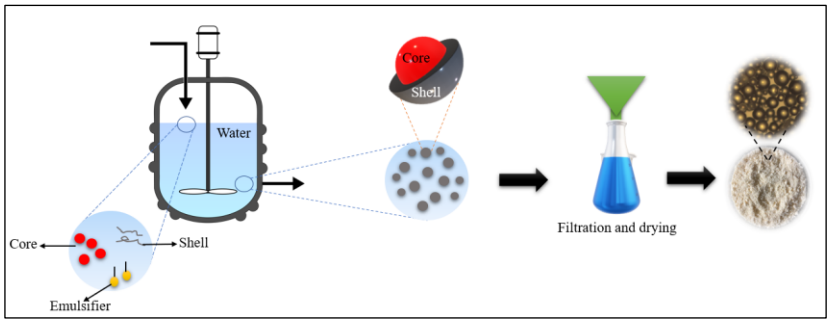

Figure 2-2. Schematic illustration of the microencapsulation process.

2.3.3 Preparation of Self-healing Composite

In the presence of DBTL catalyst, DMS-S12 can go through the hydrolysis and condensation reactions and form a viscoelastic material that is able to fill formed cracks; this polymerization can continue even at low temperatures, making this combination suitable for a wide range of applications. To form the crosslinked network, multifunctional alkoxysilanes can participate in the reaction as crosslinkers. For preparing the self-healing composites, the microcapsules were thoroughly dispersed within a polydimethylsiloxane resin (SYLGARD 184) and mixed with its hardener. TEOS was added to the mixture by 20 wt.% of the SYLGARD 184. For the excess bubbles to be removed, the silicone composite was then vacuum-filtered and cured at 90 ℃ for 1 h. The concentration of microcapsules and the matrix were fixed at a ratio of 100:20:10:1.2 for the matrix: TEOS: PDMS microcapsules: DBTL microcapsule weight ratios.

2.3.4 Characterization

2.3.4.1 Fourier-Transform Infrared Spectrometry (FTIR)

The chemical composition of microcapsules was investigated using a Cary 630 FTIR spectrometer (Agilent, USA) in the attenuated total reflection (diamond ATR) mode at an infrared range of 400–4000 cm^{-1}. The FTIR was carried out on a diamond surface cleaned with isopropyl alcohol prior to the test. The microcapsules were then clamped with a consistent pressure to be broken. The FTIR test was performed for all types of microcapsules, the core materials, and the extracted shells to verify the encapsulation of core components and the formation of the MUF shell.

2.3.4.2 Microscopy

Optical microscopy was performed using a Nikon polarizing microscope (Nikon ECLIPSE E600Pol) to measure the size distribution of microcapsules. Scanning Electron Microscope (SEM) images were taken on a JSM-6480 LV SEM instrument, manufactured by JEOL, Japan, to observe the morphology of microcapsules, their size distribution, and the shell thickness of the microcapsules. The samples were sputter-coated with gold, and the SEM scans were observed at 20 kV voltage.

2.3.4.3 Differential Scanning Calorimetry (DSC)

The thermal behavior of the microcapsules was examined via DSC using a TA instrument DSC in the heating range of 0℃ to 400℃ at a heating rate of 10°C/min under nitrogen atmosphere to avoid oxidation. The average sample weight was 6 ± 0.2 mg.

2.3.4.4 Self-healing Testing

The self-healing performance of the silicone composites were evaluated qualitatively via SEM observation. The composite was scratched by a razor blade prior to SEM observation and kept at room temperature to ensure the healing was underway.

To quantify the self-healing efficiency, mechanical testing was employed. Tensile and tear tests were performed using a universal testing machine (UTM ADMET, eXpert 7603, USA, loadcell 4.4 kN). Both tests were operated to measure the healing efficiency of the healed composites based on their references under specific standards. The as-prepared composites were poured into dumbbell and rectangular aluminum molds, then fully degassed and placed in the oven to be cured.

The ASTM D638 standard was adopted for tensile tests for three to five iterations for each specimen at a crosshead rate of 50 $mm.min^{-1}$ at room temperature. The initial length was recorded, and the device stretched the samples until rupture occurred. Stress-strain curves were obtained, and the healing efficiency was calculated by dividing the recovered toughness—the area under the stress-strain curve—of the healed sample compared to the non-defected self-healing composite.

For the trouser tear test, ASTM D624 was utilized, and samples were prepared based on type T geometry. The trouser test specimens had legs (**Figure 2-3b**) that were extended in opposite directions to obtain load-displacement curves. For measuring the healing efficiency, the rectangular samples were cut from one end to 40 mm using a sharp razor blade. Then, a crack was applied at the end of the cut and placed at room temperature for 24 h for the self-healing action. The reference was the self-healing composite that was cut for 40 mm without applying a crack. The extension rate of 100 mm/min was applied to each sample and the legs were pulled in opposite directions until the point of complete failure of the sample. The healing efficiency was calculated by dividing the tearing energy of the healed sample to the tearing energy of the virgin sample. Tearing energy is calculated from the area under the load versus displacement curves divided by the cross-sectional area of the fractured surface (the sample thickness, multiplied by the length of the fractured path) [307]·[406]·[407].

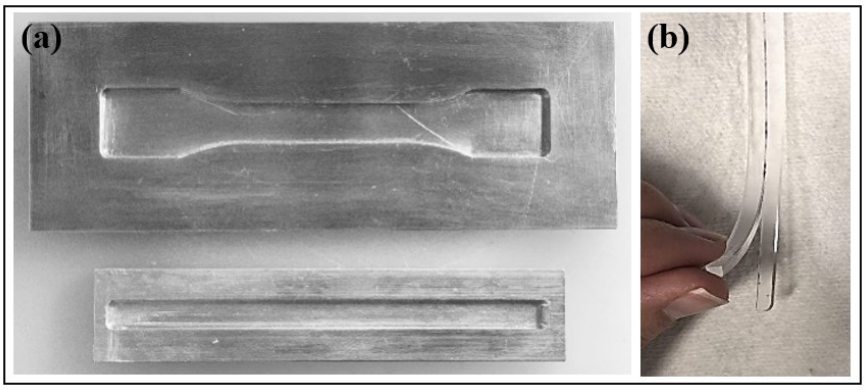

Figure 2-3. a) Aluminum molds for tensile and trouser tear tests; b) Preparation of samples for tear test.

2.4 Results and Discussions

2.4.1 Optimization of Synthesis and Encapsulation Efficacy

To produce microcapsules having an appropriate size, morphology, dispersal ability and flowability of the powder, handling, etc., the main parameters, i.e., agitation rate, emulsifiers, core: shell ratio, and working temperature, were optimized using various experimental analyses. The details of these optimization experiments are provided in Appendix I.

The primary objective was focused on producing a free-flowing powder of spherical microcapsules, in a size range to be well filtered and dispersed within the matrix [408]. To acquire optimal microcapsules, polymerizations were performed under agitation speeds of 300, 600, and 900 rpm. The optimal results with a size range of 10-110 μm and average diameter of 56 μm were found at 600 rpm (**Table A-I. 1**, Appendix I). In the polymerization media, the shell forming components could be polymerized in the bath, rather than the oil-water interface, while the latter is the ideal polymerization site for encapsulation. The formation of large quantities of these polymerized shells which are named as debris, could lead to poor-quality capsules, due to less available material for shell formation, and a more difficult filtration is also observed [368], [409] (**Table A-I. 2**, Appendix I). The type and concentration of emulsifiers are also highly important factors for the microencapsulation process. Emulsifiers lower the interfacial tension between the two phases of oil and water. This forms a stable emulsion and prevents particles from coalescing [345], [388], [410], [411]. Increasing the emulsifier concentration reduces the average size of core droplets in the media and the formed microcapsules. When we replaced about 8% of the EMA with anionic sodium dodecyl sulfate (SDS) surfactant, particle size decreased significantly, and the resultant product turned into a sticky agglomerate rather than the desired free-flowing powder (**Table A-I. 2**, Appendix I). This effect may be caused by the smaller core droplets, which can enlarge the active surface area of the core that should be covered with shell materials. [345], [412], [413].The core/shell ratio may need to be fine-tuned to overcome this issue.

The core/shell ratio effects on the morphology and the quality of microcapsules. Core to shell ratios of 2:1, 4:1, and 6:1 were selected for investigating the appropriate proportions of components (**Table A-I. 3**, Appendix I). Microcapsule size increases with greater amounts of core material, and larger microcapsules are formed by increasing the core to shell weight ratio while holding all other parameters constant. At the same time, excess core materials can reduce the quality of the powders and form a sticky aggregate of fragile microcapsules, which has a poorer dispersional ability [414].

A certain amount of roughness on the surface of microcapsules enhances the mechanical interlocking and adhesion of microcapsules to the matrix [408], [415]. The polymerization time and temperature have significant effects on shell properties. The effect of temperature on microcapsule

synthesis procedures are investigated as reported in **Table A-I. 4** and **Table A-I. 5** (Appendix I). Extremely low temperatures, or short reaction times, produce microcapsules having an inadequate mechanical strength because of a too-thin shell thickness and the imperfect polymerization of the shell materials. Extending the polymerization time leads to a narrower size distribution of microcapsules, which is comparable to the Ostwald ripening mechanism in the crystal growth approach [416]. The smaller sol particles in the media can re-dissolve and deposit on larger particles. This minimizes the surface area that is a spontaneous and more thermodynamically stable state. On the other hand, very long polymerization times lead to very thick shells, which can reduce the self-healing efficacy by decreasing the core to shell ratio in the synthesized microcapsules [417], [418]. As well, high temperatures can lead to an uneven distribution of microcapsule size and produce debris in the emulsion bath or on the shell surface because of the increased reaction rate [368], [374], [419]. Therefore, appropriate polymerization conditions play a key role in the functional performance of self-healing microcapsules.

To investigate the efficacy of microcapsule fabrication, the yield of microencapsulation was calculated by dividing the weight of total obtained dried microcapsules, W_{cap}, by the amount of raw capsule-forming ingredients initially added to the reactor, $W_{shell} + W_{core}$, as defined by equation 2-1.

$$Yield\% = (W_{cap}/W_{shell} + W_{core}) \times 100 \quad \text{(Eq. 2-1)}$$

Microcapsules core content was calculated using solvent extraction method. For this purpose, a specific weight of microcapsules, W_{cap}, were crushed and heated to 150°C. Then crushed powders were added to a proper solvent, ultrasonicated for 10 minutes and filtered. The residue was dried under vacuum at room temperature for 48 h to obtain W_{shell}. The core content of both types of microcapsules was measured according to equation 2-2.

$$Core\ content\% = (1 - (W_{shell}/W_{cap})) \times 100 \quad \text{(Eq. 2-2)}$$

For the optimized encapsulation processes, the encapsulation yield was calculated for three batches of each type of microcapsules, and the results showed yields of 82% and 84.5% for PDMS and

DBTL encapsulation, respectively. While the obtained core content for PDMS-MUF and DBTL-MUF microcapsules were 52 ± 5% and 59 ± 8%.

2.4.2 Chemical Composition of Microcapsules

For both types of microcapsules, shell formation occurs through the polymerization of melamine, urea, and formaldehyde on the interface of the dispersed cores inside the continuous phase. At the initial stage, these materials react to form a low molecular weight prepolymer. The prepolymer grows as time and temperature increase and deposits on the interface of water and the core material. The solid and non-permeable capsule shell forms by continuing the polycondensation reaction between urea, melamine, and formaldehyde on this interface [323], [403], [420]–[422]. As illustrated in **Figure 2-4**, the triazine ring, which is a nitrogen-containing heterocyclic ring, provides evidence of the formation of the MUF shell.

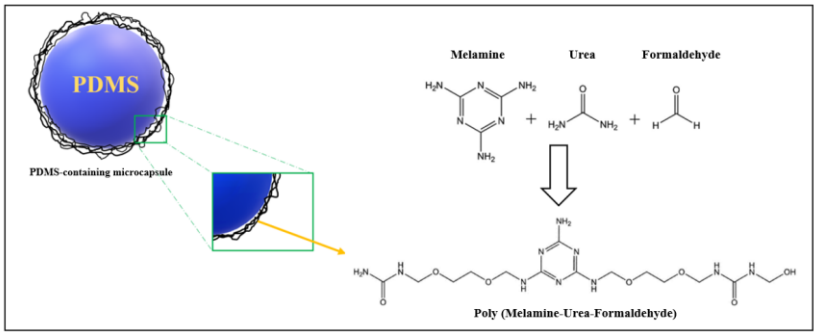

Figure 2-4. Schematic illustration of the melamine-urea-formaldehyde shell-forming reaction.

To investigate the chemical composition of microcapsules, FTIR spectroscopy was used while the formed microcapsules should show characteristic peaks of both the core and shell components. In **Figure 2-5 a** (encapsulation of PDMS), the transmission FTIR spectra of core and shell compounds are represented as is the FTIR result of the formed microcapsules. The peaks at a high wavenumber range of 3400–3300 cm^{-1} are attributed to the stretching vibrations of the O-H and N-H groups existing in the melamine-urea-formaldehyde structure as well as the O-H in the silanol bands of PDMS. The bending vibrations of $–CH_2$ are visible at 1353 cm^{-1}. In the region between 1500 and 1700 cm^{-1}, the transmission peaks can be assigned to the coupling vibrations between $N-H_2$ shearing and the stretching of C=N, which provide evidence for the structure of the triazine ring. In the low wavenumber range of 600–1100

cm^{-1}, the vibrational bands are further evidence for the formation of the triazine ring at around 800 cm^{-1} because of the out of plane deformation of the ring. Therefore, all characteristic peaks of the MUF shell and PDMS core are observed in the microcapsule FTIR spectra, which confirms the successful encapsulation process of the PDMS-loaded microcapsules.

In **Figure 2-5b** (encapsulation of DBTL), the characteristic bands of triazine ring visible at 1550 cm^{-1} and around 800 cm^{-1}, following the C=O vibrations at 1626 cm^{-1}, confirm the formation of a melamine-urea-formaldehyde shell. C–O–C stretching because of the ether bridge at around 1020 cm^{-1} is also present. The OH deformation in CH_2OH is visible at around 1240 cm^{-1}. The FTIR spectra for the DBTL-loaded microcapsules (shown in blue), containing both DBTL and MUF typical absorption peaks, indicate DBTL encapsulation inside the MUF shell.

The FTIR spectra of the formed microcapsules contain all the characteristic peaks of PDMS, DBTL, and the MUF shell. These spectra indicate the encapsulation of core materials inside the shell, whereas no chemical reaction occurs between the cores and the shell-forming components.

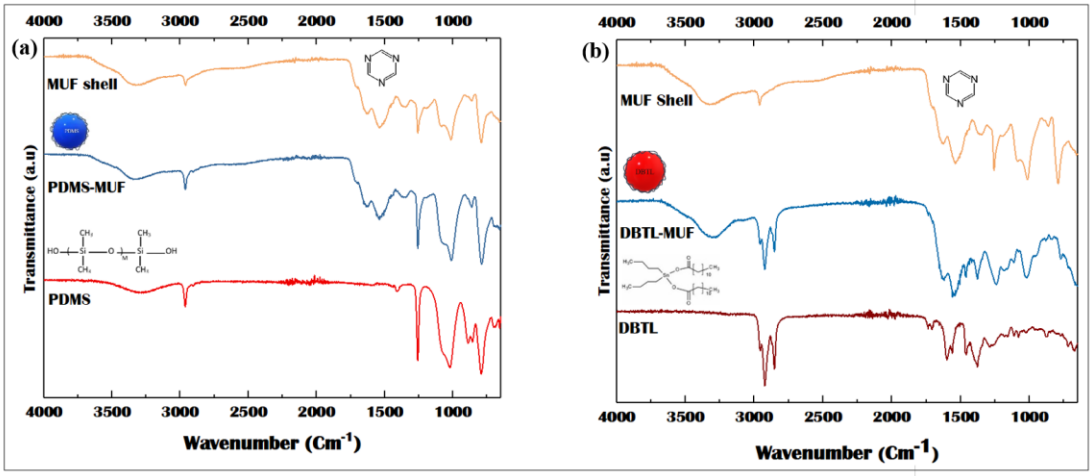

Figure 2-5. FTIR spectra for (a) encapsulation of DMS-S12 inside a MUF shell; (b) encapsulation of DBTL inside a MUF shell.

2.4.3 Size Distribution of Microcapsules

The size distribution of both types of microcapsules was investigated by measuring capsule diameters among different batches of microcapsules. For imaging and measurements, SEM and optical

microscope images were used in Image J software. The optical images and particle size histograms are shown in **Figure 2-6a, b** and **Figure 2-6c, d** for PDMS-MUF and DBTL-MUF microcapsules, respectively. Usually, the size distribution is quite wide because of the different flow patterns of agitation in the polymerization bath. The smaller microcapsules are formed in the vicinity of the agitator blades, whereas the larger microcapsules are formed in the more distant regions [423]. The size distribution of PDMS- and DBTL-loaded microcapsules falls within the range of 10–110 µm with an average size of 56 µm, and 10–80 µm with an average of 42 µm, respectively. This particle size distribution can provide sufficient core material in case of cracking and at the same time, they are applicable for use in polymeric composites.

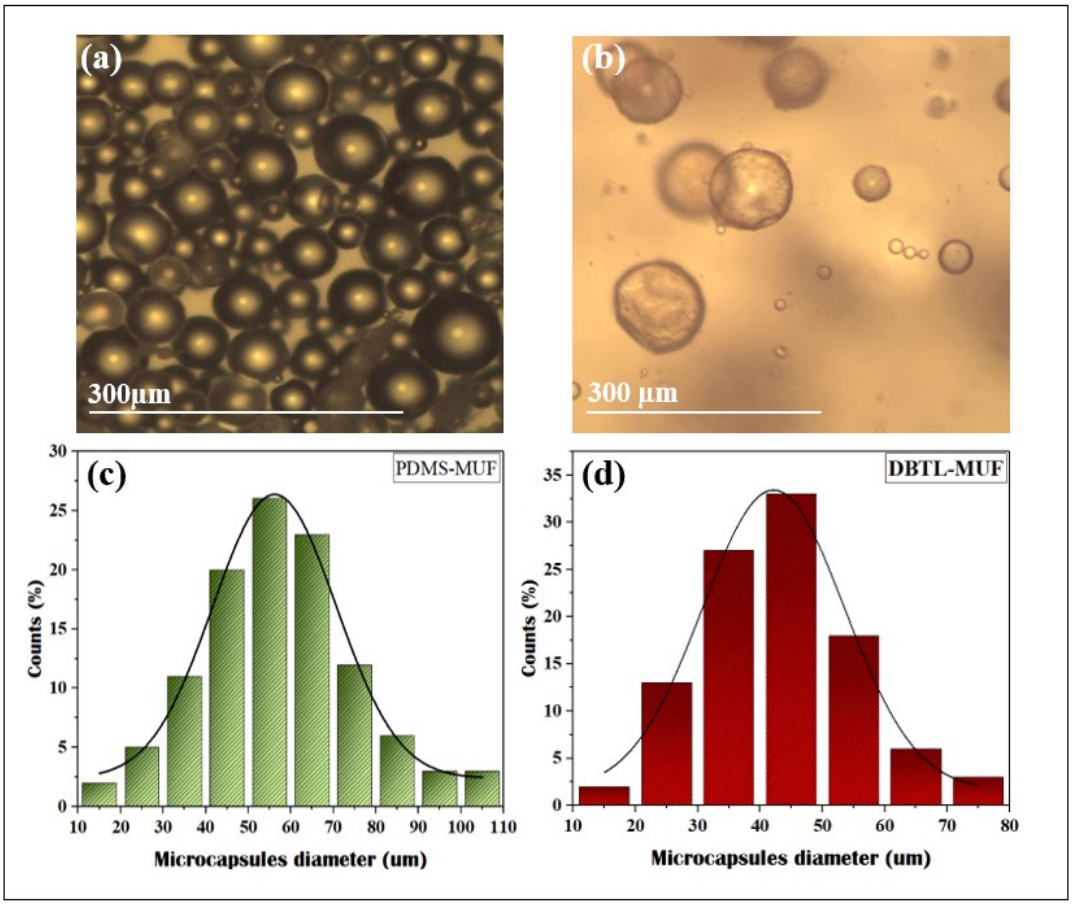

Figure 2-6. Optical microscope images and histogram plots of (a, b) PDMS-MUF microcapsules and (c, d) DBTL-MUF microcapsules.

2.4.4 Morphology of Microcapsules

SEM images of synthesized microcapsules are presented in **Figure 2-7**. As observed in **Figure 2-7a** (PDMS microcapsules) and **Figure 2-7d** (DBTL microcapsules), both types of microcapsules are spherical, show no signs of coalescence between particles, and present a slight roughness on the outer shells owing to the re-deposition of small particles on the surface of larger particles, as mentioned in **Section 2.4.1**.

Figure 2-7b, e presents SEM images of single microcapsules of PDMS-MUF and DBTL-MUF, respectively. Brown et al. suggested that the precipitation of higher molecular weight prepolymer (melamine-urea-formaldehyde in this case) causes the roughness of the outer surface—given that a smooth shell is formed through the deposition of low molecular weight prepolymer at the core–water interface [415], [424]. The DBTL-MUF capsules show rougher capsule walls than those of the PDMS-MUF microcapsules. This greater roughness of the DBTL-MUF capsules may occur because of the larger formaldehyde ratio in their fabrication than that for PDMS-MUF synthesis; the greater the formaldehyde ratio, the higher the condensation reaction rate, and thus the faster deposition of poly(melamine-urea-formaldehyde) nanoparticles onto the shells [388]. The same pattern has been observed in urea-formaldehyde shells, where increasing the formaldehyde content also increases the precipitation of high-molecular-weight prepolymer onto the shell wall [424].

To investigate the shell morphology and measure the shell thickness of microcapsules, we ruptured some microcapsules using a razor blade prior to gold-sputtering. The ruptured shells are shown in **Figure 2-7c, f**. The inner surfaces of microcapsule shells are uniform, compact, and smooth having a thickness of around 200 ± 30 nm and 100 ± 20 nm for the PDMS-MUF and DBTL-MUF microcapsules, respectively. The formed shells ensured the sealing of core materials with no leakage and failure during the processing steps, yet they were not too thick to prevent the rupture of the microcapsules when necessary.

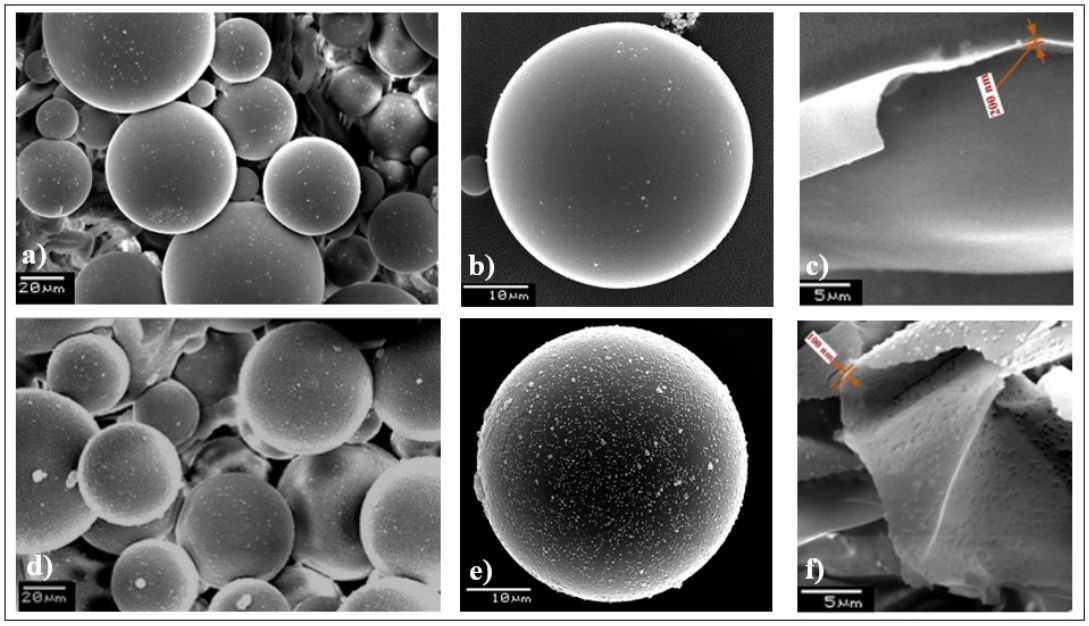

Figure 2-7. SEM images of (a) PDMS-MUF microcapsules having a spherical shape; (b) a single PDMS-MUF microcapsule with a more detailed shell morphology; (c) shell thickness measurement (PDMS-MUF): 200 nm; (d) spherical DBTL-MUF microcapsules; (e) a single DBTL-MUF microcapsule; (f) shell thickness measurement (DBTL-MUF): 100 nm.

2.4.5 Thermal Stability of Microcapsules

Differential scanning calorimetry (DSC) can confirm whether the microcapsules contain the encapsulated core. This verification is possible by knowing the physical and chemical properties of the shell and core components by observing their distinct transition temperatures. The thermal stability of microcapsules is an important factor for self-healing applications. DSC curves determine the temperature range of the microcapsules for which they are chemically and thermally stable [408], [424]. As well, the boiling points of PDMS and DBTL can indicate the presence of the encapsulated core materials inside the shell.

To investigate the thermal properties of the polymeric MUF shell, a small mass of microcapsules was broken apart, washed several times in solvent to extract the cores, dried at room temperature, and analyzed the material using DSC. The resulting DSC curves of extracted MUF shell, PDMS, PDMS-MUF, DBTL, and DBTL-MUF are shown in **Figure 2-8**.

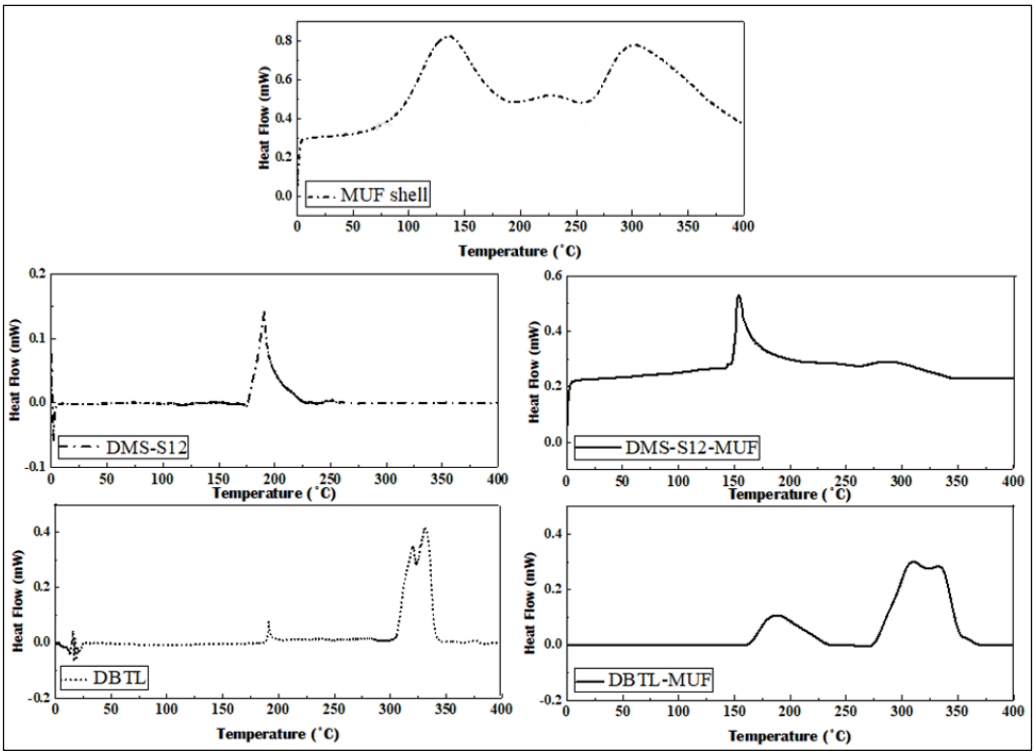

Figure 2-8. DSC thermographs of the extracted MUF shell PDMS, PDMS-MUF, DBTL, DBTL-MUF.

In the extracted MUF shell DSC curve, the first endothermic peak around 100℃ relates to the evaporation of residual water and unreacted formaldehyde in the melamine-urea-formaldehyde polymers. The series of degradation steps of the MUF shell are observed by the two endothermic peaks at around 220℃ and 300℃ [404], [425].

Telechelic hydroxyl-terminated silicones can be prepared by the ring-chain equilibration or redistribution polymerization of cyclosiloxanes, in which, at the end of reaction, 10-15% of cyclic unit could be remained in the media depending on the equilibrium conditions [426]–[428]. In the PDMS DSC curve, the endothermic peak at < 200℃ could be attributed to the boiling point of the residual D_4 monomers (octamethylcyclotetrasiloxane). Considering this transition peak for PDMS, the peak at around 170℃ in the PDMS-MUF curve confirms the encapsulation of PDMS inside the microcapsules. The peak around 300–350℃ can be attributed to the gradual diffusion of the core over the shell, which leads to the decomposition of microcapsules. Therefore, as the PDMS-MUF curve does not show any transition related to the decomposition or chemical reaction up to 300℃, the DSC testifies to the good

thermal stability of the formed microcapsules. For the microcapsule DSC curves, because of the smaller fraction of the shell to the core, the transition peaks related to the MUF shell are mostly neglected [429].

In the DBTL DSC curve, the indicative boiling transition peak also occurs at around 200°C whereas the peaks at 300–350°C demonstrate the decomposition of the material. In the DBTL-MUF DSC curve, both peaks are also observed, and the microcapsules are stable when used at these temperatures [429].

2.4.6 Self-healing Performance of Silicone Composite

The cross-sections of the prepared self-healing composite, as explained in **Section 2.3.3**, are displayed in **Figure 2-9**. The SEM images show that there is no specific interface between the microcapsules and the silicone matrix that suggests good compatibility between the components. Also, a hollow site remained after the breakage of a 100 μm-microcapsule and the shell residues are illustrated in **Figure 2-9a** and **b**, confirming the rupturing of microcapsules in case of damage.

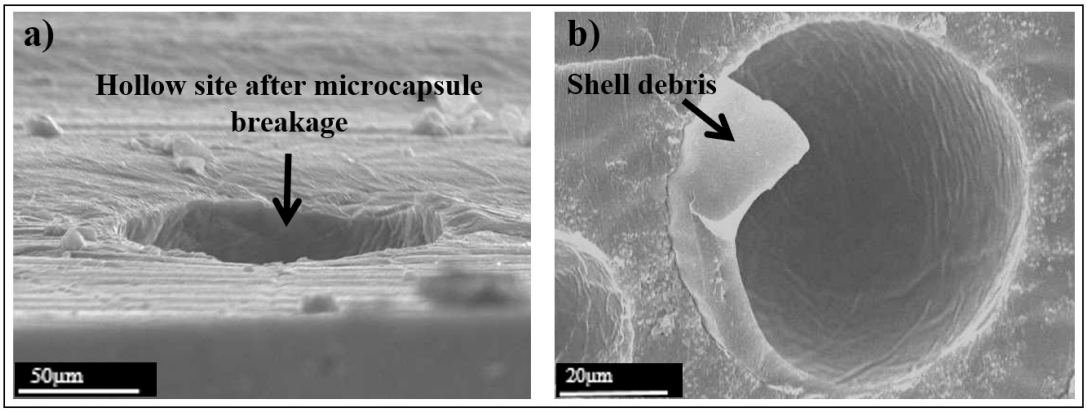

Figure 2-9. SEM images of the cross-section of a self-healing composite and a) hollow sites after microcapsule breakage and with b) a remnant of microcapsule shell.

The self-healing performance of this composite occurs because of the polycondensation reaction of the PDMS and remaining ethoxy groups in the presence of the tin-based catalyst (DBTL) (**Figure 2-10**) [401]. Firstly, the resultant polycondensate product of PDMS could adhere to the matrix because of its viscous nature and form as an adhesive layer between the crack faces. Secondly, the viscous product can continue its polycondensation reaction with the unreacted ethoxy groups in the

matrix and form the crosslinked network in the crack plane. As this chemistry is quite similar to the host matrix, the self-healing imparts no heterogeneity to the composite. Additionally, successful crack filling occurs as both PDMS and DBTL have good flow properties stemming from their low viscosity, and there is no need for a diluent in the self-healing process of this matrix.

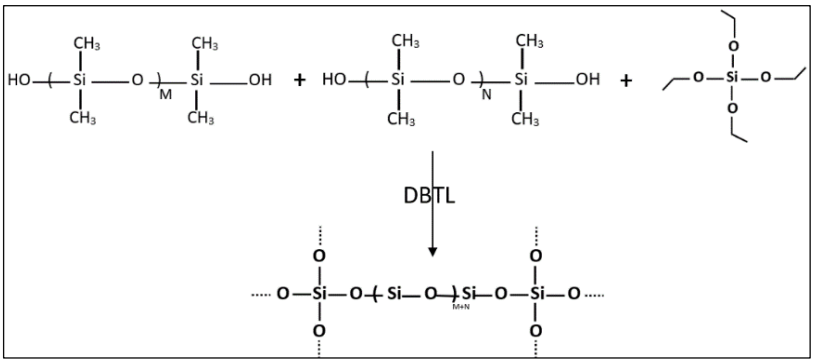

Figure 2-10. Condensation polymerization of PDMS in the presence of the DBTL catalyst.

The self-healing performance of the composite was observed by monitoring the changes to a crack through SEM (**Figure 2-11a, b)**. After scratching the surface to form a crack, the samples were kept at room temperature for at least 24 hours. Crack filling is highly dependent on the width and depth of the crack and the self-healing agent ratio inside the matrix. A good dispersion of the healing agents ensures that appropriate amounts of healing agents are found across the surface of the composite. Here, we observed that for a crack width of around 10 μm, the crack was fully filled by the healing agents—these agents were released and filled the crack through capillary movement—and cured in situ.

Representatives of stress-strain and load-displacement data for the samples are shown in **Figure 2-11c** and **d**, respectively. The tensile test was performed on four types of samples (including the pristine SYLGARD184+20%TEOS and the cracked one, the pristine self-healing composite and the healed composite) to investigate the effect of self-healing microcapsules on the overall mechanical performance of the composite. Here, the incorporation of microcapsules reduced the mechanical properties (tensile strength, ultimate tensile strength, toughness, and strain at break of the composite), green line, compared to the pristine matrix, SYLGARD184+TEOS, (black line). However, when a crack is formed in the pristine matrix, the sample ruptures easily (blue line) in the absence of self-healing microcapsules. After the healing occurrence, the self-healed composite could show a self-healing efficiency of 67% for an

average of five iterations through the tensile testing. For the tear testing, an average healing efficiency of about 55% was obtained for the composites in which the tear path propagated through the healed regions.

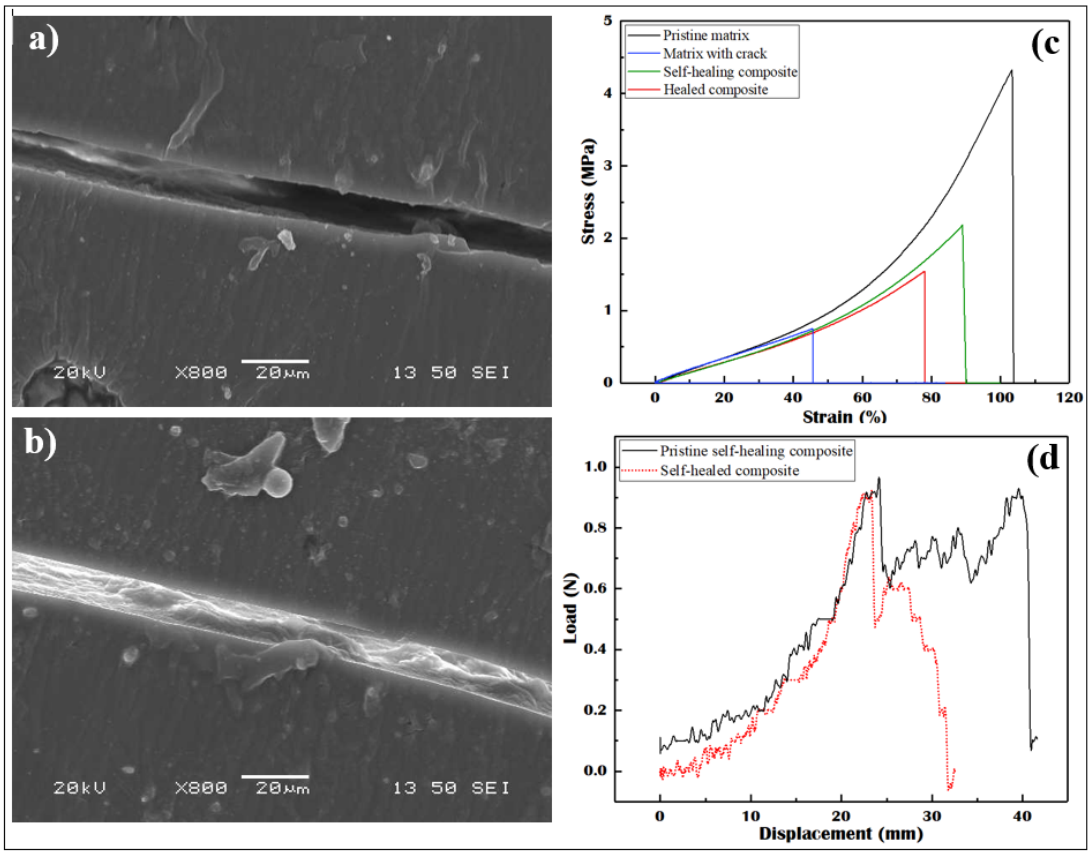

Figure 2-11. Self-healing performance of the dual-microcapsule-integrated silicone composite; a) immediately after cracking and b) After at least 24 h of after cracking at room temperature; c) Stress-strain curve obtained by tensile test, d) Load-displacement data by trouser tear test.

2.5 Conclusion

Silanol-terminated polydimethylsiloxane (DMS-S12) and dibutyltin dilaurate (DBTL) were successfully encapsulated as the healing agent and the catalyst inside poly (melamine-urea-formaldehyde) shells separately through in situ emulsion polymerization techniques. Melamine-urea-formaldehyde shells are preferred over both urea-formaldehyde and melamine-formaldehyde shells owing to their higher robustness to lower cost. The resultant products were free-flowing powders of spherical-shaped microcapsules. These microcapsules had a compact and uniform shell morphology and good thermal properties. The average diameter of the PDMS-MUF and DBTL-MUF microcapsules was

56 μm and 42 μm, respectively. The uniform and compact MUF shells with thickness of 100–200 nm showed sufficient sealing, handling, and processing properties during the fabrication steps yet easily ruptured when microcracks were formed. The synthesized microcapsules showed promise as a healing pair inside a silicone matrix having a unique feature namely the same PDMS chemistry for the healed area and the host matrix. For investigating the healing performance of microcapsules SEM imaging was utilized observing the self-repair of a microcrack. Also, tensile and tear tests performed on the self-healed composites to attain the self-healing efficiency, ensured 67 and 55% of recovery by the proposed system.

Acknowledgments

The authors acknowledge the financial support from the Natural Sciences and Engineering Research Council of Canada (NSERC), Hydro-Québec, Québec, Canada, PRIMA Québec, Canada. We also thank Pauline Moniot for her generous contributions to the laboratory experiments, and Caroline Potvin at the Université du Québec à Chicoutimi for providing us the instruments used for the chemical analyses.

CHAPTER 3 - ARTICLE 2

TRANSPARENT NON-FLUORINATED SUPERHYDROPHOBIC COATING WITH ENHANCED ANTI-ICING PERFORMANCE

A. Allahdini *, R. Jafari, G. Momen

Department of Applied Sciences, University of Quebec in Chicoutimi (UQAC)
555, boul. de l'Université, Chicoutimi, Québec, G7H 2B1, Canada
E-mail: Anahita.Allahdini-Hesarouyeeh1@uqac.ca

3.1 Abstract

A major challenge of non-fluorinated superhydrophobic coatings is the low robustness of the infused nanoparticles in coating films compromising their non-wetting properties. In this paper we developed a robust transparent superhydrophobic coating using an alkoxysilane binder, fumed silica nanoparticles, and methyltriethoxysilane (MTES), in which MTES can act as a coupling agent between the nanoparticles and the binder to increase the stability of the hierarchical structures. The surface wettability was assessed in terms of contact angle (CA) and contact angle hysteresis (CAH) of water at different subfreezing temperatures. The spray-coated superhydrophobic coating with WCA of 163° showed appropriate adhesion to different substrates, optical transmittance of 80% in the visible-light region, and great non-wetting properties even after various extreme treatments, i.e., waterjet impacting, immersing in pollutants and acid/base solutions for 24 h, tape peeling test, and sandpaper abrasion. Self-cleaning tests demonstrated that the superhydrophobic surface could shed various contaminants in both wet and dry conditions leaving a clear surface behind. Ice-adhesion strength and delay of freezing were studied, and it was found that this superhydrophobic coating displayed excellent durability in icephobic properties. The push-off ice adhesion strength of 13.3 kPa on the superhydrophobic coating after 15 icing/de-icing cycles increased only 15% reaching to 15.4 kPa, confirming the superior icephobic behavior of the coating.

3.2 Introduction

In recent years laboratory and industrial interest in multifunctional coatings has widely increased. Among them, superhydrophobic coatings have shown to be promising candidates owing to

their outstanding non-wettability, self-cleaning, icephobic, anti-fouling, and anticorrosion properties [18], [25], [28]. Inspired by nature, superhydrophobic surfaces having a static WCA of more than 150° and a dynamic contact angle (CAH, and sliding angle, SA) of less than 10° can be achieved by a combination of low surface energy materials and micro-nanostructures [1,4–6].

Ice formation and its accumulation on structures in cold regions is a challenging issue that has led to several failures in power lines, telecommunication services, transportation systems, energy harvesting devices, off-shore structures, etc. [11], [13], [431], [432]. Common passive anti-icing strategies can be categorized into two main groups, liquid trapping surfaces and air-trapping surfaces [11,12]. The "air trapping" strategy, where the mechanism is inspired by lotus leaves and used in superhydrophobic surfaces, is mostly based on the rapid removal of water prior to freezing [28]. On one hand, this strategy functions by preventing the nucleation of ice by rapidly eliminating water droplets arriving on the surface. It has been shown that SHPS can potentially prevent ice nucleation on the solid surface by decreasing both contact time and contact area, and also increasing droplet roll-off [194], [435], [436]. On the other hand, the trapped air pockets on the structures of superhydrophobic coatings are beneficial in decreasing the contact area leading to the reduction in the adhesion of ice [437]. Besides, the presence of air cushions at the ice/coating interface plays a role in reducing heat transfer as well as providing stress locations for crack initiation during ice removal [17,18]. The "liquid trapping" strategy, or slippery liquid infused porous surfaces (SLIPS), is inspired by the pitcher plant and involves using an infused lubricant to eliminate the condensation of water in pores and to reduce ice adhesion [19,20].

Silicone resins have been widely used in many industrial and protective coating systems owing to their unique chemical and physical characteristics and abundance of a wide range for material synthesis. Highly crosslinked networks of PDMS form very stable chemical bonds, and their low surface energy makes them suitable binders and precursors in several applications to develop superhydrophobic and icephobic materials and surface coatings [26], [442], [443]. The backbone and chemical functionality of the utilized silicone binder can strongly affect the performance and behavior of the developed coating [444], [445].

A hierarchical micro-nanostructure is another important factor governing the wettability of surfaces that are expected to maintain air pockets underneath water droplets, forming a stable non-wetting Cassie-Baxter state [64], [446]. Silica NPs are attractive options to create micro/nano-scale roughness for superhydrophobic coatings and surfaces due to their low toxicity, optical transparency, and low environmental impacts [25], [447]. Superhydrophobic coatings could be achieved via a combination of silicone resins and hydrophobically modified silica NPs. The durability issues have always been a challenge for superhydrophobic coatings, bottlenecking the transfer of these technologies into real-world applications. Optical transparency is another important parameter for superhydrophobic coatings in many applications. Generally, transparency and superhydrophobicity are conflicting since higher surface roughness, which is favorable for non-wetting durability, could hinder the transparency of the coating by increasing light scattering [33].

The interaction between the NPs and the matrix is crucial for the durability of the non-fluorinated superhydrophobic coatings. If there is a weak interaction the nanostructures are removed easily by abrasion or erosion leading to superhydrophobic failure. The mechanical properties of the nanomaterials, resistance of the matrix against wearing, and adhesion of the coating to the substrate are other factors which should be considered in designing such coatings to enhance their life-time and efficiency in order to obtain a mechanically durable superhydrophobic surface [249]. A recent approach for elevating the robustness of a polymeric coating is to increase the possible cross-linking sites between the functional groups in the formulation [242]. Ming et al. [253] reported a procedure for preparing hierarchically roughened superhydrophobic films by using raspberry-like silica particles in an epoxy-amine matrix. The raspberry particles were prepared by covalently bonding epoxy-functionalized monodisperse silica particles of about 700 nm and amine-functionalized silica particles of about 70 nm via the reaction of epoxy and amine groups. Then raspberry-like silica particles with an amine-functionalized surface were chemically deposited onto the epoxy films, generating roughness with dual-size length scales. Finally, a layer of mono epoxy-end-capped PDMS was grafted onto the particles to render the film surface hydrophobic, resulting in the films showing a WCA of 165° and CAH of 2°. Yang et al. [254] used a mixture of TEOS, heptadecafluoro-1,1,2,2-tetrahydrodecyl triethoxysilane, and nanosilica in an ethanol solution to

formulate a bridged NPs/sol solution for spray coating, leading to a transparent superamphiphobic coating. The coating showed enhanced robustness against sand abrasion, heating, and water jetting. However, the incorporation of fluorinated agents, which are expensive and toxic, is a major drawback.

Over several reports on fabricating superhydrophobic coatings the most widely reported methods are sol-gel [448], [449], chemical and electrical deposition [95], plasma etching techniques [450], and self-assembly [451]. On one hand, in a majority of the reports, fluorinated compounds have been used for creating superhydrophobic surfaces due to their ultra-low surface energy; while their application is a global concern because of their potential toxicity, biomagnification, and bioaccumulation effects [452], [453]. On the other hand, many of these traditional methods are costly and/or require sophisticated equipment in the laboratory and cannot be used in large-scale, low-cost, and rapid fabrication. This issue is still a major drawback specifically for the fabrication of transparent superhydrophobic coatings, in which lithographic processes or the usage of nanoscale roughened templates are pricy for applying superhydrophobic coatings to the large area of glass or polymeric surfaces. Besides, very few articles in this field focus on the industrial applications, the durability and robustness issues of the fabricated superhydrophobic surfaces. Among the application methods, the coatings which are applied using the spraying method have shown promise in the development of superhydrophobic coatings [176], [454] and could be one of the very best choices for industrial applications. Therefore, despite a growing amount of recent research, there is still a need for developing new facile strategies to enhance the consistency of the superhydrophobic coatings [455], [456].

In this work we proposed a method to create a transparent superhydrophobic/icephobic coating of methoxy-functional silicone resin, fumed silica NPs, and MTES that can be applied on various substrates such as glass and metals. Transparent superhydrophobic coatings could endow the surface with the superhydrophobic characteristics while not altering their optical properties, making them promising candidates for solar cell systems, dust-free windows, optical equipment, etc. [457]. Organofunctional silanes, represented as $RSiX_3$ (in which X is substituted by methoxy or ethoxy groups) are used as coupling agents to increase the interface interactions between an organic filler and a polymer matrix [458], [459]. Here, the methyltriethoxysilane could act as a coupling agent to form a bridge

between the nano silica particles and the methoxy-functional silicone resin, helping to increase the robustness of the hierarchical structures.

3.3 Experimental Section

3.3.1 Materials and Method

Glass, aluminum (Al), stainless steel, and porcelain plates were washed with acetone to be used as the coating substrates. A methoxy functional silicone resin, SILIKOPHEN AC1000, was provided from Evonik Co., and tetra-n-butyl titanate was used as its catalyst. Ethanol and butyl acetate were utilized as the solvents. To prepare the non-fluorinated superhydrophobic mixture, MTES, Sigma, and HMDS-treated fumed silica, AEROSIL R812S from Evonik Co., were used to impart surface structure and chemical surface treatment to the coating. The two steps for preparing the superhydrophobic coating are represented in **Figure 3-1**.

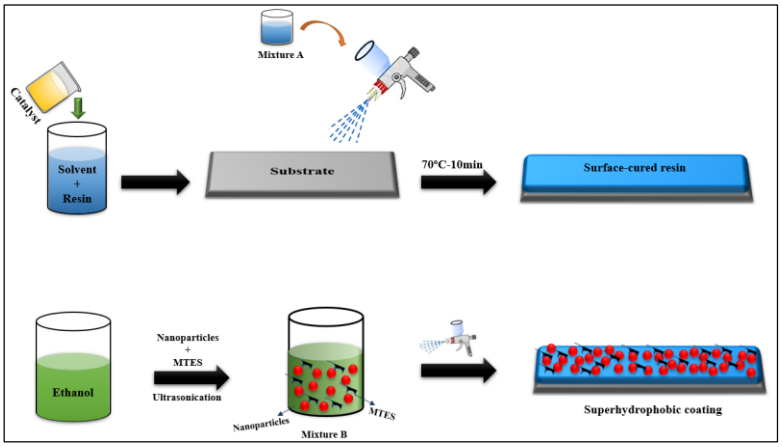

Figure 3-1. Schematic of the preparation steps of the superhydrophobic coating.

The first step, to prepare mixture A, SILIKOPHEN AC 1000 was added to butyl acetate and stirred for 15 minutes. Tetra-n-butyl titanate catalyst was added and mixed for an extra 5 minutes. Mixture A was sprayed on the substrates and placed in the oven at 70°C for 10 minutes to obtain surface curing. After reaching the appropriate surface curing, a thin layer of mixture B was sprayed on the samples and cured at 70°C for 2 hours.

Mixture B was prepared by thoroughly dispersing 0.7 g of fumed silica in 60 ml of ethanol, followed by the addition of 0.5 g MTES to the mixture and ultrasonication for 15 minutes. The role of each step and materials are further explained in the Results and discussions (**Section 3.4**).

3.3.2 Characterizations

The optical transparency of the coating applied on a glass slide was measured by a Cary 5000 UV–Vis spectrophotometer in the visible range.

The coating thickness was measured using DeFelsko`s PosiTector 200 and Elektrophysik MiniTest70 coating thickness gauges. A cross-cut test was performed by cutting a grid of 6 × 6 orthogonal lines with 2 mm spacing. Compressed air was gently applied to remove the chipped-off coating particles and the area was visually inspected. A rating was assigned to the coating according to ASTM D3359, ranging from 5B for an intact coating to 0B for a coating peeled off completely. It is worth noting that a distinction should be drawn between cohesion failure, when the failure occurs in the coating layer between single adsorbent particles, and adhesion failure, in which the point of failure is located at the interface of the substrate and coating.

The chemical composition of the samples was assessed by Fourier Transform Infrared (FTIR) in Attenuated Total Reflection (ATR) mode using a Cary 630 FTIR spectrometer (Agilent, USA) in the range of 400-4000 cm^{-1}.

Scanning Electron Microscopy (SEM) was conducted to survey the surface morphology of the superhydrophobic coating. All samples were sputter-coated with a thin layer of gold prior to SEM analysis, performed by a JSM-6480 LV microscope utilized by the energy dispersive spectroscopy to characterize the elemental composition of the coating. Surface roughness was obtained using the Bruker MultiMode-8 atomic force microscope with scanning in the ScanAsyst mode using PeakForce Tapping. The scanned area was 1 μm ×1 μm and the average data for three scans are reported.

Measuring the CA of a liquid droplet placed on a solid surface is used to quantify its wettability. To measure the WCAs, the sessile drop method was carried out using a Kruss™ DSA100 goniometer at

room temperature and sub-zero temperatures. For the static WCA measurements, a 4-µl distilled water droplet was deposited onto the sample surface and drop shape analysis software was utilized according to the Young-Laplace approximation method. For the evaluation of CAH, a 4-µl water droplet was brought into contact with the surface and held with a stationary needle. The substrate was moved slowly in one direction using a micrometer screw. The CAs appearing at the front and back of the droplet are called advancing and receding CAs, respectively, and the difference between the advancing and receding CAs is reported as the CAH. The measurements were repeated for five different spots on each surface and the average values were reported with the associated standard deviations.

A high-speed charged-coupled device (CCD) camera at fps 5400 was used to record the contact process of an 10 µl water droplet impacted on to the superhydrophobic surface, and the contact time was obtained from the high speed camera. In this measurement the water droplets were released from a fixed height of 10 cm over the surface.

The self-cleaning property of the superhydrophobic coating was assessed by contaminating the samples under both wet and dry conditions. For the wet conditions the coated substrates were completely immersed in a multi-contaminant suspension (20 $g.l^{-1}$ dirty suspension consisting of SiO_2 particles, carbon black, and kaolin, $Al_2Si_2O_5(OH)_4$, in water) for 24 h. Then the samples were placed in the oven at 70°C for 30 minutes to evaporate the water and investigate the presence of pollution residues on the surface through precisely weighing the surface before and after being exposed to the pollution suspension. For the dry condition carbon black and kaolin contaminants were sieved and applied to the substrate. The sample was left for 30 minutes and then a 20-µl water droplet was used to wash the pollution layer.

To assess the icephobic characteristic of the superhydrophobic coating two different analyses of centrifuge tests and push-off tests were used to measure the ice adhesion strength. The freezing delay time was determined using the cold chamber of the Kruss™ DSA100 goniometer where sample stage temperatures can reach to -30°C. First the sample was placed in the chamber, and the temperature of the chamber was adjusted to the designated temperature (-10, -15, and -20°C), then a 4-µl distilled water

droplet was deposited on the cooled surface. For the observation of different stages of freezing the video recording was started from the onset of placing the droplet on the surface.

For the ice adhesion measurement using the push-off test, in a cold chamber at -10°C, a thin cylindrical plastic mold, 1.2 cm in diameter, was placed on the surface and filled with deionized water to form a cylinder of ice over 24 h. Using a remote computer-controlled interface, the force gauge measured the shear force until the ice was detached. Therefore, the adhesion stress can be calculated by knowing the maximum force and the icing area. For the ice centrifuge test, the samples (2.5 cm × 3.5 cm) were iced covered by spraying supercooled water microdroplets to simulate the icing conditions under freezing drizzle in a climatic chamber at -8°C for about 35 minutes to obtain around 5.5 ± 0.5 g of ice. After 1 h the iced samples were transferred to a cold room equipped with a centrifugal instrument to measure the ice adhesion strength at -10°C ± 0.2°C, and the samples were installed at the end of a beam and rotated at a controlled frequency. The force applied to the ice at the breaking point was measured and the adhesion stress was calculated by dividing the force by the icing area. Furthermore, adhesion reduction factor (ARF) is defined by following equation:

$$ARF = \frac{\tau_{pristine}}{\tau_{coating}} \quad \text{(Eq. 3-1)}$$

Where, $\tau_{pristine}$ is the shear stress of ice removal on the reference (Aluminum and pristine resin) and $\tau_{coating}$ is the shear stress of ice removal on the coating.

Sandpaper abrasion and adhesive peeling tests are commonly used to evaluate the mechanical durability of superhydrophobic coatings. For the tape peeling test the adhesive tape (3M scotch tape, USA) was applied and pressed to the coating to confirm complete contact between the tape and coating surface, and then peeled off to observe the coating stability. This process was repeated for 30 cycles and the WCA and CAH were measured every 10 cycles. The abrasion test was conducted using an abrasion apparatus (Manual Clemen Unit, Elcometer 3000, USA) equipped with an adjustable loaded force. For each abrasion cycle the sample was dragged along #1200 sandpaper for 20 cm at an abrasion force of 5.0 kPa. The WCA and CAH were measured after 10 and 20 cycles.

As the performance of coatings against chemical solutions is of great importance, the effect of harsh acidic and basic conditions on the wetting properties of the coating was evaluated by immersing the coated samples into various pHs ranging from 2 to 14 for 24 h and measuring the WCA and CAH afterwards.

3.4 Results and Discussions

3.4.1 Contact Angle Measurements

The pristine SILIKOPHEN AC1000 film showed a WCA of 79° ± 2.3° while the developed superhydrophobic coating exhibited a WCA of 163° ± 2.1°. Water droplets placed on the superhydrophobic coating rolled rapidly off the surface even in very low surface slopes, while the pristine surface was easily wetted by water and no movement of the droplet was observed up to tilted angles of > 30°. Comparison of CAH and SA of the pristine resin and those of the superhydrophobic samples (**Table 3-1**) demonstrated that the surface structures on the superhydrophobic surface, in combination with the low surface energy materials, lead to achieving a composite solid-liquid-air interface, resulting in a Cassie-Baxter state responsible for such superhydrophobic behavior [64].

Table 3-1. WCA, CAH, and SA of water droplet on SILIKOPHEN AC1000 and the superhydrophobic coating.

Sample	WCA (°)	CAH (°)	SA (°)
SILIKOPHEN AC 1000	79 ± 2.0 	9.3 ± 1.5	>30
Superhydrophobic Coating	163 ± 2.0 	2.3 ± 0.3	≤ 5

3.4.2 Physico-Mechanical Properties of Coating

The developed superhydrophobic coating could be applied to different substrates such as glass, aluminum, stainless steel, and porcelain, as shown in **Figure 3-2a, b, d,** and **Figure A-II. 1**. The

thickness of coatings was in the range of 100-150 micrometers. For a water-repellent surface to be optically transparent the dimensions of the surface structures must be in a range that permits the transmittance of light in the visible spectrum, i.e., 400-700 nm. It has been shown that surface features with dimensions of less than one-quarter of the visible light wavelength are able to show this behavior [460]. Optical transmittance of the superhydrophobic coating was measured on glass slides. The blank glass slides had an approximately 90% visible light transmission, and the superhydrophobic coating showed 80% visible light transmission as shown in **Figure 3-2c**. Therefore, the surface structures of the developed coating are in the appropriate size range to show high optical transparency.

A cross-cut adhesion value was assigned to the coating on steel, aluminum and glass substrates depending on the amount of peeled-off coating (the digital photos of the cross-cut test are available in Appendix II, **Figure A-II. 2**). The superhydrophobic coating showed good adhesion to aluminum, steel, glass, and porcelain plates rating as 2B, 3B, 4B and 4B (ASTM D3359), respectively. To investigate the flexibility of the coating and its adhesion properties while bending, a coated aluminum plate was bended as illustrated in **Figure 3-2d**, showing that the coating could maintain its non-wetting properties in the bended region. **Figure 3-2e** illustrates a water meniscus of approx. 4.8 mm formed around the coated aluminum, called the Moses effect.

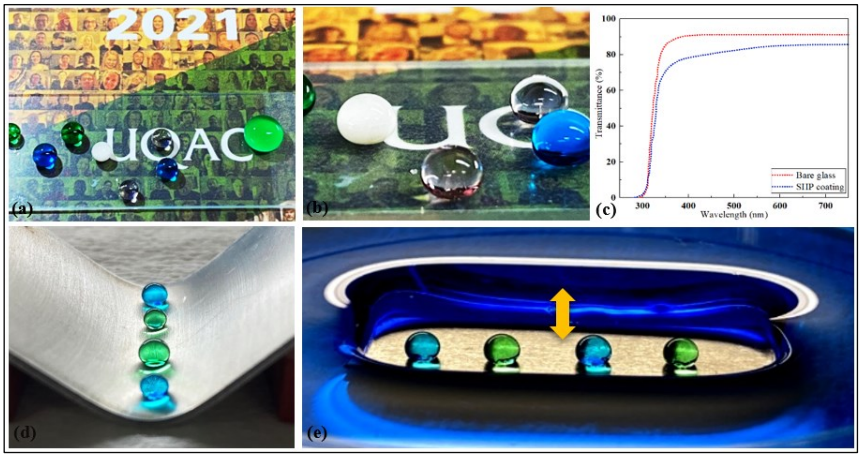

Figure 3-2. a), b) transparent SHP coating on glass; c) UV-visible spectrophotometry of the glass slide and SHP coating; d) Water droplets on a bended aluminum substrate showing that the coating could maintain its non-wetting properties in the bended region; e) Moses effect on the coated aluminum substrate by showing 4.8 mm water meniscus.

3.4.3 Non-Wettability and Cassie-Baxter Regime Study

Formation of a stable interface in a water-repellent surface is guaranteed by the robustness of the Cassie-Baxter regime. The consistency of the Cassie-Baxter regime to create and maintain low CAH on the sample was investigated via various tests including the trapped air layer, waterjet, severe pressing droplet, and water droplet impact, as shown in **Figure 3-3**.

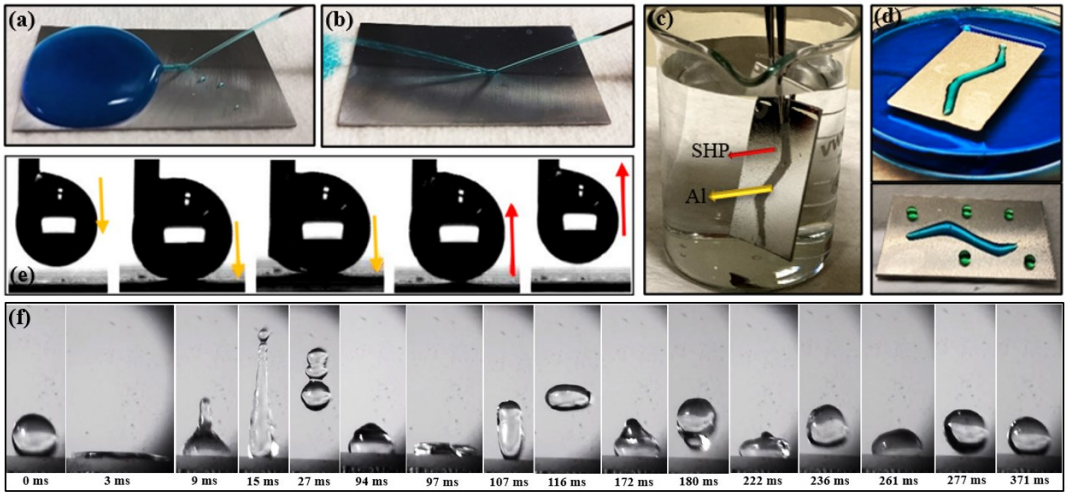

Figure 3-3. a, b) Water-jet impact on SILIKOPHEN AC1000 and superhydrophobic coating; c) Demonstration of the mirror-like phenomenon on the surface of the submerged SHP coating, the masked area is completely wetted by water; d) Showing the wettability difference between the superhydrophobic parts and the masked area; e) Severe pressing of a water droplet to the surface of coating, initial contact, pressing, and lifting stages; f) Impact of 10 µl water droplet on the superhydrophobic coating, showing different stages of impact and five rebounds.

A water jet can compromise the Cassie-Baxter regime by diminishing the air pockets entrapped in between the structures and by the penetration of water into the structures [461]. So, the impact of a waterjet on the superhydrophobic coating was used to evaluate the stability of the water repelling property of the surface. The waterjet adheres to the pristine coating film and accumulates on the surface upon reaching it (**Figure 3-3a**). In the case of the superhydrophobic coating, the waterjet rebounds fully off the surface without leaving any residual water adhering to the coating (**Figure 3-3b**), which shows the stability of the Cassie-Baxter state. In this situation the cylindrical shape of the water jet is unaltered upon rebounding from the surface and water accumulation on the coating is not observed. The WCA of the superhydrophobic coating was measured after 10 cycles of waterjet test (equal to ~50 ml of waterjet) and the results showed no significant change in WCA and CAH even after the repetitive tests, confirming

the robustness of the superhydrophobic coating against the waterjet (WCA = 162.4° and CAH = 2.8° after 10 cycles).

Formation of a plastron layer is a characteristic sign which can be used to distinguish the under-water appearance of a superhydrophobic coating from a pristine coating, confirming the non-wettability properties of the superhydrophobic structures. Thus, a pathway on the aluminum substrate was masked before spraying the superhydrophobic mixture to observe different wetting behavior of the superhydrophobic parts and the masked area. The submerged sample (**Figure 3-3c)**, exhibited an obvious bright plastron layer similar to an optical mirror-like effect in the superhydrophobic parts, which is due to the total reflectance of light at the air layer trapped on the surface structures in which water could not penetrate, confirming the stable conformation to the Cassie-Baxter regime [462]. This phenomenon does not occur on the masked pathway due to the complete contact of the water with the surface interstices. When the aluminum slide was removed from the water, the superhydrophobic parts were completely dry without residual water while the non-coated parts were completely wetted by water (colored by blue dye in **Figure 3-3d**).

The behavior of the superhydrophobic coating against applied additional forces could be evaluated by severe contact with a water droplet [463]. For this test, a 4-µl water droplet adhering to a needle was brought to the surface. After the initial contact between the droplet and the surface, the droplet was pushed toward the surface using the needle. The droplet was then lifted upward. Here the droplet detached easily and rapidly from the surface without leaving any traces of water due to its ultra-water repellency property as shown in **Figure 3-3e.**

To explore the dynamic behavior of a water droplet on the superhydrophobic coating, a water droplet impact test was performed as shown in **Figure 3-3f**. Due to the viscous dissipation triggered by the air pockets at the interface, and depending on the impact velocity, a water droplet usually exhibits either a complete rebound, a partial rebound, or splashing upon reaching a superhydrophobic surface. Here the droplet impacting on the superhydrophobic coating manifests the three stages of spreading, retraction, and complete rebound. When the droplet collides with the surface the droplet spreads until reaching a maximum diameter at t = 3 ms. The kinetic energy of the water droplet is altered during the

spreading stage. A portion of the kinetic energy is dissipated, and the rest is converted into interfacial energy which is responsible for the spreading and deformation of the droplet. The extent of energy dissipation and wetting transition governs the rebound characteristics during the impact [464]. The low energy dissipation on the superhydrophobic surface led to the retraction process and transformation of part of the surface energy into kinetic energy. During the retraction process the droplet was reshaped into a vertical liquid column to reduce its interfacial energy. Afterwards, when the inertia force in the vertical direction exceeded the gravity and adhesion force of the droplet, the droplet rebounded from the surface [48,49]. The droplet was in contact with the surface for around 19 ms before bouncing off and the surface showed five full bounces. After almost 371 ms the droplet came to rest on the surface dissipating all its kinetic energy.

3.4.4 Surface Characterization

To study surface structures for superhydrophobicity, the morphology of the superhydrophobic coating was observed by SEM as illustrated in **Figure 3-4a, b,** and **c.** Also, the energy dispersive spectroscopy results are presented in the supplementary information, in which, the data show 57.69, 40.87 and 1.44% of silicone, oxygen and carbon atoms on the surface of the superhydrophobic coating. The incorporation of fumed silica NPs resulted in the formation of a hierarchical micro-nano structure on the surface. This structure favors the entrapment of air pockets and formation of a layer of air cushion underneath the water droplets which is responsible for the superhydrophobic behavior, i.e., high values of WCA and low values of CAH. When incorporating a fumed silica NPs, the nanometric size leads to a very high surface area and a huge increase in the surface energy, which is not favorable. Therefore, the agglomeration of NPs reduces the total surface energy. Whereas the resin assists the binding of the particles, and results in the formation of highly packed quasi-spherical shapes of multiple size ranges, a hierarchical structure is consequently formed. This hierarchical structure is then favorable in the two aspects of lowering the total surface energy and the superhydrophobic characteristics [460]. In the proposed procedure for the fabrication of superhydrophobic coating in this paper it is note-worthy that as the NPs are dispersed in the solvent phase, the size of agglomerations would be smaller, and the outcome would be a superhydrophobic coating with high optical transparency.

The surface geometry of superhydrophobic coatings has been shown to play an important role in the robustness of superhydrophobicity as well as the icephobicity [467]. Atomic force microscopic (AFM) analysis was also used for quantitatively measuring the dimensional surface roughness and visualizing the surface texture of the superhydrophobic coating and the pristine silicone resin (**Figure 3-4 d, e**). The surface roughness parameters are also presented in **Figure 3-4 f**. The arithmetic average roughness is the absolute average relative to the base length, i.e., the average roughness between peaks and valleys, while the root mean square (RMS) roughness shows the standard deviation of the distribution of surface roughness height. Pristine silicone resin had a relatively smooth surface with the RMS (S_q) and arithmetic average roughness (S_a) values of 4.373 and 3.645 nm, respectively. After the incorporation of fumed silica NPs and formation of the superhydrophobic structure, the Sq and Sa values increased to 57.05 and 46.67 nm, respectively. When the roughness dimensions are smaller than ¼ of the light wavelength, the coating becomes transparent by reducing the intensity of refraction at the interface of air and coating. Here the roughness patterns of below 100 nm can effectively lower the intensity of Mie scattering and concurrently maintain non-wettable characteristics [51,52].

Skewness (S_{sk}) is a scale of the features distribution relative to the mean, where $S_{sk} > 1$ indicates a surface dominated by peaks and $S_{sk} < 0$ indicates a surface with pits or valleys. The $S_{sk} = -0.117$ for the superhydrophobic coating showing slight domination of valleys across the scanned area. The ratio of the actual area to the projected area shows an almost 37% increase in the surface roughness for superhydrophobic coating.

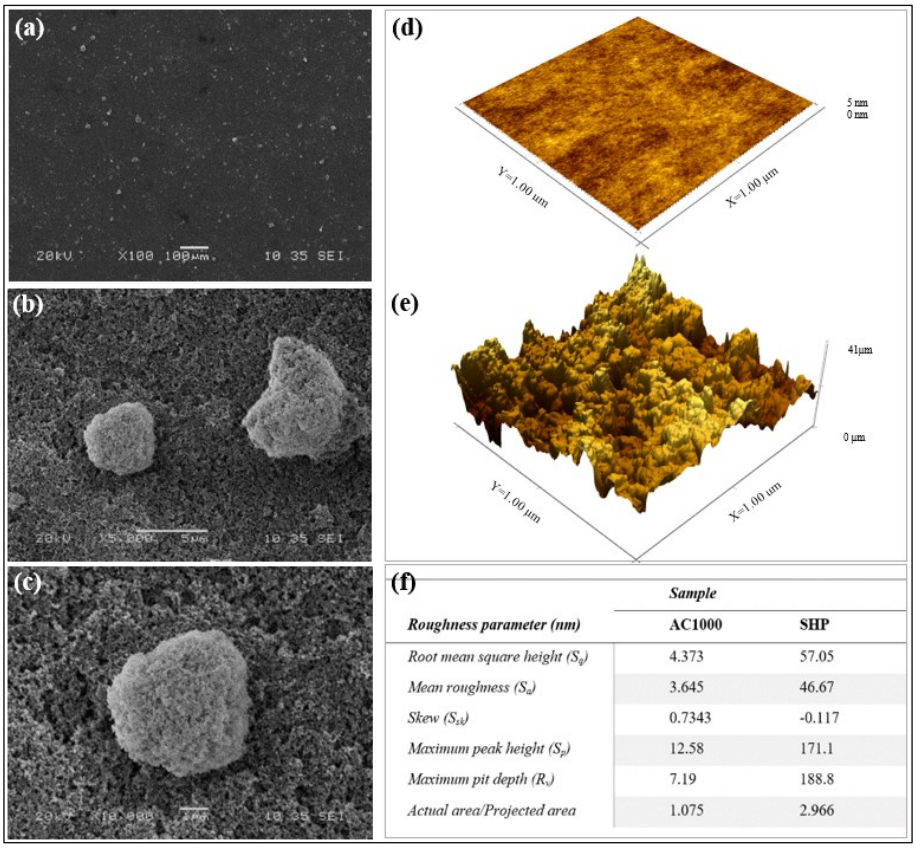

Roughness parameter (nm)	Sample AC1000	SHP
Root mean square height (S_q)	4.373	57.05
Mean roughness (S_a)	3.645	46.67
Skew (S_{sk})	0.7343	-0.117
Maximum peak height (S_p)	12.58	171.1
Maximum pit depth (R_v)	7.19	188.8
Actual area/Projected area	1.075	2.966

Figure 3-4. SEM images of the superhydrophobic coating at magnifications: a)100X; b)5kX; c)10kX; d) AFM image of SILIKOPHEN AC1000; e) AFM image of the superhydrophobic coating film; f) Average surface roughness parameters for the AFM images.

3.4.5 Chemistry of the Superhydrophobic Coating

As explained in the experimental procedure, when the first layer (the SILIKOPHEN AC 1000) reached some extent of a surface curing, the mixture of NPs, MTES, and ethanol were sprayed as the top layer. The solvent helped the NPs embed and fix on the matrix surface, aiding the reduction of total nanoparticle weight ratio in the coating, resulting in a superhydrophobic coating with a high optical transparency of 80%. MTES could participate in the coating formulation through two possible reactions. On one hand, it could be hydrolyzed in the presence of humidity and participate in the condensation reaction with the hydrolyzed methoxy functional silicone resin, as well as the present OH groups on the surface of silica NPs acting as the coupling agent between the particles and the matrix, leading to enhancement of the robustness and durability of the nano-silica inside the coating. On the other hand, MTES, which is highly hydrophobic, can be condensed with the hydrolyzed resin and increase the

hydrophobic characteristic of the coating. Possible hydrolysis and condensation steps of the coating moieties are presented in **Figure 3-5 a, b**, and **c**.

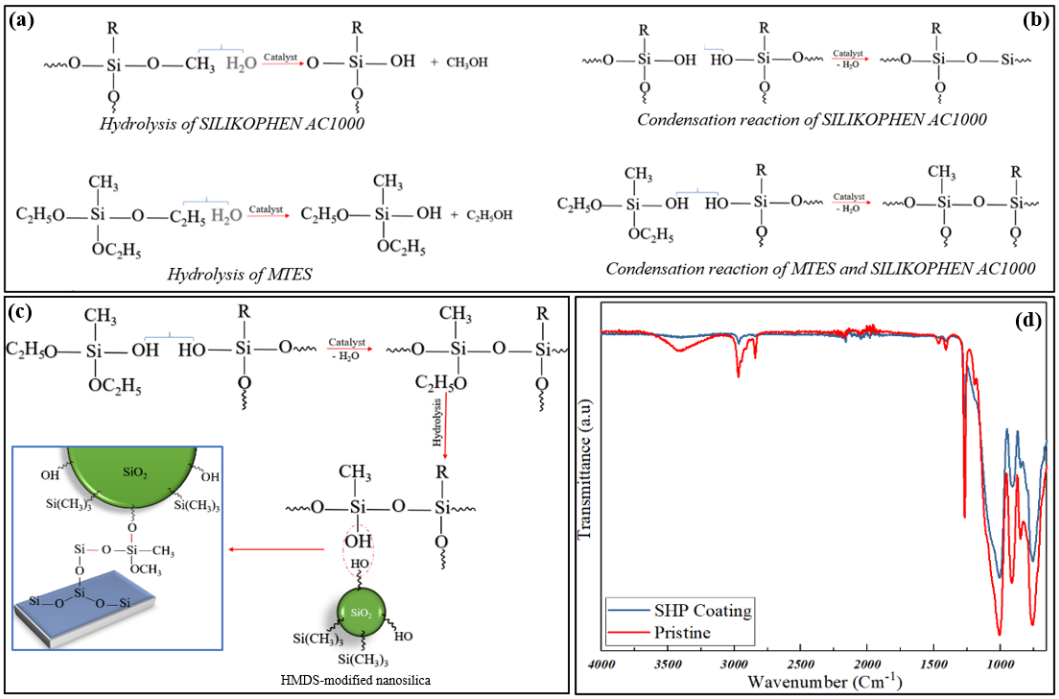

Figure 3-5. Possible a) hydrolysis and b) condensation reactions; c) MTES acts as the coupling agent between silica NPs and SILIKOPHEN AC1000 that is responsible for robustness of NPs in the coating; d) FTIR spectroscopy of the superhydrophobic coating and surface-cures SILIKOPHEN AC1000.

The FTIR spectroscopy (**Figure 3-5 d)** was used to investigate the chemical composition of the superhydrophobic coating and the surface cured SILIKOPHEN AC1000. The methoxy-functional SILIKOPHEN AC1000 cures in the presence of tetra butyl orthotitanate catalyst through a twostep (hydrolysis and condensation) reaction. The peaks at the high wavenumber range of 3500 cm^{-1} in the pristine film are attributed to the presence of Si-OH groups due to the hydrolysis step. Obviously, these peaks are not observed in the superhydrophobic coating which shows the completion of the reaction and elimination of the hydrophilic groups on the surface. The other peaks at around 1260 cm^{-1}, 1020-1070 cm^{-1}, and 780-790 cm^{-1} are related to the CH_3 deformation in Si-CH_3, stretching of Si-O-Si and asymmetric Si-O-C vibrations, and CH_3 rocking and Si-C stretching in Si-CH_3, respectively. Also, the peaks at around 2950 cm^{-1} are attributed to the asymmetric CH_3 stretching in Si-CH_3.

3.4.6 Self-cleaning Behavior

Self-cleaning surfaces are inspired by the lotus plant, the symbol of purity in some ancient religions, in which the water droplets can slide and roll over the surface and pick up dirt particles on their way down [183], [469], [470]. To better represent the outdoor pollution conditions we can consider two dry and wet pollution scenarios in which the behavior of the coating is evaluated against both solid contamination and a suspension of pollutants.

Here, as explained, the coated substrates were completely immersed in a multi-contaminant suspension (20 $g.l^{-1}$ dirty suspension consisting of SiO_2 particles, carbon black, and kaolin in water). Then the samples were placed in the oven at 70°C for 30 minutes to evaporate the water and investigate the presence of pollutant residues on the surface through precisely weighing the surface before and after being exposed to the pollutant suspension. Following this method, the contamination on the surface of the pristine sample is illustrated in **Figure 3-6 a1**, whereas the superhydrophobic surface remained clean and showed no evidence of accumulation or residues of contamination (**Figure 3-6 a2)**. Weighing the samples after washing, the pristine sample showed $\Delta m = 0.19\ g$ while for the superhydrophobic coating the weight of the sample remained unaltered up to the third decimal digit.

The self-cleaning behavior of the superhydrophobic coating was also evaluated using carbon black particles which were sprinkled on the surface and removed by water droplets. As shown in **Figure 3-6 b1, b2** on the superhydrophobic coating, the water droplets removed the contamination on the way down and the surface was cleaned. However, on the pristine surface, the water droplets were stuck to the contaminated surface. This phenomenon is due to the greater adhesion of the water droplet to contaminants compared to the adhesion of water to the superhydrophobic surface when rolling and the lower adhesion of water to the contaminant in case of the pristine surface as shown in the schematic images. **Figure 3-6 c** also represents the water droplet which has collected the sprinkled carbon black particles on its way.

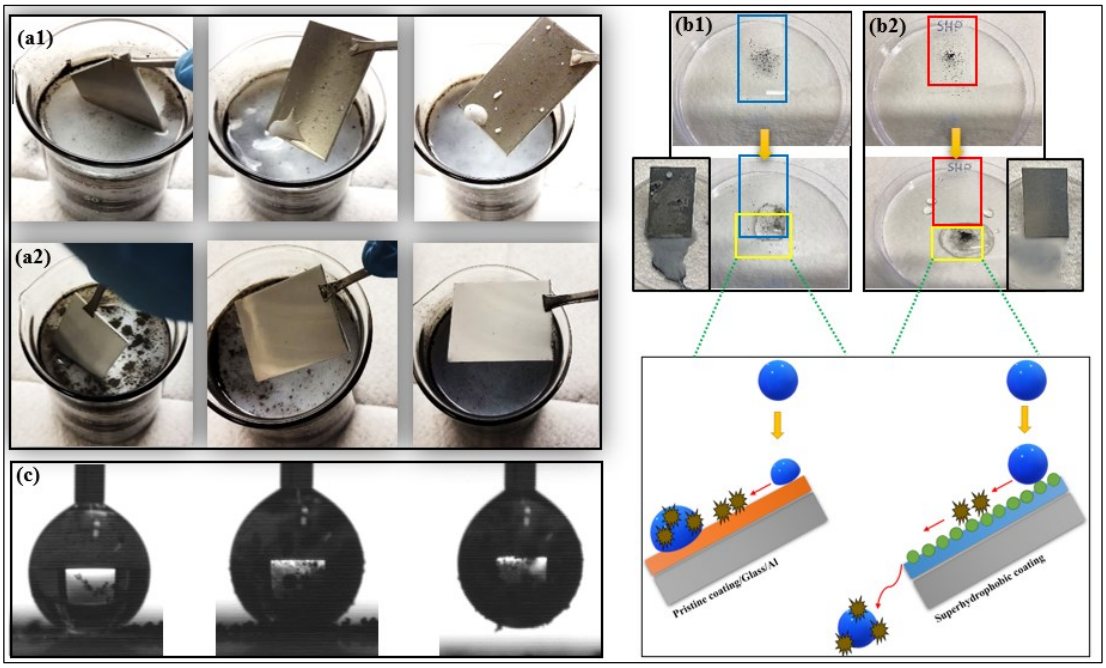

Figure 3-6. Self-cleaning evaluation of the developed coating in wet and dry pollution scenarios. Wet scenario: submerged a1) SILIKOPHEN AC1000 a2) superhydrophobic coating in multi-contaminant suspension. Dry scenario: sprinkled carbon black particles on b1) SILIKOPHEN AC1000 and b2) superhydrophobic coating, and the schematic representation of the movement of water droplets on polluted surfaces; c) attached water droplet collecting pollutants on its way on the superhydrophobic coating.

3.4.7 Durability Assessment

The broad-ranging application of superhydrophobic coatings has always been restricted by their poor mechanical durability. To assess the durability of the superhydrophobic coating, the WCA and CAH measurements are represented after each 10 cycles of sandpaper abrasion and tape peeling in **Figure 3-7 a, c** following the SEM images of the coatings after the tests (The effect of presence of MTES on the mechanical durability of the coating is represented in **Figure A-II. 5**, Appendix II).

After 30 cycles of tape peeling the coating still showed appropriate superhydrophobic behavior and good water roll-off with WCA of 157.8° and CAH of 7°. Also, after 20 cycles of sandpaper abrasion, the coating was still superhydrophobic, however its WCA and CAH reached 152.6° and 9.5°, respectively. Albeit, in the SEM images, the coating structures are compromised in some parts after the mechanical testing (shown by yellow dash-lines), the superhydrophobic coating still possesses appropriate mechanical durability by retaining its non-wetting properties after repetitive cycles.

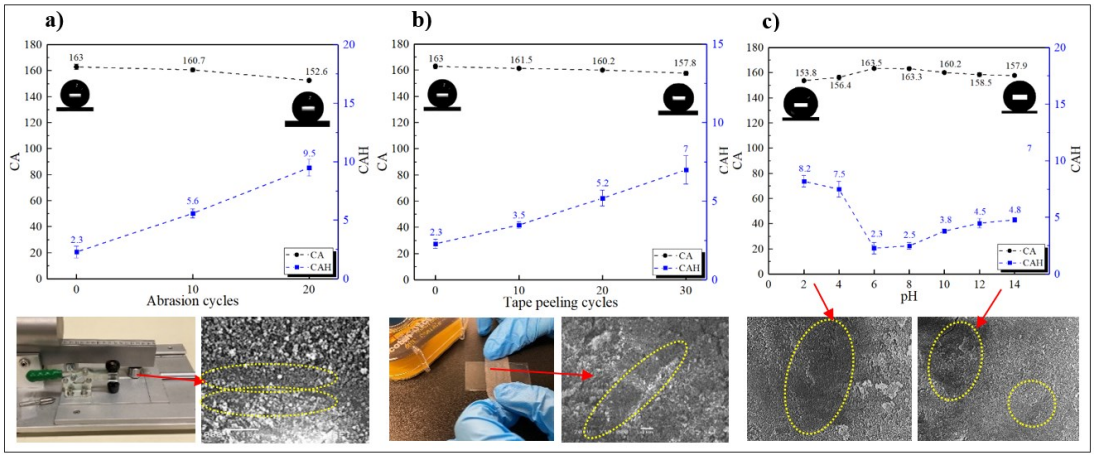

Figure 3-7. Durability assessment of the superhydrophobic coating. WCA and CAH measurements after a) 10 and 20 cycles of abrasion; b) 10, 20, and 30 cycles of tape-peeling; c) immersion in pH ranges of 2 to 14 for 24 h; d) abrasion apparatus and SEM image after 20 cycles of abrasion; e) tape peeling tests and SEM image after 30 cycles; f) SEM images after acid and base treatments.

To investigate the chemical durability of the superhydrophobic coating, the coating was immersed in different pH solutions of 2, 4, 10, 12, and 14 for 24 hours, and the WCA and CAH were measured. In pH = 2, The WCA of the coating decreased and reached to 153.8° and CAH increased to the value of 8.2° while at pH = 14, WCA and CAH were 157.9° and 4.8°, respectively, indicating that pH values of the aqueous solution have little effect on the non-wettability of the as-prepared coating. Therefore, such a surface is superhydrophobic for not only pure water but also corrosive liquids and can be used in all pH environments (The transparency of the coating after immersion in corrosive solutions is illustrated in **Figure A-II. 4**, Appendix II)

3.4.8 Icephobicity

The ice adhesion strength measurements are reported on aluminum, pristine SILIKOPHEN AC1000, and the superhydrophobic coating in **Figure 3-8 a**. The ice adhesion strengths of 13.3 and 126 kPa were obtained for push-off and centrifuge tests on the superhydrophobic coating, equaling to ARF of 4.89 and 3.88 based on the pristine silicone resin.

The icephobic durability of the superhydrophobic coating was also investigated through 15 icing/de-icing cycles of ice push-off tests (**Figure 3-8 b)**. Showing ice adhesion strength of lower than

20 kPa, even after 15 cycles of icing/de-icing, the developed superhydrophobic coating could be considered as an appropriate surface for the passive removal of ice [471]. During the ice formation process on a superhydrophobic coating, if the Cassie to Wenzel transition does not occur, the icephobic behavior of the coating is governed by the trapped air pockets underneath the formed ice leading to a reduction in ice adhesion strength [472]. Here the durability of the icephobic behavior also verifies the robustness of the Cassie-Baxter state for the developed superhydrophobic coating even in sub-zero temperatures [473].

Another parameter to assess the icephobic behavior of coatings is to measure the delay in the onset of freezing on different surfaces. **Figure 3-8 c, d** show the WCA and freezing delays for the SILIKOPHEN AC1000, superhydrophobic coating, and aluminum surface at different temperatures, and the stages of freezing of water droplets at -20°C are represented in **Figure 3-8 e**.

Comparing the freezing delay times of the superhydrophobic coating and the pristine resin (**Figure 3-8 d** yellow and blue lines), the superhydrophobic coating could improve the freezing delay times from 122 s to 483 s ($T = -20°C$), 329 s to 2116 s ($T = -15°C$), and 1517 s to 3294 s ($T = -10°C$). The pristine surface shows lower water CA, and consequently a higher contact area between the water droplet and the surface occurred. The lower the contact area between the water droplet and the surface, the lower the thermal conduction and the longer the delay of freezing. The superhydrophobic coating also benefits from the presence of thermal insulation of the air pockets trapped in between the surface structures in order to extend the onset of freezing [474], [475]. It could be claimed that the superhydrophobic surface showed a longer freezing delay, and so had a greater anti-icing potential, leading to less ice accumulation over time [475].

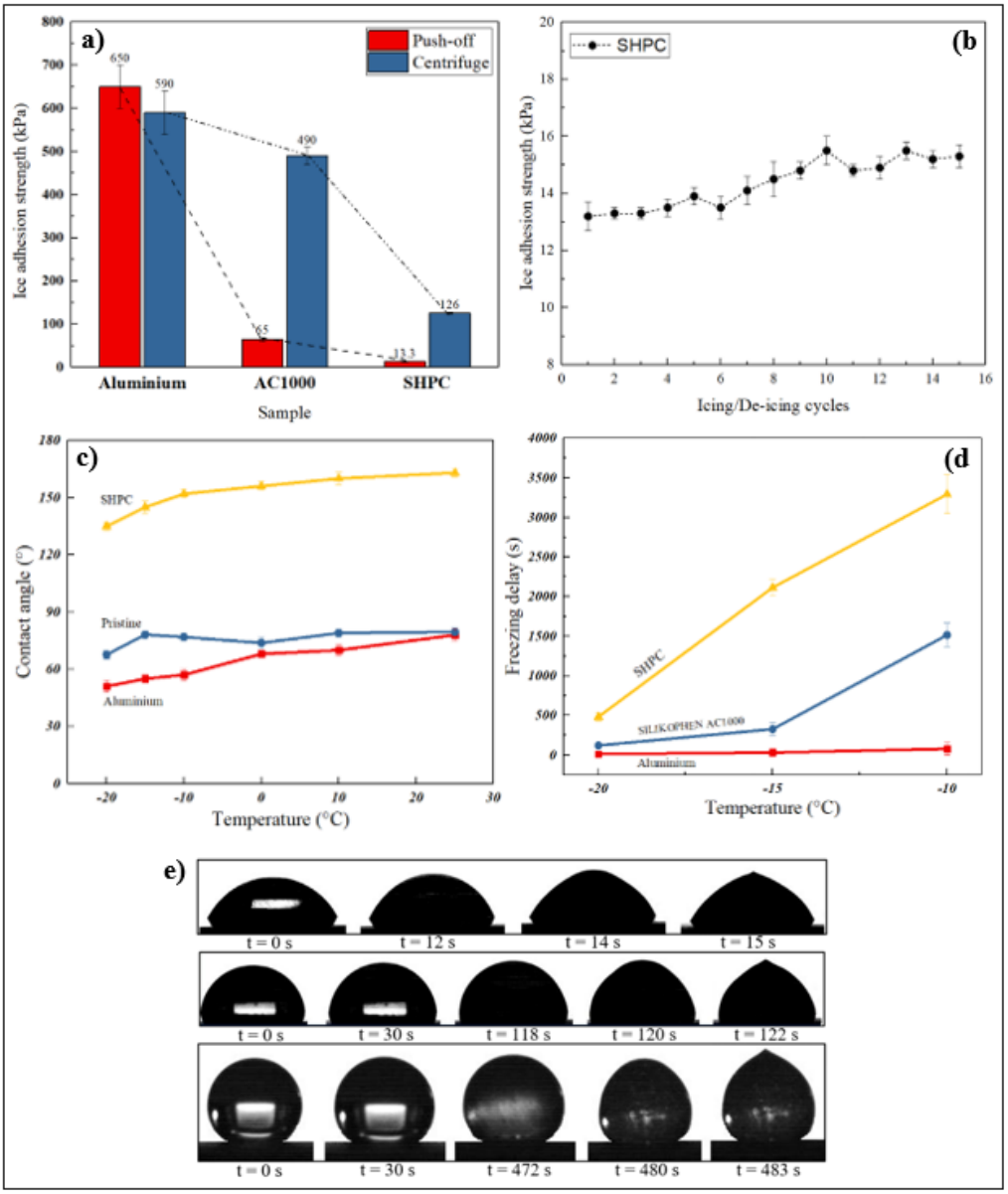

Figure 3-8. a) Ice adhesion strength measurements by push-off and centrifuge tests on bare aluminum, SILIKOPHEN AC1000, and SHP coating; b) icing/de-icing durability of the SHP coating for 15 cycles; c) CA of water droplets on the samples at different temperatures, d) the freezing time of water droplets on different samples at different sub-freezing temperatures; e) stages of water droplet freezing on aluminum, SILIKOPHEN AC1000, and SHP coating at -30°c.

3.5 Conclusion

Among different types of coatings, superhydrophobic coatings have attracted considerable attention due to their water repellency, icephobic properties, self-cleaning ability, etc. In this paper we fabricated a transparent non-fluorinated superhydrophobic coating based on alkoxysilane resin using a

spraying technique. Superhydrophobicity was obtained through the combination of low surface energy materials and hierarchical structures in the submicron range leading to high optical transparency. The final coating showed optical transparency of 80% in the visible light region, WCA of 163 ± 2° and CAH of 2.3 ± 0.3° at room temperature, and good adhesion to glass and aluminum substrates. The robustness of the superhydrophobic structures was enhanced by increasing the possible crosslinking sites between the silica nanoparticles and the alkoxysilane binder using methyltriethoxysilane as the coupling agent. The coating exhibited great mechanical robustness (WCA = 152.6 ± 1.7°, CAH = 9.5 ± 0.7° after 20 cycles of sandpaper abrasion and WCA = 158.7 ± 1.8°, CAH = 7 ± 0.9° after 30 cycles of tape-peeling) maintaining its superhydrophobicity. Also, the non-wetting properties of the coating was shown to be acceptable in harsh chemical environments (after 24 h: WCA = 153.8 ± 1.2° @ pH = 2 and WCA = 157.9 ± 0.9° @ pH = 14).

The adhesion of both bulk and glaze ice was measured on the developed superhydrophobic coating via ice push-off and centrifuge tests, showing remarkable icephobicity (ARF = 4.89 and 3.88 for push-off and centrifuge compared to a pristine resin). After 15 icing/deicing cycles the push-off ice adhesion strength was kept lower than 20 kPa, confirming the icephobic durability of the coating. Also, compared to bare aluminum, the superhydrophobic coating could increase the delay of the ice formation time by 97, 63, and 31% at -10, -15 and -20°C, respectively.

The water-repellency, self-cleaning, icephobic properties, and transparent characteristics of such coatings could find applications in different fields of industry such as windows, electrical insulators, solar cells, etc.

Acknowledgment

The authors acknowledge the financial support from the Natural Sciences and Engineering Research Council of Canada (NSERC); Hydro-Québec, Québec, Canada; and le Pôle Recherche Innovation en Matériaux avancés du Québec (PRIMA Québec), Québec, Canada. We also thank Caroline Blackburn of Anti-icing Materials International Laboratory (AMIL) for performing the

Centrifuge Adhesion Test (CAT) and Caroline Potvin at the Université du Québec à Chicoutimi for providing us the instruments used for the chemical analyses.

CHAPTER 4 - ARTICLE 3

PERFORMANCE OF A NANOTEXTURED SUPERHYDROPHOBIC COATING DEVELOPED FOR HIGH-VOLTAGE OUTDOOR PORCELAIN INSULATORS

Anahita Allahdini, Gelareh Momen, Frédérick Munger, Stephan Brettschneider, Issouf Fofana, and Reza Jafari

[1] International Research Center on Atmospheric Icing and Power Engineering (CENGIVRE)
Department of Applied Sciences, University of Quebec in Chicoutimi (UQAC)
555, boul. de l'Université, Chicoutimi, Québec, G7H 2B1, Canada.
E-mail: Anahita.Allahdini-Hesarouyeeh1@uqac.ca

4.1 Abstract

We live in an era of striking advancements in various domains of science and technology, where separate fields and specializations are overlapping into new horizons. This cooperative approach is emerging rapidly in polymer science by employing the organic and physical chemistry, materials science, as well as electrical and mechanical engineering to collaborate and develop uniquely innovative materials. In outdoor high voltage power equipment, various problems such as flashover, rain, icing, pollution, and UV can compromise the performance of insulators thereby distorting the reliability of the entire system. Superhydrophobic coatings are sought-after candidates owing to their ultra-non-wettable, easy-to-clean, and anti-ice character. However, the performance of superhydrophobic coatings when they are subjected to high-voltage fields is still lacking sufficient research. Here, we aimed at designing a robust and novel non-fluorinated superhydrophobic coating in order to increase the effective life-span of high-voltage insulators by preventing and/or delaying the possible arcing and flashover driven damages. The electrical properties of the coating were investigated through various and comprehensive test methods. The coating showed high thermal and desirable weathering stability. Compared with bare porcelain in dry, wet, and polluted conditions, the superhydrophobic coating successfully increased the flashover voltage. Moreover, the superhydrophobic coating exhibited low leakage currents through the condensation test when exposed to high humidity conditions. With leakage currents of as low as 20 mA after three continuous steps of voltage increase, the superhydrophobic coating showed less tracking and erosion lines than the pristine coating in an adapted inclined plane test for thin films.

4.2 Introduction

In the power transmission system, failure of any components, including insulators, can lead to huge power and monetary losses. Outdoor high-voltage insulators must maintain a high dielectric strength under all environmental conditions. The power utility records report that nearly 70% of high-voltage line failures are due to inadequate insulations [49]. This finding reveals the importance of investigating insulator capabilities and weaknesses under electrical stresses and harsh environmental conditions to guarantee the reliability of the system in different conditions [37], [49], [476], [477]. Electrical failures at the surface of insulating materials can occur because of several issues, including flashover, thermal degradation of the surface, and surface degradation by corona discharges or progressive tiny arcs and tracking [478].

Most insulators used in power transmission and distribution lines are made of porcelain and glass; compared with composite insulators, porcelain- and glass-based insulators offer high mechanical strength, high resistivity, hardness, and resistance to aging [476], [479], [480]. However, the lifetime of porcelain-based insulators is mainly related to the electrical stresses intensified by the accumulation of water, ice, and pollution on their surface because of their high surface energy (roughly $50\ mJ.m^{-2}$) and high degrees of wettability (water contact angle [CA] of around 40°) [13], [41], [476], [481], [482]. The formation of a conductive layer by water or pollution on the surface of an insulator leads to leakage current flow. The concomitant increase in this leakage current induces dry band formation and a strong arcing or discharge, causing flashover along the insulator [45]. The magnitude of the leakage current along the insulator surface determines its performance. Dry band arcing makes the insulators prone to erosion and tracking degradation. The insulation capability of materials to withstand damage is consequently gradually reduced by erosion. High magnitudes of leakage current may accelerate the processes leading to insulation failure [46], [47], [483]. Insulator design modification, surface washing, and periodical applications of silicone grease are among the common conventional methods used by utilities to prevent the aforementioned phenomena while facing the limitations of technical and economic challenges [49]. Moreover, improving hydrophobicity by applying a hydrophobic coating shows promise because of the easy removal of water and contaminations from the surface of insulators [48], [49]. Room

temperature vulcanized (RTV) silicon rubber coatings, with polydimethylsiloxane (PDMS) as the main component, are the most used coatings for ceramic insulators [50]–[56]. The main components of RTV coatings include the PDMS polymer, reinforcing filler, low molecular weight silicone fluid, crosslinking agent, condensation catalyst and an adhesion promoter. Among various fillers, ATH helps to reduce tracking and increase erosion resistance, thus providing the long-term functionality in lowering leakage current and preventing flashover. Smaller ATH particle fillers have shown to induce longer lifetime for RTV coatings because of the better heat conduction and smoother coating surface. The type of utilized materials and the applied thickness play important roles on the properties of the RTV coating. Thickness of these coatings must not exceed 1 mm and the optimum thickness has been reported to be in the range of 0.3 and 0.5 mm. Increasing the thickness increases the thermal resistance thereby making the conduction of heat away from the insulator more difficult. A satisfactory performance of RTV coatings depends on its capability to maintain the hydrophobicity and the resistance to erosion and surface discharge. Material composition also effects on the dielectric strength of the coating. It is also expected that a thicker coating is able to maintain its hydrophobic level for a longer period of time than a thinner coating since the quantity of LMW fluid would be higher. Silica fillers are not sensitive to moisture uptake, and they can form chemical bonds with the host PDMS matrix thereby improving strength, reducing porosity, and further improving adhesion to substrates. Therefore we can conclude that the lifetime of RTV coatings and their electrical and surface properties depend on various factors, such as LMW content, rate of diffusion of LMW fluid to the surface, thermal conductivity, surface roughness, type of substrate, ATH particle size, amount of ATH and silica particles, electric stress level, coating thickness and pollution conditions [43], [484], [485].

Field experiences have shown a minimum of a 10-year lifetime for RTV coatings even in serious contamination conditions [486], [487]. Moreover, low–molecular weight PDMS chains in the bulk of coatings can migrate toward the surface and form a nonconductive weak layer, preventing the leakage current development on the insulator surface [477], [488]–[491].

It has been shown that water repellency of insulators and the severity of flashover on their surfaces have a relationship and many researchers have studied different levels of surface hydrophobicity

[492]–[495]. Superhydrophobic coatings with WCA of more than 150° and contact angle hysteresis (CAH) of less than 10°, are best known for their nonwetting, self-cleaning, and icephobic behavior [496]–[498]. The WCAs on the surface of RTV coatings are approximately 110°, much lower than those on superhydrophobic surfaces which means more delicate self-cleaning properties [499]. A superhydrophobic surface can be achieved through different approaches, including lithography, etching techniques, plasma, chemical vapor deposition, etc. [500], [501]. However, applying a superhydrophobic coating on the surface of the material instead of shifting the procedures toward expensive production techniques for superhydrophobic surfaces is more convenient and applicable for many utilities. Among several methods used to produce superhydrophobic coatings, spraying a nanocomposite coating dispersion is an effective, simple, and cost-effective way.

Most of the superhydrophobic materials and coatings on high-voltage insulators are based on inorganic nanoparticles dispersed in polysiloxanes. The inorganic oxides doped in the polysiloxane coatings can change the surface energy because of the presence of oxygen vacancies, which are predominant at a higher temperature. The incorporation of inorganic oxide nanoparticles may fill the interfacial cracks of the matrix and improve the electrical properties considerably [502]. Arshad et al. [9] reviewed the properties and applications of superhydrophobic coatings in high-voltage insulation sectors and discussed the available test methods for evaluating their performance. Seyedmehdi et al. [503] developed a polyurethane superhydrophobic coating using 8 wt.% nanosilica sprayed on porcelain insulators. The coating showed good UV durability and mechanical robustness. They also performed a dry lightning impulse voltage test in accordance with IEC 60383 to investigate the electrical durability of the coating. The withstand voltages of the coated insulator with standard noncoated insulator were nearly close to one another, and the superhydrophobic coating could pass this test. Ramalla et al. [504] used a suspension of SiO_2-powder and SiO_2-sol to develop a superhydrophobic coating via the sol–gel reaction of tetraethoxysilane, perfluorodecyltriethoxysilane, ethanol, nitric acid, and hydrochloric acid. These authors evaluated the self-cleaning ability of the coating in light, moderate, and heavy pollution levels. The application of an electrical field on the superhydrophobic-coated insulators showed better performance in all pollution levels. Chen et al. [505] studied the self-cleaning and anti-pollution flashover performance of a micro/nano-structured superhydrophobic coating to establish a DC

pollution flashover mechanism model. The experiments were done on superhydrophobic coating, RTV coating, and uncoated surface and their results showed that at any pollution degree, the superhydrophobic coating could maintain an almost constant leakage current of about 16.3μA after being completely wetted.

On one hand, there are various challenges bottlenecking the large-scale and industrial execution of superhydrophobic coatings, i.e., complicated fabrication procedures, laboratory-scale application methods, and low mechanical robustness. Thereby, the current-years research is mostly focusing on the amelioration of their performance and more specifically enhancing the mechanical durability [33], [506]. A durable and scalable superhydrophobic coating based on a methoxy functional silicone resin and silica nanoparticles with superior self-cleaning behavior in different pollution conditions and excellent icephobic performance was developed in a previous study [35]. Considering the durability issues of SHP coatings, the utilized fabrication method embosses the developed coating with an enhancement in robustness by increasing the potential interactions and crosslinking sites between the nanoparticles and the matrix via a non-complicated approach in order to reduce the coatings delamination due to abrasion or erosion.

On the other hand, despite the existence of several studies on the topic of applications for superhydrophobic coatings, research is still lacking to fully understand how they work when subjected to different high-voltage fields in harsh conditions. Most of the available and standardized test methods are intended for porcelain and glass insulators. These methods are not directly applicable to coated insulators. The lack of standard complicates the research on new insulator materials, including superhydrophobic coatings, and the detailed investigation of their performance [21], [507]. For a superhydrophobic coating to be employed in high-voltage applications within a reasonable life-span, the behavior of the coating must be carefully investigated in various aspects including thermal/weathering resistance, and in particular the dielectric stability. When the coating is exposed to electric field, different parameters such as resistivity, dielectric loss, voltage, leakage current, tracking, etc. would be important and must be inspected. Based on our literature review, there were not as many papers considering all the mentioned aspects in one comprehensive work. Therefore, we decided to evaluate how the developed

coating behaves in various conditions and under different electric field stresses. To put it in a nutshell, the ultra-nonwettability, multifunctionality of the coating and surface insulation of the coating based on the binder/nanoparticle approach were discussed through wide range of testing conditions (including dielectric spectroscopy, thermogravimetric analyses, weathering resistance, flashover voltage measurements, condensation test, and inclined plane test (IPT)). Accordingly, the results revealed that the as-prepared coating can endow high DC flashover strength, low leakage current, acceptable tracking resistance, and superhydrophobicity, with universal applicability to various substrate materials.

4.3 Materials and Methods

4.3.1 Materials and Coating Preparations

The materials utilized for the fabrication of superhydrophobic coating are introduced in **Table 4-1**. The coating was applied by spraying a mixture of nanoparticles and organosiloxane on the surface of a methoxy functional silicone resin [33]. Firstly, a mixture of 0.7 g fumed silica nanoparticles and 0.5 g MTES in 60 ml ethanol was prepared using an ultrasonicate prob for 15 minutes. SILIKOPHEN AC 1000 (resin) was diluted in butyl acetate by mechanical agitation and tetra-n-butyl titanate (catalyst) was subsequently added and stirred for 5 minutes to obtain a homogenous mixture. The resin mixture was sprayed on the substrates and placed in the oven for an initial surface curing (10 min @ 70°C). Lastly, the nanosilica mixture was sprayed on the surface-cured resin and cured for 2h at 70°C.

Table 4-1. Materials for development of superhydrophobic coating.

Material	Company	Function
SILIKOPHEN AC1000	Evonik Co.	Resin
Tetra-n-butyl titanate	Sigma	Catalyst
Methyltriethoxysilane (MTES)	Sigma	Surface treatment/Coupling agent
AEROSIL R812S	Evonik Co.	Fumed silica NPs (BET 195-245 m^2/g)
Ethanol and Butyl acetate	Fisher scientific	Solvent
Porcelain/Glass/GPO3*	-	Substrates

*GPO3 is a glass reinforced thermoset polyester sheet material with excellent electrical properties including flame, arc, and track resistance and is used for electrical insulating applications.

The preparation of superhydrophobic coating is schematically presented in **Figure 4-1**.

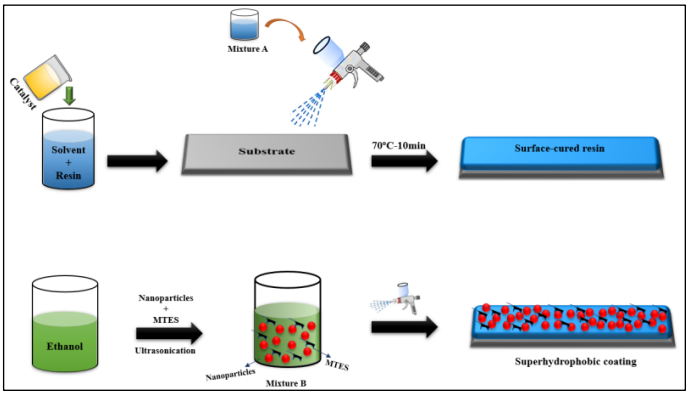

Figure 4-1. Preparation of superhydrophobic coatings [35].

4.3.2 Characterization

The Kruss ™ DSA100 CA goniometer was utilized to evaluate the wettability of samples by depositing a water droplet (4 µl) on each sample, allowing the static and dynamic CA (WCA and CAH) measurement at room temperature via Young-Laplace equation fitting. The reported values were the average of four measurements. For measuring the CAH, the droplet was brought in contact with the surface. The substrate was moved using a micrometer screw in one direction while holding the droplet with a needle, and the CAs appearing at the front and back of the droplet (called advancing and receding CAs, respectively) were measured. The difference between the advancing and receding CAs was reported as the CAH.

The chemical composition of coatings was characterized using a Cary 630 Fourier Transform Infrared spectrometer (FTIR, Agilent, USA) in attenuated total reflection (ATR) mode in the infrared range of 400–4000 cm^{-1}.

Scanning electron microscopy (SEM) images were taken on a JSM-6480 LV SEM instrument manufactured by JEOL Japan to observe the micro-nanostructure morphology of the developed coatings. The samples were sputter coated with a thin gold film before imaging.

An optical surface profiler (Profil3D Filmetrics, USA) was employed to measure the surface roughness. The roughness values were calculated based on the ASME B46.1 2D and ASME B46.1 3D standards.

The thermogravimetric analysis (TGA) was performed to assess the thermal stability of the coatings using a NETZSCH STA 449C thermogravimetric analyzer within the temperature range of 30–700°C and at the heating rate of 10°C/min in an argon atmosphere using graphite crucible.

A QUV accelerated weathering tester was used to evaluate the destruction of the surface nonwetting properties to simulate outdoor conditions within a controlled laboratory setting. The coatings were applied on glass plates. Accelerated weathering measurement was performed using a QUV/Spray Accelerated Weathering Test Chamber by Q-Lab Corporation USA. The tests were conducted according to ASTM G154 using UVA-340 fluorescent lamps. The test comprised a cycle of 8 h UV radiation (temperature of 60°C), followed by 4 h condensation (temperature of 50°C) and irradiance of 0.89 $W.m^{-2}$. Then, the WCA measurement was performed.

The dielectric response of the coatings was investigated with the assistance of a Novocontrol broadband dielectric spectrometer (Microtonic Alpha-A high-performance frequency analyzer). The measurements were carried out at room temperature and over a wide range of frequencies varying from 10^{-4} Hz to 10^{3} Hz. For each measurement, the disk-shaped samples with a diameter of 46 mm and a thickness of approximately 2 mm were placed between the two solid electrodes, forming a plane–plane capacitor. The applied AC voltage was 3 V.

The flashover voltage measurements on the coating surface were conducted using a rod-plate configuration under the application of AC voltage (shown in **Figure 4-2 a, b**). The coatings were applied on porcelain plates that were cut from real high voltage insulators. These samples were fixed into a custom-made setup between two electrodes to eliminate the effect of distance and sample size (fixed distance = 36 mm). First, the voltage was increased rapidly to a certain value before any visible discharge activity (up to 50% of the estimated flashover value). Then, the voltage was continuously increased by 0.5 kV/s rate and stopped automatically at the first complete discharge. The procedure was repeated 10

times on each sample with 2 min intervals to allow possible residual charges to dissipate. For this test, porcelain, pristine resin, and superhydrophobic coating were tested in nonpolluted/dry/horizontal, polluted/dry/horizontal, and polluted/wet/horizontal conditions, respectively. Kaolin was mixed with deionized water and used as the pollutant mixture. A certain amount of pollutants was placed on the surfaces, and the samples were left at room temperature for water evaporation. Then, the samples were washed with 5 ml of water droplets by a syringe. The as-prepared samples were used for the polluted states. For the wet states, a spray of water droplets was applied to the samples before each voltage application.

In order to do tests under wet surface conditions, the condensation test was performed under electric field stress using the test suggested by J. Wu et al. [508]. The moisture can be condensed on the surface when the surrounding air contains high humidity levels, and the air temperature exceeds the superficial insulator temperature. Under these circumstances a thin wet layer (dew) can be formed on the surface. The coatings were applied on GPO3 substrates and placed inside a chamber with controllable temperature and humidity. Then, the temperature inside the chamber was varied between 35 and 10°C once in an hour while keeping the relative humidity constant at 95%. The leakage current was monitored while an electric field stress of 4 kV/cm was applied to the sample. This test could be used to evaluate the performance of superhydrophobic coatings under high voltage in humid conditions.

The erosion and tracking resistance of the coatings were evaluated using the IPT based on an adapted version of IEC 60587 to be suitable for thin films. In this test, the coatings were applied on rectangular standard size GPO3 substrates (50 mm width, 120 mm length, and 5.5 mm thickness) and placed at an inclination angle of 45° while applying an AC voltage through electrodes. An electrolyte solution (a mixture of 0.1 wt.% NH_4Cl and 0.02 wt.% Triton X100 in deionized water; conductivity of the solution, 3.95 Ωm ± 0.05 Ωm @ 23° ± 1°C) was streamed along the coating surface at a constant flow rate of 0.6 ml/min between the two electrodes through filter papers placed under the top electrode. The mounted sample is shown in **Figure 4-2 c, d.** A 60 Hz-high voltage was applied to the samples when a uniform flow of the contaminant covered the surface of the tested sample. The adapted test method is based on the stepwise voltage increase method in the IEC 60587 and consists of three steps,

each lasting 45 mins at 2.5, 3, and 3.5 kV. This test intends to promote partial arc discharge formations to evaluate the material's resistance to erosion and tracking. A carbonaceous path, called a track, appears during the test because of the arcing on the surface. Therefore, the parameters analyzed here are the tracking and erosion lines on the coating surface, leakage current, visual observation of the arcing activity, and the temperature evolution along the surface using a thermal camera. The existence of a wetting agent (Triton X100) in the streaming solution destroys the inherent hydrophobicity of the samples, which can simulate the aged phase of the coatings.

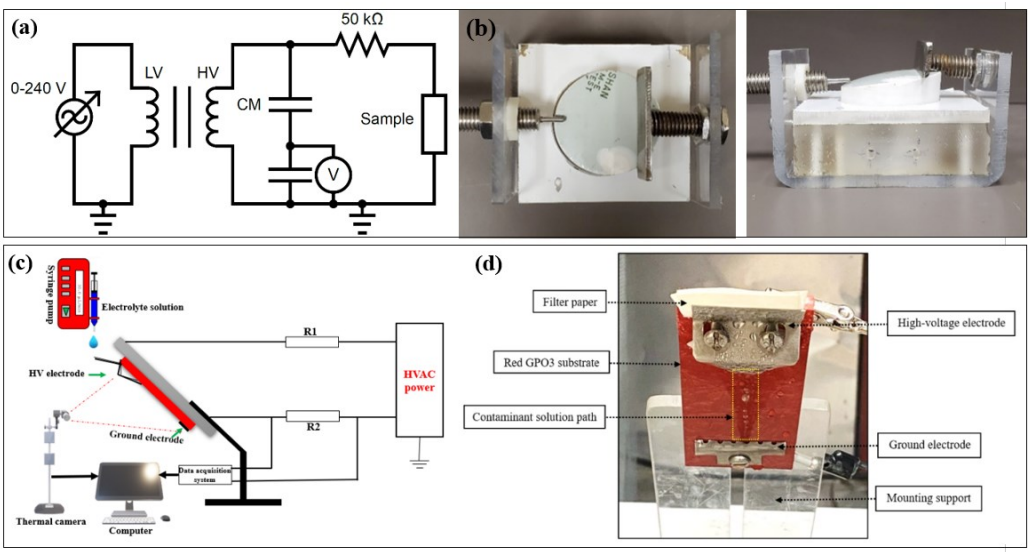

Figure 4-2. a) Electrical circuit for the FoV measurements; b) Top and front view of the flashover setup; c) Test setup for the IPT; d) Parts utilized for mounting the specimen.

4.4 Results and Discussion

4.4.1 Wettability Measurement

The WCA and CAH of the samples were measured and reported in **Table 4-2**. to quantify the degree of nonwettability. The pristine sample is referred to as the coating layer of SILIKOPHEN AC1000 before being superhydrophobically treated.

Table 4-2. WCA and CAH data for samples.

Sample	WCA (°)	CAH (°)
Superhydrophobic coating	163 ± 2	2.3 ± 0.3
Pristine coating	79 ± 2	9.3 ± 1.5
Porcelain	34 ± 1.8	32.5 ± 1.7
GPO3	82 ± 1.5	39.3 ± 1.5

The surfaces with CAs less than 90° show hydrophilic behaviors and are wetted with water easily. CAH is responsible for the rolling or sliding of droplets on the surface, which plays a crucial role in the accumulation of water on surfaces, i.e., the lower the CAH is, the higher the sliding/rolling of water is on the surface. Therefore, the pristine, porcelain, and GPO3 samples are hydrophilic. The pristine sample shows low CAH, whereas the porcelain and GPO3 samples depict high CAH values, leading to inevitable water accumulation on their surfaces. The wettability of different samples is shown in **Figure 4-3** by colored water droplets.

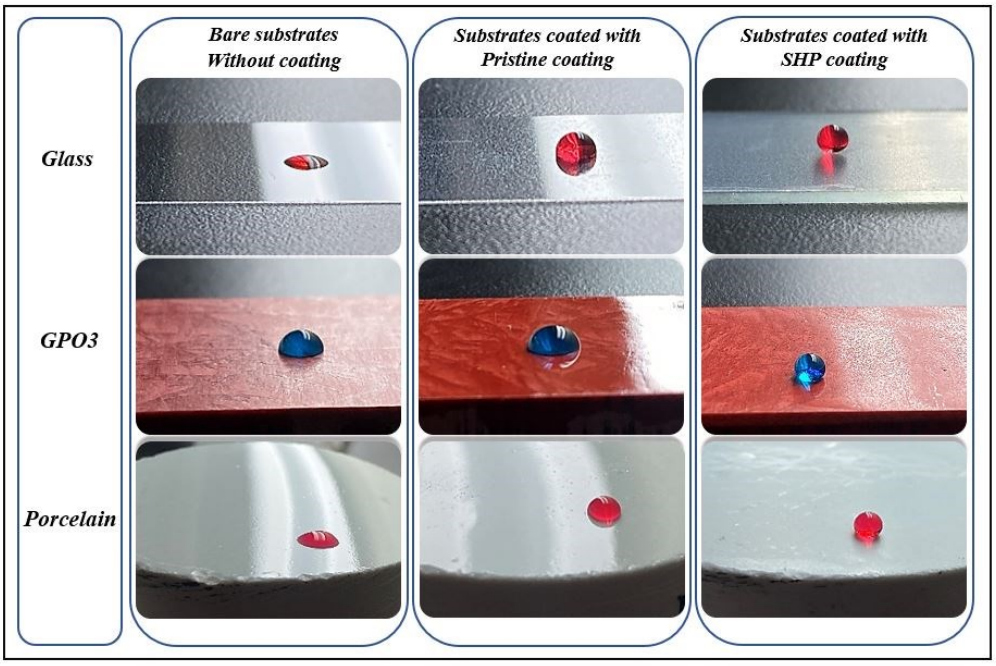

Figure 4-3. Wettability of bare substrates, pristine, and SHP coatings shown by colored water droplets.

4.4.2 FTIR

To investigate the chemical composition of the coatings, the FTIR spectroscopy results for pristine resin and SHP coatings are presented in **Figure 4-4.** As detected in the FTIR spectra, the pristine sample contains polar groups (Si-OH) in the high wavenumber range of 3500–3000 cm^{-1}. These polar groups are responsible for the hydrophilic nature of the pristine sample. After the superhydrophobic modification, as observed for the SHP sample, these peaks are eliminated in the blue-line spectra indicating that the surface is thoroughly covered with nonpolar moieties. The other peaks at1260 cm^{-1} and 1020–1070 cm^{-1} are associated to CH_3 deformations in Si-CH_3 and stretching of Si-O-Si bonds and asymmetric Si-O-C vibrations. The CH_3 rocking and Si-C stretching in Si-CH_3 are also detected in low wavenumber ranges of 780–790 cm^{-1}.

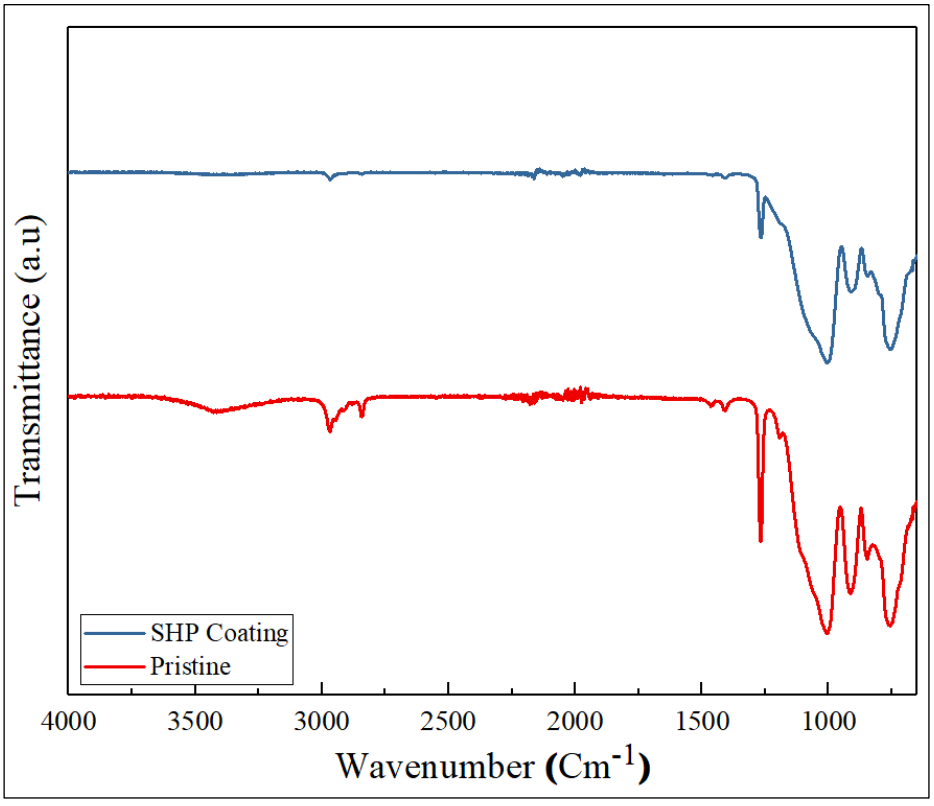

Figure 4-4. FTIR spectra for the pristine resin and superhydrophobic coating.

4.4.3 SEM

As shown in **Figure 4-5 t**he SEM images were taken to understand the surface morphology of the samples. The SEM images of the pristine sample exhibit a smooth and homogenous surface (**Figure 4-5 a**). The incorporation of silica nanoparticles leads to the formation of a compact network of nanoparticles bonded with the assistance of resin as observed in the SHP sample (**Figure 4-5 b, c, d**). The resin possesses good wetting properties for nanoparticles because the SEM images have no signs of huge aggregations or phase separation. The established hierarchical porous conformation is responsible for lowering the total surface energy and imparting superhydrophobic behavior to the coating by favoring the entrapment of air pockets and the formation of an air cushion layer underneath the water droplets.

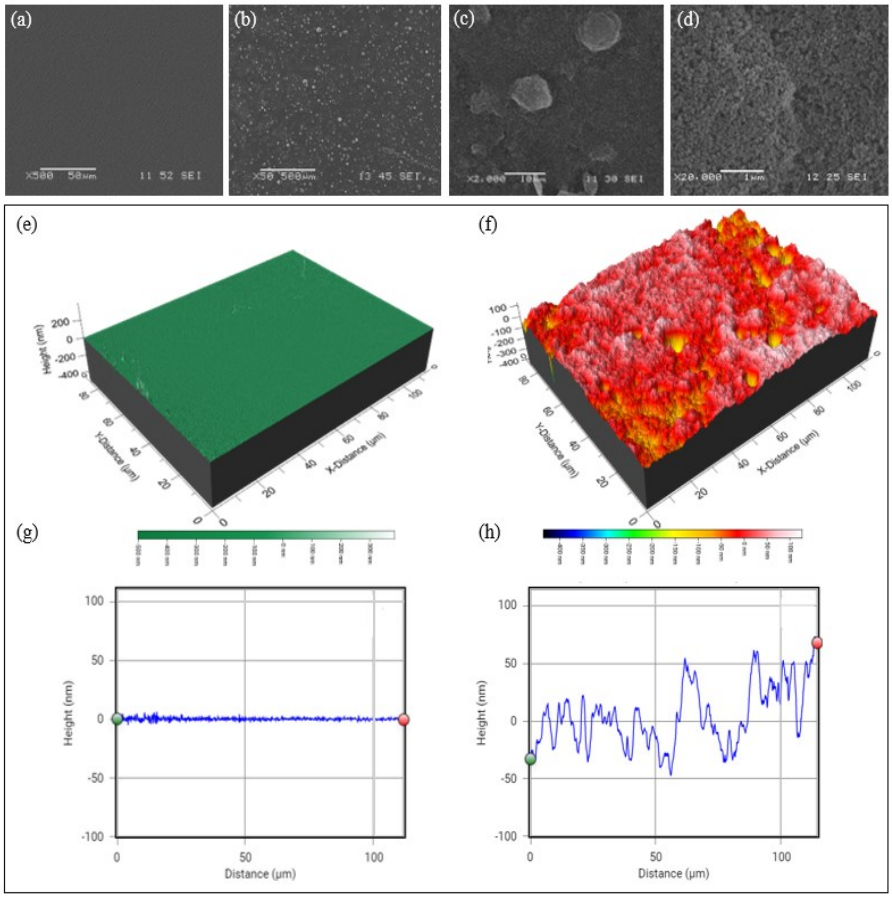

Figure 4-5. SEM picture of a) pristine sample with 500X magnification; SEM picture of SHP coating with b)500X magnification, c)2000X magnification, and d) 20KX magnification; 3D surface profiles in tilted view of e) pristine sample, f) SHP coating; Typical roughness profile traced across the surface of g) pristine and h) SHP coating.

4.4.4 Profilometry Analyses

The surface geometry plays a crucial role in the robustness of superhydrophobic coatings [28]. The surface profiles of the pristine and superhydrophobic coating are illustrated in **Figure 4-5 e-h**. The root mean square (RMS) roughness value represents the standard deviation of the distribution of surface roughness height within the scanned area. The pristine sample has a smooth surface roughness, as observed in the SEM pictures, with the root mean square (RMS) and arithmetic average (S_a) roughness value of 4.759 and 1.786 nm, respectively. Hierarchical structures were created on the surface after the silica NPs were incorporated. Thus, the S_a value increases by up to 38 nm, leading to the formation of a superhydrophobic and transparent coating. The roughness values obtained from profilometry analysis are tabulated in **Table 4-3**.

Table 4-3. Roughness values of the pristine and SHP coatings.

Roughness parameter (nm)	Pristine coating	SHP coating
RMS (S_q)	4.759	54.48
Mean roughness (S_a)	1.786	38
Maximum peak height (S_p)	25.6	277.7
Maximum pit height (S_v)	18.54	347.7

4.4.5 TGA

The thermal stability of the coatings was studied with thermogravimetric analyses. **Figure 4-6 a** shows that the weight loss steps of the pristine resin are slightly more significant than those of the superhydrophobic coating. Silica-based fillers play a vital role in suppressing destructive thermal degradation of silicone resins because of their superior physical reinforcement effect. Thus, the slight enhancement of thermal stability of the pristine resin is triggered by the incorporation of silica nanoparticles within the temperature range of the test. The methyl functionality can intensify the thermal stability of the silicone backbone. This effect can be observed in the TGA results of the SILIKOPHEN AC1000, which is a methyl silicone resin with high thermal stability of up to 700°C and only 13% of

weight loss. Therefore, the developed coating shows to be distinctly stable in high temperatures which can plays a crucial role in high-voltage applications due to the possibility of arcing in which the energy is released as heat on the surface.

4.4.6 Accelerated Weathering

The WCA and CAH results of the superhydrophobic coating within 28 days of the accelerated weathering test are presented in **Figure 4-6 b**. As observed, the coating can maintain its hydrophobic properties during the first 21 days, whereafter the superhydrophobicity of coating is lost. The CAs and CAH values reached 140.1° and 15.2°, respectively. Polymeric materials are prone to degradation when exposed to harsh environmental conditions, particularly UV, resulting in gradual decomposition of chemical structural units. This UV-induced aging could cause hydrophobicity loss, chalking, cracking, and weakening of mechanical strength which leads to shorter service life [509]. Here, the detected superhydrophobic loss can be attributed to the segregation of nanoparticles from the matrix due to the breakage of the formed bonds between them. This scenario leads to the demolition of hierarchical structures. For the pristine resin, the WCA was also decreased moderately within the 28th days and a slight yellowing and haziness was observed.

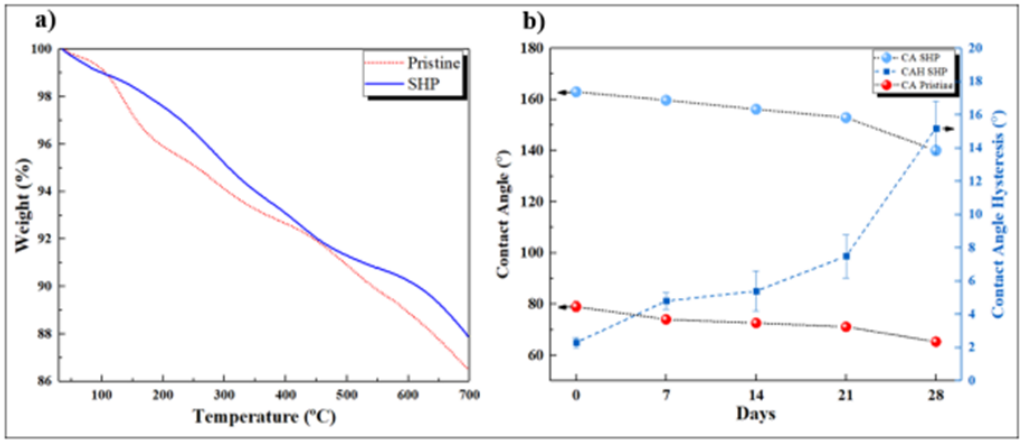

Figure 4-6. a) TGA data for the pristine and SHP coating; b) Wettability variations of the superhydrophobic and pristine coatings exposed to QUV test within 28 days (672 h).

4.4.7 Dielectric Spectra Analyses

Dielectric spectroscopy is used to investigate the coating response when the coating is subjected to an applied electric field of fixed or changing frequency [503]. The dielectric behavior of the superhydrophobic coating and pristine resin has been investigated in a wide range of frequency (f) at room temperature. The real and imaginary parts of dielectric permittivity (ε' and ε'') are presented by

$$\varepsilon' = \frac{C_s d}{\varepsilon_0 A} \quad \text{(Eq. 4-1)}$$

$$\varepsilon'' = \frac{\sigma}{2\pi f \varepsilon_0} \quad \text{(Eq. 4-2)}$$

In these equations, C_s is the measured capacitance of the sample, d is the thickness, A is the electrode cross-sectional area, and $\varepsilon_0 = 8.854 \times 10^{-12}$ F/m is the permittivity of free space.

Figure 4-7a, b represent the variation of ε′ and ε″ as a function of frequency. The graphs in these two figures have the same behavior, where the dielectric permittivity values are high at low frequency, followed by a drastic decrease with increasing frequency.

For the pristine resin, the presence of polar groups, such as C=O and –OH, can induce an imbalance distribution of electrons; thus, dipoles build up [510]. The dipole orientation can be changed by applying the electric field, leading to an increase in the dipole polarization. The absorption of moisture may increase because of the existence of polar functional groups, thereby increasing the dielectric constant and reducing the resistivity.

The high values of ε′ at low frequencies ($f \leq 0.001\ Hz$) are attributed to the alternations of the field's direction, which provide sufficient time for the dipoles to align themselves in accordance with the field. This occurrence improves the interfacial polarization and, consequently, the value of permittivity. The permittivity values for the superhydrophobic coating are lower than those for the pristine resin because the superhydrophobic coating contains minimal polar groups. This improvement stems from the Maxwell–Wagner–Sillars polarization effect, in which the charge carriers inside the

matrix can migrate and accumulate at the interface, thereby enhancing the equivalent capacitance value [511].

In the frequency range ($0.001 \leq f \leq 0.01\,Hz$), ε' values show a substantial decrease. This drastic reduction can be ascribed to the inability of the induced charge carriers to follow the recurring alternation in the field direction, leading to the accumulation of charge carriers [510].

Given the continuous increase in frequency ($f \geq 0.01\,Hz$), the insignificant change in the value of dielectric permittivity can be traced to the small contribution of ionic and electronic polarizations to the dielectric relaxation phenomenon of the induced charge carriers congregated at the interface.

A behavior similar to the real part of permittivity is observed for the imaginary part of permittivity. However, this behavior is more extensive in magnitude in the imaginary permittivity than it is in the real part of permittivity (**Figure 4-7b**).

The dependence of the loss tangent (tan δ) of the coatings on the frequency at room temperature is displayed in **Figure 4-7c**. The loss tangent is computed using the following approximation (by neglecting the loss by conduction):

$$\tan\delta \cong \varepsilon'' / \varepsilon' \qquad \text{(Eq. 4-3)}$$

The tan δ value abruptly decreases within the low-frequency range and stabilizes within the high-frequency range with increasing frequency. The dielectric loss is due to the interfacial polarization within a low-frequency range. However, the incorporation of nanosilica particles can disturb electron mobility within the high-frequency range [512]**.**

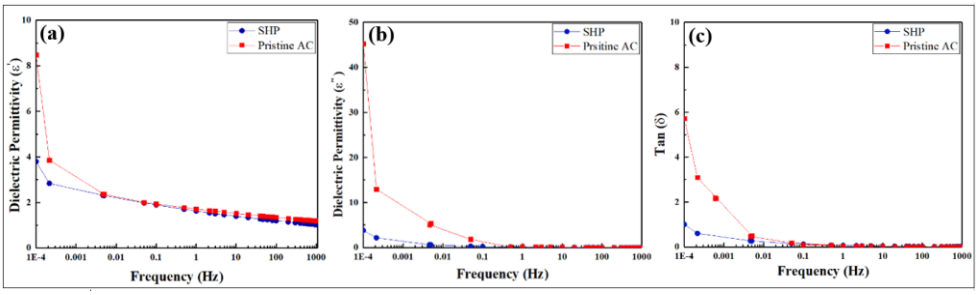

Figure 4-7. a) Real part of permittivity versus frequency; b) Imaginary part of permittivity versus frequency; c) loss tangent of the pristine and SHP coating in different frequencies.

4.4.8 Flashover Voltage

The dielectric strength tests were performed on the coated and uncoated porcelain samples to determine the flashover voltage levels and to evaluate whether the superhydrophobic coating improves the performance of the porcelain insulators under different conditions. **Figure 4-8 a, b, c** shows the results for the flashover voltage for ten repetitive tests on uncoated porcelain, pristine resin coating, and superhydrophobic coating in nonpolluted/dry/horizontal, polluted/dry/horizontal, and polluted/wet/horizontal conditions, respectively. It can be seen in **Figure 4-8 a, b** that the insulation performance is conserved with the two types of coating on the porcelain under dry surface condition (with less than 10% differences in the obtained results). **Figure 4-8 c** shows that the flashover voltage is higher under wet surface condition for superhydrophobic coating during the first tests. This can be explained by the fact that the water film is not continuous on the superhydrophobic coating, but only separate water droplets are present. Thus, the wetted superhydrophobic coating preserves an insulation capacity almost similar to dry surface. However, after a certain number of discharges, the water film becomes more and more continuous, and the flashover voltage decreases during the subsequent tests. After several tests, similar results are obtained than for uncoated porcelain and pristine coating. The experiment seems to indicate that repeated electrical arcing may cancel the superhydrophobic property of the coating on the pathways of sever arcs.

Figure 4-8 d summarizes the voltage for the first flashover tests in different conditions (the following abbreviations are used: D: Dry, P: Polluted, Non-P: Non-polluted, HM95: Humidity 95%, H: Horizontal, V: Vertical, W-S: Wet-state). The results reveal that the superhydrophobic coating can successfully maintain or increase the flashover voltage in all tested conditions. The superhydrophobic

coating shows good performance in particular for the wet state under the nonpolluted and polluted conditions for the first 1–3 flashovers because of the nonwetting and self-cleaning behavior of the superhydrophobic coating. Thus, the positive effect of surface nonwettability on delaying flashover-driven issues could be observed.

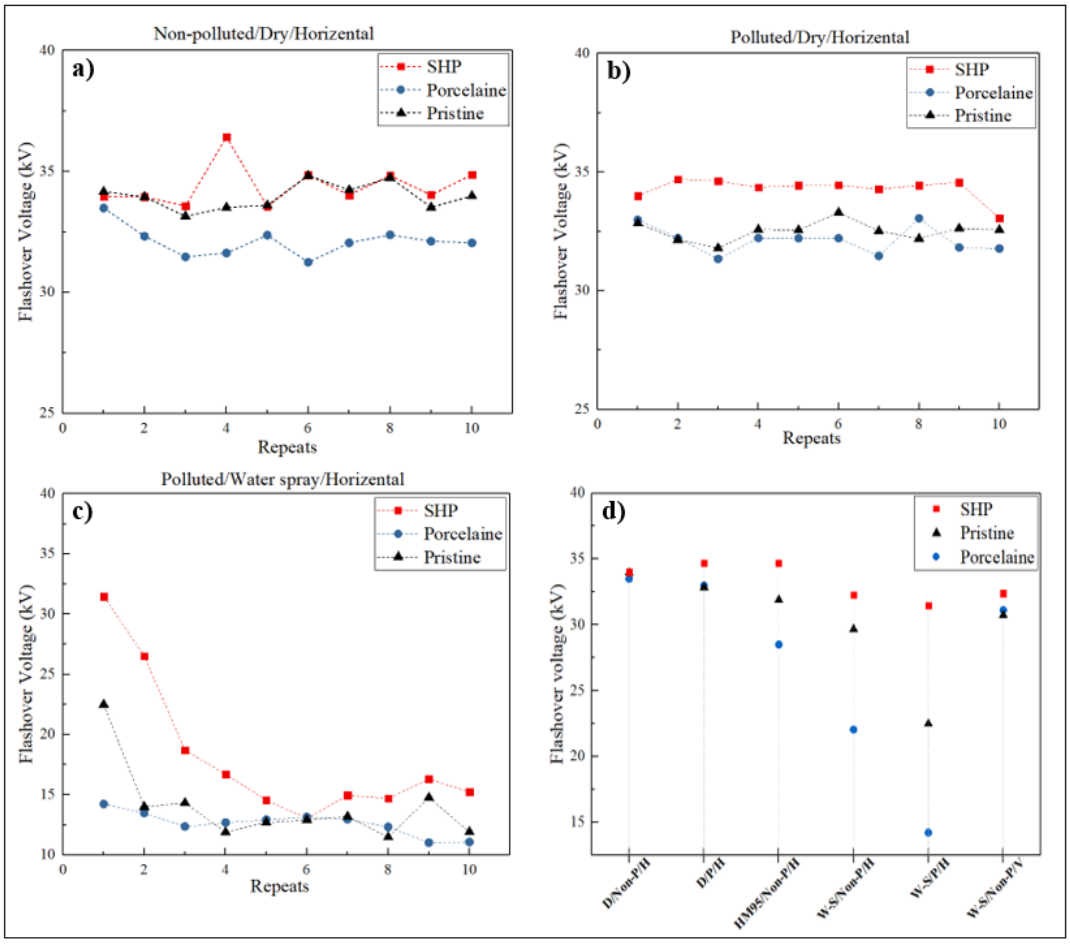

Figure 4-8. Ten repetitive flashover tests in a) nonpolluted/dry/horizontal, b) polluted/dry/horizontal, and c) polluted/wetted/horizontal conditions; d) FoV measurement in different conditions (first FoV).

4.4.9 Condensation Test

The condensation test was used as a second experimental method to investigate the electrical insulation performance of the superhydrophobic coating. The applied high voltage during this condensation test was adjusted so that no visible discharges were created. **Figure 4-9** shows the test results for three different surfaces: uncoated GPO3, pristine resin coating, and superhydrophobic coating. **Figure 4-9 a** shows the results for the leakage current measurements during several heating and

cooling cycles and **Figure 4-9 b** shows the average of the three cycles. It can be observed that all three types of surfaces exhibit similar leakage current values for dry surface condition (time period between 30 and 60 minutes in **Figure 4-9 b**). However, the leakage current of the coatings was much lower for wet surface condition (time period between 0 and 30 minutes in **Figure 4-9 b**). The smallest leakage current was obtained for the superhydrophobic coating. Furthermore, the decrease in leakage current was observed in all repetitive test cycles.

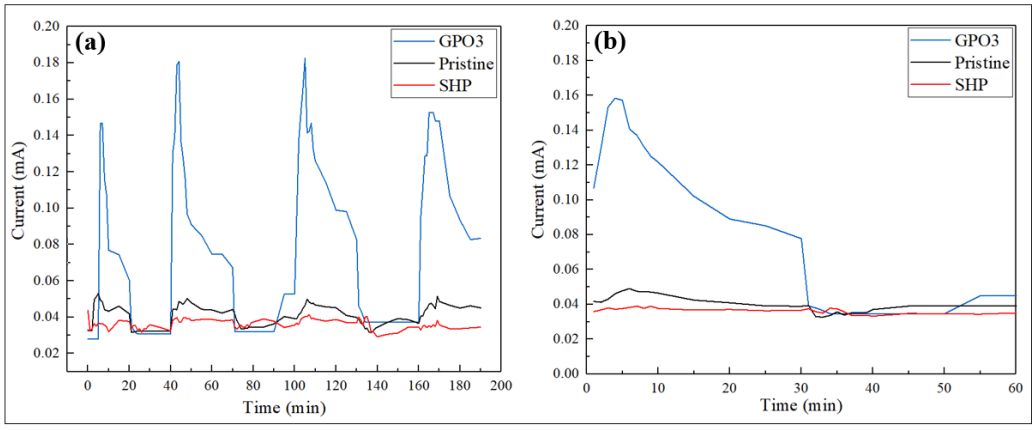

Figure 4-9. Leakage current plots versus time on different samples for the condensation test. a) Three repetitive cycles and b) average of the three cycles.

This experiment provides indications that the superhydrophobic coating can decrease the leakage current in humid atmospheres. The leakage current is one of the important factors for judging the level of insulation [513], [514]. Thus, the low leakage current values for the developed superhydrophobic coating indicate that the insulation performance of this coating is better than that of the surfaces with high degrees of wettability. This improvement was conserved during several repetitive test cycles. However, the obtained test data is not yet sufficient to draw any conclusions on the long-term stability of the insulation properties of the superhydrophobic coating. A test series with a much higher number of repetitions is planned on order to gain such data in the future.

4.4.10 Inclined Plane Test

The visual aspects of the erosion and tracking of samples were inspected after the IPT, as shown in **Figure 4-10 a**. The tracking usually starts at the lower ground electrode because of the continuous

sparks and moves toward the high-voltage electrode. The erosion usually follows a defined area on the sample surface. The leakage current flows on the contaminant path, causing discharges. Concomitant failure of the material may happen with time because of tracking and erosion. In this scenario, the pristine resin shows severe tracks and cracks on its surface, whereas the superhydrophobic coating depicts minimal tracks. This phenomenon can be due to the incorporation of silica nanoparticles into the SHP coating formulation that plays an important role when the surface is exposed to leakage current and/or arcing. Consequently, resistance to degradation at high temperatures is improved. The silica nanoparticles effectively delay the induction of hot spots, dissipating them during the dry band arcing and suppressing progressive erosion [515], [516]. The arcs with temperatures up to 700°C were monitored during the test via a thermal camera (**Figure 4-10 c**). The surface temperature does not exceed 80–90°C. The development of the leakage current on the surface of the samples was also monitored during the test. At first, no discharges were observed on the samples when the voltage was applied. However, as the test continued, discharges initiated from the top electrode and moved downward along the contaminant stream as blue lights. Intense bright yellow arcs were occasionally observed, rooted at the lower electrode. These current arcs are responsible for the erosion of the surfaces during the test time. **Figure 4-10 b** shows the comparison between the average current evolution results for the pristine coating, superhydrophobic coating, and bare GPO3 substrate. The peak values were at the low levels within 5–12 mA for the initial step, 12–17 mA for the second step, and 17–23 mA for the final step for the test duration on all the samples. The GPO3 substrate showed the lowest leakage current in the IPT. During the test, the pristine resin performed better than the superhydrophobic coating in the case of leakage current when exposed to 2.5 and 3 kV. However, the superhydrophobic coating showed lower leakage current values by increasing the voltage to 3.5 kV. This behavior can be attributed to the increased degradation of pristine coating in time compared with the SHP coating. This finding means a considerable loss in its performance, i.e., the pristine coating is degraded, and high leakage currents flow through the damaged surface.

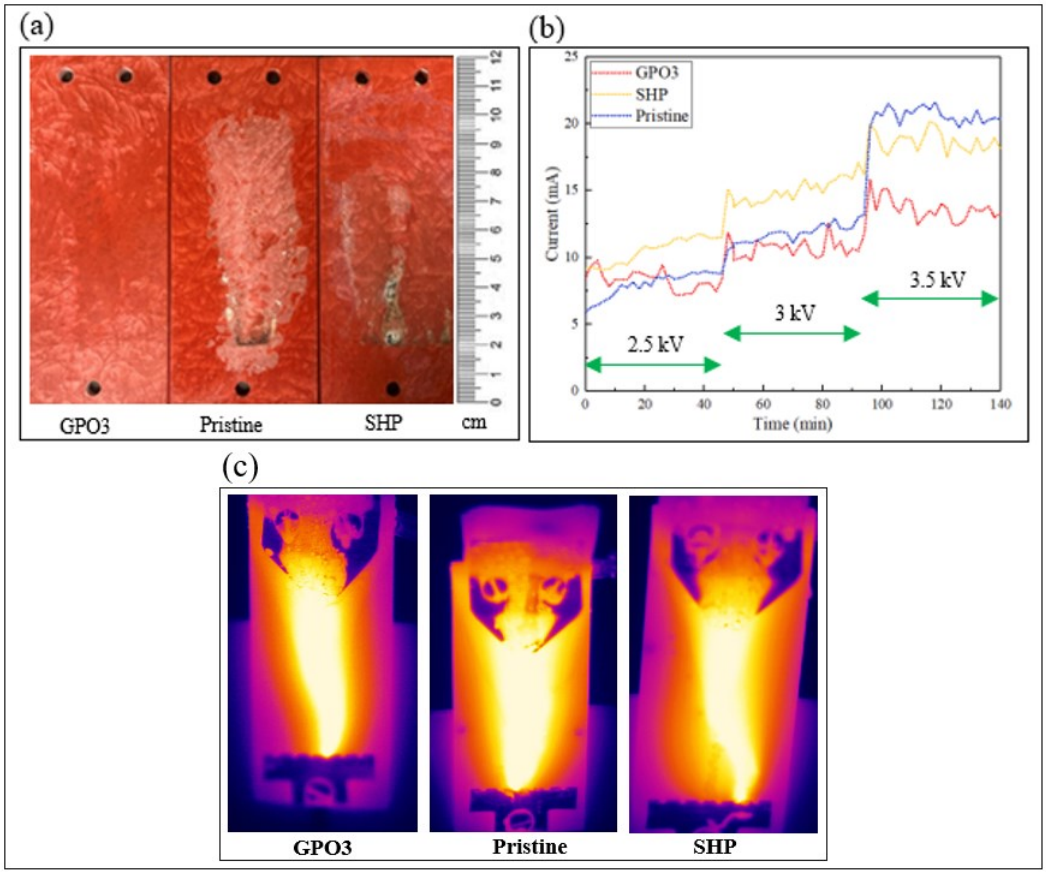

Figure 4-10. a) Visual inspection of the samples after the IPT; b) Leakage current plots versus time on different samples in the IPT; c) Thermal camera images of the samples at the final minutes of the test.

The SHP coating loses its superhydrophobicity because of the degradation effect of high voltages. However, a part of its hydrophobicity was restored within one week.

4.5 Conclusion

Controlling surface wettability is a promising solution to avoid unexpected failures for outdoor insulators. Superhydrophobic nanocomposite coatings are promising alternatives for conventional silicon rubber coatings because of their high water repellency, icephobic properties, and the possibility of surface self-cleaning. However, it is still a complex challenge to obtain a robust non-fluorinated superhydrophobic coating within a simple and substrate-independent fabrication method that is capable to withstand harsh conditions for multifunctional purposes. A silicone-based superhydrophobic coating was developed via spraying method. For enhancing the robustness of the hierarchical structures resulting in non-wettable behavior, the possible crosslinking sites between the silica nanoparticles and the

methoxysilane binder were increased using methyltriethoxysilane as coupling agent. The coating, applied on the porcelain and glass substrates showed a high WCA of 163° and a low CAH of 2.3°. These characteristics led to easy water roll-off, self-cleaning, and very low ice adhesion on its surface, as shown in a previous study [35]. The observed ultra-nonwetting behavior was triggered by the low surface energy of silicone resin and a hierarchically roughened surface morphology due to the incorporation of nanoparticles, as investigated through FTIR, SEM, and surface profilometer. TGA was also utilized to assess the thermal resistance of the coating. The results confirmed the stability of coating even at high temperatures. The coating could withstand harsh condensation cycles and UV radiance through an accelerated QUV weathering test.

A comprehensive set of experiment was designed and performed in order to thoroughly evaluate the behavior of the coating under various electric field conditions.

Firstly, to measure the dielectric permittivity and loss factor of the SHP coating, a dielectric spectrometer was utilized, and the results revealed that superhydrophobic modification of the surface could decrease both these values compared to those of the pristine sample within the frequency range of 10^{-4} Hz to 10^{3} Hz.

Secondly, a condensation test was employed to investigate the coating's performance when exposed to dew conditions to know whether superhydrophobicity is capable of enhancing the insulation performance of the system. The leakage current results showed that compared with a pristine coating with high degrees of wettability (WCA = 79°), the superhydrophobic coating successfully reduced the leakage current on the surface in humid environments.

Thirdly, the flashover voltage was measured on the SHP coating and a bare porcelain sample which was cut from a real insulator. The observed values in particular for wet and polluted conditions verified the beneficial effect of superhydrophobicity on increasing the flashover voltage.

Lastly, the erosion and tracking of the samples were monitored through an inclined plane test setup. The superhydrophobic coating depicted minimal tracks by the end of the test. As well, monitoring

the leakage current values showed more stable behavior for the superhydrophobic coating even by increasing the voltage to 3.5 kV.

To conclude, the results indicated that the developed superhydrophobic coating shows promise in the laboratory experiments. The authors would like to investigate the real-life insulators to confirm the results in actual scenarios.

Acknowledgment

The authors acknowledge the financial support from the Natural Sciences and Engineering Research Council of Canada (NSERC); Hydro-Québec, Québec, Canada; and le Pôle Recherche Innovation en Matériaux avancés du Québec (PRIMA Québec), Québec, Canada. They also thank M. Luc Chatigny, technician of Laboratoire Revêtements glaciophobes et ingénierie des surfaces (LARGIS), for performing the high voltage tests, Ms. Kouba Marie Lucia Yapi for the dielectric spectroscopy analyses, and Ms. Caroline Potvin at the Université du Québec à Chicoutimi for providing access to the instruments used for the chemical analyses.

CHAPTER 5:

DEVELOPMENT OF ALL-SILICONE SPRAYABLE SELF-HEALING SUPERHYDROPHOBIC COATING

6.1 Abstract

The impressive advancements in new materials and processes attained since the 20th and the 21st century, the demand for new generations of materials with specific functionalities is highly emerging. Self-healing ability is striking in the current environmental circumstances as-far-as the demand for prolonging the lifespan of products and reducing waste is irresistible. In this paper, the self-healing ability of microcracks was introduced into a fluorine-free superhydrophobic coating via the incorporation of microcapsules containing a silicone resin (DMS-S12) and catalyst (dibutyltin dilaurate, DBTL) inside poly (melamine urea formaldehyde) shells. The designed self-healing system is well aligned with the chemistry of the superhydrophobic coating from two points of view. Firstly, the silicone nature of the coating will remain almost unchanged after healing action, and secondly, the present free ethoxy groups of the superhydrophobic coating could act as bridge linkage between the healed region and the matrix. The synthesized microcapsules showing mean diameters of 18 and 16 were sought-after for the application in surface coating. The water contact angle on the coating reached to 165°, while the contact angle hysteresis value of 3.6° verified the superb non-wettability of the coating. The self-healing ability of the coating was visually inspected using microscopy imaging of a microcrack. Also, electrochemical impedance spectroscopy (EIS) was utilized to quantify the self-healing ability of the as-prepared coating. The self-healing efficiency and delamination index of the coating were calculated using charge transfer resistance (R_{ct}) and impedance ($Z_{0.01\ Hz}$) data indicating self-healing efficiency of up to 96% comparing to the blank superhydrophobic coating. The self-healing sample also showed lower delamination index value validating the reparation of the formed microcrack after 48 hours.

6.2 Introduction

Designing multifunctional mechanisms has been a striking methodology within the recent decades aiming at extending the efficient service life of protective coatings [517]. These coatings are able to respond to a variety of external stimulus thereby withstanding harsh conditions.

Superhydrophobic coatings with superior self-cleaning, icephobic and anti-corrosion characteristics have been lately well executed in scientific literature. However, as the coatings service life increases, the occurrence of cracks, abrasions, and mechanical damages will be inevitable [518]. Such mechanical defects in a polymeric coating can lead to major losses in their functionality [519], [520]. Self-healing ability is a distinguished feature of the living organism helping them prevent losing their functions. As a particular example, human skin is healed through an inflammatory response of cells below the dermis layer via increasing the production of collagen and regenerating epithelial cells and tissue [266]. The impressive advancements in new materials and processes on smart materials has led to the design and fabrication of different types of self-healing coatings capable of restoring their structural integrity after damage [24], [367], [415], [520]–[524]. In the recent years, self-healing polymers have been widely used in different fields of biomedicine, tissue engineering, and protective coatings [268]–[272]. However, despite the existence of several techniques, reservoir-based self-healing mechanisms are yet the most widely reported methods for conferring the auto-repair ability to the composites and coatings [374], [396], [406], [415], [525]. This method has been categorized within different aspects based on the arrangement of the healing agents and catalysts while the most extensive arrangement consists of five types: single-capsule, double-capsule, capsule and dispersed catalyst, phase-separated droplet and capsules, and all-in-one capsules [274], [374], [526]–[529]. Comparing to other techniques, the biggest strength of microcapsule-based self-healing approach is that the capsules containing the active materials could be incorporated inside almost any matrix via dispersion and release their core materials only under specific stimuli, in desired situations [521], [530], [531]. Supposing a superhydrophobic coating being scratched and the underneath substrate is exposed to the environment, the crack area could be considered as a domain with different wettability characteristics which might compromise the consistency of the non-wettable surface. Therefore, the film needs to be repaired from the bulk in order to fill the damaged region. Qin et al. [532] fabricated a self-healing superhydrophobic conductor composite which was able to heal through the application of voltage after the surface was severely damaged. The researchers used a mixture of $FeCl_3$, acetylene black (AB), and gallic acid (GA) modified PDMS to develop a conductor material. After the surface modification with nanoparticles and 1H,1H,2H,2H-perfluorodecyl triethoxysilane (PFDS), a composite conductor with water WCA of 155° and CAH of 3° was obtained.

This conductor was able to be re-aligned after it was cut into halves when subjected to 10 V DC power for 1 min via SEM observation. In another study, Xu et al. [533] developed a multifunctional waterborne polyurethane (WPU) coating with self-healing and temperature stimuli-responsive microcapsules. Multicompartment microcapsules were synthesized via Pickering emulsion polymerization using phase change materials (PCMs) and titanium dioxide (TiO_2) nanocapsules as Pickering emulsifiers. The coating using microcapsules exhibited thermal insulation and antireflection properties owing to the application of PCMs and TiO_2, and it also achieved superhydrophobicity. The coating exhibited dual self-healing ability including intrinsically from the self-healing ability of WPU, and superficially due to the release of hydrophobic and fluorinated moieties from microcapsules.

In this paper, the self-healing ability was introduced into a silicone-based superhydrophobic coating by incorporation of microcapsules containing a silicone resin and DBTL catalyst using poly(melamine-urea-formaldehyde) shells via a procedure explained in a recent work [34] with some modifications in order to obtain a size range of sub-50 μm which would be applicable for surface coatings. The self-healing ability of the superhydrophobic coating is investigated via monitoring an applied scratch using SEM imaging and electrochemical impedance spectroscopy in a corrosive media. The utilized encapsulated healing agent is hydrophobic in nature and does not have negative effect on the overall hydrophobic character of the surface. Also, as the surface layers of the coating are thoroughly covered with silica NPs and methyltriethoxysilane (MTES), the scratched region showed similar non-wetting behavior as the undamaged regions after healing of the microcracks. Moreover, the free ethoxy groups of MTES could contribute in the polycondensation reaction of the encapsulated silanol-terminated PDMS (DMS-S12) in the presence of DBTL catalyst, and form an adhesive layer between the crack faces, increasing the robustness of the repaired sample.

6.3 Experimental

6.3.1 Materials and Equipment

The utilized chemicals and their functions are represented in **Table 6-1**. The in-situ polymerizations were conducted in a double-walled reactor (ACE Glass Inc.). To maintain a constant

temperature for the polymerization, a circulating water bath was used. A homogenizer and digital overhead stirrer were used to obtain fine distribution of microcapsules and properly mix the emulsion bath.

Table 6-1. The materials used in the fabrication of self-healing microcapsules and superhydrophobic coating.

Role of material	Material	Company
Core healing agent	Silanol terminated polydimethylsiloxane (DMS-S12)	Gelest
Core catalyst	Dibutyltin dilaurate (DBLT)	Fisher Scientific
Shell forming components	Urea	Alfa Aesar
	Formaldehyde (37% solution)	Alfa Aesar
	Melamine 99%	Alfa Aesar
	Resorcinol 99%	Alfa Aesar
Electrolyte	Ammonium chloride 98%	Alfa Aesar
Emulsifiers	Poly (ethylene-alt-maleic anhydride) (EMA)	Sigma Aldrich
	Sodium dodecylbenzene sulfonate (SDBS)	Fisher Scientific
Matrix	SILIKOPHEN AC1000	Evonik Co.
Catalyst	Tetra-n-butyl titanate	Sigma
Nanoparticles	AEROSIL R812S	Evonik Co.
Crosslinking agent	Methyltriethoxysilane	Sigma
Solvent	Ethanol	Fisher Scientific

6.3.2 Preparation of microcapsules

The PDMS and DBTL microcapsules were prepared according to the procedures shown in **Figure 6-1**. Firstly, emulsifier (poly (ethylene-alt-maleic anhydride), EMA, and Sodiumdodecylbenzenesulfonate, SDBS) was dissolved in deionized (DI) water followed by the addition of core material and homogenization process in order to obtain very fine droplets of core material emulsified in water. After addition and dissolution of shell forming materials and pH adjustments, the bath was heated to reach the appropriate temperature. The polymerization process was continued for 3 h, then cooled and filtered by the help of vacuum pump and washed thoroughly by DI

water and ethanol. The dried microcapsules were obtained after 24 h of air and vacuum drying at room temperature.

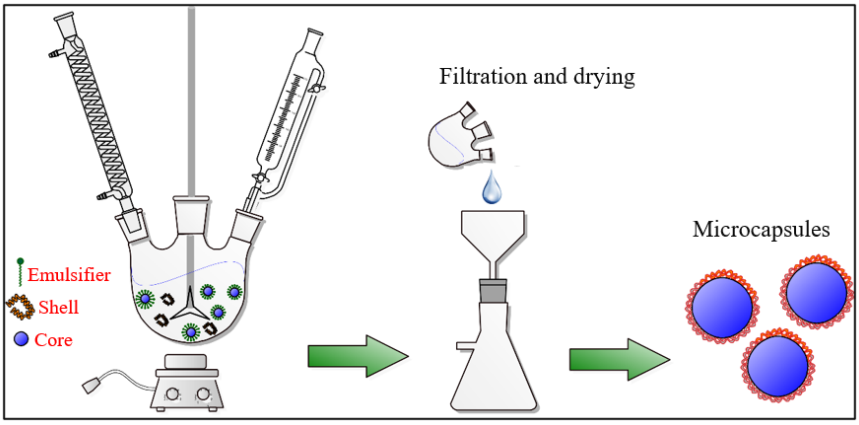

Figure 6-1. The synthesis procedure for microencapsulation of DMS-S12 and DBTL in MUF shell.

The fabrication procedure was optimized based on parameters mentioned in **Table 6-2** to acquire a size distribution of 10-50 µm. For this purpose mechanical agitation with overhead stirrer was replaced by a homogenizer in order to decrease the particle size of core droplets in the water phase. Core:shell ratio was also adjusted to provide sufficient shell material for the core droplets as explained in 2, Section 2.4.1. Microcapsules within this size range could be well-dispersed inside the coating and provide appropriate amount of healing agent for the possibly formed microcracks.

Table 6-2. The synthesis and process parameters for the preparation of PDMS and DBTL microcapsules.

PDMS-MUF microcapsules	DBTL-MUF microcapsules
Agitation: Homogenizer, 5000 W, 15 minutes; Core/shell ratio: 1.5; EMA wt.%: 1.5; Temperature: 70°C; Reaction time: 3h.	Agitation: Homogenizer, 5000 W, 15 minutes; Core/shell ratio: 2; SDBS wt.%: 1.5; Temperature: 70°C; Reaction time: 3h.

6.3.3 Preparation of Self-healing Superhydrophobic Coating

The as-prepared microcapsules were dispersed in a mixture of butyl acetate (solvent) and SILIKOPHEN AC 1000 (resin) in weight ratio of PDMS-MUF: DBTL-MUF: Resin ratio of 10:1:100

via mechanical agitation. Tetra-n-butyl titanate (catalyst) was added and stirred for 5 minutes to obtain a homogenous mixture. The mixture was spray coated on the substrates and placed in the oven for curing. A mixture of 0.7 g fumed silica nanoparticles and 0.5 g MTES in 60 ml ethanol was prepared using an ultrasonicator prob for 15 minutes and sprayed on surface-cured samples to obtain the superhydrophobic structure. The schematic of the preparation of self-healing superhydrophobic coating is illustrated in **Figure 6-2**.

The coding of the samples used in this paper are SHP-self healing (superhydrophobic coating with 10% of self-healing microcapsules), SHP-bare (superhydrophobic coating without self-healing microcapsules), and Pristine (blank SILIKOPHEN AC1000 cured resin).

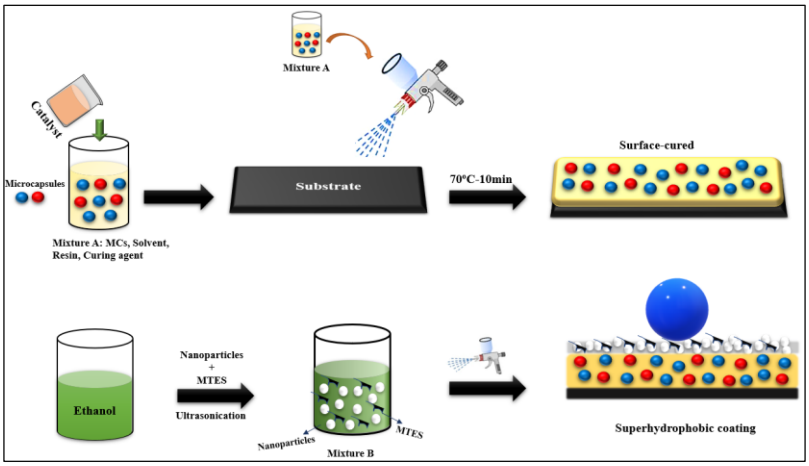

Figure 6-2. The schematic presentation of developing self-healing superhydrophobic coating.

6.4 Characterization

6.4.1 Microcapsules Characterization

Scanning electron microscope (JSM-6480 LV SEM, JEOL, Japan) was utilized to observe the synthesized microcapsules. The size distribution of microcapsules was obtained via measuring the diameter of microcapsules using ImageJ software.

6.4.2 Surface Characterization

The coatings were applied on stainless steel substrates and thickness was measured using Elektrophysik MiniTest70 coating thickness gage.

The sessile drop method was carried out using a Kruss™ DSA100 goniometer to measure the water contact angle of the coating. For estimating the CAH, a 4-µL water droplet was brought into contact with the surface and held with a stationary needle. The contact angles appearing at the front and back of the droplet while moving the substrate by a micrometric screw were measured as advancing and receding contact angles, respectively. The tests were repeated on five different spots and the average values were reported with the associated standard deviations. Sliding angle was measured by a home-made tilting stage. A 10 µL water droplet was placed on the samples which were fixed on a tilting stage. The stage was inclined until the droplet began to slide or roll off. Sliding angle was measured as the stage angle at 0.5 s before the droplet began to slide.

Self-cleaning properties of the coating was investigated using dye powders as contaminants. A layer of the dye was placed on the coating and water droplets were used to investigate the ability of surface to remain clean.

Scanning Electron Microscopy (SEM) was performed by a JSM-6480 LV microscope to survey the surface morphology of the self-healing superhydrophobic coating. Samples were sputter-coated with a thin layer of gold prior to SEM analyses.

6.4.3 Self-healing Characterization

6.4.3.1 Imaging

For observing the self-healing function of the coating, a razor blade was utilized, and 20-30 µm-width cracks were applied. The scratched samples were placed at room temperature to ensure the healing action prior to SEM observation.

6.4.3.2 Electrochemical Impedance Spectroscopy analyses (EIS)

EIS analysis is employed as non-invasive technique to indirectly assess the self-healing process by monitoring the coatings corrosion resistance in time [534], [535]. EIS tests were conducted using BioLogic SP300 potentiostat equipped with LClab software and measurements were repeated at least two times to ensure reproducibility. A scratch was made on the coating samples (Pristine, SHP-bare, and SHP-self healing) by a razor blade, and the samples were left at room temperature for 24 h prior immersion in 0.05 M NaCl solution (Scratch 25 μm was obtained ensuring to reach the metallic substrate).

EIS measurements were conducted in a conventional three-electrode cell with a graphite rod counter electrode and a saturated Ag/AgCl electrode as reference electrode. The working electrodes were coated carbon steels (surface area of 1 cm^2). The cell was placed in a Faraday cage to avoid interferences with external electromagnetic fields and stray currents. The experiments were carried out keeping the working electrode at the open circuit potential (OCP), sweeping the frequency of the perturbing ±10 mV amplitude signal in the range within 10 mHz -10 kHz. Bode and Nyquist plots of the impedance data were analyzed with NOVA 1.11 software.

6.4.4 Icephobic Characterizations

For the ice adhesion measurements, the push-off test was conducted in a cold chamber at -10˚C. A thin cylindrical plastic mold (1.2 cm in diameter) was placed on the surface and filled with deionized water to form a cylinder of ice over 24 h. Using a remote computer-controlled interface, the force gauge measured the shear force until the ice was detached. The ice adhesion stress can be calculated by knowing the detachment force and the icing area. The ice adhesions were measured on both damaged/healed and undamaged self-healing samples to investigate whether the healed area shows significant change on the icephobic properties of the superhydrophobic coating.

6.5 Result and Discussion

6.5.1 Microcapsules Characterization

The SEM images of the PDMS-MUF and DBTL-MUF microcapsules are shown in **Figure 6-3 a, c.** The images show uniform spherical surface morphology for both types of microcapsules. The size distributions of the obtained capsules are plotted in **Figure 6-3 b, d.** The PDMS-MUF microcapsules are mostly within a size range of 5-35 µm with a mean diameter of 18 µm and DBTL-MUF microcapsules are mainly in 5-30 µm size range by a mean diameter of 16 µm. The acquired size distribution is supposed as a suitable size range for self-healing microcapsules for surface coating applications.

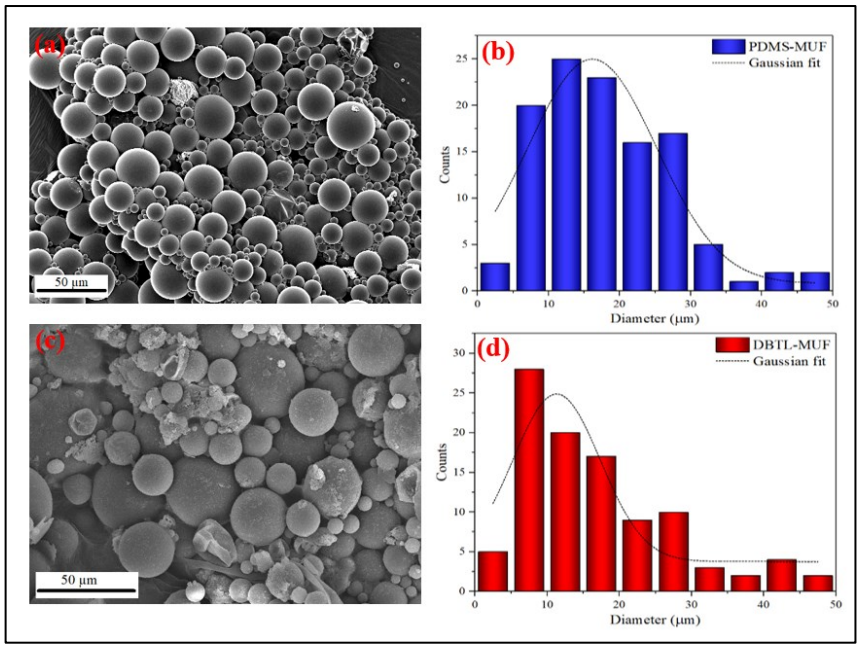

Figure 6-3. a) SEM image of PDMS-MUF microcapsule; b) Size distribution histograms of PDMS-MUF microcapsule; c) SEM image of DBTL-MUF microcapsules, d) Size distribution histograms DBTL-MUF microcapsules.

6.5.2 Surface Characterization

The thickness of the applied coatings on stainless steel substrates were varied in the range of 150-200 µm. This thickness range could ensure the adequate distribution of microcapsules within the coating with minimum adverse effect on the superhydrophobic characteristics of the coating.

CA, CAH, and SA values of the prepared samples are represented in **Table 6-3**.

Table 6-3. The surface wettability of prepared samples using CA, CAH, and SA values.

	Sample		
	Pristine	***SHP bare***	***SHP-Self healing***
CA	79° ± 2.3°	163° ± 2.1°	165° ± 1.5°
CAH	9.3° ± 1.5°	2.3° ± 0.3°	3.6° ± 1.5°
SA	> 30°	≤ 5°	≤ 5°

Though the self-healing microcapsules are incorporated in the SHP-self healing coating, the sample shows almost identical surface characteristics compared to the SHP-bare sample. This similar behavior is because the microcapsules are dispersed inside the first layer while the top layer that governs the non-wettability properties has not been altered. SEM imaging was also employed to observe the surface morphology of the self-healing superhydrophobic samples. The images shown in **Figure 6-4** confirm the similar superhydrophobic structures on the surface of the coating with no significant differences observed compared to the samples without incorporation of self-healing microcapsules inside the base layer (**Figure 3-4**).

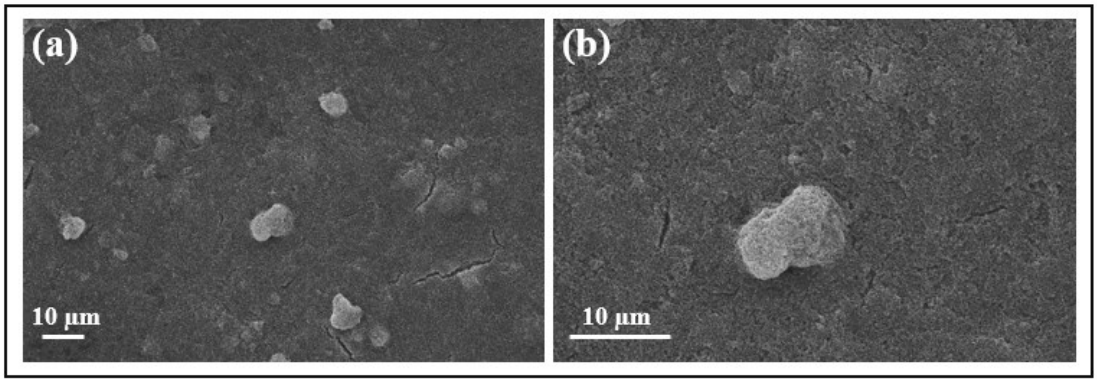

Figure 6-4. SEM images of the SHP-self healing sample with different magnifications of a) 1000X; b) 2500X.

To represent the self-cleaning properties of the SHP coating, the behavior of the coating was evaluated against solid contamination. As shown in **Figure 6-5**, when water droplets reach the SHP

coating surface, the pollutants stick to water due to the greater adhesion of water to contaminant comparing to the adhesion of water to the superhydrophobic surface.

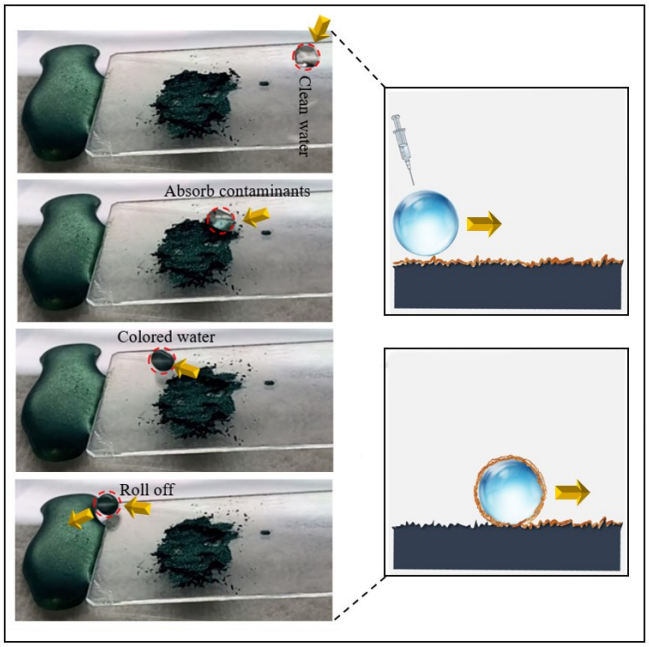

Figure 6-5. Self-cleaning behavior of the SHP coating using dye powder as contaminant. While rolling off, the water droplet absorbs the pollutants on its way down.

6.5.3 Self-healing Characterization

For monitoring the healing performance, the SEM images of the scratched SHP-bare and SHP-self healing samples are illustrated in **Figure 6-6 a, b.** The applied scratch on the SHP-self healing sample was shown to be filled with the released healing agents.

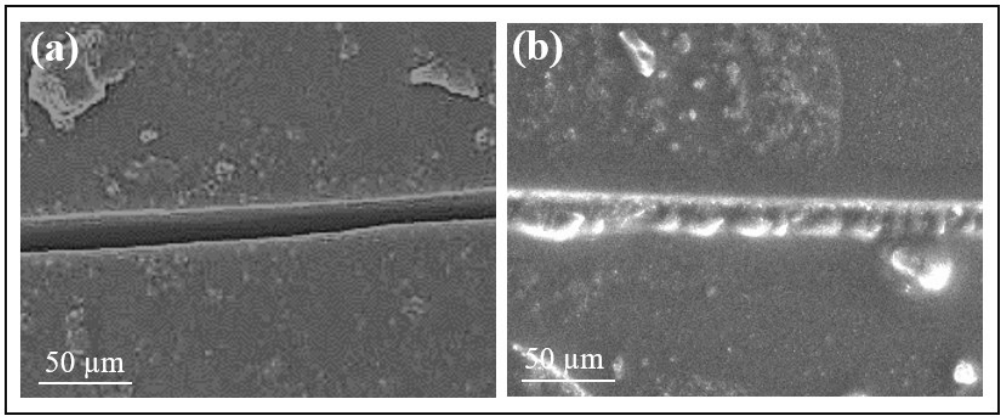

Figure 6-6. SEM observation of a crack on a) SHP-bare sample, b) SHP-self healing sample after 24 h of crack formation.

The healing of microcracks is an important ability for the coatings that could be highly manifested in the functional applications and harsh environments. For this purpose, the EIS analysis was employed to investigate the performance of the self-healing coating in corrosive media. EIS analysis provides detailed information on the electrochemical behaviour of the interfaces generated by dipping the coated samples in the electrolyte solution (i.e., naturally aerated 0.05 M NaCl). The Bode and Nyquist plots of the coatings were derived at time intervals of 1h, 24h, and 48h after immersion as shown in **Figure 6-7 a-c**.

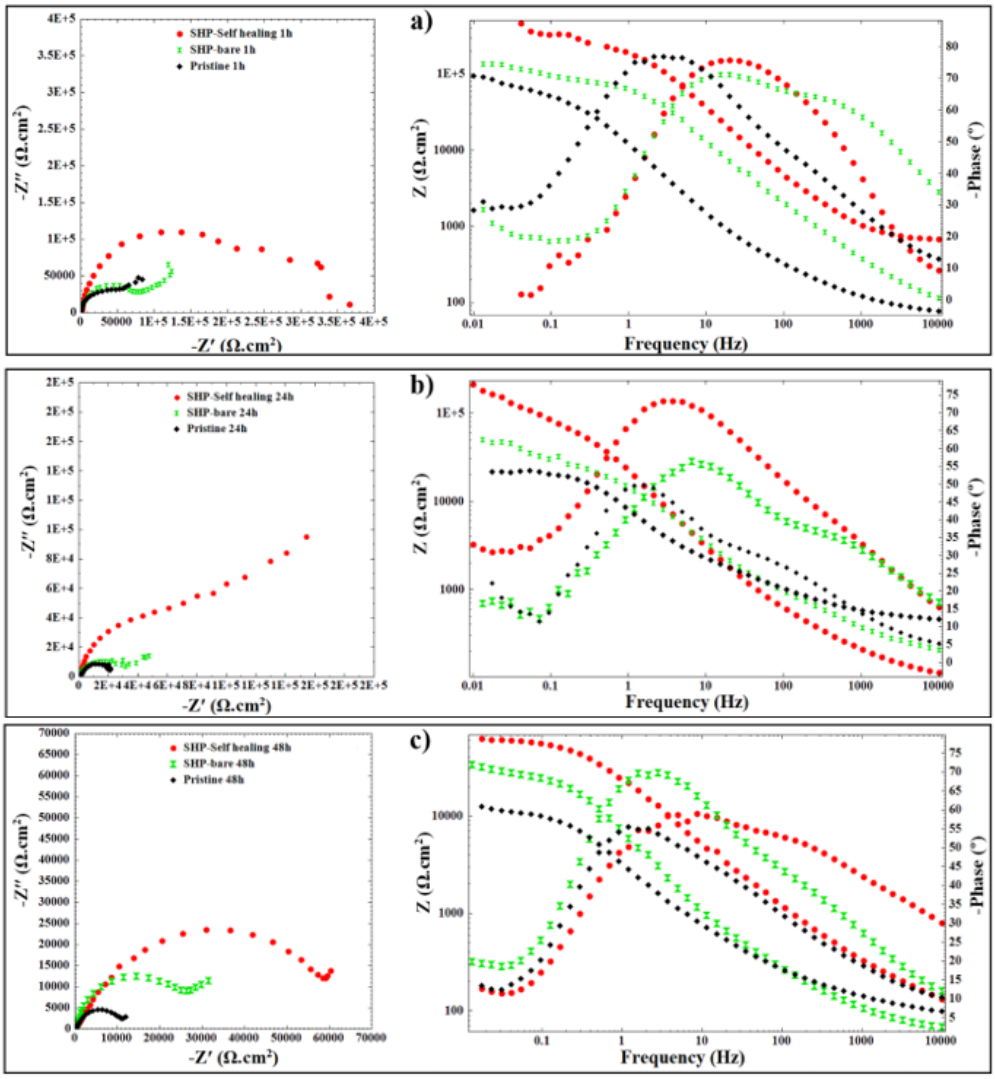

Figure 6-7. Obtained Bode and Nyquist plots for the pristine, SHP-bare, and SHP-self healing samples after a) 1 h immersion, b) 24 h immersion and c) 48 h immersion in corrosive media.

The acquired results from EIS analysis are reported in **Table 6-4**. In corrosion studies, the impedance value at the lowest frequency could be considered as the total resistance of the system against corrosion [536]. It is observed that the impedance of the self-healing coating at low frequency (4.65×10^5 $\Omega.cm^2$) increased by 50 times compared to the pristine (9.52×10^4 $\Omega.cm^2$) and 4 times compared to the SHP-bare coating (1.35×10^5 $\Omega.cm^2$) in the first one hour. The phase angles of the three samples are almost within the same range in the first hour, while after 24 and 48h, the higher phase angles for the self-healing system could also verify the intactness property.

Table 6-4. The EIS parameters of various coatings at different times of 1, 24 and 48 h after immersion.

Scratched Sample	*Time (h)*	R_f *(Ω.cm²)*	CPE_f		R_{ct} *(Ω.cm²)*	CPE_{dl}		$\lvert Z\rvert_{lf}$
			$Y_0 \times 10^6$ *(mW^{-1} cm^{-2} s^n)*	*n*		$Y_0 \times 10^6$ *(mW^{-1} cm^{-2} s^n)*	*n*	
Pristine	***1***	6.15×10^4	21.85	0.82	4.39×10^4	28.7	0.88	9.52×10^4
	24	2.29×10^3	27.29	0.76	2.03×10^4	26.0	0.90	2.33×10^4
	48	1.13×10^4	26.97	0.61	3.14×10^3	25.9	0.85	1.24×10^4
SHP-bare	***1***	8.80×10^4	50.19	0.89	6.15×10^4	19.1	0.85	1.35×10^5
	24	3.71×10^4	34.86	0.80	2.16×10^4	26.4	0.90	4.95×10^4
	48	2.69×10^4	31.52	0.89	8.35×10^3	78.2	0.91	3.34×10^4
SHP-Self healing	***1***	2.46×10^5	24.58	0.82	1.41×10^5	18.6	0.91	4.65×10^5
	24	1.20×10^5	30.81	0.97	5.22×10^5	19.7	0.82	2.12×10^5
	48	1.65×10^3	25.15	0.57	5.91×10^4	28.9	0.85	6.17×10^5

A two-time constant electrical equivalent circuit (EEC) model was utilized to fit the EIS results as shown in **Figure 6-8**. This circuit consists of two-time constants in cascade, considering film capacitance (CPE_f) and film resistance (R_f), and double layer capacitance (CPE_{dl}) and charge transfer resistance (R_{ct}).

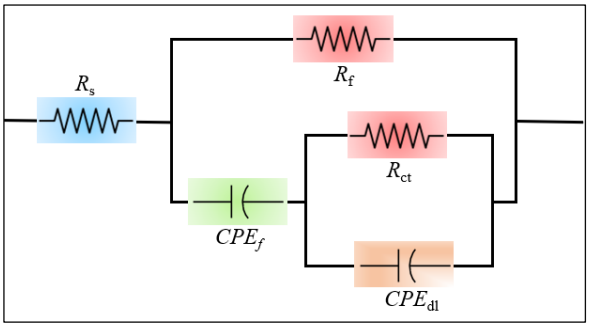

Figure 6-8. The electric equivalent circuit used to analyze the EIS data.

Corrosion takes place when water, oxygen, and aggressive ions are transferred to the interface of metal and coating through the scratched area [537], [538]. In a self-healing system, when the coating is damaged, the embedded microcapsules can rupture and release the healing agents leading to the formation of a protective layer at the interface that would function to prevent corrosion. Therefore, from the EIS results, the charge transfer resistance (R_{ct}) could be an appropriate indicator of the healing action. Based on the charge transfer variations, we can define a parameter, namely inhibition efficiency, via the following equation:

$$Inhibition\ Efficiency\ (\%) = \frac{R_{ct}^{Self\ healing} - R_{ct}^{Reference}}{R_{ct}^{Self\ healing}} \times 100 \qquad \text{(Eq. 5-1)}$$

With the evolution of self-healing, the inhibition efficiency (IE%) would be increased due to the progression in the protective layer thereby decreasing the charge transfer to the damaged area. However, since the coating is exposed to the corrosive media, the corrosion will take place after a certain time leading to a further decrease in the IE%. The inhibition efficiency at its maximum value could be thus attributed to the maximum self-healing efficiency (SHE%) of the system (i.e., $IE_{max}\% \approx SHE\%$)

A sufficient amount of healing agent provided in the damaged area would be helpful to achieve high self-healing efficiency. **Table 6-5** shows the inhibition efficiencies at different test intervals based on the R_{ct} values. The inhibition efficiency could be computed based on two references including the pristine sample and the SHP-bare. The data trends show an increase in IE% within the first 24 h (from 56.38% @ 1 h to 95.86% @ 24 h) and a further decrease from 95.86 @ 24 h to 85.87 @ 48 h. Therefore, based on the presented definition, the self-healing efficiency of the coating could be estimated by 95.86% compared to the bare superhydrophobic coating, and 96.11% in comparison to the pristine coating.

Table 6-5. The calculated charge transfer resistances and the corresponding inhibition efficiencies for the references and the self-healing coating.

Time (h)	***R_{ct} ($\Omega.cm^2$)***			***Inhibition Efficiency (%)***	
	Pristine	***SHP bare***	***SHP-Self healing***	***Ref: Pristine***	***Ref: SHP bare***
1	4.39×10^4	6.15×10^4	1.41×10^5	68.86	56.38

24	2.03×10^4	2.16×10^4	5.22×10^5	96.11	95.86
48	3.14×10^3	8.35×10^3	5.91×10^4	94.68	85.87

Reaching to maximum inhibition efficiency values at 24 h after immersion, we can claim that the appropriate time for self-healing of the present system would be roughly 48 h (Considering that the coatings were left at room temperature for 24 h prior to immersion).

Delamination occurs in coatings when the electrolyte and aggressive ions reach the interface of metal and coating, leading to the initiation of the corrosion reactions [539]. The delamination of the coatings can be estimated through the electrochemical data obtained from Bode plots. The delamination index of coatings can be calculated by the following equation [540]

$$DI\ (\%) = \left(\frac{Z_1 - Z_2}{Z_1}\right)_{0.01\ Hz} \times 100 \qquad \text{(Eq. 5-2)}$$

where Z_1 and Z_2 are the logarithms of the impedance values after 1 h and 48 h immersion, respectively. The calculated DI for the pristine. SHP-bare and SHP self-healing are represented in **Table 6-6**.

Table 6-6. Delamination index of the samples.

Sample	**Pristine**	**SHP-bare**	**SHP-self healing**
DI (%)	17.7	11.89	-2.3

The SHP-self healing sample shows a negative delamination index value. The negative value is due to the higher resistance of the damaged coating after 48 h compared to 1 h immersion time, which could be attributed to the healing of the damaged area.

6.5.4 Ice adhesion Measurements

The measured ice adhesion strength on the Pristine, SHP-bare, and SHP-self healing samples are reported in **Table 6-7**.

Table 6-7. Ice adhesion strength values for the pristine, SHP-bare, and SHP-self-healing samples.

Sample	Pristine	SHP-bare	SHP-self healing	
			Virgin	Healed
Ice adhesion strength (kPa)	65	13.3 ± 1.5	14.1 ± 1.2	18.6 ± 1.5

The measured values show that the incorporation of self-healing microcapsules does not have obvious adverse effect on the adhesion of ice to the superhydrophobic coating. However, the ice adhesion strength on the scratched and healed region was followed by a slight increase of up to 18.6 ± 1.5 kPa. Yet, the healed samples show appropriate de-icing performance.

6.6 Conclusion

This chapter aimed at developing a multifunctional self-healing superhydrophobic coating that is able to self-repair the possible microcracks. For this purpose, two types of microcapsules were prepared carrying a silicone resin and its catalyst in order to be incorporated into a superhydrophobic coating. The successful self-healing ability of the dual-capsule system was presented earlier in *CHAPTER 2* inside a bulk silicone matrix. Also, superhydrophobic, self-cleaning and anti-icing properties of the coating was previously discussed in *CHAPTER 3*. Here, we adjusted the process parameters resulting in the synthesis of microcapsules within size ranges of sub-50 μm.

Scanning electron microscopy was utilized to observe the morphology of microcapsules, as well as the healing function of a microcrack. Also, WCA values and microscopic images confirmed that the incorporation of self-healing microcapsules does not change the surface characteristics of the superhydrophobic coating. To verify and quantify the healing performance of the coating, corrosion behavior of the scratch samples was investigated via EIS analysis and the R_{ct}, $Z_{0.01}$ parameters were utilized to calculate inhibition efficiency (IE), self-healing efficiency (SHE) and delamination index (DI). The self-healing superhydrophobic coating showed SHE of up to 96% compared to the bare superhydrophobic coating and the pristine sample. The delamination index of the scratched self-healing sample also confirmed the healing of the scratch after 48 h thank to the increasing of the total resistance

of the coating in time. The ice adhesion strength values were measured using ice push-off test, and obtained results showed only a slight increase on the healed region of the sample compared to the virgin self-healing superhydrophobic coating.

Acknowledgment

The authors acknowledge the financial support from the Natural Sciences and Engineering Research Council of Canada (NSERC); Hydro-Québec, Québec, Canada; and le Pôle Recherche Innovation en Matériaux avancés du Québec (PRIMA Québec), Québec, Canada. They also thank Dr. Shamim Roshan, Researcher at Laboratoire Revêtements glaciophobes et ingénierie des surfaces (LARGIS), for performing the EIS measurements.

CONCLUSIONS

In the following, an overview of the important findings of this project is presented as both partial and general conclusions. As the partial conclusion, the important results obtained in the papers are separately provided in the same order as their presentation in this thesis. The general conclusions are provided afterwards.

Development of a dual capsule self-healing silicone composite using silicone chemistry and poly (melamine-urea-formaldehyde) shells

- Firstly, we employed the microencapsulation technique as the most common self-healing mechanism for polymeric matrices. A telechelic silanol terminated polydimethylsiloxane (DMS-S12) and dibutyltin dilaurate catalyst were chosen as the core materials and encapsulated inside poly(melamine-urea-formaldehyde) shells. Introduction of melamine into the urea-formaldehyde has shown to increase its mechanical and thermal stabilities.
- The microcapsules were synthesized via emulsion polymerization. In this method, the shell materials are dissolved in the water phase, and the oil phase (core material) is further added to the emulsion bath. The polymerization of the shell-forming components at the interface of oil/water leads to the formation of a compact shell around the emulsified core droplet.
- The formation of spherical and compact microcapsules containing the healing agents, as well as the characteristics of microcapsules were analyzed via SEM, FTIR and DSC tests. The results showed spherical microcapsules within a size range of 10-110 μm with appropriate properties for being used as self-healing microcapsules.
- The synthesized microcapsules were incorporated inside the SYLGARD 184 matrix (with weight ratio SYLGARD 184: DMS-S12 MCs: DBTL MCs of 100:10:1.2 wt.%.).
- The self-healing evolution of the system was monitored via SEM imaging of an applied microcrack, and the successful crack healing was observed.
- To quantify the self-healing efficiency of the system, mechanical properties of a composite with and without microcapsules was evaluated after scratch application. The self-healed composite showed 67% and 55% recovery based on the toughness and tearing energy calculations via tensile and tear tests.

Transparent non-fluorinated superhydrophobic coating with enhanced anti-icing performance

- The wetting behavior of a surface is governed mainly by two factors of surface chemistry and surface geometry. Superhydrophobicity or ultra-non-wettability is observed for surfaces with low surface energy and appropriate hierarchical micro/nano structures. Therefore, a methoxy functional silicone resin (SILIKOPHEN AC 1000) and HMDS-modified silica nanoparticles were utilized to fabricate a non-fluorinated superhydrophobic coating. Given the acquired coating had a contact angle of 163° and contact angle hysteresis of 2.3°, it showed excellent non-wetting behavior and water rolled off easily on the surface.
- The superhydrophobic coatings are prone to lose their functional properties due to durability challenges. One of the available methodologies for increasing the robustness of SHP coatings is to increase the possible crosslinking sites between the incorporated materials (i.e., matrix and nanoparticles). In this thesis, methyltriethoxysilane (MTES) was introduced to the coating mixture acting as a coupling agent between the silicone matrix and nanoparticles.
- The self-cleaning ability of the coating was evaluated in both wet and dry pollutant conditions and the SHP coating was able to stay clean and contaminant-free after being exposed to artificial pollution scenarios.
- For investigating the mechanical and chemical durability of the coating, sand-paper abrasion, tape peeling, and acidic/basic stability tests were employed. The SHP coating depicted appropriate robustness against repetitive cycles of test by maintaining non-wettability characteristics, i.e., WCA = 152.6 ± 1.7°, CAH = 9.5 ± 0.7° after 20 cycles of sandpaper abrasion; WCA = 158.7 ± 1.8°, CAH = 7 ± 0.9° after 30 cycles of tape-peeling; WCA = 153.8 ± 1.2° after 24 h @ pH = 2 and WCA = 157.9 ± 0.9° after 24 h @ pH = 14).
- Icephobic performance of the developed coating was investigated in terms of ice-adhesion strength and the freezing delay time. The adhesion of bulk and glaze ice were measured via ice push-off and centrifuge tests, showing remarkably low ice adhesion strengths (ARF = 4.89 and 3.88 for push-off and centrifuge compared to a pristine coating). Also, the push-off ice adhesion strength was kept lower than 20 kPa even after 15 icing/deicing cycles verifying its icephobic durability. Moreover, the ice formation on the SHP coating was delayed for 97, 63, and 31% at -10, -15 and -20°C compared to bare aluminum, respectively.

Performance of a nano-textured superhydrophobic coating developed for high-voltage outdoor porcelain insulators

- Considering that the SHP coating is developed for the high-voltage porcelain insulator section, the performance of the coating under electrical stress is highly important. Therefore, the dielectric characteristics of the coating were investigated by different test methods including measuring the flashover voltage on the surface, measuring leakage current in a condensation chamber, and observing the erosion and tracking performance of the coating in an inclined plane test setup.
- Dielectric permittivity and loss factor of the developed coating was investigated via a dielectric spectroscopy instrument. The SHP coating showed lower permittivity and tan δ values compared to a pristine coating.
- The accelerated weathering test depicted that the coating has acceptable weathering resistance since it is a crucial factor for the coatings being exposed to outdoor conditions.
- The thermogravimetric analyses (TGA) illustrated that the SHP coating was thermally stable and showed only 13% of weight loss up to 700°C.
- The flashover voltage on the surface of bare porcelain and SHP-coated porcelain were measured in different polluted, non-polluted, dry, and wet conditions. The results revealed that the coating could successfully increase the flashover level on the surface of the SHP-coated porcelain compared to the bare porcelain in all conditions. In the polluted and wet condition, the flashover occurred at 33 kV on the SHP-coated porcelain, while for the bare porcelain the flashover voltage value was 14 kV (which is representative of its excellent self-cleaning properties).
- In highly humid climates, the moisture could be condensed on the insulator surface (dew formation) leading to an increased leakage current and formation of arc on the surface. Here, the SHP coating was able to decrease the leakage current in a condensation test (test method suggested by J. Wu et al. [508]), which could be attributed to its better insulation performance compared to the surfaces with higher degrees of wettability.
- The inclined plane test was performed in an adopted version for thin coatings, and the results showed less erosion and tracking lines on the surface of SHP coating compared to a pristine sample.

Development of all-silicone self-healing superhydrophobic coating

- The aim of this thesis was to develop a superhydrophobic coating which has the ability to repair the microcracks that occurred on its surface. Therefore, the synthesized microcapsules were adopted to be applicable in a coating layer with film thickness of less than 200 µm. For this goal, it is better to obtain a size distribution of sub-50 µm in order to provide enough active agent in the place of damage as well as being well-dispersed inside the coating.
- To decrease the particle size distribution, the process parameters were optimized, and the diameter of the obtained microcapsules were measured via SEM observations and the help of ImageJ software. The synthesized PDMS-MUF MCs were obtained within a range of 5-35 µm with a mean diameter of 18 µm and DBTL-MUF MCs were in 5-30 µm size range and a mean diameter of 16 µm. The acquired size distribution fulfills the requirements of self-healing microcapsules aimed for surface coating applications.
- The microcapsules were incorporated in the developed SHP coating formulation in a weight ratio of 10 wt.%, and the as-prepared coating showed WCA = 165° and CAH = 3.6°.
- For the self-healing testing, the SEM observation and electrochemical impedance spectroscopy (EIS) were utilized. The microscopic images confirmed the repair of a 25 µm-deep scratch on the surface of the SHP coating.
- The EIS measurements were conducted on the scratched samples (Pristine, SHP-bare, and SHP-self healing) after 1, 24 and 48 hours of immersion in NaCl solution. The Bode and Nyquist plots were obtained from the EIS data and the healing efficiency was calculated based on the variations in the charge transfer resistance (Rct) for the self-healing and reference samples. The self-healing efficiency was shown to be 95.86% compared to the bare-SHP coating, and 96.11% considering to the pristine coating as the reference.
- Delamination index for the samples was also calculated based on the impedance values at 0.01 Hz frequency, verifying the complete repair of the crack on the self-healing sample after 48 hours.

General Conclusion

In this thesis, to address the catastrophic risks of the failure of high-voltage porcelain insulators due to internal or external mechanical damages as well as ice and pollution accumulation on their surfaces, two bio-inspired mechanisms are opted to effectively create a self-healing coating with superhydrophobic surface characteristics. The introduction of self-healing ability into the polymeric

materials, that have a resemblance with the biological wound healing process, have been increasingly desirable in many applications in order to trigger a self-repair response to a formed damage without human intervention. The superhydrophobic surfaces are also well known for their superb self-cleaning function and enhanced icephobic performance.

To fully address the objectives of the current thesis, initially, a room temperature self-healing system was designed. The microencapsulation method was employed for this purpose and a silicone resin and catalyst were encapsulated inside poly(melamine-urea-formaldehyde) shells. The physical and chemical properties of the microcapsules were investigated by different means. The microcapsules were then incorporated inside a bulk silicone resin and the healing of microcracks were carefully assessed by quantitative and qualitative methods. The imaging techniques depicted the filling of a microcrack, while by the aid of tensile and tear tests, the self-healing efficiency of the polymer was calculated. The results showed self-healing efficiencies of 67% and 55% based on the recovered toughness and tearing energy measurements for the self-healing sample compared to a reference sample without self-healing microcapsules.

For the development of a superhydrophobic coating, a methoxy functional silicone resin and hydrophobic-treated fumed silica nanoparticles were chosen as the main ingredients. The coating was applied via a spraying method which is industrially applicable for large scale productions. The application of superhydrophobic coatings has been always limited owing to their low durability that leads to the loss of its surface non-wetting function. To enhance the robustness of the coating, MTES was incorporated into the formulation to create more possible crosslinking sites and increase the interactions between the nanoparticles and the matrix. The mechanical tests showed an enhancement in the durability of the coating with MTES compared to the coating without MTES.

The consistency of the Cassie-Baxter regime was verified by various analyses including water jetting, droplet pressure test and droplet impact. The self-cleaning behavior of the SHP coating was verified based on wet and dry contamination methods. Furthermore, the pronounced delayed ice formation and notable low ice adhesion strength of the SHP coating depicted its significant anti-icing and de-icing capabilities. Relatively good mechanical durability and substantial chemical stability were

also observed after multiple tests, including sand-paper abrasion, tape peeling and immersion in corrosive chemicals.

The electrical properties of the developed coating were also studied to investigate the performance of the SHP coating under high voltage conditions and electric stress. The dielectric spectroscopy was used to obtain the dielectric permittivity and loss factors of the samples, showing acceptable characteristics. The flashover voltage and leakage current on the surface of SHP coating was also evaluated by means of various test methods. The superhydrophobic characteristic of the surface showed positive effect on increasing the flashover voltage in wet and polluted conditions and decreasing the leakage current in humid environment compared with a non-SHP coating.

Lastly, the as-prepared microcapsules were adopted to be used inside the SHP coating formulation for self-healing function. The self-healing superhydrophobic coating represented successful repair after a scratch was made on its surface and left at room temperature. The self-healing performance of the coating was quantified by EIS analyses and visualized via SEM observation.

The results revealed that the self-healing and superhydrophobic characteristics were effectively introduced into a coating with acceptable performance under electrical stress, confirming its multifunctional capacity.

RECOMMENDATIONS

In this Ph.D. thesis, self-healing and superhydrophobic surfaces were produced. The developed surfaces demonstrated successful self-repair without human intervention, significant superhydrophobicity, self-cleaning, icephobicity, and mechanical/chemical robustness. Nevertheless, there are still several suggestions worth considering for further investigations. These recommendations are presented as follows.

- The self-healing mechanism here was based on the microencapsulation approach, which is yet the most feasible approach among other methods. However, this approach suffers from the limited number of healing actions. To address this issue, other self-healing approaches could be also employed to produce self-healing coatings with several cycles of self-healing in a certain area of the coating. As and example, silicone rubber has shown to be repaired through heat-activated reversible bonding. Introduction of reversible bonding chemistries into the silicone backbone (e.g., imine bonds, hydrogen bonding, etc.) could be promising approaches to obtain unlimited intrinsic self-healing.

- The optimum size distribution, and microcapsules weight ratio could also be further evaluated using other process parameters, other matrix composition, etc.

- The self-healing performance was assessed in this thesis at room temperature. Though, the possibility of self-healing action should be investigated at lower temperatures when a coating is applied in cold climates. Also, the kinetic of the self-healing reaction could also be investigated with more details.

- Although the fabricated superhydrophobic coating demonstrated acceptable durability, these coatings are still prone to lose their surface properties under much severe conditions due to the disruption of their low surface energy by various factors. Recently, the superhydrophobic coatings that are able to regenerate their chemistry have been progressively gaining attention. Therefore, it is suggested to introduce regeneration mechanisms into the as-prepared coating to increase its efficient life-time.

- The performance of the coating under electrical stress was evaluated in laboratory setups and small samples. It is also suggested to conduct some experiments on whole porcelain insulators to assess the performance of coating in more realistic conditions and have a better understanding of its functionality.

- Optical transparency is an important parameter in many applications. Here, the developed SHP coating depicted high optical transparency due to specific length-scales of the surface textures. Therefore, the performance of this coating could also be investigated on the surfaces where optical transparency and superhydrophobicity are required simultaneously (e.g., windows, solar panels, etc.).

APPENDIX I

SUPPORTING INFORMATION FOR ARTICLE 1

DEVELOPMENT OF A DUAL CAPSULE SELF-HEALING SILICONE COMPOSITE USING SILICONE CHEMISTRY AND POLY(MELAMINE-UREA-FORMALDEHYDE) SHELLS

A. Allahdini *, R. Jafari, G. Momen

Department of Applied Sciences, University of Quebec in Chicoutimi (UQAC)

555, boul. de l'Université, Chicoutimi, Québec, G7H 2B1, Canada

E-mail: Anahita.Allahdini-Hesarouyeeh1@uqac.ca

This article has been accepted in:

Applied Polymer Science Journal

Optimization of Microencapsulation

This study aimed to optimize the microcapsules for use in a self-healing silicone matrix. Herein, it is necessary to investigate the optimized conditions for producing the applicable microcapsules. These conditions include microcapsule size and morphology, dispersal capability and flowability of the powder, handling, and thermal stabilities. Therefore, we altered the parameters (emulsifier, agitation rate, core: shell ratio, and polymerization temperature) within a range of experiments to identify the appropriate reaction parameters given the laboratory conditions. The visual results of microcapsule quality are also provided in the various sections.

Effect of Agitation Rate

The effect of agitation rate on particle size and the quality of the produced powders are presented in **Table A-I. 1**. Increasing the agitation speed forms smaller microcapsules, which enhances the active surface area of the core material that should be covered by shell materials. This occurrence could negatively affect the stability of microcapsules, the formation of thinner shells, or the existence of excess core in the media.

Table A-I. 1. Effect of agitation rate on microcapsule synthesis.

Number of experiments		**1**	**2**	**3**
Agitation rate (rpm)		300	600	900
Result	PDMS MCs	Particle size: 150–500 µm, Free-flowing powder.	Particle size: 10–110 µm, Free-flowing powder.	Particle size: too small, Agglomerated powder.
	DBTL MCs	Particle size: 100–300 µm, Free-flowing powder.	Particle size: 10–80 µm, Free-flowing powder.	Particle size: too small, Sticky agglomerate.

Effect of Emulsifier Type and Concentration

We carried out the microencapsulation of PDMS using different concentrations of EMA and SDS, as presented in **Table A-I. 2**, while keeping all other parameters constant.

Table A-I. 2. Effect of emulsifier type and concentration on PDMS-MUF microcapsule synthesis.

Number of experiments	**1**	**2**	**3**	**4**
EMA (g)	0.8	1.6	2.4	2.2
SDS (g)	0	0	0	0.2
Optical microscope image	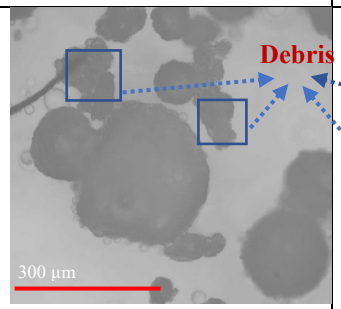	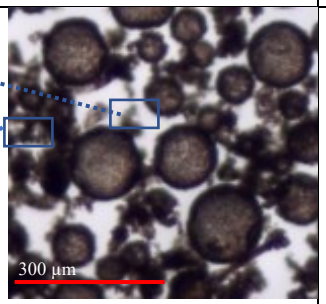	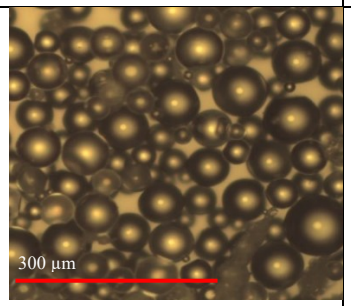	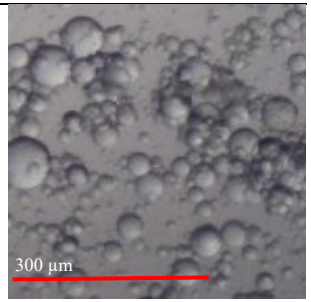
Result	Very large microcapsules having non-uniform shapes, Large amounts of debris, Rough exterior shell.	Large microcapsules, Debris still present, Rough exterior shell.	Appropriate size of microcapsules, Smooth shell morphology, Free-flowing powder.	Microcapsules are too small, Sticky agglomerate.

Effect of the Core to Shell Ratio

The core to shell ratio is one of the most important factors affecting the quality of formed microcapsules. This ratio should be controlled precisely to obtain microcapsules having an appropriate size, morphology, and shell wall thickness. If this quantity is too large, there may be inadequate shell material to cover the surface of core droplets leading to the poor mechanical stability of the microcapsules. On the other hand, a low core to shell ratio produces thick walls that might not be able to rupture and decreases the local core content, which may decrease the healing efficacy. Our investigation of the effect of the core to shell ratio on the microencapsulation of PDMS is presented in **Table A-I. 3**.

Table A-I. 3. Effect of the core to shell ratio on the microencapsulation of PDMS inside the MUF shell.

Number of experiments	**1**	**2**	**3**
Core: shell ratio	2:1	4:1	6:1
Result	Very rough surface of microcapsules and large quantities of debris due to the existence of excess shell materials.	Well-formed microcapsules, Shell wall thickness is 100–200 nm, Free-flowing powder.	Weak microcapsules, Sticky agglomerate.
SEM images of formed microcapsules	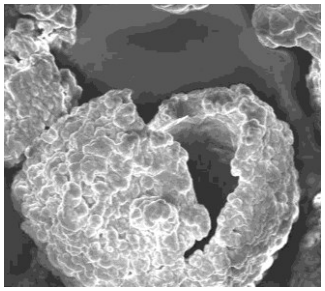	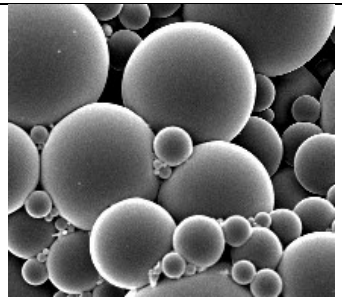	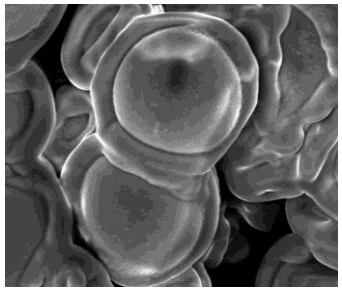
Quality of powder microcapsules		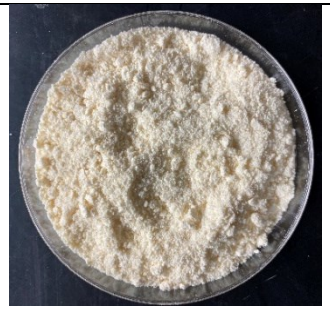	

Effect of Polymerization Temperature

The effect of polymerization temperature on microcapsule formation is indicated in **Table A-I. 4** and **Table A-I. 5**. The optimal temperature for the synthesis of these microcapsules occurs at 70℃. However, some reports offer different polymerization temperatures because of variable interlaboratory conditions.

Table A-I. 4. Effect of polymerization temperature on the synthesis of the PDMS-MUF microcapsules.

Number of experiments	**1**	**2**	**3**
Temperature (°C)	55	70	85
Result	Almost no reaction occurred, Observed only emulsified PDMS in the media.	Reaction occurred, Appropriate size, Smooth shell, Free-flowing powder.	Good size, Large quantities of debris within the media.

Table A-I. 5. Effect of polymerization temperature on the synthesis of DBTL-MUF microcapsules.

Number of experiments	**1**	**2**
Temperature (°C)	Room temperature	70
Result	Incomplete reaction, Very thin shells leading to microcapsules that are very poor in quality, Sticky powder.	Reaction occurred, Appropriate size, Free-flowing powder.

APPENDIX II

SUPPORTING INFORMATION FOR ARTICLE 2

TRANSPARENT NON-FLUORINATED SUPERHYDROPHOBIC COATING WITH ENHANCED ANTI-ICING PERFORMANCE

A. Allahdini *, R. Jafari, G. Momen

Department of Applied Sciences, University of Quebec in Chicoutimi (UQAC)

555, boul. de l'Université, Chicoutimi, Québec, G7H 2B1, Canada

E-mail: Anahita.Allahdini-Hesarouyeeh1@uqac.ca

This article has been accepted in:

Progress in Organic Coatings Journal

The developed superhydrophobic coating could be applied on different substrates, as mentioned in the manuscript. The coating applied on glass and aluminum were presented in **Figure 3-2**, however, we applied the coating on steel and porcelain for our further analysis. The coated steel and porcelain surfaces are represented in **Figure A-II. 1**.

Figure A-II. 1. The developed superhydrophobic coating applied on a) stainless steel and b) Porcelain substrates.

Adhesion Test

The digital photos of the crosscut adhesion test on different substrates of glass, porcelain, steel, and Aluminum are presented in **Figure A-II. 2**.

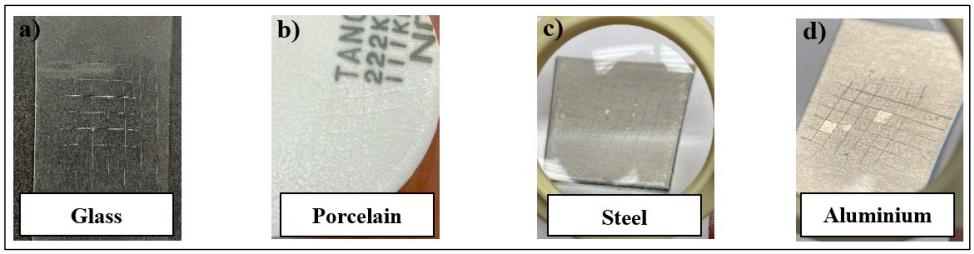

Figure A-II. 2. Images of the crosscut adhesion test on different substrates of glass, porcelain, stainless steel, and aluminum

Energy Dispersive Spectroscopy (EDS)

The EDS data of the superhydrophobic coating is shown in **Figure A-II. 3**.

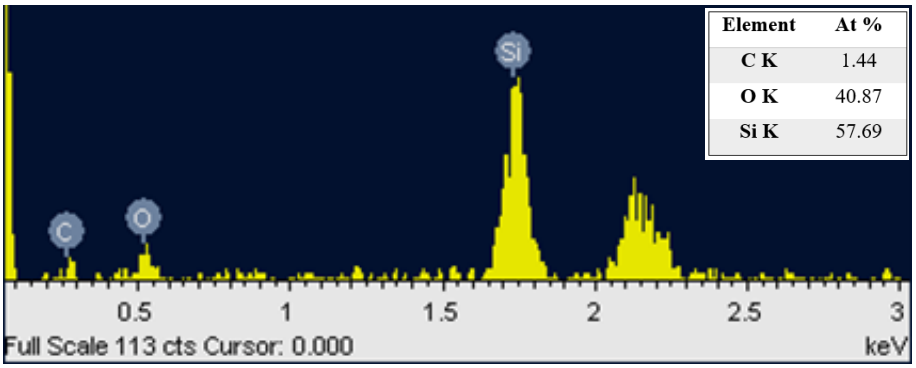

Figure A-II. 3. Result of EDS analysis on the superhydrophobic coating and the atomic percentages of elements.

Optical Transparency

The coating could maintain its optical transparency even after immersion in pollutant mixture and waterjet impacting, as well as the acid treatment, as presented in **Figure A-II. 4**. However, acidic solutions with pH as low as 2 could slightly alter the transparency of the coating compared to other extreme treatments.

Figure A-II. 4. Optical transparency of the superhydrophobic coating a) After immersion in pollutant mixture; b) After waterjet impacting; and c) After 24 h acid treatment (pH = 2).

Mechanical Durability

The sandpaper abrasion and tape peeling test were conducted on the superhydrophobic coating without MTES as the coupling agent. The results showed that the CAH is highly affected by sandpaper and tape peeling in the coating without MTES, and the water droplet does not show rolling on the coatings after these tests (**Figure A-II. 5**).

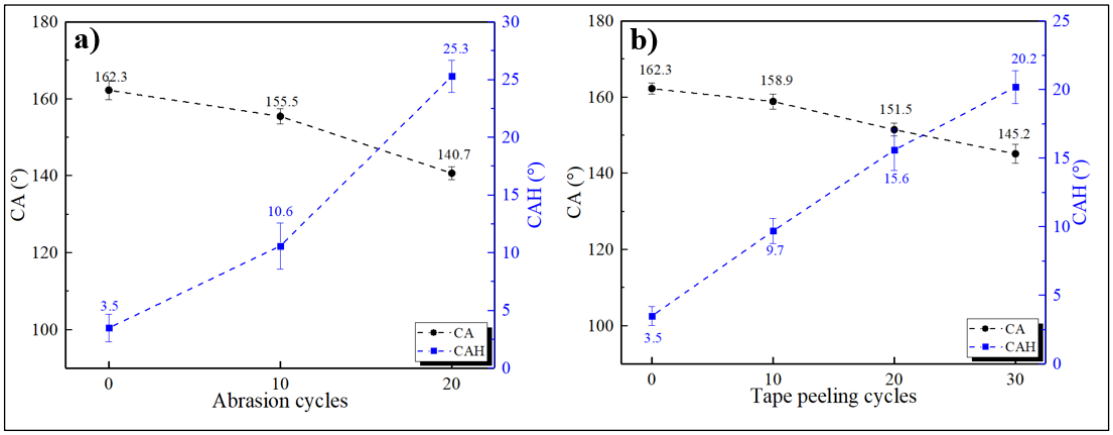

Figure A-II. 5. Mechanical durability of the superhydrophobic coating without MTES; a) WCA and CAH of the coating after 10 and 20 cycles of sandpaper abrasion; b) WCA and CAH after 10,20, and 30 cycles of tape peeling test.

REFERENCES

[1] T. Morocutti, T. Berg, M. Muhr, and G. Godel, "Developments of high voltage porcelain post-insulators," *Conf. Rec. IEEE Int. Symp. Electr. Insul.*, pp. 395–398, 2012, doi: 10.1109/ELINSL.2012.6251497.

[2] K. O. Papailiou and F. Schmuck, "Silicone Composite Insulators: Materials, Design, Applications," *Power Syst.*, vol. 75, 2013, doi: 10.1007/978-3-642-15320-4.

[3] A. Al-Gheilani, W. Rowe, Y. Li, and K. L. Wong, "Stress Control Methods on a High Voltage Insulator: A Review," 2017, doi: 10.1016/j.egypro.2017.03.112.

[4] M. Farzaneh, *Atmospheric Icing of Power*, vol. 84. 2008.

[5] X. Li, B. Yang, Y. Zhang, G. Gu, M. Li, and L. Mao, "A study on superhydrophobic coating in anti-icing of glass/porcelain insulator," *J. Sol-Gel Sci. Technol.*, vol. 69, no. 2, pp. 441–447, 2014, doi: 10.1007/s10971-013-3243-y.

[6] Muhsin Tunay Gençoğlu, "the comparison of ceramic and non-ceramic insulators," *New World Sci. Acad.*, vol. 2, no. 4, pp. 274–294, 2007, [Online]. Available: http://dergipark.gov.tr/download/article-file/186445.

[7] M. Farzaneh and W. A. Chisholm, *Insulators for Icing and Polluted Environments*. Institute of Electrical and Electronics Engineers (IEEE), 2009.

[8] G. Momen and M. Farzaneh, "Survey of micro/nano filler use to improve silicone rubber for outdoor insulators," *Rev. Adv. Mater. Sci.*, vol. 27, no. 1, pp. 1–13, 2011.

[9] Arshad, G. Momen, M. Farzaneh, and A. Nekahi, "Properties and applications of superhydrophobic coatings in high voltage outdoor insulation: A review," *IEEE Transactions on Dielectrics and Electrical Insulation*. 2017, doi: 10.1109/TDEI.2017.006725.

[10] H. C. Hillborg, "Loss and recovery of hydrophobicity of polydimethylsiloxane after exposure to electrical discharges of polydimethylsiloxane after exposure to electrical discharges," Royal Institute of Technology , Stockholm, Sweden, 2001.

[11] M. Farzaneh, "Ice accretions on high-voltage conductors and insulators and related phenomena," *Philos. Trans. R. Soc. A Math. Phys. Eng. Sci.*, vol. 358, pp. 2971–3005, 2000, doi: 10.1098/rsta.2000.0692.

[12] J. F. J. Zhang and M. Farzaneh, "Experimental study and mathematical modelling of fl ashover on extra-high voltage insulators covered with ice," vol. 3480, no. April, pp. 3471–3480, 2004, doi: 10.1002/hyp.5807.

[13] CIGRE Working Group B2.44, "Coatings for the protection of power network equipment in winter conditions," 2015.

[14] M. Farzaneh, "Ice Accretions on High-Voltage Conductors and Insulators and Related Phenomena," *Philos. Trans. R. Soc. A*, vol. 358, no. 1776, pp. 2971–3005, 2000, doi: https://doi.org/10.1098/rsta.2000.0692.

[15] K. L. Chrzan and F. Moro, "Concentrated Discharges and Dry Bands on Polluted Outdoor Insulators," *IEEE Trans. Power Deliv.*, vol. 22, no. 1, pp. 466–471, 2007.

[16] M. Farzaneh, "coatings for protecting overhead power network equipment in winter conditions," 2015.

[17] X. Wu, V. V. Silberschmidt, Z. T. Hu, and Z. Chen, "When superhydrophobic coatings are icephobic: Role of surface topology," *Surf. Coatings Technol.*, 2019, doi: 10.1016/j.surfcoat.2018.11.039.

[18] S. S. Latthe *et al.*, "Self – cleaning superhydrophobic coatings: Potential industrial applications," *Prog. Org. Coatings*, vol. 128, pp. 52–58, Mar. 2019, doi: 10.1016/J.PORGCOAT.2018.12.008.

[19] P. Irajizad, S. Nazifi, and H. Ghasemi, "Historical Perspective Icephobic surfaces: Definition and figures of merit," *Adv. Colloid Interface Sci.*, vol. 269, pp. 203–218, 2019, doi: 10.1016/j.cis.2019.04.005.

[20] J. Blackett, "Voltshield - anti-pollutant treatment for glass and glazed porcelain insulators," *IET Conf. Publ.*, no. 550 CP, 2009, doi: 10.1049/CP.2009.1137.

[21] H. de Santos and M. Sanz-Bobi, "Research on the pollution performance and degradation of superhydrophobic nano-coatings for toughened glass insulators," *Electr. Power Syst. Res.*, vol. 191, p. 106863, Feb. 2021, doi: 10.1016/J.EPSR.2020.106863.

[22] K. Jud, H. H. Kausch, and J. G. Williams, “Fracture mechanics studies of crack healing and welding of polymers,” *J. Mater. Sci.*, vol. 16, pp. 204–210, 1981, doi: 10.1007/BF00552073.

[23] C. M. Dry and N. R. Sottos, “Passive smart self-repair in polymer matrix composite materials,” 1993, doi: 10.1117/12.148501.

[24] S. R. White *et al.*, “Autonomic healing of polymer composites,” *Nature*, vol. 409, pp. 794–797, 2001, doi: 10.1038/35057232.

[25] J. Jeevahan, M. Chandrasekaran, G. Britto Joseph, R. B. Durairaj, and G. Mageshwaran, “Superhydrophobic surfaces: a review on fundamentals, applications, and challenges,” *Journal of Coatings Technology and Research*, vol. 15, no. 2. Springer New York LLC, pp. 231–250, Mar. 01, 2018, doi: 10.1007/s11998-017-0011-x.

[26] S. S. Latthe *et al.*, “Recent developments in air-trapped superhydrophobic and liquid-infused slippery surfaces for anti-icing application,” *Prog. Org. Coatings*, vol. 137, p. 105373, 2019, doi: 10.1016/J.PORGCOAT.2019.105373.

[27] K. Guo *et al.*, “The Principle and the Application of Self-cleaning Anti-pollution Coating in Power System,” *Mater. Sci. Eng.*, vol. 269, no. 1, p. 012044, 2017, doi: 10.1088/1757-899X/269/1/012044.

[28] S. Parvate, P. Dixit, and S. Chattopadhyay, “Superhydrophobic Surfaces: Insights from Theory and Experiment,” *J. Phys. Chem. B*, vol. 124, no. 8, pp. 1323–1360, Feb. 2020, doi: 10.1021/ACS.JPCB.9B08567.

[29] B. Bhushan and V. Multanen, “Designing liquid repellent, icephobic and self-cleaning surfaces with high mechanical and chemical durability,” *Philos. Trans. R. Soc. A Math. Phys. Eng. Sci.*, vol. 377, p. 20180270, 2019, doi: 10.1098/rsta.2018.0270.

[30] A. Hooda, M. S. Goyat, J. K. Pandey, A. Kumar, and R. Gupta, “A review on fundamentals, constraints and fabrication techniques of superhydrophobic coatings,” *Prog. Org. Coatings*, vol. 142, p. 105557, May 2020, doi: 10.1016/J.PORGCOAT.2020.105557.

[31] D. Wang *et al.*, “Design of robust superhydrophobic surfaces,” *Nat. 2020 5827810*, vol. 582, no. 7810, pp. 55–59, Jun. 2020, doi: 10.1038/s41586-020-2331-8.

[32] U. Eduok, O. Faye, and J. Szpunar, “Recent developments and applications of protective silicone coatings: A review of PDMS functional materials,” *Prog. Org. Coatings*, vol. 111, pp. 124–163, Oct. 2017, doi: 10.1016/J.PORGCOAT.2017.05.012.

[33] H. Y. Erbil, “Practical Applications of Superhydrophobic Materials and Coatings: Problems and Perspectives,” *Langmuir*, vol. 36, no. 10, pp. 2493–2509, Mar. 2020, doi: 10.1021/ACS.LANGMUIR.9B03908.

[34] A. Allahdini, R. Jafari, and G. Momen, “Development of a dual capsule self-healing silicone composite using silicone chemistry and poly(melamine-urea-formaldehyde) shells,” *J. Appl. Polym. Sci.*, vol. 139, no. 8, p. 51670, Feb. 2022, doi: 10.1002/APP.51670.

[35] A. Allahdini, R. Jafari, and G. Momen, “Transparent non-fluorinated superhydrophobic coating with enhanced anti-icing performance,” *Prog. Org. Coatings*, vol. 165, p. 106758, Apr. 2022, doi: 10.1016/J.PORGCOAT.2022.106758.

[36] A. Allahdini, G. Momen, F. Munger, S. Brettschneider, I. Fofana, and R. Jafari, “Performance of a nanotextured superhydrophobic coating developed for high-voltage outdoor porcelain insulators,” *Colloids Surfaces A Physicochem. Eng. Asp.*, vol. 649, no. June, p. 129461, 2022, doi: 10.1016/j.colsurfa.2022.129461.

[37] W. M. Carty and U. Senapati, “Porcelain - Raw materials, processing, phase evolution, and mechanical behavior,” *J. Am. Ceram. Soc.*, 1998, doi: 10.1111/j.1151-2916.1998.tb02290.x.

[38] J. E. Contreras and E. A. Rodríguez, “Nanostructured insulators – A review of nanotechnology concepts for outdoor ceramic insulators,” *Ceram. Int.*, vol. 43, no. 12, pp. 8545–8550, 2017, doi: 10.1016/j.ceramint.2017.04.105.

[39] K. Dana, S. Das, and S. K. Das, “Effect of substitution of fly ash for quartz in triaxial kaolin–quartz–feldspar system,” *J. Eur. Ceram. Soc.*, vol. 24, no. 10–11, pp. 3169–3175, Sep. 2004, doi: 10.1016/J.JEURCERAMSOC.2003.10.008.

[40] S. M. Gubanski, “Editorial: Outdoor high voltage insulation,” *IEEE Trans. Dielectr. Electr. Insul.*, vol. 17, no. 2, p. 325, Apr. 2010, doi: 10.1109/TDEI.2010.5448084.

[41] R. S. Gorur, “High voltage outdoor insulation technology,” in *Control and Dynamic Systems*, Elsevier B.V., 1991, pp.

131–191.

[42] A. P. Mishra, R. S. Gorur, and S. Venkataraman, “Evaluation of porcelain and toughened glass suspension insulators removed from service,” *IEEE Trans. Dielectr. Electr. Insul.*, vol. 15, no. 2, pp. 467–475, Apr. 2008, doi: 10.1109/TDEI.2008.4483466.

[43] S. Braini, “Coatings for outdoor high voltage insulators,” Cardiff University, 2013.

[44] R. Hackam, “Outdoor HV composite polymeric insulators,” *IEEE Trans. Dielectr. Electr. Insul.*, vol. 6, no. 5, pp. 557–585, 1999, doi: 10.1109/94.798114.

[45] P. Charalampidis, M. Albano, H. Griffiths, A. Haddad, and R. T. Waters, “Silicone rubber insulators for polluted environments part 1: Enhanced artificial pollution tests,” *IEEE Trans. Dielectr. Electr. Insul.*, 2014, doi: 10.1109/TDEI.2013.004015.

[46] Khumbulani Mafasigodo, “Using inclined plane test to compare tracking on silicon rubber under HVAC and HVDC,” University of Kwazulu-Natal, 2018.

[47] R. A. Ghunem, S. H. Jayaram, and E. A. Cherney, “Inclined plane initial tracking voltage for AC, +DC and -DC,” *Conf. Rec. IEEE Int. Symp. Electr. Insul.*, pp. 459–463, 2012, doi: 10.1109/ELINSL.2012.6251510.

[48] K. L. Chrzan, “Application of Silicone coatings on porcelain insulators in Poland, a case study,” in *Proceedings of the 4th International Scientific Symposium on Electric Power Engineering, ELEKTROENERGETIKA 2007*, 2007, pp. 19–21.

[49] M. A. Talebi, A. Gholami, M. R. Shariati, and M. Hasanzadeh, “Technical & economical evaluation of using silicone rubber RTV coating for H.V. substation in polluted area,” *CIRED 2005, 18th Int. Conf. Exhib. Electr. Distrib.*, pp. 1–4, 2005, doi: 10.1049/cp:20050895.

[50] A. N. Chaudhry and N. C. Billingham, “Characterisation and oxidative degradation of a room-temperature vulcanised poly(dimethylsiloxane) rubber,” *Polym. Degrad. Stab.*, vol. 73, no. 3, pp. 505–510, 2001, doi: 10.1016/S0141-3910(01)00139-2.

[51] J. E. Mark, “Some interesting things about polysiloxanes,” *Acc. Chem. Res.*, vol. 37, no. 12, pp. 946–953, 2004, doi: 10.1021/ar030279z.

[52] W. Zhou, H. Yang, X. Guo, and J. Lu, “Thermal degradation behaviors of some branched and linear polysiloxanes,” *Polym. Degrad. Stab.*, vol. 91, no. 7, pp. 1471–1475, 2006, doi: 10.1016/j.polymdegradstab.2005.10.005.

[53] Suwarno, A. Basuki, F. Lendy, and Sumedi, “Improving outdoor insulator performances installed at coastal area using silicone rubber coating,” 2012, doi: 10.1109/CMD.2012.6416361.

[54] I. Ramirez, R. Hernandez, and G. Montoya, “Salt fog testing of RTV coated ceramic insulators and comparison with HTV silicone rubber insulators,” 2012, doi: 10.1109/CEIDP.2012.6378900.

[55] E. A. Cherney, R. Hackam, and S. H. Kim, “Porcelain insulator maintenance with RTV silicone rubber coatings,” *IEEE Trans. Power Deliv.*, 1991, doi: 10.1109/61.85865.

[56] K. Siderakis and D. Agoris, “Performance of RTV silicone rubber coatings installed in coastal systems,” *Electr. Power Syst. Res.*, 2008, doi: 10.1016/j.epsr.2007.02.013.

[57] A. M. Robin H.A. Ras, *Non-wettable Surfaces: Theory, Preparation and Applications*. Royal Society of Chemistry, 2016.

[58] J. T. Simpson, S. R. Hunter, and T. Aytug, “Superhydrophobic materials and coatings: A review,” *Reports on Progress in Physics*, vol. 78, no. 8. Institute of Physics Publishing, p. 086501, Jul. 01, 2015, doi: 10.1088/0034-4885/78/8/086501.

[59] A. K. Padhan and D. Mandal, “Chapter 2: Types of chemistries involved in self-healing polymeric systems,” in *Self-Healing Polymer-Based Systems*, A. S. Sabu Thomas, Ed. Elsevier Inc., 2020, pp. 17–74.

[60] G. Romero-Sabat *et al.*, “Development of a highly efficient extrinsic and autonomous self-healing polymeric system at low and ultra-low temperatures for high-performance applications,” *Compos. Part A Appl. Sci. Manuf.*, vol. 145, p. 106335, Jun. 2021, doi: 10.1016/J.COMPOSITESA.2021.106335.

[61] P. S. Tan, A. A. Somashekar, P. Casari, and D. Bhattacharyya, “Healing efficiency characterization of self-repairing polymer composites based on damage continuum mechanics,” *Compos. Struct.*, vol. 208, pp. 367–376, Jan. 2019, doi: 10.1016/J.COMPSTRUCT.2018.09.091.

[62] T. Young, “An Essay on the Cohesion of Fluids,” *Philos. Trans. R. Soc. London*, vol. 95, no. 0, pp. 65–87, 1805, doi: 10.1098/rstl.1805.0005.

[63] R. N. Wenzel, “Resistance of solid surfaces to wetting by water,” *Ind. Eng. Chem.*, vol. 28, no. 8, pp. 988–994, 1936, doi: 10.1021/ie50320a024.

[64] A. B. D. Cassie and S. Baxter, “Wettability of porous surfaces,” *Trans. Faraday Soc.*, vol. 40, pp. 546–551, 1944, doi: 10.1039/tf9444000546.

[65] O. Tricinci, T. Terencio, B. Mazzolai, N. M. Pugno, F. Greco, and V. Mattoli, “3D Micropatterned Surface Inspired by Salvinia molesta via Direct Laser Lithography,” *ACS Appl. Mater. Interfaces*, vol. 7, no. 46, pp. 25560–25567, 2015, doi: 10.1021/acsami.5b07722.

[66] Faraday Society., “Wettability of porous surfaces,” *Trans. faraday Soc.*, vol. 40, pp. 546–551, 1944, doi: 10.1103/PhysRevLett.70.3796.

[67] H. S. Grewal, I. J. Cho, J. E. Oh, and E. S. Yoon, “Effect of topography on the wetting of nanoscale patterns: Experimental and modeling studies,” *Nanoscale*, vol. 6, no. 24, pp. 15321–15332, 2014, doi: 10.1039/c4nr04069d.

[68] C. E. Cansoy, H. Y. Erbil, O. Akar, and T. Akin, “Effect of pattern size and geometry on the use of Cassie-Baxter equation for superhydrophobic surfaces,” *Colloids Surfaces A Physicochem. Eng. Asp.*, vol. 386, no. 1–3, pp. 116–124, 2011, doi: 10.1016/j.colsurfa.2011.07.005.

[69] B. Bhushan, Y. C. Jung, and K. Koch, “Micro-, nano- and hierarchical structures for superhydrophobicity, self-cleaning and low adhesion,” *Philos. Trans. R. Soc. A Math. Phys. Eng. Sci.*, vol. 367, no. 1894, pp. 1631–1672, May 2009, doi: 10.1098/RSTA.2009.0014.

[70] S. Ebnesajjad, “Adhesives for medical and dental applications,” in *Handbook of Adhesives and Surface Preparation*, Elsevier Inc., 2011, pp. 345–368.

[71] S. Vedantam and M. V. Panchagnula, “Constitutive modeling of contact angle hysteresis,” *J. Colloid Interface Sci.*, vol. 321, no. 2, pp. 393–400, May 2008, doi: 10.1016/J.JCIS.2008.01.056.

[72] I. S. Bayer, C. M. Megaridis, J. Zhang, D. Gamota, and A. Biswas, “Analysis and surface energy estimation of various model polymeric surfaces using contact angle hysteresis,” *http://dx.doi.org/10.1163/156856107782844800*, vol. 21, no. 15, pp. 1439–1467, Nov. 2012, doi: 10.1163/156856107782844800.

[73] E. Chibowski and F. Gonzalez-Caballero, “Interpretation of contact angle hysteresis,” *J. Adhes. Sci. Technol.*, vol. 7, no. 11, pp. 1195–1209, 2012, doi: 10.1163/156856193X00051.

[74] R. E. Johnson and R. H. Dettre, “Contact angle hysteresis. III. Study of an idealized heterogeneous surface,” *J. Phys. Chem.*, 1964, doi: 10.1021/j100789a012.

[75] R. J. Good, “Contact angle, wetting, and adhesion: a critical review,” *J. Adhes. Sci. Technol.*, vol. 6, no. 12, pp. 1269–1302, 2012, doi: 10.1163/156856192X00629.

[76] H. Y. Erbil, “The debate on the dependence of apparent contact angles on drop contact area or three-phase contact line: A review,” *Surf. Sci. Rep.*, vol. 69, no. 4, pp. 325–365, Dec. 2014, doi: 10.1016/J.SURFREP.2014.09.001.

[77] A.B. Pridmore; R.P. Ojdrovic, “Trenchless Repair of Concrete Pipelines Using Fiber-reinforced Polymer Composites,” in *Rehabilitation of pipelines using fiber-reinforced polymer (FRP) composites*, no. 2001, Vistasp M. Karbhari, Ed. Elsevier Ltd, 2015, pp. 17–38.

[78] G. McHale, N. J. Shirtcliffe, and M. I. Newton, “Contact-angle hysteresis on super-hydrophobic surfaces,” *Langmuir*, vol. 20, no. 23, pp. 10146–10149, 2004, doi: 10.1021/la0486584.

[79] C. G. L. Furmidge, “Studies at phase interfaces. I. The sliding of liquid drops on solid surfaces and a theory for spray retention,” *J. Colloid Sci.*, vol. 17, no. 4, pp. 309–324, Apr. 1962, doi: 10.1016/0095-8522(62)90011-9.

[80] S. Parvate, P. Dixit, and S. Chattopadhyay, “Superhydrophobic Surfaces: Insights from Theory and Experiment,” *J.*

Phys. Chem. B, vol. 124, no. 8, pp. 1323–1360, Feb. 2020, doi: 10.1021/ACS.JPCB.9B08567.

[81] A. B. D. Cassie, "Contact angles," *Discuss. Faraday Soc.*, vol. 3, no. 0, pp. 11–16, Jan. 1948, doi: 10.1039/DF9480300011.

[82] H. Y. Erbil, *Surface Chemistry of Solid and Liquid Interfaces*, vol. 83, no. 5. Wiley, 2006.

[83] J. D. Andrade, L. M. Smith, and D. E. Gregonis, "The Contact Angle and Interface Energetics," in *Surface and Interfacial Aspects of Biomedical Polymers*, Springer US, 1985, pp. 249–292.

[84] C. Neinhuis and W. Barthlott, "Characterization and Distribution of Water-repellent, Self-cleaning Plant Surfaces," *Ann. Bot.*, vol. 79, no. 6, pp. 667–677, Jun. 1997, doi: 10.1006/ANBO.1997.0400.

[85] Z. Guo, W. Liu, and B. L. Su, "Superhydrophobic surfaces: From natural to biomimetic to functional," *J. Colloid Interface Sci.*, vol. 353, no. 2, pp. 335–355, Jan. 2011, doi: 10.1016/J.JCIS.2010.08.047.

[86] H. J. Ensikat, P. Ditsche-Kuru, C. Neinhuis, and W. Barthlott, "Superhydrophobicity in perfection: the outstanding properties of the lotus leaf," *Beilstein J. Nanotechnol.*, vol. 2, no. 1, p. 152, 2011, doi: 10.3762/BJNANO.2.19.

[87] B. B. Nosonovsky M., *Lotus Effect: Roughness-Induced Superhydrophobicity.* Springer, Berlin, Heidelberg, 2007.

[88] P. Li, L. Wang, S. Tang, Y. Xing, H. Zhao, and J. Liu, "Shape Control of Lotus Leaf Induced by Surface Submillimeter Texture," *Adv. Mater. Interfaces*, vol. 7, no. 8, p. 2000040, Apr. 2020, doi: 10.1002/ADMI.202000040.

[89] Z. Guo and W. Liu, "Biomimic from the superhydrophobic plant leaves in nature: Binary structure and unitary structure," *Plant Sci.*, vol. 172, no. 6, pp. 1103–1112, Jun. 2007, doi: 10.1016/J.PLANTSCI.2007.03.005.

[90] T. B. H. Schroeder, J. Houghtaling, B. D. Wilts, and M. Mayer, "It's Not a Bug, It's a Feature: Functional Materials in Insects," *Adv. Mater.*, vol. 30, no. 19, 2018, doi: 10.1002/adma.201705322.

[91] G. S. Watson *et al.*, "Insect Analogue to the Lotus Leaf: A Planthopper Wing Membrane Incorporating a Low-Adhesion, Nonwetting, Superhydrophobic, Bactericidal, and Biocompatible Surface," *ACS Appl. Mater. Interfaces*, vol. 9, no. 28, pp. 24381–24392, Jul. 2017, doi: 10.1021/ACSAMI.7B08368/SUPPL_FILE/AM7B08368_SI_001.PDF.

[92] T. Nishino, M. Meguro, K. Nakamae, M. Matsushita, and Y. Ueda, "The Lowest Surface Free Energy Based on $-CF_3$ Alignment," *Langmuir*, vol. 15, no. 13, pp. 4321–4323, 1999, doi: 10.1021/la981727s.

[93] T. Onda, S. Shibuichi, N. Satoh, and K. Tsujii, "Super-water-repellent fractal surfaces," *Langmuir*, vol. 12, no. 9, pp. 2125–2127, May 1996, doi: 10.1021/LA950418O.

[94] M. Ma and R. M. Hill, "Superhydrophobic surfaces," *Curr. Opin. Colloid Interface Sci.*, vol. 11, no. 4, pp. 193–202, Oct. 2006, doi: 10.1016/J.COCIS.2006.06.002.

[95] G. Barati Darband, M. Aliofkhazraei, S. Khorsand, S. Sokhanvar, and A. Kaboli, "Science and Engineering of Superhydrophobic Surfaces: Review of Corrosion Resistance, Chemical and Mechanical Stability," *Arab. J. Chem.*, vol. 13, no. 1, pp. 1763–1802, Jan. 2020, doi: 10.1016/J.ARABJC.2018.01.013.

[96] X. Gao and Z. Guo, "Biomimetic superhydrophobic surfaces with transition metals and their oxides: A review," *J. Bionic Eng. 2017 143*, vol. 14, no. 3, pp. 401–439, Sep. 2017, doi: 10.1016/S1672-6529(16)60408-0.

[97] J. Liu, X. Fang, C. Zhu, X. Xing, G. Cui, and Z. Li, "Fabrication of superhydrophobic coatings for corrosion protection by electrodeposition: A comprehensive review," *Colloids Surfaces A Physicochem. Eng. Asp.*, vol. 607, p. 125498, Dec. 2020, doi: 10.1016/J.COLSURFA.2020.125498.

[98] Y. Wu, M. Zhao, and Z. Guo, "Robust, heat-resistant and multifunctional superhydrophobic coating of carbon microflowers with molybdenum trioxide nanoparticles," *J. Colloid Interface Sci.*, vol. 506, pp. 649–658, Nov. 2017, doi: 10.1016/J.JCIS.2017.07.091.

[99] T. J. Young, J. Jackson, S. Roy, H. Ceylan, and S. Sundararajan, "Tribological behavior and wettability of spray-coated superhydrophobic coatings on aluminum," *Wear*, vol. 376–377, pp. 1713–1719, Apr. 2017, doi: 10.1016/J.WEAR.2016.12.050.

[100] T. Ren, G. Tang, B. Yuan, Z. Yan, L. Ma, and X. Huang, "One-step fabrication of robust superhydrophobic coatings with corrosion resistance by a self-curing epoxy-resin-based adhesive," *Surf. Coatings Technol.*, vol. 380, p. 125086,

Dec. 2019, doi: 10.1016/J.SURFCOAT.2019.125086.

[101] K. Fu *et al.*, "Mechanically robust, self-healing superhydrophobic anti-icing coatings based on a novel fluorinated polyurethane synthesized by a two-step thiol click reaction," *Chem. Eng. J.*, vol. 404, p. 127110, Jan. 2021, doi: 10.1016/J.CEJ.2020.127110.

[102] C. Xie *et al.*, "ZnO/Acrylic Polyurethane Nanocomposite Superhydrophobic Coating on Aluminum Substrate Obtained via Spraying and Co-Curing for the Control of Marine Biofouling," *Surfaces and Interfaces*, vol. 22, p. 100833, Feb. 2021, doi: 10.1016/J.SURFIN.2020.100833.

[103] X. Gong and S. He, "Highly Durable Superhydrophobic Polydimethylsiloxane/Silica Nanocomposite Surfaces with Good Self-Cleaning Ability," *ACS Omega*, vol. 5, no. 8, pp. 4100–4108, Mar. 2020, doi: 10.1021/ACSOMEGA.9B03775/SUPPL_FILE/AO9B03775_SI_001.PDF.

[104] C. Ma *et al.*, "Preparation and characterization of polyacrylate composite and its application in superhydrophobic coating based on silicone-modified ZnO," *J. Coatings Technol. Res.*, vol. 18, no. 2, pp. 415–433, Mar. 2021, doi: 10.1007/S11998-020-00411-7/FIGURES/12.

[105] D. E. Packham, "Surface energy, surface topography and adhesion," *Int. J. Adhes. Adhes.*, vol. 23, no. 6, pp. 437–448, Jan. 2003, doi: 10.1016/S0143-7496(03)00068-X.

[106] Y. Cao, A. Salvini, and M. Camaiti, "Superhydrophobic fluorinated oligomers as protective agents for outdoor stone artworks," *J. Cult. Herit.*, vol. 44, pp. 90–97, Jul. 2020, doi: 10.1016/J.CULHER.2020.01.005.

[107] T. Jan Kadoski, U. Gryglewicz Mateusz Staczyk, and T. Kadoski, "investigations on lubricity and surface properties of selected perfluoropolyether oils," *J. KONES Powertrain Transp.*, vol. 18, no. 1, pp. 199–212, 2011.

[108] R. R. Thomas, "Material Properties of Fluoropolymers and Perfluoroalkyl-based Polymers," *Fluoropolymers 2*, pp. 47–67, Feb. 2002, doi: 10.1007/0-306-46919-7_4.

[109] J. C. Fielding, "Fluorination of silicone rubber by plasma polymerization," University of Cincinnati, 2004.

[110] K. Aleksandrov *et al.*, "Waste incineration of Polytetrafluoroethylene (PTFE) to evaluate potential formation of per- and Poly-Fluorinated Alkyl Substances (PFAS) in flue gas," *Chemosphere*, vol. 226, pp. 898–906, 2019, doi: 10.1016/j.chemosphere.2019.03.191.

[111] S. Pan, M. Chen, and L. Wu, "Smart Superhydrophobic Surface with Restorable Microstructure and Self-Healable Surface Chemistry," *ACS Appl. Mater. Interfaces*, vol. 12, no. 4, pp. 5157–5165, Jan. 2020, doi: 10.1021/ACSAMI.9B22693/SUPPL_FILE/AM9B22693_SI_003.AVI.

[112] S. M. R. Razavi *et al.*, "Superhydrophobic Surfaces Made from Naturally Derived Hydrophobic Materials," *ACS Sustain. Chem. Eng.*, vol. 5, no. 12, 2017, doi: 10.1021/acssuschemeng.7b02424.

[113] T. Darmanin and F. Guittard, "Superoleophobic surfaces with short fluorinated chains?," *Soft Matter*, vol. 9, no. 25, pp. 5982–5990, Jun. 2013, doi: 10.1039/C3SM50643F.

[114] X. Zhao *et al.*, "Environmentally benign and durable superhydrophobic coatings based on SiO2 nanoparticles and silanes," *J. Colloid Interface Sci.*, vol. 542, pp. 8–14, Apr. 2019, doi: 10.1016/J.JCIS.2019.01.115.

[115] J. E. Mates *et al.*, "Environmentally-safe and transparent superhydrophobic coatings," *Green Chem.*, vol. 18, no. 7, pp. 2185–2192, Mar. 2016, doi: 10.1039/C5GC02725J.

[116] Q. Wang, G. Sun, Q. Tong, W. Yang, and W. Hao, "Fluorine-free superhydrophobic coatings from polydimethylsiloxane for sustainable chemical engineering: Preparation methods and applications," *Chem. Eng. J.*, vol. 426, p. 130829, Dec. 2021, doi: 10.1016/J.CEJ.2021.130829.

[117] G. Lorenz and A. Kandelbauer, "Silicones," in *Handbook of Thermoset Plastics*, H. Dodiuk, Ed. William Andrew Publishing, 2014, pp. 555–575.

[118] L. Li, B. Li, J. Dong, and J. Zhang, "Roles of silanes and silicones in forming superhydrophobic and superoleophobic materials," *J. Mater. Chem. A*, vol. 4, no. 36, pp. 13677–13725, 2016, doi: 10.1039/c6ta05441b.

[119] Q. S. Bhatia, J. K. Chen, J. T. Koberstein, J. E. Sohn, and J. A. Emerson, "The measurement of polymer surface tension by drop image processing: Application to PDMS and comparison with theory," *J. Colloid Interface Sci.*, vol. 106, no. 2,

pp. 353–359, 1985, doi: 10.1016/S0021-9797(85)80009-6.

[120] G. Wang *et al.*, "A Review on Fabrication Methods and Research Progress of Superhydrophobic Silicone Rubber Materials," *Adv. Mater. Interfaces*, vol. 8, no. 1, pp. 1–19, 2021, doi: 10.1002/admi.202001460.

[121] J. N. Wang *et al.*, "Wearable Superhydrophobic Elastomer Skin with Switchable Wettability," *Adv. Funct. Mater.*, vol. 28, no. 23, p. 1800625, Jun. 2018, doi: 10.1002/ADFM.201800625.

[122] E. Yilgör, Y. Yilgör, and I. Yilgör, "Silicone containing copolymers: Synthesis, properties and applications," *Prog. Polym. Sci.*, vol. 39, pp. 1165–1195, 2014, doi: 10.1016/j.progpolymsci.2013.11.003.

[123] H. Wang *et al.*, "Multifunctional superhydrophobic surface with dynamically controllable micro/nanostructures for droplet manipulation and friction control," *Chem. Eng. J.*, vol. 417, p. 127944, Aug. 2021, doi: 10.1016/J.CEJ.2020.127944.

[124] B. Cortese, S. D'Amone, M. Manca, I. Viola, R. Cingolani, and G. Gigli, "Superhydrophobicity Due to the Hierarchical Scale Roughness of PDMS Surfaces," *Langmuir*, vol. 24, no. 6, pp. 2712–2718, Mar. 2008, doi: 10.1021/LA702764X.

[125] J. Yong *et al.*, "Femtosecond laser weaving superhydrophobic patterned PDMS surfaces with tunable adhesion," *J. Phys. Chem. C*, vol. 117, no. 47, pp. 24907–24912, Nov. 2013, doi: 10.1021/JP408863U/SUPPL_FILE/JP408863U_SI_010.AVI.

[126] T. Zhu *et al.*, "A transparent superhydrophobic coating with mechanochemical robustness for anti-icing, photocatalysis and self-cleaning," *Chem. Eng. J.*, vol. 399, p. 125746, Nov. 2020, doi: 10.1016/j.cej.2020.125746.

[127] T. He *et al.*, "Facile fabrication of superhydrophobic Titanium dioxide-composited cotton fabrics to realize oil-water separation with efficiently photocatalytic degradation for water-soluble pollutants," *Colloids Surfaces A Physicochem. Eng. Asp.*, vol. 585, p. 124080, Jan. 2020, doi: 10.1016/J.COLSURFA.2019.124080.

[128] H. Zhou *et al.*, "Fabrication of ZnO/epoxy resin superhydrophobic coating on AZ31 magnesium alloy," *Chem. Eng. J.*, vol. 368, pp. 261–272, Jul. 2019, doi: 10.1016/J.CEJ.2019.02.032.

[129] W. Stöber, A. Fink, and E. Bohn, "Controlled growth of monodisperse silica spheres in the micron size range," *J. Colloid Interface Sci.*, vol. 26, no. 1, pp. 62–69, Jan. 1968, doi: 10.1016/0021-9797(68)90272-5.

[130] L. Dashairya, D. D. Barik, and P. Saha, "Methyltrichlorosilane functionalized silica nanoparticles-treated superhydrophobic cotton for oil–water separation," *J. Coatings Technol. Res. 2019 164*, vol. 16, no. 4, pp. 1021–1032, Feb. 2019, doi: 10.1007/S11998-018-00177-Z.

[131] M. Manca, A. Cannavale, L. De Marco, A. S. Aricò, R. Cingolani, and G. Gigli, "Durable Superhydrophobic and Antireflective Surfaces by Trimethylsilanized Silica Nanoparticles-Based Sol−Gel Processing," *Langmuir*, vol. 25, no. 11, pp. 6357–6362, Jun. 2009, doi: 10.1021/LA804166T.

[132] N. Ullah *et al.*, "Fabrication and characterization of functionalized nano-silica based transparent superhydrophobic surface," *Mater. Chem. Phys.*, vol. 267, p. 124694, Jul. 2021, doi: 10.1016/J.MATCHEMPHYS.2021.124694.

[133] S. Riaz, M. Ashraf, T. Hussain, and M. T. Hussain, "Modification of silica nanoparticles to develop highly durable superhydrophobic and antibacterial cotton fabrics," *Cellul. 2019 268*, vol. 26, no. 8, pp. 5159–5175, Apr. 2019, doi: 10.1007/S10570-019-02440-X.

[134] A. Idris, Z. Man, A. S. Maulud, M. A. Bustam, H. A. Mannan, and I. Ahmed, "Investigation on particle properties and extent of functionalization of silica nanoparticles," *Appl. Surf. Sci.*, vol. 506, p. 144978, Mar. 2020, doi: 10.1016/J.APSUSC.2019.144978.

[135] C. Petcu *et al.*, "The Influence of New Hydrophobic Silica Nanoparticles on the Surface Properties of the Films Obtained from Bilayer Hybrids," *Nanomater. 2017, Vol. 7, Page 47*, vol. 7, no. 2, p. 47, Feb. 2017, doi: 10.3390/NANO7020047.

[136] Y. Wang, L. Zhang, Y. Hu, and C. Li, "In situ Surface Functionalization of Hydrophilic Silica Nanoparticles via Flame Spray Process," *J. Mater. Sci. Technol.*, vol. 31, no. 9, pp. 901–906, Sep. 2015, doi: 10.1016/J.JMST.2015.07.001.

[137] D. Heiman-Burstein, A. Dotan, H. Dodiuk, and S. Kenig, "Hybrid sol-gel superhydrophobic coatings based on alkyl silane-modified nanosilica," *Polymers (Basel).*, vol. 13, no. 4, pp. 1–15, 2021, doi: 10.3390/polym13040539.

[138] J.-D. Brassard, D. K. Sarkar, and J. Perron, "Synthesis of Monodisperse Fluorinated Silica Nanoparticles and Their

Superhydrophobic Thin Films," *ACS Appl. Mater. Interfaces*, vol. 3, no. 9, pp. 3583–3588, Sep. 2011, doi: 10.1021/AM2007917.

[139] A. B. M. Giasuddin, A. Cartwright, and D. W. Britt, "Silica Nanoparticles Synthesized from 3,3,3-Propyl(trifluoro)trimethoxysilane or n-Propyltrimethoxysilane for Creating Superhydrophobic Surfaces," *ACS Appl. Nano Mater.*, vol. 4, no. 4, pp. 4092–4102, Apr. 2021, doi: 10.1021/ACSANM.1C00398.

[140] Y. Cai, J. Li, L. Yi, X. Yan, and J. Li, "Fabricating superhydrophobic and oleophobic surface with silica nanoparticles modified by silanes and environment-friendly fluorinated chemicals," *Appl. Surf. Sci.*, vol. 450, pp. 102–111, Aug. 2018, doi: 10.1016/J.APSUSC.2018.04.186.

[141] A. Yildirim, H. Budunoglu, B. Daglar, H. Deniz, and M. Bayindir, "One-Pot Preparation of Fluorinated Mesoporous Silica Nanoparticles for Liquid Marble Formation and Superhydrophobic Surfaces," *ACS Appl. Mater. Interfaces*, vol. 3, no. 6, pp. 1804–1808, Jun. 2011, doi: 10.1021/AM200359E.

[142] A. R. Jennings and S. T. Iacono, "Progress in fluorinated organically modified silicas," *Polym. Int.*, vol. 65, no. 1, pp. 6–10, Jan. 2016, doi: 10.1002/PI.4984.

[143] X. Wang, X. Li, Q. Lei, Y. Wu, and W. Li, "Fabrication of superhydrophobic composite coating based on fluorosilicone resin and silica nanoparticles," doi: 10.1098/rsos.180598.

[144] V. S. Saji, "Wax-based artificial superhydrophobic surfaces and coatings," *Colloids Surfaces A Physicochem. Eng. Asp.*, vol. 602, p. 125132, Oct. 2020, doi: 10.1016/J.COLSURFA.2020.125132.

[145] M. Li, W. Luo, H. Sun, J. Xu, Y. Liu, and X. Cheng, "Superhydrophobic coatings fabricated by paraffin wax and silica nanoparticles with enhanced adhesion stability," *Mater. Lett.*, vol. 309, p. 131316, Feb. 2022, doi: 10.1016/J.MATLET.2021.131316.

[146] I. S. Bayer and I. S. Bayer, "Superhydrophobic Coatings from Ecofriendly Materials and Processes: A Review," *Adv. Mater. Interfaces*, vol. 7, no. 13, p. 2000095, Jul. 2020, doi: 10.1002/ADMI.202000095.

[147] Z. Wei, D. Jiang, J. Chen, S. Ren, and L. Li, "Fabrication of mechanically robust superhydrophobic aluminum surface by acid etching and stearic acid modification," *http://dx.doi.org/10.1080/01694243.2017.1302698*, vol. 31, no. 21, pp. 2380–2397, Nov. 2017, doi: 10.1080/01694243.2017.1302698.

[148] H. Wang, S. Dong, and Z. Wang, "One-step fabrication of superhydrophobic surface on beryllium copper alloys and corrosion protection application," *Colloids Surfaces A Physicochem. Eng. Asp.*, vol. 556, pp. 291–298, Nov. 2018, doi: 10.1016/J.COLSURFA.2018.08.044.

[149] M. Ghasemlou, F. Daver, E. P. Ivanova, and B. Adhikari, "Bio-inspired sustainable and durable superhydrophobic materials: from nature to market," *J. Mater. Chem. A*, vol. 7, no. 28, pp. 16643–16670, Jul. 2019, doi: 10.1039/C9TA05185F.

[150] I. S. Bayer, "Superhydrophobic Coatings from Ecofriendly Materials and Processes: A Review," *Adv. Mater. Interfaces*, vol. 7, no. 13, p. 2000095, Jul. 2020, doi: 10.1002/ADMI.202000095.

[151] S. Naderizadeh *et al.*, "Bioresin-based superhydrophobic coatings with reduced bacterial adhesion," *J. Colloid Interface Sci.*, vol. 574, pp. 20–32, Aug. 2020, doi: 10.1016/J.JCIS.2020.04.031.

[152] J. M. Morrissette, P. J. Carroll, I. S. Bayer, J. Qin, D. Waldroup, and C. M. Megaridis, "A methodology to produce eco-friendly superhydrophobic coatings produced from all-water-processed plant-based filler materials," *Green Chem.*, vol. 20, no. 22, pp. 5169–5178, Nov. 2018, doi: 10.1039/C8GC02439A.

[153] A. Diego-Taboada, S. T. Beckett, S. L. Atkin, and G. Mackenzie, "Hollow Pollen Shells to Enhance Drug Delivery," *Pharm. 2014, Vol. 6, Pages 80-96*, vol. 6, no. 1, pp. 80–96, Mar. 2014, doi: 10.3390/PHARMACEUTICS6010080.

[154] Sumio Sakka, "History of the Sol-Gel Chemistry and Technology," in *Handbook of sol-gel science and technology; Processing, Characterization, and Applications.*, Second Edi., A. J. Lisa Klein, Mario Aparicio, Ed. Springer, Cham, 2018, pp. 3–29.

[155] M. Poddighe and P. Innocenzi, "Hydrophobic Thin Films from Sol–Gel Processing: A Critical Review," *Mater. 2021, Vol. 14, Page 6799*, vol. 14, no. 22, p. 6799, Nov. 2021, doi: 10.3390/MA14226799.

[156] C. Ke, C. Zhang, X. Wu, and Y. Jiang, "Highly transparent and robust superhydrophobic coatings fabricated via a facile sol-gel process," *Thin Solid Films*, vol. 723, p. 138583, Apr. 2021, doi: 10.1016/J.TSF.2021.138583.

[157] M. G. N. C. Barry Carter, “Sols, Gels, and Organic Chemistry,” in *Ceramic Materials*, Springer, New York, NY, 2007, pp. 400–411.

[158] S. Xu, Q. Wang, and N. Wang, “Chemical Fabrication Strategies for Achieving Bioinspired Superhydrophobic Surfaces with Micro and Nanostructures: A Review,” *Adv. Eng. Mater.*, vol. 23, no. 3, p. 2001083, Mar. 2021, doi: 10.1002/ADEM.202001083.

[159] T. Darmanin, E. T. De Givenchy, S. Amigoni, and F. Guittard, “Superhydrophobic Surfaces by Electrochemical Processes,” *Adv. Mater.*, vol. 25, no. 10, pp. 1378–1394, Mar. 2013, doi: 10.1002/ADMA.201204300.

[160] H. Bellanger, T. Darmanin, E. Taffin De Givenchy, and F. Guittard, “Chemical and Physical Pathways for the Preparation of Superoleophobic Surfaces and Related Wetting Theories,” *Chem. Rev.*, vol. 114, no. 5, pp. 2694–2716, Mar. 2014, doi: 10.1021/CR400169M.

[161] L. Cao, H. A. Hu, and D. Gao, “Design and Fabrication of Micro-textures for Inducing a Superhydrophobic Behavior on Hydrophilic Materials,” *Langmuir*, vol. 23, no. 8, pp. 4310–4314, Apr. 2007, doi: 10.1021/LA063572R.

[162] Wei Chen and Thomas J. McCarthy, “Layer-by-layer deposition: A tool for polymer surface modification,” *Macromolecules*, vol. 30, no. 1, pp. 78–86, 1997, doi: https://doi.org/10.1021/ma961096d.

[163] Y. Li, X. Wang, and J. Sun, “Layer-by-layer assembly for rapid fabrication of thick polymeric films,” *Chem. Soc. Rev.*, vol. 41, no. 18, pp. 5998–6009, Aug. 2012, doi: 10.1039/C2CS35107B.

[164] H. A. M. Mustafa and D. A. Jameel, “Modeling and the main stages of spin coating process: A review,” *J. Appl. Sci. Technol. Trends*, vol. 2, no. 03, pp. 91–95, 2021, doi: 10.38094/jastt203109.

[165] Z. Ji, Y. Liu, and F. Du, “Rational design of superhydrophobic, transparent hybrid coating with superior durability,” *Prog. Org. Coatings*, vol. 157, p. 106294, Aug. 2021, doi: 10.1016/J.PORGCOAT.2021.106294.

[166] Z. Ji, Y. Liu, and F. Du, “Facile synthesis of solvent-free and mechanically robust coating with self-cleaning property,” *Prog. Org. Coatings*, vol. 149, p. 105923, Dec. 2020, doi: 10.1016/J.PORGCOAT.2020.105923.

[167] H. Ye *et al.*, “Durable and Robust Self-Healing Superhydrophobic Co-PDMS@ZIF-8-Coated MWCNT Films for Extremely Efficient Emulsion Separation,” *ACS Appl. Mater. Interfaces*, vol. 11, no. 41, pp. 38313–38320, Oct. 2019, doi: 10.1021/ACSAMI.9B13539/SUPPL_FILE/AM9B13539_SI_001.PDF.

[168] L. Chen *et al.*, “Facile fabrication of robust and healable superhydrophobic cotton fabric with flower-like Ni(OH)2@ODA micro-nanoparticles,” *Cellulose*, vol. 28, no. 1, pp. 581–592, Jan. 2021, doi: 10.1007/S10570-020-03546-3/FIGURES/9.

[169] M. J. Nine, T. T. Tung, F. Alotaibi, D. N. H. Tran, and D. Losic, “Facile Adhesion-Tuning of Superhydrophobic Surfaces between ‘Lotus’ and ‘Petal’ Effect and Their Influence on Icing and Deicing Properties,” *ACS Appl. Mater. Interfaces*, vol. 9, no. 9, pp. 8393–8402, Mar. 2017, doi: 10.1021/ACSAMI.6B16444/SUPPL_FILE/AM6B16444_SI_004.AVI.

[170] C. Cao *et al.*, “Robust fluorine-free superhydrophobic PDMS–ormosil@fabrics for highly effective self-cleaning and efficient oil–water separation,” *J. Mater. Chem. A*, vol. 4, no. 31, pp. 12179–12187, Aug. 2016, doi: 10.1039/C6TA04420D.

[171] H. Sun *et al.*, “Superhydrophobic Activated Carbon-Coated Sponges for Separation and Absorption,” *ChemSusChem*, vol. 6, no. 6, pp. 1057–1062, Jun. 2013, doi: 10.1002/CSSC.201200979.

[172] X. Li, M. Cao, H. Shan, F. Handan Tezel, and B. Li, “Facile and scalable fabrication of superhydrophobic and superoleophilic PDMS-co-PMHS coating on porous substrates for highly effective oil/water separation,” *Chem. Eng. J.*, vol. 358, pp. 1101–1113, 2018, doi: 10.1016/j.cej.2018.10.097.

[173] Y. X. Chao Hua, Wenhui Chena, Tan Lia, Yanxi Dinga, Han Yanga, Shuangjie Zhaob, Emmanuel Acheampong Tsiwaha, Xiujian Zhaoa, “Constructing non-fluorinated porous superhydrophobic SiO2-based films with robust mechanical properties,” *Colloids Surfaces A Physicochem. Eng. Asp. surfaces*, vol. 551, pp. 65–73, 2018.

[174] C. Li, M. Boban, J. M. Beebe, D. E. Bhagwagar, J. Liu, and A. Tuteja, “Non-Fluorinated, Superhydrophobic Binder-Filler Coatings on Smooth Surfaces: Controlled Phase Separation of Particles to Enhance Mechanical Durability,” *Langmuir*, vol. 37, no. 10, pp. 3104–3112, Mar. 2021, doi: 10.1021/ACS.LANGMUIR.0C03455/SUPPL_FILE/LA0C03455_SI_001.PDF.

[175] H. Ye, L. Zhu, W. Li, H. Liu, and H. Chen, “Simple spray deposition of a water-based superhydrophobic coating with

high stability for flexible applications," *J. Mater. Chem. A*, vol. 5, no. 20, pp. 9882–9890, May 2017, doi: 10.1039/C7TA02118F.

[176] L. Li, J. Zhu, and Z. Zeng, "A sky-blue superhydrophobic coating and applications," *Prog. Org. Coatings*, vol. 147, p. 105863, Oct. 2020, doi: 10.1016/J.PORGCOAT.2020.105863.

[177] K. Golovin, M. Boban, J. M. Mabry, and A. Tuteja, "Designing Self-Healing Superhydrophobic Surfaces with Exceptional Mechanical Durability," *ACS Appl. Mater. Interfaces*, vol. 9, no. 12, pp. 11212–11223, Mar. 2017, doi: 10.1021/ACSAMI.6B15491/SUPPL_FILE/AM6B15491_SI_005.AVI.

[178] X. Li, B. Li, Y. Li, and J. Sun, "Nonfluorinated, transparent, and spontaneous self-healing superhydrophobic coatings enabled by supramolecular polymers," *Chem. Eng. J.*, vol. 404, p. 126504, Jan. 2021, doi: 10.1016/J.CEJ.2020.126504.

[179] Y. Shen *et al.*, "Spraying Preparation of Eco-Friendly Superhydrophobic Coatings with Ultralow Water Adhesion for Effective Anticorrosion and Antipollution," *ACS Appl. Mater. Interfaces*, vol. 12, no. 22, pp. 25484–25493, Jun. 2020, doi: 10.1021/ACSAMI.0C06074/SUPPL_FILE/AM0C06074_SI_003.AVI.

[180] J. Zhang, L. Zhang, and X. Gong, "Large-Scale Spraying Fabrication of Robust Fluorine-Free Superhydrophobic Coatings Based on Dual-Sized Silica Particles for Effective Antipollution and Strong Buoyancy," *Langmuir*, vol. 37, no. 19, pp. 6042–6051, 2021, doi: 10.1021/acs.langmuir.1c00706.

[181] A. Elzaabalawy and S. A. Meguid, "Development of novel superhydrophobic coatings using siloxane-modified epoxy nanocomposites," *Chem. Eng. J.*, vol. 398, p. 125403, 2020, doi: 10.1016/j.cej.2020.125403.

[182] M. Long *et al.*, "Robust and thermal-healing superhydrophobic surfaces by spin-coating of polydimethylsiloxane," *Colloid interface Sci.*, vol. 508, pp. 18–27, 2017, doi: 10.1016/j.jcis.2017.08.027.

[183] V. A. Ganesh, H. K. Raut, A. S. Nair, and S. Ramakrishna, "A review on self-cleaning coatings," *J. Mater. Chem.*, vol. 21, pp. 16304–16322, 2011, doi: 10.1039/c1jm12523k.

[184] S. P. Dalawai *et al.*, "Recent Advances in durability of superhydrophobic self-cleaning technology: A critical review," *Progress in Organic Coatings*, vol. 138. Elsevier B.V., p. 105381, Jan. 01, 2020, doi: 10.1016/j.porgcoat.2019.105381.

[185] Y. L. Zhang, H. Xia, E. Kim, and H. B. Sun, "Recent developments in superhydrophobic surfaces with unique structural and functional properties," *Soft Matter*, vol. 8, no. 44. The Royal Society of Chemistry, pp. 11217–11231, Oct. 23, 2012, doi: 10.1039/c2sm26517f.

[186] H. Sojoudi, M. Wang, N. D. Boscher, G. H. McKinley, and K. K. Gleason, "Durable and scalable icephobic surfaces: Similarities and distinctions from superhydrophobic surfaces," *Soft Matter*. 2016, doi: 10.1039/c5sm02295a.

[187] A. J. Meuler, J. D. Smith, K. K. Varanasi, J. M. Mabry, G. H. McKinley, and R. E. Cohen, "Relationships between water wettability and ice adhesion," *ACS Appl. Mater. Interfaces*, vol. 2, no. 11, pp. 3100–3110, 2010, doi: 10.1021/am1006035.

[188] R. Menini and M. Farzaneh, "Elaboration of Al2O3/PTFE icephobic coatings for protecting aluminum surfaces," *Surf. Coatings Technol.*, 2009, doi: 10.1016/j.surfcoat.2009.01.030.

[189] P. Kim, T. S. Wong, J. Alvarenga, M. J. Kreder, W. E. Adorno-Martinez, and J. Aizenberg, "Liquid-infused nanostructured surfaces with extreme anti-ice and anti-frost performance," *ACS Nano*, 2012, doi: 10.1021/nn302310q.

[190] S. Jung, M. Dorrestijn, D. Raps, A. Das, C. M. Megaridis, and D. Poulikakos, "Are superhydrophobic surfaces best for icephobicity?," *Langmuir*, vol. 27, no. 6, pp. 3059–3066, 2011, doi: 10.1021/la104762g.

[191] S. Jung, M. K. Tiwari, N. V. Doan, and D. Poulikakos, "Mechanism of supercooled droplet freezing on surfaces," *Nat. Commun.*, vol. 3, p. 615, 2012, doi: 10.1038/ncomms1630.

[192] P. Guo, Y. Zheng, M. Wen, C. Song, Y. Lin, and L. Jiang, "Icephobic/anti-icing properties of micro/nanostructured surfaces," *Adv. Mater.*, vol. 24, no. 19, pp. 2642–2648, 2012, doi: 10.1002/adma.201104412.

[193] L. Zheng *et al.*, "Exceptional superhydrophobicity and low velocity impact icephobicity of acetone-functionalized carbon nanotube films," *Langmuir*, vol. 27, no. 16, pp. 9936–9943, 2011, doi: 10.1021/la201548k.

[194] D. Mangini, C. Antonini, M. Marengo, and A. Amirfazli, "Runback ice formation mechanism on hydrophilic and superhydrophobic surfaces," *Cold Reg. Sci. Technol.*, vol. 109, pp. 53–60, 2015, doi:

10.1016/j.coldregions.2014.09.012.

[195] G. Wang, Y. Shen, J. Tao, X. Luo, L. Zhang, and Y. Xia, “Fabrication of a superhydrophobic surface with a hierarchical nanoflake-micropit structure and its anti-icing properties,” *RSC Adv.*, vol. 7, no. 16, pp. 9981–9988, 2017, doi: 10.1039/c6ra28298a.

[196] M. Qian, G. H. Tan, Z. Y. Lee, C. W. Koh, and L. Y. L. Wu, “Nanostructure-induced icephobic sol–gel coating for glass application,” *J. Sol-Gel Sci. Technol.*, vol. 81, pp. 127–137, 2017, doi: 10.1007/s10971-016-4069-1.

[197] S. Yang *et al.*, “Condensation frosting and passive anti-frosting,” *Cell Reports Phys. Sci.*, vol. 2, no. 7, p. 100474, Jul. 2021, doi: 10.1016/J.XCRP.2021.100474.

[198] S. Farhadi, M. Farzaneh, and S. A. Kulinich, “Anti-icing performance of superhydrophobic surfaces,” *Appl. Surf. Sci.*, vol. 257, no. 14, pp. 6264–6269, 2011, doi: 10.1016/j.apsusc.2011.02.057.

[199] Y. Shen, J. Tao, H. Tao, S. Chen, L. Pan, and T. Wang, “Anti-icing Potential of Superhydrophobic Ti6Al4V Surfaces: Ice Nucleation and Growth,” *Langmuir*, vol. 31, no. 39, pp. 10799–10806, 2015, doi: 10.1021/acs.langmuir.5b02946.

[200] T. Bharathidasan, S. V. Kumar, M. S. Bobji, R. P. S. Chakradhar, and B. J. Basu, “Effect of wettability and surface roughness on ice-adhesion strength of hydrophilic, hydrophobic and superhydrophobic surfaces,” *Appl. Surf. Sci.*, vol. 314, pp. 241–250, 2014, doi: 10.1016/j.apsusc.2014.06.101.

[201] E. Vazirinasab, R. Jafari, and G. Momen, “Application of superhydrophobic coatings as a corrosion barrier: A review,” *Surf. Coatings Technol.*, vol. 341, pp. 40–56, May 2018, doi: 10.1016/J.SURFCOAT.2017.11.053.

[202] A. Bahgat Radwan *et al.*, “Electrospun highly corrosion-resistant polystyrene–nickel oxide superhydrophobic nanocomposite coating,” *J. Appl. Electrochem.*, vol. 51, no. 11, pp. 1605–1618, Nov. 2021, doi: 10.1007/S10800-021-01603-8/FIGURES/11.

[203] S. Dong *et al.*, “Construction and corrosion resistance of Ni-B4C superhydrophobic composite coatings on Q235 steel,” *Surf. Coatings Technol.*, vol. 422, p. 127551, Sep. 2021, doi: 10.1016/J.SURFCOAT.2021.127551.

[204] Y. Chen, Y. W. Liu, Y. Xie, H. H. Zhang, and Z. Zhang, “Preparation and anti-corrosion performance of superhydrophobic silane/graphene oxide composite coating on copper,” *Surf. Coatings Technol.*, vol. 423, p. 127622, Oct. 2021, doi: 10.1016/J.SURFCOAT.2021.127622.

[205] S. Das, S. Kumar, S. K. Samal, S. Mohanty, and S. K. Nayak, “A Review on Superhydrophobic Polymer Nanocoatings: Recent Development and Applications,” vol. 57, no. 8, pp. 2727–2745, 2018, doi: 10.1021/acs.iecr.7b04887.

[206] K. Liu and L. Jiang, “Metallic surfaces with special wettability,” *Nanoscale*, vol. 3, no. 3, pp. 825–838, Mar. 2011, doi: 10.1039/C0NR00642D.

[207] N. Wang and D. Xiong, “Superhydrophobic membranes on metal substrate and their corrosion protection in different corrosive media,” *Appl. Surf. Sci.*, vol. 305, pp. 603–608, 2014, doi: 10.1016/j.apsusc.2014.03.142.

[208] J. Gould, “Learning from nature’s best,” *Nat. 2015 5197544*, vol. 519, no. 7544, pp. S2–S3, Mar. 2015, doi: 10.1038/519s2a.

[209] N. Kanovsky, S. Cohen, and S. Margel, “In-situ design, characterization and use of durable superhydrophobic thin coatings applied on polymeric films,” *Mater. Res. Bull.*, vol. 146, p. 111598, Feb. 2022, doi: 10.1016/J.MATERRESBULL.2021.111598.

[210] Y. Lu, S. Sathasivam, J. Song, C. R. Crick, C. J. Carmalt, and I. P. Parkin, “Robust self-cleaning surfaces that function when exposed to either air or oil,” *Science (80-.).*, vol. 347, no. 6226, pp. 1132–1135, Mar. 2015, doi: 10.1126/SCIENCE.AAA0946/SUPPL_FILE/LU-SM.PDF.

[211] K. K. Varanasi, T. Deng, J. D. Smith, M. Hsu, and N. Bhate, “Frost formation and ice adhesion on superhydrophobic surfaces,” *Appl. Phys. Lett.*, vol. 97, no. 23, p. 234102, Dec. 2010, doi: 10.1063/1.3524513.

[212] M. Elsharkawy, D. Tortorella, S. Kapatral, and C. M. Megaridis, “Combating Frosting with Joule-Heated Liquid-Infused Superhydrophobic Coatings,” *Langmuir*, vol. 32, no. 17, pp. 4278–4288, May 2016, doi: 10.1021/ACS.LANGMUIR.6B00064/SUPPL_FILE/LA6B00064_SI_002.AVI.

[213] X. Yin *et al.*, “Integration of Self-Lubrication and Near-Infrared Photothermogenesis for Excellent Anti-Icing/Deicing

Performance," *Adv. Funct. Mater.*, vol. 25, no. 27, pp. 4237–4245, Jul. 2015, doi: 10.1002/ADFM.201501101.

[214] L. Battisti and R. Fedrizzi, "2D Numerical Simulation of a Wind Turbine De-Icing System, Using Cycled Heating:," *Wind Eng.*, vol. 31, no. 1, pp. 33–42, Nov. 2007, doi: 10.1260/030952407780811375.

[215] T. Zhu *et al.*, "A transparent superhydrophobic coating with mechanochemical robustness for anti-icing, photocatalysis and self-cleaning," *Chem. Eng. J.*, vol. 399, p. 125746, Nov. 2020, doi: 10.1016/J.CEJ.2020.125746.

[216] C. Wang, A. H. F. Wu, and R. N. Lamb, "Superhydrophobicity and Optical Transparency in Thin Films: Criteria for Coexistence," *J. Phys. Chem.*, vol. 118, no. 10, pp. 5328–5335, 2014, doi: 10.1021/jp411062u.

[217] G. Mie, "Beiträge zur Optik trüber Medien, speziell kolloidaler Metallösungen," *Ann. Phys.*, vol. 330, no. 3, pp. 377–445, Jan. 1908, doi: 10.1002/ANDP.19083300302.

[218] A. Nakajima, K. Hashimoto, T. Watanabe, K. Takai, G. Yamauchi, and A. Fujishima, "Transparent Superhydrophobic Thin Films with Self-Cleaning Properties," *Langmuir*, vol. 16, no. 17, pp. 7044–7047, Aug. 2000, doi: 10.1021/LA000155K.

[219] S. Yu, Z. Guo, and W. Liu, "Biomimetic transparent and superhydrophobic coatings: from nature and beyond nature," *Chem. Commun.*, vol. 51, no. 10, pp. 1775–1794, Jan. 2015, doi: 10.1039/C4CC06868H.

[220] B. Yunfeng Li *et al.*, "Biomimetic Surfaces for High-Performance Optics," *Adv. Mater.*, vol. 21, no. 46, pp. 4731–4734, Dec. 2009, doi: 10.1002/ADMA.200901335.

[221] J. Lyu *et al.*, "Green preparation of transparent superhydrophobic coatings with persistent dynamic impact resistance for outdoor applications," *Chem. Eng. J.*, vol. 404, p. 126456, Jan. 2021, doi: 10.1016/J.CEJ.2020.126456.

[222] X. Tian, T. Verho, and R. H. A. Ras, "Moving superhydrophobic surfaces toward real-world applications," *Science (80-.).*, vol. 352, no. 6282, pp. 142–143, Apr. 2016, doi: 10.1126/SCIENCE.AAF2073.

[223] D. Quéré, "Non-sticking drops," *Reports Prog. Phys.*, vol. 68, no. 11, p. 2495, Sep. 2005, doi: 10.1088/0034-4885/68/11/R01.

[224] T. N. Krupenkin, J. A. Taylor, E. N. Wang, P. Kolodner, M. Hodes, and T. R. Salamon, "Reversible wetting-dewetting transitions on electrically tunable superhydrophobic nanostructured surfaces," *Langmuir*, vol. 23, no. 18, pp. 9128–9133, Aug. 2007, doi: https://doi.org/10.1021/la7008557.

[225] Y. Li, D. Quéré, C. Lv, and Q. Zheng, "Monostable superrepellent materials," *Proc. Natl. Acad. Sci. U. S. A.*, vol. 114, no. 13, pp. 3387–3392, Mar. 2017, doi: 10.1073/PNAS.1614667114/-/DCSUPPLEMENTAL.

[226] Y. Yamauchi, M. Tenjimbayashi, S. Samitsu, and M. Naito, "Durable and Flexible Superhydrophobic Materials: Abrasion/Scratching/Slicing/Droplet Impacting/Bending/Twisting-Tolerant Composite with Porcupinefish-Like Structure," *ACS Appl. Mater. Interfaces*, vol. 11, no. 35, pp. 32381–32389, Sep. 2019, doi: 10.1021/ACSAMI.9B09524/SUPPL_FILE/AM9B09524_SI_007.MP4.

[227] Z. S. Huang *et al.*, "Multifunctional superhydrophobic composite materials with remarkable mechanochemical robustness, stain repellency, oil-water separation and sound-absorption properties," *Chem. Eng. J.*, vol. 358, pp. 1610–1619, Feb. 2019, doi: 10.1016/J.CEJ.2018.10.123.

[228] D. Zhi, Y. Lu, S. Sathasivam, I. P. Parkin, and X. Zhang, "Large-scale fabrication of translucent and repairable superhydrophobic spray coatings with remarkable mechanical, chemical durability and UV resistance," *J. Mater. Chem. A*, vol. 5, no. 21, pp. 10622–10631, May 2017, doi: 10.1039/C7TA02488F.

[229] T. Yang *et al.*, "Superhydrophobic Coating Derived from the Spontaneous Orientation of Janus Particles," *ACS Appl. Mater. Interfaces*, vol. 13, no. 21, pp. 25392–25399, 2021, doi: 10.1021/ACSAMI.1C05571/SUPPL_FILE/AM1C05571_SI_005.PDF.

[230] Z. Liu *et al.*, "Fabrication of robust superhydrophobic organic-inorganic hybrid coating through a novel two-step phase separation method," *Prog. Org. Coatings*, vol. 157, p. 106320, Aug. 2021, doi: 10.1016/J.PORGCOAT.2021.106320.

[231] C. Peng, Z. Chen, and M. K. Tiwari, "All-organic superhydrophobic coatings with mechanochemical robustness and liquid impalement resistance," *Nat. Mater.*, vol. 17, no. 4, pp. 355–360, 2018, doi: 10.1038/s41563-018-0044-2.

[232] L. Xu, Z. Geng, J. He, and G. Zhou, "Mechanically robust, thermally stable, broadband antireflective, and

superhydrophobic thin films on glass substrates," *ACS Appl. Mater. Interfaces*, vol. 6, no. 12, pp. 9029–9035, Jun. 2014, doi: 10.1021/AM5016777/SUPPL_FILE/AM5016777_SI_001.PDF.

[233] X. Li and B. Bhushan, "A review of nanoindentation continuous stiffness measurement technique and its applications," *Mater. Charact.*, vol. 48, no. 1, pp. 11–36, Feb. 2002, doi: 10.1016/S1044-5803(02)00192-4.

[234] W. Zhang, D. Wang, Z. Sun, J. Song, and X. Deng, "Robust superhydrophobicity: Mechanisms and strategies," *Chem. Soc. Rev.*, vol. 50, no. 6, pp. 4031–4061, 2021, doi: 10.1039/d0cs00751j.

[235] V. Kondrashov and J. Rühe, "Microcones and Nanograss: Toward Mechanically Robust Superhydrophobic Surfaces," *Langmuir*, vol. 30, no. 15, pp. 4342–4350, Apr. 2014, doi: 10.1021/LA500395E.

[236] A. Checco, A. Rahman, and C. T. Black, "Robust Superhydrophobicity in Large-Area Nanostructured Surfaces Defined by Block-Copolymer Self Assembly," *Adv. Mater.*, vol. 26, no. 6, pp. 886–891, Feb. 2014, doi: 10.1002/ADMA.201304006.

[237] H. Zhao, K. Y. Law, and V. Sambhy, "Fabrication, surface properties, and origin of superoleophobicity for a model textured surface," *Langmuir*, vol. 27, no. 10, pp. 5927–5935, Jun. 2011, doi: 10.1021/LA104872Q/SUPPL_FILE/LA104872Q_SI_001.PDF.

[238] T. Verho, C. Bower, P. Andrew, S. Franssila, O. Ikkala, and R. H. A. Ras, "Mechanically Durable Superhydrophobic Surfaces," *Adv. Mater.*, vol. 23, no. 5, pp. 673–678, Feb. 2011, doi: 10.1002/ADMA.201003129.

[239] L. Wang, X. Zhang, Y. Fu, B. Li, and Y. Liu, "Bioinspired Preparation of Ultrathin SiO 2 Shell on ZnO Nanowire Array for Ultraviolet-Durable Superhydrophobicity," *Langmuir*, vol. 25, no. 23, pp. 13619–13624, 2009, doi: 10.1021/la901998p.

[240] J. Groten and J. Rgen Rü, "Surfaces with Combined Microscale and Nanoscale Structures: A Route to Mechanically Stable Superhydrophobic Surfaces?," *Langmuir*, vol. 29, no. 11, pp. 3765–3772, 2013, doi: 10.1021/la304641q.

[241] A. Y. Fadeev and T. J. McCarthy, "Self-Assembly Is Not the Only Reaction Possible between Alkyltrichlorosilanes and Surfaces: Monomolecular and Oligomeric Covalently Attached Layers of Dichloro- and Trichloroalkylsilanes on Silicon," *Langmuir*, vol. 16, no. 18, pp. 7268–7274, Sep. 2000, doi: 10.1021/LA000471Z.

[242] S. K. Lahiri, P. Zhang, C. Zhang, and L. Liu, "Robust Fluorine-Free and Self-Healing Superhydrophobic Coatings by H3BO3 Incorporation with SiO2–Alkyl-Silane@PDMS on Cotton Fabric," *ACS Appl. Mater. Interfaces*, vol. 11, no. 10, pp. 10262–10275, Mar. 2019, doi: 10.1021/ACSAMI.8B20651.

[243] M. Z. Khan, J. Militky, V. Baheti, J. Wiener, and M. Vik, "Development of durable superhydrophobic and UV protective cotton fabric via TiO2/trimethoxy(octadecyl)silane nanocomposite coating," *J. Text. Inst.*, vol. 112, no. 10, pp. 1639–1650, 2021, doi: 10.1080/00405000.2020.1834235.

[244] H. Li *et al.*, "Durable superhydrophobic and oleophobic cotton fabric based on the grafting of fluorinated POSS through silane coupling and thiol-ene click reaction," *Colloids Surfaces A Physicochem. Eng. Asp.*, vol. 630, p. 127566, Dec. 2021, doi: 10.1016/J.COLSURFA.2021.127566.

[245] L. Zhang, A. G. Zhou, B. R. Sun, K. S. Chen, and H. Z. Yu, "Functional and versatile superhydrophobic coatings via stoichiometric silanization," *Nat. Commun. 2021 121*, vol. 12, no. 1, pp. 1–7, Feb. 2021, doi: 10.1038/s41467-021-21219-y.

[246] X. Jing, Y. Xia, F. Chen, C. Yang, Z. Yang, and S. H. I. Jaffery, "Preparation of superhydrophobic glass surface with high adhesion," *Colloids Surfaces A Physicochem. Eng. Asp.*, vol. 633, p. 127861, Jan. 2022, doi: 10.1016/J.COLSURFA.2021.127861.

[247] E. P. Plueddemann, *Silane Coupling Agents*. Springer US, 1982.

[248] J. Zhang, S. Liu, Y. Huang, Y. Lv, M. Kong, and G. Li, "Durable fluorinated-SiO2/epoxy superhydrophobic coatings on polycarbonate with strong interfacial adhesion enhanced by solvent-induced crystallization," *Prog. Org. Coatings*, vol. 150, p. 106002, Jan. 2021, doi: 10.1016/J.PORGCOAT.2020.106002.

[249] C. H. Xue and J. Z. Ma, "Long-lived superhydrophobic surfaces," *J. Mater. Chem. A*, vol. 1, no. 13, pp. 4146–4161, 2013, doi: 10.1039/c2ta01073a.

[250] T. Tian *et al.*, "An Elastic Interfacial Transistor Enabled by Superhydrophobicity," *Small*, vol. 14, no. 51, p. 1804006, Dec. 2018, doi: 10.1002/SMLL.201804006.

[251] Y. Shen *et al.*, "Spraying Fabrication of Durable and Transparent Coatings for Anti-Icing Application: Dynamic Water Repellency, Icing Delay, and Ice Adhesion," *ACS Appl. Mater. Interfaces*, vol. 11, no. 3, pp. 3590–3598, Jan. 2019, doi: 10.1021/ACSAMI.8B19225/SUPPL_FILE/AM8B19225_SI_002.AVI.

[252] J. Ju, X. Yao, X. Hou, Q. Liu, Y. S. Zhang, and A. Khademhosseini, "A highly stretchable and robust non-fluorinated superhydrophobic surface," *J. Mater. Chem. A*, vol. 5, no. 31, pp. 16273–16280, Aug. 2017, doi: 10.1039/C6TA11133E.

[253] W. Ming, D. Wu, R. Van Benthem, and G. De With, "Superhydrophobic films from raspberry-like particles," *Nano Lett.*, vol. 5, pp. 2298–2301, 2005, doi: 10.1021/nl0517363.

[254] D. Ge, L. Yang, Y. Zhang, Y. Rahmawan, and S. Yang, "Transparent and Superamphiphobic Surfaces from One-Step Spray Coating of Stringed Silica Nanoparticle/Sol Solutions," *Part. Part. Syst. Charact.*, vol. 31, no. 7, pp. 763–770, Jul. 2014, doi: 10.1002/PPSC.201300382.

[255] R. P. Wool, "Self-healing materials: A review," *Soft Matter*, vol. 4, no. 3, pp. 400–418, 2008, doi: 10.1039/b711716g.

[256] S. Pan *et al.*, "Coatings super-repellent to ultralow surface tension liquids," *Nat. Mater.*, vol. 17, pp. 1040–1047, 2018, doi: 10.1038/s41563-018-0178-2.

[257] D. Weng, F. Xu, X. Li, Y. Li, and J. Sun, "Bioinspired photothermal conversion coatings with self-healing superhydrophobicity for efficient solar steam generation," *J. Mater. Chem. A*, vol. 6, no. 47, pp. 24441–24451, Dec. 2018, doi: 10.1039/C8TA08706G.

[258] R. Zhao, Y. Chen, G. Liu, Y. Jiang, and K. Chen, "Fabrication of self-healing waterbased superhydrophobic coatings from POSS modified silica nanoparticles," *Mater. Lett.*, vol. 229, pp. 281–285, 2018, doi: 10.1016/j.matlet.2018.07.040.

[259] M. E. Vlachopoulou, P. S. Petrou, S. E. Kakabakos, A. Tserepi, K. Beltsios, and E. Gogolides, "Effect of surface nanostructuring of PDMS on wetting properties, hydrophobic recovery and protein adsorption," *Microelectron. Eng.*, vol. 86, no. 4–6, pp. 1321–1324, 2009, doi: 10.1016/j.mee.2008.11.050.

[260] J. L. Fritz and M. J. Owen, "Hydrophobic recovery of plasma-treated polydimethylsiloxane," *J. Adhes.*, vol. 54, no. 1–4, pp. 33–45, 1995, doi: 10.1080/00218469508014379.

[261] A. Oláh, H. Hillborg, and G. J. Vancso, "Hydrophobic recovery of UV/ozone treated poly(dimethylsiloxane): Adhesion studies by contact mechanics and mechanism of surface modification," *Appl. Surf. Sci.*, vol. 239, no. 3–4, pp. 410–423, 2005, doi: 10.1016/j.apsusc.2004.06.005.

[262] J. Kim, M. K. Chaudhury, M. J. Owen, and T. Orbeck, "The mechanisms of hydrophobic recovery of polydimethylsiloxane elastomers exposed to partial electrical discharges," *J. Colloid Interface Sci.*, vol. 244, no. 1, pp. 200–207, 2001, doi: 10.1006/jcis.2001.7909.

[263] M. Meincken, T. A. Berhane, and P. E. Mallon, "Tracking the hydrophobicity recovery of PDMS compounds using the adhesive force determined by AFM force distance measurements," *Polymer (Guildf).*, vol. 46, no. 1, pp. 203–208, 2005, doi: 10.1016/j.polymer.2004.11.012.

[264] K. Senshu, S. Yamashita, H. Mori, M. Ito, A. Hirao, and S. Nakahama, "Time-Resolved Surface Rearrangements of Poly(2-hydroxyethyl methacrylate- block -isoprene) in Response to Environmental Changes," *Langmuir*, vol. 15, no. 5, pp. 1754–1762, 1999, doi: 10.1021/la980815+.

[265] W. Wang, J. Salazar, H. Vahabi, A. Joshi-Imre, W. E. Voit, and A. K. Kota, "Metamorphic Superomniphobic Surfaces," *Adv. Mater.*, vol. 29, no. 27, p. 1700295, Jul. 2017, doi: 10.1002/ADMA.201700295.

[266] M. C. E. Robert F Diegelmann, "Wound healing: An overview of acute, fibrotic and delayed healing," *Front. Biosci.*, vol. 9, pp. 283–289, 2004, doi: 10.2741/1184.

[267] R. París, L. Lamattina, and C. A. Casalongué, "Nitric oxide promotes the wound-healing response of potato leaflets," *Plant Physiol. Biochem.*, vol. 45, no. 1, pp. 80–86, Jan. 2007, doi: 10.1016/J.PLAPHY.2006.12.001.

[268] Z. Wei *et al.*, "Self-healing gels based on constitutional dynamic chemistry and their potential applications," *Chem. Soc. Rev.*, vol. 43, no. 23, pp. 8114–8131, Nov. 2014, doi: 10.1039/C4CS00219A.

[269] J. Wu *et al.*, "Development of a new class of self-healing and therapeutic dental resins," *Polym. Degrad. Stab.*, vol. 163, pp. 87–99, May 2019, doi: 10.1016/J.POLYMDEGRADSTAB.2019.02.024.

[270] S. Li, L. Wang, W. Zheng, G. Yang, and X. Jiang, “Rapid Fabrication of Self-Healing, Conductive, and Injectable Gel as Dressings for Healing Wounds in Stretchable Parts of the Body,” *Adv. Funct. Mater.*, vol. 30, no. 31, p. 2002370, Aug. 2020, doi: 10.1002/ADFM.202002370.

[271] D. M. Kim *et al.*, “Healing Performance of a Self-Healing Protective Coating According to Damage Width,” *Coatings 2020, Vol. 10, Page 543*, vol. 10, no. 6, p. 543, Jun. 2020, doi: 10.3390/COATINGS10060543.

[272] D. M. Kim, I. H. Song, J. Y. Choi, S. W. Jin, K. N. Nam, and C. M. Chung, “Self-Healing Coatings Based on Linseed-Oil-Loaded Microcapsules for Protection of Cementitious Materials,” *Coatings 2018, Vol. 8, Page 404*, vol. 8, no. 11, p. 404, Nov. 2018, doi: 10.3390/COATINGS8110404.

[273] M. H. Quinlan, “Materials with Variable Bonding,” *Arch. Ration. Mech. Anal.*, vol. 67, no. 2, pp. 165–181, 1978.

[274] S. Utrera-Barrios, R. Verdejo, M. A. López-Manchado, and M. Hernández Santana, “Evolution of self-healing elastomers, from extrinsic to combined intrinsic mechanisms: a review,” *Mater. Horizons*, vol. 7, no. 11, pp. 2882–2902, Nov. 2020, doi: 10.1039/D0MH00535E.

[275] E. B. S. van der Zwaag, Ed., *Self healing materials : pioneering research in the Netherlands*, Reprint. IOS press, 2015.

[276] N. Wen *et al.*, “Recent advancements in self-healing materials: Mechanicals, performances and features,” *React. Funct. Polym.*, vol. 168, p. 105041, Nov. 2021, doi: 10.1016/J.REACTFUNCTPOLYM.2021.105041.

[277] X. F. Wu *et al.*, “Electrospinning core-shell nanofibers for interfacial toughening and self-healing of carbon-fiber/epoxy composites,” *J. Appl. Polym. Sci.*, vol. 129, no. 3, pp. 1383–1393, Aug. 2013, doi: 10.1002/APP.38838.

[278] V. K. Mohonee, K. Lim Goh, L. Mishnaevsky, and P. Pasbakhsh, “Capsule based self-healing composites: New insights on mechanical behaviour based on finite element analysis,” *Comput. Mater. Sci.*, vol. 192, p. 110203, May 2021, doi: 10.1016/J.COMMATSCI.2020.110203.

[279] W. Sima *et al.*, “Magnetically gradient-distributed microcapsule/epoxy composites: Low capsule load and highly targeted self-healing performance,” *Chem. Eng. J.*, vol. 405, p. 126908, Feb. 2021, doi: 10.1016/J.CEJ.2020.126908.

[280] N. Zheng, J. Liu, Y. Wang, C. Li, and Q. Zhang, “Preparation of chitosan-reduced graphene oxide (CS-RGO) microcapsules and its application in UV/moisture-induced self-healing coatings,” *Prog. Org. Coatings*, vol. 151, p. 106055, Feb. 2021, doi: 10.1016/J.PORGCOAT.2020.106055.

[281] X. Fu *et al.*, “Nanofiber Composite Coating with Self-Healing and Active Anticorrosive Performances,” *ACS Appl. Mater. Interfaces*, vol. 13, no. 48, pp. 57880–57892, Dec. 2021, doi: 10.1021/ACSAMI.1C16052/SUPPL_FILE/AM1C16052_SI_001.PDF.

[282] U. S. Chung, J. H. Min, P. C. Lee, and W. G. Koh, “Polyurethane matrix incorporating PDMS-based self-healing microcapsules with enhanced mechanical and thermal stability,” *Colloids Surfaces A Physicochem. Eng. Asp.*, vol. 518, pp. 173–180, Apr. 2017, doi: 10.1016/j.colsurfa.2017.01.044.

[283] M. W. Lee, S. An, Y. Il Kim, S. S. Yoon, and A. L. Yarin, “Self-healing three-dimensional bulk materials based on core-shell nanofibers,” *Chem. Eng. J.*, vol. 334, pp. 1093–1100, Feb. 2018, doi: 10.1016/J.CEJ.2017.10.034.

[284] J. Zhao, R. Xu, G. Luo, J. Wu, and H. Xia, “A self-healing, re-moldable and biocompatible crosslinked polysiloxane elastomer,” *J. Mater. Chem. B*, vol. 4, no. 5, pp. 982–989, Jan. 2016, doi: 10.1039/C5TB02036K.

[285] A. Nasresfahani and P. M. Zelisko, “Synthesis of a self-healing siloxane-based elastomer cross-linked via a furan-modified polyhedral oligomeric silsesquioxane: investigation of a thermally reversible silicon-based cross-link,” *Polym. Chem.*, vol. 8, no. 19, pp. 2942–2952, May 2017, doi: 10.1039/C7PY00215G.

[286] L. Feng, Z. Yu, Y. Bian, J. Lu, X. Shi, and C. Chai, “Self-healing behavior of polyurethanes based on dual actions of thermo-reversible Diels-Alder reaction and thermal movement of molecular chains,” *Polymer (Guildf).*, vol. 124, pp. 48–59, Aug. 2017, doi: 10.1016/J.POLYMER.2017.07.049.

[287] B. Willocq, J. Odent, P. Dubois, and J. M. Raquez, “Advances in intrinsic self-healing polyurethanes and related composites,” *RSC Adv.*, vol. 10, no. 23, pp. 13766–13782, Apr. 2020, doi: 10.1039/D0RA01394C.

[288] J. Araujo-Morera, M. H. Santana, R. Verdejo, and M. A. López-Manchado, “Giving a Second Opportunity to Tire Waste: An Alternative Path for the Development of Sustainable Self-Healing Styrene–Butadiene Rubber Compounds Overcoming the Magic Triangle of Tires,” *Polym. 2019, Vol. 11, Page 2122*, vol. 11, no. 12, p. 2122, Dec. 2019, doi: 10.3390/POLYM11122122.

[289] Y. Zhu *et al.*, "Ultra-Tough, Strong, and Defect-Tolerant Elastomers with Self-Healing and Intelligent-Responsive Abilities," *ACS Appl. Mater. Interfaces*, vol. 11, no. 32, pp. 29373–29381, 2019, doi: 10.1021/ACSAMI.9B11041/SUPPL_FILE/AM9B11041_SI_005.PDF.

[290] Q. Guo *et al.*, "Protein-Inspired Self-Healable Ti3C2 MXenes/Rubber-Based Supramolecular Elastomer for Intelligent Sensing," *ACS Nano*, vol. 14, no. 3, pp. 2788–2797, Mar. 2020, doi: 10.1021/ACSNANO.9B09802/SUPPL_FILE/NN9B09802_SI_004.MOV.

[291] R. Li *et al.*, "Autonomous Self-Healing, Antifreezing, and Transparent Conductive Elastomers," *Chem. Mater.*, vol. 32, no. 2, pp. 874–881, Jan. 2020, doi: 10.1021/ACS.CHEMMATER.9B04592/SUPPL_FILE/CM9B04592_SI_003.MOV.

[292] P. Tanasi, M. Hernández Santana, J. Carretero-González, R. Verdejo, and M. A. López-Manchado, "Thermo-reversible crosslinked natural rubber: A Diels-Alder route for reuse and self-healing properties in elastomers," *Polymer (Guildf).*, vol. 175, pp. 15–24, Jun. 2019, doi: 10.1016/J.POLYMER.2019.04.059.

[293] G. Li, P. Xiao, S. Hou, and Y. Huang, "Rapid and efficient polymer/graphene based multichannel self-healing material via Diels-Alder reaction," *Carbon N. Y.*, vol. 147, pp. 398–407, Jun. 2019, doi: 10.1016/J.CARBON.2019.03.021.

[294] X. Li *et al.*, "Self-Healing Polyurethane Elastomers Based on a Disulfide Bond by Digital Light Processing 3D Printing," *ACS Macro Lett.*, vol. 8, no. 11, pp. 1511–1516, Nov. 2019, doi: 10.1021/ACSMACROLETT.9B00766/SUPPL_FILE/MZ9B00766_SI_001.PDF.

[295] M. Zhu *et al.*, "Polysaccharide-based fast self-healing ion gel based on acylhydrazone and metal coordination bonds," *Mater. Des.*, vol. 192, p. 108723, Jul. 2020, doi: 10.1016/J.MATDES.2020.108723.

[296] Y. Cao *et al.*, "Self-healing electronic skins for aquatic environments," *Nat. Electron.*, vol. 2, no. 2, pp. 75–82, Feb. 2019, doi: 10.1038/s41928-019-0206-5.

[297] J. Cao *et al.*, "Multiple Hydrogen Bonding Enables the Self-Healing of Sensors for Human-Machine Interactions," *Angew. Chemie*, vol. 129, no. 30, pp. 8921–8926, Jul. 2017, doi: 10.1002/ANGE.201704217.

[298] C. Li, J. Tan, Z. Guan, and Q. Zhang, "A Three-Armed Polymer with Tunable Self-Assembly and Self-Healing Properties Based on Benzene-1,3,5-tricarboxamide and Metal–Ligand Interactions," *Macromol. Rapid Commun.*, vol. 40, no. 17, p. 1800909, Sep. 2019, doi: 10.1002/MARC.201800909.

[299] Y. Kobayashi, T. Hirase, Y. Takashima, A. Harada, and H. Yamaguchi, "Self-healing and shape-memory properties of polymeric materials cross-linked by hydrogen bonding and metal–ligand interactions," *Polym. Chem.*, vol. 10, no. 33, pp. 4519–4523, Aug. 2019, doi: 10.1039/C9PY00450E.

[300] N. N. Xia, X. M. Xiong, M. Z. Rong, M. Q. Zhang, and F. Kong, "Self-Healing of Polymer in Acidic Water toward Strength Restoration through the Synergistic Effect of Hydrophilic and Hydrophobic Interactions," *ACS Appl. Mater. Interfaces*, vol. 9, no. 42, pp. 37300–37309, Oct. 2017, doi: 10.1021/ACSAMI.7B11230/SUPPL_FILE/AM7B11230_SI_001.PDF.

[301] Y. Peng, Y. Yang, Q. Wu, S. Wang, G. Huang, and J. Wu, "Strong and tough self-healing elastomers enabled by dual reversible networks formed by ionic interactions and dynamic covalent bonds," *Polymer (Guildf).*, vol. 157, pp. 172–179, Nov. 2018, doi: 10.1016/J.POLYMER.2018.09.038.

[302] S. Terryn *et al.*, "A review on self-healing polymers for soft robotics," *Mater. Today*, vol. 47, pp. 187–205, Jul. 2021, doi: 10.1016/J.MATTOD.2021.01.009.

[303] D. Ratna and J. Karger-Kocsis, "Recent advances in shape memory polymers and composites: A review," *J. Mater. Sci.*, vol. 43, no. 1, pp. 254–269, Jan. 2008, doi: 10.1007/S10853-007-2176-7/FIGURES/13.

[304] M. L. D. Hang jerry Qi, "Thermomechanical Behavior and Modeling Approaches," in *Shape-Memory polymers and multifunctional composites*, CRC Press, 2010, pp. 75–100.

[305] B. Aïssa, D. Therriault, E. Haddad, and W. Jamroz, "Self-healing materials systems: Overview of major approaches and recent developed technologies," *Adv. Mater. Sci. Eng.*, vol. 2012, pp. 1–17, 2012, doi: 10.1155/2012/854203.

[306] S. Wang and M. W. Urban, "Self-healing polymers," *Nat. Rev. Mater. 2020 58*, vol. 5, no. 8, pp. 562–583, Jun. 2020, doi: 10.1038/s41578-020-0202-4.

[307] M. W. Keller, S. R. White, and N. R. Sottos, "A Self-Healing Poly(Dimethyl Siloxane) Elastomer," *Adv. Funct. Mater.*, vol. 17, no. 14, pp. 2399–2404, Sep. 2007, doi: 10.1002/ADFM.200700086.

[308] X. Chen *et al.*, "A thermally re-mendable cross-linked polymeric material," *Science (80-.).*, vol. 295, no. 5560, pp. 1698–1702, Mar. 2002, doi: 10.1126/SCIENCE.1065879/SUPPL_FILE/1065879S3_THUMB.GIF.

[309] P. Cordier, F. Tournilhac, C. Soulié-Ziakovic, and L. Leibler, "Self-healing and thermoreversible rubber from supramolecular assembly," *Nat. 2008 4517181*, vol. 451, no. 7181, pp. 977–980, Feb. 2008, doi: 10.1038/nature06669.

[310] K. S. Toohey, N. R. Sottos, J. A. Lewis, J. S. Moore, and S. R. White, "Self-healing materials with microvascular networks," *Nat. Mater. 2007 68*, vol. 6, no. 8, pp. 581–585, Jun. 2007, doi: 10.1038/nmat1934.

[311] I. G. Loscertales, A. Barrero, I. Guerrero, R. Cortijo, M. Marquez, and A. M. Gañán-Calvo, "Micro/nano encapsulation via electrified coaxial liquid jets," *Science (80-.).*, vol. 295, no. 5560, pp. 1695–1698, 2002, doi: 10.1126/science.1067595.

[312] H. Qu, S. Wei, and Z. Guo, "Coaxial electrospun nanostructures and their applications," *J. Mater. Chem. A*, vol. 1, no. 38, pp. 11513–11528, 2013, doi: 10.1039/c3ta12390a.

[313] X. Qin, "Coaxial electrospinning of nanofibers," in *Electrospun Nanofibers; Woodhead Publishing Series in Textiles*, Mehdi Afshari, Ed. Elsevier Ltd, 2017, pp. 41–71.

[314] R. Xue, P. Behera, J. Xu, M. S. Viapiano, and J. J. Lannutti, "Polydimethylsiloxane core-polycaprolactone shell nanofibers as biocompatible, real-time oxygen sensors," *Sensors Actuators, B Chem.*, vol. 192, pp. 697–707, 2014, doi: 10.1016/j.snb.2013.10.084.

[315] S. An *et al.*, "Highly flexible transparent self-healing composite based on electrospun core–shell nanofibers produced by coaxial electrospinning for anti-corrosion and electrical insulation," *Nanoscale*, vol. 7, no. 42, pp. 17778–17785, Oct. 2015, doi: 10.1039/C5NR04551G.

[316] M. W. Lee, S. An, C. Lee, M. Liou, A. L. Yarin, and S. S. Yoon, "Self-healing transparent core–shell nanofiber coatings for anti-corrosive protection," *J. Mater. Chem. A*, vol. 2, no. 19, pp. 7045–7053, Apr. 2014, doi: 10.1039/C4TA00623B.

[317] C. Zhang, F. Feng, and H. Zhang, "Emulsion electrospinning: Fundamentals, food applications and prospects," *Trends Food Sci. Technol.*, vol. 80, pp. 175–186, 2018, doi: 10.1016/j.tifs.2018.08.005.

[318] M. Buzgo, A. Mickova, M. Rampichova, and M. Doupnik, "Blend electrospinning, coaxial electrospinning, and emulsion electrospinning techniques," in *Core-Shell Nanostructures for Drug Delivery and Theranostics: Challenges, Strategies, and Prospects for Novel Carrier Systems*, Maria Letizia Focarete and Anna Tampieri, Ed. Elsevier Ltd, 2018, pp. 325–347.

[319] H. Yang, Q. Mo, W. Li, and F. Gu, "Preparation and Properties of Self-Healing and Self-Lubricating Epoxy Coatings with Polyurethane Microcapsules Containing Bifunctional Linseed Oil," *Polym. 2019, Vol. 11, Page 1578*, vol. 11, no. 10, p. 1578, Sep. 2019, doi: 10.3390/POLYM11101578.

[320] M. Hu, J. Guo, Y. Yu, L. Cao, and Y. Xu, "Research advances of microencapsulation and its prospects in the petroleum industry," *Materials (Basel).*, vol. 10, no. 4, p. 369, 2017, doi: 10.3390/ma10040369.

[321] Swapan Kumar Ghosh, Ed., *Functional Coatings by Polymer Microencapsulation*. Wiley-VCH Verlag, 2006.

[322] H. Peng *et al.*, "N -Alkanes Phase Change Materials and Their Microencapsulation for Thermal Energy Storage: A Critical Review," *Energy and Fuels*, vol. 32, no. 7, pp. 7262–7293, 2018, doi: 10.1021/acs.energyfuels.8b01347.

[323] N. V. N. Jyothi, P. M. Prasanna, S. N. Sakarkar, K. S. Prabha, P. S. Ramaiah, and G. Y. Srawan, "Microencapsulation techniques, factors influencing encapsulation efficiency," *J. Microencapsul.*, vol. 27, no. 3, pp. 187–197, 2010, doi: 10.3109/02652040903131301.

[324] E. Koh, N. K. Kim, J. Shin, and Y. W. Kim, "Polyurethane microcapsules for self-healing paint coatings," *RSC Adv.*, vol. 4, no. 31, pp. 16214–16223, 2014, doi: 10.1039/c4ra00213j.

[325] H. Ullah, K. Azizli, Z. B. Man, and M. B. C. Ismail, "Synthesis and Characterization of Urea-formaldehyde Microcapsules Containing Functionalized Polydimethylsiloxanes," *Procedia Eng.*, vol. 148, pp. 168–175, 2016, doi: 10.1016/j.proeng.2016.06.519.

[326] F. Cotting, A. Koebsch, and I. V. Aoki, "Epoxy Self-Healing Coating by Encapsulated Epoxy Ester Resin in Poly (Urea-Formaldehyde-Melamine) Microcapsules," *Front. Mater.*, vol. 6, p. 314, Dec. 2019, doi: 10.3389/FMATS.2019.00314/BIBTEX.

[327] R. Amini-Nejad, A. Ghasemi-Ghalebahman, A. Fereidoon, and N. Golshan-Ebrahimi, "In situ encapsulation technique for fabrication of self-healing thermosetting polyurethane with tungsten (VI) chloride," *Polym. Adv. Technol.*, vol. 32, no. 2, pp. 789–802, Feb. 2021, doi: 10.1002/PAT.5131.

[328] H. Jin, C. L. Mangun, D. S. Stradley, J. S. Moore, N. R. Sottos, and S. R. White, "Self-healing thermoset using encapsulated epoxy-amine healing chemistry," *Polymer (Guildf).*, vol. 53, no. 2, pp. 581–587, Jan. 2012, doi: 10.1016/J.POLYMER.2011.12.005.

[329] P. C. JE *et al.*, "Manufacturing challenges in self-healing technology for polymer composites — a review," *J. Mater. Res. Technol.*, vol. 9, no. 4, pp. 7370–7379, Jul. 2020, doi: 10.1016/J.JMRT.2020.04.082.

[330] X. Yan, Y. Tao, and X. Qian, "Effect of Microcapsules with Waterborne Coating as Core Material on Properties of Coating for Tilia Europaea and Comparison with Other Microcapsules," *Polymers (Basel).*, vol. 13, no. 18, Sep. 2021, doi: 10.3390/POLYM13183167.

[331] G. Farzi, A. Davoodi, A. Ahmadi, R. E. Neisiany, M. K. Anwer, and M. A. Aboudzadeh, "Encapsulation of Cerium Nitrate within Poly(urea-formaldehyde) Microcapsules for the Development of Self-Healing Epoxy-Based Coating," *ACS Omega*, vol. 6, no. 46, pp. 31147–31153, Nov. 2021, doi: 10.1021/ACSOMEGA.1C04597.

[332] Y. T. Zhang, H. C. Yu, M. C. Shen, Y. T. Chern, and C. C. Li, "Synthesis and application of self-healing microcapsules containing curable glue," *Mater. Chem. Phys.*, vol. 240, p. 122161, Jan. 2020, doi: 10.1016/J.MATCHEMPHYS.2019.122161.

[333] N. Sharma, S. Sharma, S. K. Sharma, and R. Mehta, "Evaluation of corrosion inhibition and self healing capabilities of nanoclay and tung oil microencapsulated epoxy coatings on rebars in concrete," *Constr. Build. Mater.*, vol. 259, p. 120278, Oct. 2020, doi: 10.1016/J.CONBUILDMAT.2020.120278.

[334] E. N. Browny, M. R. Kessler}, N. R. Sottosy, and S. R. Whitez, "In situ poly(urea-formaldehyde) microencapsulation of dicyclopentadiene," *J. Microencapsul.*, vol. 20, no. 6, pp. 719–730, 2003, doi: 10.1080/0265204031000154160.

[335] S. Then, G. S. Neon, and N. H. Abu Kasim, "Performance of melamine modified urea–formaldehyde microcapsules in a dental host material," *J. Appl. Polym. Sci.*, vol. 122, no. 4, pp. 2557–2562, Nov. 2011, doi: 10.1002/APP.34361.

[336] Y. Ren, N. Abbas, G. Zhu, and J. Tang, "Synthesis and mechanical properties of large size silica shell microcapsules for self-healing cementitious materials," *Colloids Surfaces A Physicochem. Eng. Asp.*, vol. 587, p. 124347, Feb. 2020, doi: 10.1016/J.COLSURFA.2019.124347.

[337] Y. Jinglei, M. W. Keller, J. S. Moore, S. R. White, and N. R. Sottos, "Microencapsulation of isocyanates for self-healing polymers," *Macromolecules*, vol. 41, no. 24, pp. 9650–9655, Dec. 2008, doi: 10.1021/MA801718V/SUPPL_FILE/MA801718V_SI_001.PDF.

[338] M. Attaei *et al.*, "Autonomous self-healing in epoxy coatings provided by high efficiency isophorone diisocyanate (IPDI) microcapsules for protection of carbon steel," *Prog. Org. Coatings*, vol. 139, p. 105445, Feb. 2020, doi: 10.1016/J.PORGCOAT.2019.105445.

[339] Z. Tao, J. Cui, H. Qiu, J. Yang, S. Gao, and J. Li, "Microcapsule/silica dual-fillers for self-healing, self-reporting and corrosion protection properties of waterborne epoxy coatings," *Prog. Org. Coatings*, vol. 159, p. 106394, Oct. 2021, doi: 10.1016/J.PORGCOAT.2021.106394.

[340] Y. Song, K. F. Chen, J. J. Wang, Y. Liu, T. Qi, and G. L. Li, "Synthesis of Polyurethane/Poly(urea-formaldehyde) Double-shelled Microcapsules for Self-healing Anticorrosion Coatings," *Chinese J. Polym. Sci. 2019 381*, vol. 38, no. 1, pp. 45–52, Sep. 2019, doi: 10.1007/S10118-019-2317-X.

[341] C. Zotiadis, I. Patrikalos, V. Loukaidou, D. M. Korres, A. Karantonis, and S. Vouyiouka, "Self-healing coatings based on poly(urea-formaldehyde) microcapsules: In situ polymerization, capsule properties and application," *Prog. Org. Coatings*, vol. 161, p. 106475, Dec. 2021, doi: 10.1016/J.PORGCOAT.2021.106475.

[342] S. Parsaee, S. M. Mirabedini, R. Farnood, and F. Alizadegan, "Development of self-healing coatings based on urea-formaldehyde/polyurethane microcapsules containing epoxy resin," *J. Appl. Polym. Sci.*, vol. 137, no. 41, p. 49663, Nov. 2020, doi: 10.1002/app.49663.

[343] S. Tzavidi, C. Zotiadis, A. Porfyris, D. M. Korres, and S. Vouyiouka, "Epoxy loaded poly(urea-formaldehyde) microcapsules via in situ polymerization designated for self-healing coatings," *J. Appl. Polym. Sci.*, vol. 137, no. 43, p. 49323, Nov. 2020, doi: 10.1002/app.49323.

[344] H. Es-haghi, S. M. Mirabedini, M. Imani, and R. R. Farnood, “Preparation and characterization of pre-silane modified ethyl cellulose-based microcapsules containing linseed oil,” *Colloids Surfaces A Physicochem. Eng. Asp.*, vol. 447, pp. 71–80, Apr. 2014, doi: 10.1016/J.COLSURFA.2014.01.021.

[345] F. Safaei, S. N. Khorasani, H. Rahnama, R. E. Neisiany, and M. S. Koochaki, “Single microcapsules containing epoxy healing agent used for development in the fabrication of cost efficient self-healing epoxy coating,” *Prog. Org. Coatings*, vol. 114, pp. 40–46, 2018, doi: 10.1016/j.porgcoat.2017.09.019.

[346] Y. Tian *et al.*, “Preparation and characterization of self-healing microcapsules of asphalt,” *Constr. Build. Mater.*, vol. 263, p. 120174, Dec. 2020, doi: 10.1016/J.CONBUILDMAT.2020.120174.

[347] Martin D. Hager Sybrand van der Zwaag Ulrich S. Schubert, *Self-healing Materials*, vol. 273. Cham: Springer International Publishing, 2016.

[348] S. Bode *et al.*, “Characterization of self-healing polymers: From macroscopic healing tests to the molecular mechanism,” in *Advances in Polymer Science*, vol. 273, 2016, pp. 113–142.

[349] H. Feng, F. Yu, Y. Zhou, M. Li, L. Xiao, and Y. Ao, “Fabrication of microcapsule-type composites with the capability of underwater self-healing and damage visualization,” *RSC Adv.*, vol. 10, no. 56, pp. 33675–33682, Sep. 2020, doi: 10.1039/D0RA03197F.

[350] Y. K. Song *et al.*, “Dual Monitoring of Cracking and Healing in Self-healing Coatings Using Microcapsules Loaded with Two Fluorescent Dyes,” *Molecules*, vol. 24, no. 9, p. 1679, Apr. 2019, doi: 10.3390/MOLECULES24091679.

[351] L. T. T. Nguyen *et al.*, “Healable shape memory (thio)urethane thermosets,” *Polym. Chem.*, vol. 6, no. 16, pp. 3143–3154, Apr. 2015, doi: 10.1039/C5PY00126A.

[352] J. Kötteritzsch, S. Stumpf, S. Hoeppener, J. Vitz, M. D. Hager, and U. S. Schubert, “One-Component Intrinsic Self-Healing Coatings Based on Reversible Crosslinking by Diels–Alder Cycloadditions,” *Macromol. Chem. Phys.*, vol. 214, no. 14, pp. 1636–1649, Jul. 2013, doi: 10.1002/MACP.201200712.

[353] M. Kashif and Y. W. Chang, “Supramolecular hydrogen-bonded polyolefin elastomer/modified graphene nanocomposites with near infrared responsive shape memory and healing properties,” *Eur. Polym. J.*, vol. 66, pp. 273–281, May 2015, doi: 10.1016/J.EURPOLYMJ.2015.02.007.

[354] H. Wang, J. Xu, X. Du, Z. Du, X. Cheng, and H. Wang, “A self-healing polyurethane-based composite coating with high strength and anti-corrosion properties for metal protection,” *Compos. Part B Eng.*, vol. 225, p. 109273, Nov. 2021, doi: 10.1016/J.COMPOSITESB.2021.109273.

[355] C. Sun *et al.*, “Self-healing polymers using electrosprayed microcapsules containing oil: Molecular dynamics simulation and experimental studies,” *J. Mol. Liq.*, vol. 325, p. 115182, Mar. 2021, doi: 10.1016/J.MOLLIQ.2020.115182.

[356] H.-C. Yu, Y.-T. Zhang, M.-J. Wang, and C.-C. Li, “Dispersion of Poly(urea-formaldehyde)-Based Microcapsules for Self-Healing and Anticorrosion Applications,” *Langmuir*, vol. 35, pp. 7871–7878, 2019, doi: 10.1021/acs.langmuir.9b00526.

[357] S. H. Cho, S. R. White, P. V Braun, P. V Braun, B. Institute, and S. H. Cho, “Self-Healing Polymer Coatings,” *Adv. Mater.*, vol. 21, no. 6, pp. 645–649, Feb. 2009, doi: 10.1002/ADMA.200802008.

[358] F. Ahangaran, M. Hayaty, A. H. Navarchian, Y. Pei, and F. Picchioni, “Development of self-healing epoxy composites via incorporation of microencapsulated epoxy and mercaptan in poly(methyl methacrylate) shell,” *Polym. Test.*, vol. 73, pp. 395–403, Feb. 2019, doi: 10.1016/J.POLYMERTESTING.2018.11.041.

[359] E. N. Brown, “Use of the tapered double-cantilever beam geometry for fracture toughness measurements and its application to the quantification of self-healing,” *J. strain Anal. Eng. Des.*, vol. 46, no. 3, pp. 167–186, 2011, doi: 10.1177/0309324710396018.

[360] M. R. Kessler, N. R. Sottos, and S. R. White, “Self-healing structural composite materials,” *Compos. Part A Appl. Sci. Manuf.*, vol. 34, no. 8, pp. 743–753, Aug. 2003, doi: 10.1016/S1359-835X(03)00138-6.

[361] E. N. Brown, S. R. White, and N. R. Sottos, “Fatigue crack propagation in microcapsule-toughened epoxy,” *J. Mater. Sci.*, vol. 41, no. 19, pp. 6266–6273, Oct. 2006, doi: 10.1007/S10853-006-0512-Y/FIGURES/8.

[362] ASTM D624-00 (2020), “Standard Test Method for Tear Strength of Conventional Vulcanized Rubber and Thermoplastic Elastomers.” 2020, [Online]. Available: https://www.astm.org/d0624-00r20.html.

[363] M. Raji, M. El Achaby, R. Bouhfid, and A. el kacem Qaiss, “Self-healing based on composites and nanocomposites materials: from synthesis to application and modeling,” in *Polymer Nanocomposite-Based Smart Materials*, no. 1, A. el K. Q. and M. J. Rachid Bouhfid, Ed. Elsevier Ltd, 2020, pp. 41–60.

[364] S. Utrera-Barrios, M. Hernández Santana, R. Verdejo, and M. A. López-Manchado, “Design of Rubber Composites with Autonomous Self-Healing Capability,” *ACS Omega*, vol. 5, no. 4, pp. 1902–1910, Feb. 2020, doi: 10.1021/ACSOMEGA.9B03516/SUPPL_FILE/AO9B03516_SI_001.PDF.

[365] S. S. Chee, M. Jawaid, M. T. H. Sultan, O. Y. Alothman, and L. C. Abdullah, “Thermomechanical and dynamic mechanical properties of bamboo/woven kenaf mat reinforced epoxy hybrid composites,” *Compos. Part B Eng.*, vol. 163, pp. 165–174, Apr. 2019, doi: 10.1016/J.COMPOSITESB.2018.11.039.

[366] R. A. Chowdhury *et al.*, “Self-healing epoxy composites: preparation, characterization and healing performance,” *J. Mater. Res. Technol.*, vol. 4, no. 1, pp. 33–43, Jan. 2015, doi: 10.1016/J.JMRT.2014.10.016.

[367] S. Neon Gan and N. Shahabudin, “Applications of Microcapsules in Self-Healing Polymeric Materials,” in *Microencapsulation - Processes, Technologies and Industrial Applications*, F. Salaün, Ed. IntechOpen, 2019.

[368] H. Ullah, K. A. M. Azizli, Z. B. Man, M. B. Che Ismail, and M. I. Khan, “The potential of microencapsulated self-healing materials for microcracks recovery in self-healing composite systems: A review,” *Polym. Rev.*, vol. 56, no. 3, pp. 429–485, 2016, doi: 10.1080/15583724.2015.1107098.

[369] Q. Wang *et al.*, “Self-healing coatings containing core-shell nanofibers with pH-Responsive performance,” *ACS Appl. Mater. Interfaces*, vol. 13, no. 2, pp. 3139–3152, Jan. 2021, doi: 10.1021/acsami.0c18933.

[370] S. An, M. W. Lee, A. L. Yarin, and S. S. Yoon, “A review on corrosion-protective extrinsic self-healing: Comparison of microcapsule-based systems and those based on core-shell vascular networks,” *Chem. Eng. J.*, vol. 344, pp. 206–220, Jul. 2018, doi: 10.1016/j.cej.2018.03.040.

[371] J. F. Su *et al.*, “Experimental observation of the vascular self-healing hollow fibers containing rejuvenator states in bitumen,” *Constr. Build. Mater.*, vol. 201, pp. 715–727, Mar. 2019, doi: 10.1016/j.conbuildmat.2019.01.001.

[372] P. C. JE *et al.*, “Manufacturing challenges in self-healing technology for polymer composites — a review,” *J. Mater. Res. Technol.*, vol. 9, no. 4, pp. 7370–7379, Jul. 2020, doi: 10.1016/j.jmrt.2020.04.082.

[373] H. Liu, Y. Wang, D. Li, X. Yan, and R. Li, “Preparation and characterization of poly(melamine-formaldehyde) microcapsules filled with propisochlor,” *J. Macromol. Sci. Part A Pure Appl. Chem.*, vol. 56, no. 7, pp. 676–685, 2019, doi: 10.1080/10601325.2019.1596746.

[374] D. Y. Zhu, M. Z. Rong, and M. Q. Zhang, “Self-healing polymeric materials based on microencapsulated healing agents: From design to preparation,” *Prog. Polym. Sci.*, vol. 49–50, pp. 175–220, 2015, doi: 10.1016/j.progpolymsci.2015.07.002.

[375] E. N. Brown, N. R. Sottos, and S. R. White, “Fracture testing of a self-healing polymer composite,” *Exp. Mech.*, vol. 42, no. 4, pp. 372–379, Dec. 2002, doi: 10.1007/bf02412141.

[376] A. S. Jones, J. D. Rule, J. S. Moore, N. R. Sottos, and S. R. White, “Life extension of self-healing polymers with rapidly growing fatigue cracks,” *J. R. Soc. Interface*, vol. 4, no. 13, pp. 395–403, Apr. 2007, doi: 10.1098/rsif.2006.0199.

[377] H. Ebrahimnezhad-Khaljiri and R. Eslami-Farsani, “Experimental investigation of flexural properties of glass fiber–epoxy self-healable composite structures containing capsulated epoxy healing agent and $NiCl_2$ (imidazole) $_4$ catalyst,” *J. Ind. Text.*, p. 152808371989292, Dec. 2019, doi: 10.1177/1528083719892923.

[378] H. Ebrahimnezhad-Khaljiri, R. Eslami-Farsani, and S. Arbab Chirani, “Microcapsulated epoxy resin with nanosilica-urea formaldehyde composite shell,” *J. Appl. Polym. Sci.*, vol. 137, no. 16, p. 48580, Apr. 2020, doi: 10.1002/app.48580.

[379] S. Xu, J. Li, H. Qiu, Y. Xue, and J. Yang, “Repeated self-healing of composite coatings with core-shell fibres,” *Compos. Commun.*, vol. 19, pp. 220–225, Jun. 2020, doi: 10.1016/j.coco.2020.04.007.

[380] Z. Yin, J. Guo, J. Qiao, and X. Chen, “Improved self-healing properties and crack growth resistance of polydimethylsiloxane elastomers with dual-capsule room-temperature healing systems,” *Colloid Polym. Sci.*, vol. 298, no. 1, pp. 67–77, Jan. 2020, doi: 10.1007/s00396-019-04587-2.

[381] S. H. Cho, S. R. White, and P. V. Braun, “Room-temperature polydimethylsiloxane-based self-healing polymers,” *Chem. Mater.*, vol. 24, no. 21, pp. 4209–4214, Nov. 2012, doi: 10.1021/cm302501b.

[382] W. R. K. Weihermann, M. M. Meier, and S. H. Pezzin, "Microencapsulated amino-functional polydimethylsiloxane as autonomous external self-healing agent for epoxy systems," *J. Appl. Polym. Sci.*, vol. 136, no. 23, p. 47627, Jun. 2019, doi: 10.1002/app.47627.

[383] M. Attaei, M. Vale, A. Shakoor, R. Kahraman, M. F. Montemor, and A. C. Marques, "Hybrid shell microcapsules containing isophorone diisocyanate with high thermal and chemical stability for autonomous self-healing of epoxy coatings," *J. Appl. Polym. Sci.*, vol. 137, no. 22, p. 48751, Jun. 2020, doi: 10.1002/app.48751.

[384] G. Kurt Çömlekçi and S. Ulutan, "Encapsulation of linseed oil and linseed oil based alkyd resin by urea formaldehyde shell for self-healing systems," *Prog. Org. Coatings*, vol. 121, pp. 190–200, Aug. 2018, doi: 10.1016/j.porgcoat.2018.04.027.

[385] S. Habib, E. Fayyed, R. A. Shakoor, R. Kahraman, and A. Abdullah, "Improved self-healing performance of polymeric nanocomposites reinforced with talc nanoparticles (TNPs) and urea-formaldehyde microcapsules (UFMCs)," *Arab. J. Chem.*, vol. 14, no. 2, p. 102926, Feb. 2021, doi: 10.1016/j.arabjc.2020.102926.

[386] H. Ebrahimnezhad-Khaljiri, R. Eslami-Farsani, and S. Arbab Chirani, "Microcapsulated epoxy resin with nanosilica-urea formaldehyde composite shell," *J. Appl. Polym. Sci.*, vol. 137, no. 16, p. 48580, Apr. 2020, doi: 10.1002/app.48580.

[387] A. K. Asadi, M. Ebrahimi, and M. Mohseni, "Preparation and characterisation of melamineurea-formaldehyde microcapsules containing linseed oil in the presence of polyvinylpyrrolidone as emulsifier," *Pigment Resin Technol.*, vol. 46, no. 4, pp. 318–326, 2017, doi: 10.1108/PRT-04-2016-0043.

[388] S. N. Khorasani, S. Ataei, and R. E. Neisiany, "Microencapsulation of a coconut oil-based alkyd resin into poly(melamine–urea–formaldehyde) as shell for self-healing purposes," *Prog. Org. Coatings*, vol. 111, pp. 99–106, 2017, doi: 10.1016/j.porgcoat.2017.05.014.

[389] X.-M. Tong, M. Zhang, M.-S. Wang, and Y. Fu, "Effects of surface modification of self-healing poly(melamine-urea-formaldehyde) microcapsules on the properties of unsaturated polyester composites," *J. Appl. Polym. Sci.*, vol. 127, no. 5, pp. 3954–3961, Mar. 2013, doi: 10.1002/app.37711.

[390] F. Ahangaran, M. Hayaty, and A. H. Navarchian, "Morphological study of polymethyl methacrylate microcapsules filled with self-healing agents," *Appl. Surf. Sci.*, vol. 399, pp. 721–731, Mar. 2017, doi: 10.1016/j.apsusc.2016.12.116.

[391] R. Rodriguez, D. G. Bekas, S. Flórez, M. Kosarli, and A. S. Paipetis, "Development of self-contained microcapsules for optimised catalyst position in self-healing materials," *Polymer (Guildf).*, vol. 187, p. 122084, Jan. 2020, doi: 10.1016/j.polymer.2019.122084.

[392] F. Ahangaran, A. H. Navarchian, and F. Picchioni, "Material encapsulation in poly(methyl methacrylate) shell: A review," *J. Appl. Polym. Sci.*, vol. 136, no. 41, p. 48039, Nov. 2019, doi: 10.1002/app.48039.

[393] Y. Ren, N. Abbas, G. Zhu, and J. Tang, "Synthesis and mechanical properties of large size silica shell microcapsules for self-healing cementitious materials," *Colloids Surfaces A Physicochem. Eng. Asp.*, vol. 587, p. 124347, Feb. 2020, doi: 10.1016/j.colsurfa.2019.124347.

[394] R. Malekkhouyan, S. Nouri Khorasani, R. Esmaeely Neisiany, R. Torkaman, M. S. Koochaki, and O. Das, "Preparation and Characterization of Electrosprayed Nanocapsules Containing Coconut-Oil-Based Alkyd Resin for the Fabrication of Self-Healing Epoxy Coatings," *Appl. Sci.*, vol. 10, no. 9, p. 3171, May 2020, doi: 10.3390/app10093171.

[395] S. G. Bayryamov, "Microencapsulation of natural oils by a coacervation technique using gelatin as shell material," *J. Chem. Technol. Metall.*, vol. 55, no. 6, pp. 1985–1989, 2020.

[396] M. Samadzadeh, S. H. Boura, M. Peikari, S. M. Kasiriha, and A. Ashrafi, "A review on self-healing coatings based on micro/nanocapsules," *Prog. Org. Coatings*, vol. 68, no. 3, pp. 159–164, 2010, doi: 10.1016/j.porgcoat.2010.01.006.

[397] H. Mayer, "The chemistry and properties of silicone resins," *JOCCA - Surf. Coatings Int.*, vol. 27, no. 6, pp. 364–373, 1999, doi: 10.1007/BF02692627.

[398] U. Eduok, O. Faye, and J. Szpunar, "Recent developments and applications of protective silicone coatings: A review of PDMS functional materials," *Prog. Org. Coatings*, vol. 111, pp. 124–163, 2017, doi: 10.1016/j.porgcoat.2017.05.012.

[399] X. K. D. Hillewaere and F. E. Du Prez, "Fifteen chemistries for autonomous external self-healing polymers and composites," *Prog. Polym. Sci.*, vol. 49–50, pp. 121–153, 2015, doi: 10.1016/j.progpolymsci.2015.04.004.

[400] D. M. Kim, Y. J. Cho, J. Y. Choi, B. J. Kim, S. W. Jin, and C. M. Chung, "Low-temperature self-healing of a

microcapsule-type protective coating," *Materials (Basel).*, vol. 10, no. 9, p. 1079, 2017, doi: 10.3390/ma10091079.

[401] D. M. Kim, H. C. Yu, H. I. Yang, Y. J. Cho, K. M. Lee, and C. M. Chung, "Microcapsule-type self-healing protective coating for cementitious composites with secondary crack preventing ability," *Materials (Basel).*, vol. 10, no. 2, p. 114, 2017, doi: 10.3390/ma10020114.

[402] X. Liu, X. Sheng, J. K. Lee, and M. R. Kessler, "Synthesis and characterization of melamine- urea-formaldehyde microcapsules containing ENB-based self-healing agents," *Int. Conf. Smart Mater. Nanotechnol. Eng.*, p. 642337, 2007, doi: 10.1002/mame.200900015.

[403] Y. Konuklu, H. O. Paksoy, M. Unal, and S. Konuklu, "Microencapsulation of a fatty acid with Poly(melamine-urea-formaldehyde)," *Energy Convers. Manag.*, vol. 80, pp. 382–390, 2014, doi: 10.1016/j.enconman.2014.01.042.

[404] X. M. Tong, T. Zhang, M. Z. Yang, and Q. Zhang, "Preparation and characterization of novel melamine modified poly(urea-formaldehyde) self-repairing microcapsules," *Colloids Surfaces A Physicochem. Eng. Asp.*, vol. 371, no. 1–3, pp. 91–97, 2010, doi: 10.1016/j.colsurfa.2010.09.009.

[405] T. Nesterova, K. Dam-Johansen, and S. Kiil, "Synthesis of durable microcapsules for self-healing anticorrosive coatings: A comparison of selected methods," *Prog. Org. Coatings*, vol. 70, no. 4, pp. 342–352, 2011, doi: 10.1016/j.porgcoat.2010.09.032.

[406] G. O. Wilson, H. M. Andersson, S. R. White, N. R. Sottos, J. S. Moore, and P. V. Braun, "Self-Healing Polymers," in *Encyclopedia of Polymer Science and Technology*, Hoboken, NJ, USA: American Cancer Society, 2010.

[407] R. S. Rivlin and A. G. Thomas, "Rupture of rubber. I. Characteristic energy for tearing," *J. Polym. Sci.*, vol. 10, no. 3, pp. 291–318, Mar. 1953, doi: 10.1002/POL.1953.120100303.

[408] M. Kosarli *et al.*, "Microcapsule-based self-healing materials: Healing efficiency and toughness reduction vs. capsule size," *Compos. Part B Eng.*, vol. 171, pp. 78–86, 2019, doi: 10.1016/j.compositesb.2019.04.030.

[409] Z. Yang *et al.*, "Versatility of the microencapsulation technique via integrating microfluidic T-Junction and interfacial polymerization in encapsulating different polyamines," *Colloids Surfaces A Physicochem. Eng. Asp.*, vol. 604, p. 125097, 2020, doi: 10.1016/j.colsurfa.2020.125097.

[410] C. Fan and X. Zhou, "Effect of emulsifier on poly(urea-formaldehyde) microencapsulation of tetrachloroethylene," *Polym. Bull.*, vol. 67, pp. 15–27, 2011, doi: 10.1007/s00289-010-0355-1.

[411] J. Li, S. Wang, H. Liu, N. Liu, and L. You, "Preparation and application of poly(melamineurea- formaldehyde) microcapsules filled with sulfur," *Polym. - Plast. Technol. Eng.*, vol. 50, no. 7, pp. 689–697, 2011, doi: 10.1080/03602559.2010.551389.

[412] M. Pretzl *et al.*, "Formation and mechanical characterization of aminoplast core/shell microcapsules," *ACS Appl. Mater. Interfaces*, vol. 4, no. 6, pp. 2940–2948, 2012, doi: 10.1021/am300273b.

[413] F. Ahangaran, A. H. Navarchian, and F. Picchioni, "Material encapsulation in poly(methyl methacrylate) shell: A review," *J. Appl. Polym. Sci.*, vol. 136, no. 41, p. 48039, 2019, doi: 10.1002/app.48039.

[414] A. Olusegun *et al.*, "Applications of Microcapsules in Self-Healing Polymeric Materials," in *Microencapsulation - Processes, Technologies and Industrial Applications*, Second Edi., Fabien Salaün, Ed. IntechOpen, 2019.

[415] E. N. Brown, M. R. Kessler, N. R. Sottos, and S. R. White, "In situ poly(urea-formaldehyde) microencapsulation of dicyclopentadiene," *J. Microencapsul.*, vol. 20, no. 6, pp. 719–730, 2003, doi: 10.1080/0265204031000154160.

[416] T. Van Westen and R. D. Groot, "Effect of Temperature Cycling on Ostwald Ripening," *Cryst. Growth Des.*, vol. 18, no. 9, pp. 4952–4962, 2018, doi: 10.1021/acs.cgd.8b00267.

[417] E. Katoueizadeh, S. M. Zebarjad, and K. Janghorban, "Investigating the effect of synthesis conditions on the formation of urea-formaldehyde microcapsules," *J. Mater. Res. Technol.*, vol. 8, no. 1, pp. 541–552, 2019, doi: 10.1016/j.jmrt.2018.04.013.

[418] L. Yuan *et al.*, "Preparation and Characterization of Microencapsulated Ethylenediamine with Epoxy Resin for Self-healing Composites," *Sci. Rep.*, vol. 9, p. 18834, 2019, doi: 10.1038/s41598-019-55268-7.

[419] Rochmadi, A. Prasetya, and W. Hasokowati, "Mechanism of microencapsulation with Urea-Formaldehyde polymer,"

Am. J. Appl. Sci., vol. 7, no. 6, pp. 739–745, 2010, doi: 10.3844/ajassp.2010.739.745.

[420] B. Wu, G. Zheng, and X. Chen, "Effect of graphene on the thermophysical properties of melamine-urea-formaldehyde/N-hexadecane microcapsules," *RSC Adv.*, vol. 5, no. 90, pp. 74024–74031, 2015, doi: 10.1039/c5ra12566a.

[421] B. Likozar, R. C. Korošec, I. Poljanšek, P. Ogorelec, and P. Bukovec, "Curing kinetics study of melamine-urea-formaldehyde resin," *J. Therm. Anal. Calorim.*, vol. 109, no. 3, pp. 1413–1422, 2012, doi: 10.1007/s10973-011-1883-0.

[422] H. Zhu and S. Xu, "Preparation and fire behavior of rigid polyurethane foams synthesized from modified urea–melamine–formaldehyde resins," *RSC Adv.*, vol. 8, no. 32, pp. 17879–17887, May 2018, doi: 10.1039/C8RA01846D.

[423] R. K. Pittala, B. S. Ben, and B. A. Ben, "Self-healing performance assessment of epoxy resin and amine hardener encapsulated polymethyl methacrylate microcapsules reinforced epoxy composite," *J. Appl. Polym. Sci.*, vol. 138, no. 23, p. 50550, Jun. 2021, doi: 10.1002/app.50550.

[424] S. Then, G. S. Neon, and N. H. Abu Kasim, "Optimization of microencapsulation process for self-healing polymeric material," *Sains Malaysiana*, vol. 40, no. 7, pp. 795–802, 2011, doi: 10.5281/zenodo.811347.

[425] S. Han, Y. Chen, S. Lyu, Z. Chen, S. Wang, and F. Fu, "Effects of processing conditions on the properties of paraffin/melamine-urea-formaldehyde microcapsules prepared by in situ polymerization," *Colloids Surfaces A Physicochem. Eng. Asp.*, vol. 585, p. 124046, 2020, doi: 10.1016/j.colsurfa.2019.124046.

[426] "US Patent for Method for preparing linear organopolysiloxanediols Patent (Patent # 4,762,937 issued August 9, 1988) - Justia Patents Search." https://patents.justia.com/patent/4762937.

[427] X. Yang *et al.*, "A convenient method for preparation of hydroxyl silicone oils with ring opening polymerization of octamethylcyclotetrasiloxane (D4)," *Phosphorous, Sulfur, Silicon Relat. Elem.*, vol. 191, no. 1, pp. 117–122, 2016, doi: 10.1080/10426507.2014.986269.

[428] I. YILGÖR, J. S. RIFFLE, and J. E. McGRATH, "Reactive Difunctional Siloxane Oligomers," pp. 161–174, Jul. 1985, doi: 10.1021/BK-1985-0282.CH014.

[429] L. Yuan *et al.*, "Synthesis of poly(urea-formaldehyde) encapsulated dibutyltin dilaurate through the self-catalysis of core materials," *Polym. Bull.*, vol. 71, pp. 261–273, 2014, doi: 10.1007/s00289-013-1059-0.

[430] S. S. Latthe, R. S. Sutar, V. S. Kodag, A. K. Bhosale, and A. M. Kumar, "Progress in Organic Coatings Self – cleaning superhydrophobic coatings : Potential industrial applications," *Prog. Org. Coatings*, vol. 128, no. August 2018, pp. 52–58, 2019, doi: 10.1016/j.porgcoat.2018.12.008.

[431] M. Shamshiri, R. Jafari, and G. Momen, "Potential use of smart coatings for icephobic applications: A review," *Surf. Coatings Technol.*, vol. 424, p. 127656, Oct. 2021, doi: 10.1016/J.SURFCOAT.2021.127656.

[432] L. Foroughi Mobarakeh, R. Jafari, and M. Farzaneh, "Robust icephobic, and anticorrosive plasma polymer coating," *Cold Reg. Sci. Technol.*, vol. 151, pp. 89–93, 2018, doi: 10.1016/j.coldregions.2018.03.009.

[433] H. Sojoudi, M. Wang, N. D. Boscher, G. H. McKinley, and K. K. Gleason, "Durable and scalable icephobic surfaces: Similarities and distinctions from superhydrophobic surfaces," *Soft Matter*, vol. 12, no. 7, pp. 1938–1963, 2016, doi: 10.1039/c5sm02295a.

[434] B. Liu *et al.*, "Strategies for anti-icing: low surface energy or liquid-infused?," *RSC Adv.*, vol. 6, no. 74, pp. 70251–70260, Jul. 2016, doi: 10.1039/C6RA11383D.

[435] G. Wang, Y. Shen, J. Tao, X. Luo, L. Zhang, and Y. Xia, "Fabrication of a superhydrophobic surface with a hierarchical nanoflake-micropit structure and its anti-icing properties," *RSC Adv.*, vol. 7, p. 9981, 2017, doi: 10.1039/c6ra28298a.

[436] A. Azimi Yancheshme, G. Momen, and R. Jafari Aminabadi, "Mechanisms of ice formation and propagation on superhydrophobic surfaces: A review," *Adv. Colloid Interface Sci.*, vol. 279, p. 102155, May 2020, doi: 10.1016/J.CIS.2020.102155.

[437] A. K. Metya, J. K. Singh, and F. Müller-Plathe, "Ice nucleation on nanotextured surfaces: the influence of surface fraction, pillar height and wetting states," *Phys. Chem. Chem. Phys.*, vol. 18, no. 38, pp. 26796–26806, Sep. 2016, doi: 10.1039/C6CP04382H.

[438] X. Wu, X. Zhao, J. W. C. Ho, and Z. Chen, “Design and durability study of environmental-friendly room-temperature processable icephobic coatings,” *Chem. Eng. J.*, vol. 355, pp. 901–909, Jan. 2019, doi: 10.1016/J.CEJ.2018.07.204.

[439] J. M. Sayward, “Seeking Low Ice Adhesion,” Apr. 1979. [Online]. Available: https://apps.dtic.mil/sti/citations/ADA071040.

[440] S. Heydarian, R. Jafari, and G. Momen, “Recent progress in the anti-icing performance of slippery liquid-infused surfaces,” *Prog. Org. Coatings*, vol. 151, p. 106096, Feb. 2021, doi: 10.1016/J.PORGCOAT.2020.106096.

[441] T.-S. Wong *et al.*, “Bioinspired self-repairing slippery surfaces with pressure-stable omniphobicity,” *Nature*, vol. 477, no. 7365, pp. 443–447, Sep. 2011, doi: 10.1038/nature10447.

[442] G. Wang *et al.*, “A Review on Fabrication Methods and Research Progress of Superhydrophobic Silicone Rubber Materials,” *Adv. Mater. Interfaces*, vol. 8, no. 1, p. 2001460, Jan. 2021, doi: 10.1002/ADMI.202001460.

[443] Y. Zhuo, S. Xiao, A. Amirfazli, J. He, and Z. Zhang, “Polysiloxane as icephobic materials – The past, present and the future,” *Chem. Eng. J.*, vol. 405, p. 127088, Feb. 2021, doi: 10.1016/J.CEJ.2020.127088.

[444] R. B. Figueira, C. J. R. Silva, and E. V. Pereira, “Organic–inorganic hybrid sol–gel coatings for metal corrosion protection: a review of recent progress,” *J. Coatings Technol. Res.*, vol. 12, pp. 1–35, Aug. 2014, doi: 10.1007/S11998-014-9595-6.

[445] M. D. Soucek, D. P. Dworak, and R. Chakraborty, “A new class of silicone resins for coatings,” *J. Coatings Technol. Res.*, vol. 4, no. 3, pp. 263–274, Jul. 2007, doi: 10.1007/S11998-007-9044-X.

[446] B. Bhushan, *Biomimetics: bioinspired hierarchical-structured surfaces for green science and technology*, Second ed. Springer, 2016.

[447] P. Nguyen-Tri *et al.*, “Recent progress in the preparation, properties and applications of superhydrophobic nano-based coatings and surfaces: A review,” *Prog. Org. Coatings*, vol. 132, pp. 235–256, Jul. 2019, doi: 10.1016/J.PORGCOAT.2019.03.042.

[448] S. A. Mahadik and S. S. Mahadik, “Surface morphological and topographical analysis of multifunctional superhydrophobic sol-gel coatings,” *Ceram. Int.*, vol. 47, no. 20, pp. 29475–29482, Jul. 2021, doi: 10.1016/J.CERAMINT.2021.07.115.

[449] Ö. Kesmez, “Preparation of hybrid nanocomposite coatings via sol-gel method for hydrophobic and self-cleaning properties,” *J. Mol. Struct.*, vol. 1205, p. 127572, Apr. 2020, doi: 10.1016/J.MOLSTRUC.2019.127572.

[450] B. Subeshan, A. Usta, and R. Asmatulu, “Deicing and self-cleaning of plasma-treated superhydrophobic coatings on the surface of aluminum alloy sheets,” *Surfaces and Interfaces*, vol. 18, p. 100429, Mar. 2020, doi: 10.1016/J.SURFIN.2020.100429.

[451] Y. Yu, L. Chen, D. Weng, J. Wang, C. Chen, and A. Mahmood, “A promising self-assembly PTFE coating for effective large-scale deicing,” *Prog. Org. Coatings*, vol. 147, p. 105732, Oct. 2020, doi: 10.1016/J.PORGCOAT.2020.105732.

[452] B. Thasma Subramanian, J. P. Alla, J. S. Essomba, and N. F. Nishter, “Non-fluorinated superhydrophobic spray coatings for oil-water separation applications: An eco-friendly approach,” *J. Clean. Prod.*, vol. 256, p. 120693, May 2020, doi: 10.1016/J.JCLEPRO.2020.120693.

[453] C. E. Müller *et al.*, “Biomagnification of perfluorinated compounds in a remote terrestrial food chain: Lichen-Caribou-Wolf,” *Environ. Sci. Technol.*, vol. 45, no. 20, pp. 8665–8673, Oct. 2011, doi: 10.1021/ES201353V/SUPPL_FILE/ES201353V_SI_001.PDF.

[454] A. Bake, N. Merah, A. Matin, M. Gondal, T. Qahtan, and N. Abu-Dheir, “Preparation of transparent and robust superhydrophobic surfaces for self-cleaning applications,” *Prog. Org. Coatings*, vol. 122, pp. 170–179, Sep. 2018, doi: 10.1016/J.PORGCOAT.2018.05.018.

[455] Z. Zhang *et al.*, “One-step fabrication of robust superhydrophobic and superoleophilic surfaces with self-cleaning and oil/water separation function,” *Sci. Rep.*, vol. 8, no. 1, pp. 1–12, Mar. 2018, doi: 10.1038/s41598-018-22241-9.

[456] J. Zhao *et al.*, “Construction of a durable superhydrophobic surface based on the oxygen inhibition layer of organosilicon resins,” *Thin Solid Films*, vol. 717, p. 138467, Jan. 2021, doi: 10.1016/J.TSF.2020.138467.

[457] X. Zhao, B. Yu, and J. Zhang, “Transparent and durable superhydrophobic coatings for anti-bioadhesion,” *J. Colloid Interface Sci.*, vol. 501, pp. 222–230, Sep. 2017, doi: 10.1016/J.JCIS.2017.04.049.

[458] H. Jo and F. D. Blum, “Characterization of the Interface in Polymer−Silica Composites Containing an Acrylic Silane Coupling Agent,” *Chem. Mater.*, vol. 11, no. 9, pp. 2548–2553, 1999, doi: 10.1021/CM9902570.

[459] M. C. Li and U. R. Cho, “Effectiveness of coupling agents in the poly (methyl methacrylate)-modified starch/styrene-butadiene rubber interfaces,” *Mater. Lett.*, vol. 92, pp. 132–135, Feb. 2013, doi: 10.1016/J.MATLET.2012.10.050.

[460] S. Martin and B. Bhushan, “Transparent, wear-resistant, superhydrophobic and superoleophobic poly(dimethylsiloxane) (PDMS) surfaces,” *J. Colloid Interface Sci.*, vol. 488, pp. 118–126, Feb. 2017, doi: 10.1016/J.JCIS.2016.10.094.

[461] S. Liu *et al.*, “Self-cleaning transparent superhydrophobic coatings through simple sol-gel processing of fluoroalkylsilane,” *Appl. Surf. Sci.*, vol. 351, pp. 897–903, Oct. 2015, doi: 10.1016/j.apsusc.2015.06.016.

[462] S. Qiang, K. Chen, Y. Yin, and C. Wang, “Robust UV-cured superhydrophobic cotton fabric surfaces with self-healing ability,” *Mater. Des.*, vol. 116, pp. 395–402, Feb. 2017, doi: 10.1016/j.matdes.2016.11.099.

[463] S. Peng, D. Tian, X. Miao, X. Yang, and W. Deng, “Designing robust alumina nanowires-on-nanopores structures: Superhydrophobic surfaces with slippery or sticky water adhesion,” *J. Colloid Interface Sci.*, vol. 409, pp. 18–24, Nov. 2013, doi: 10.1016/j.jcis.2013.07.059.

[464] D. Khojasteh, M. Kazerooni, S. Salarian, and R. Kamali, “Droplet impact on superhydrophobic surfaces: A review of recent developments,” *J. Ind. Eng. Chem.*, vol. 42, pp. 1–14, Oct. 2016, doi: 10.1016/J.JIEC.2016.07.027.

[465] C. Guo, D. Zhao, Y. Sun, M. Wang, and Y. Liu, “Droplet Impact on Anisotropic Superhydrophobic Surfaces,” *Langmuir*, vol. 34, no. 11, pp. 3533–3540, Mar. 2018, doi: 10.1021/ACS.LANGMUIR.7B03752.

[466] E. Vazirinasab, R. Jafari, and G. Momen, “Evaluation of atmospheric-pressure plasma parameters to achieve superhydrophobic and self-cleaning HTV silicone rubber surfaces via a single-step, eco-friendly approach,” *Surf. Coatings Technol.*, vol. 375, pp. 100–111, Oct. 2019, doi: 10.1016/J.SURFCOAT.2019.07.005.

[467] X. Wu, V. V. Silberschmidt, Z. T. Hu, and Z. Chen, “When superhydrophobic coatings are icephobic: Role of surface topology,” *Surf. Coatings Technol.*, vol. 358, pp. 207–214, Jan. 2019, doi: 10.1016/J.SURFCOAT.2018.11.039.

[468] I. S. Bayer, “On the Durability and Wear Resistance of Transparent Superhydrophobic Coatings,” *Coatings*, vol. 7, no. 1, p. 12, Jan. 2017, doi: 10.3390/COATINGS7010012.

[469] B. Bhushan and Y. C. Jung, “Natural and biomimetic artificial surfaces for superhydrophobicity, self-cleaning, low adhesion, and drag reduction,” *Prog. Mater. Sci.*, vol. 56, no. 1, pp. 1–108, Jan. 2011, doi: 10.1016/J.PMATSCI.2010.04.003.

[470] Ç. K. Söz, S. Trosien, and M. Biesalski, “Janus Interface Materials: A Critical Review and Comparative Study,” *ACS Mater. Lett.*, vol. 2, no. 4, pp. 336–357, Apr. 2020, doi: 10.1021/ACSMATERIALSLETT.9B00489.

[471] K. Golovin, S. P. R. Kobaku, D. H. Lee, E. T. DiLoreto, J. M. Mabry, and A. Tuteja, “Designing durable icephobic surfaces,” *Sci. Adv.*, vol. 2, no. 3, pp. 1–12, Mar. 2016, doi: 10.1126/sciadv.1501496.

[472] T. Bharathidasan, S. V. Kumar, M. S. Bobji, R. P. S. Chakradhar, and B. J. Basu, “Effect of wettability and surface roughness on ice-adhesion strength of hydrophilic, hydrophobic and superhydrophobic surfaces,” *Appl. Surf. Sci.*, vol. 314, pp. 241–250, 2014, doi: 10.1016/j.apsusc.2014.06.101.

[473] M. Zou, S. Beckford, R. Wei, C. Ellis, G. Hatton, and M. A. Miller, “Effects of surface roughness and energy on ice adhesion strength,” *Appl. Surf. Sci.*, vol. 257, no. 8, pp. 3786–3792, Feb. 2011, doi: 10.1016/j.apsusc.2010.11.149.

[474] E. Vazirinasab, K. Maghsoudi, R. Jafari, and G. Momen, “A comparative study of the icephobic and self-cleaning properties of Teflon materials having different surface morphologies,” *J. Mater. Process. Technol.*, vol. 276, p. 116415, Feb. 2020, doi: 10.1016/J.JMATPROTEC.2019.116415.

[475] Q. Yang *et al.*, “Air Cushion Convection Inhibiting Icing of Self-Cleaning Surfaces,” *ACS Appl. Mater. Interfaces*, vol. 8, no. 42, pp. 29169–29178, Oct. 2016, doi: 10.1021/acsami.6b10165.

[476] S. Sanyal *et al.*, “Deterioration of Porcelain Insulators Utilized in Overhead Transmission Lines: A Review,” *Trans. Electr. Electron. Mater.*, vol. 21, pp. 16–21, 2019, doi: 10.1007/s42341-019-00143-5.

[477] F. A. Jamaludin, M. Z. Abidin Ab-Kadir, M. Izadi, N. Azis, J. Jasni, and M. S. Abd-Rahman, “Effects of RTV coating on the electrical performance of polymer insulator under lightning impulse voltage condition,” *PLoS One*, vol. 12, no. 11, 2017, doi: 10.1371/journal.pone.0187892.

[478] K. N. M. E.J.McGowan, “Surface Electrical Failure in the Presence of Contaminants : The Inclined-Plane Liquid-Contaminant Test,” *Trans. Am. Inst. Electr. Eng. Part I Commun. Electron.*, vol. 80, no. 3, pp. 281–289, 1961.

[479] Electric Power Research. Institute Report, “Visual Inspection of Porcelain and Glass Disc Insulators, Project 3002005628.”

[480] LÁSZLÓ MATTYASOVSZKY-ZSOLNAY, “Mechanical Strength of Porcelain,” *J. Am. Ceram. Soc.*, vol. 40, no. 9, pp. 299–306, 1957, doi: 10.1111/j.1151-2916.1957.tb12626.x.

[481] G. BLAISE and W. SARJEANT, “Electrical Aging and Breakdown in Dielectric Materials,” in *Handbook of Low and High Dielectric Constant Materials and Their Applications*, H. S. Nalwa, Ed. Elsevier, 1999.

[482] W. Group, *Coatings for Protecting Overhead Power Network Equipment in Winter Conditions Network Equipment*. 2015.

[483] V. Pevtsov, N. D. Jacob, and B. Kordi, “Evaluation of Erosion Discharge Characteristics in Inclined Plane Tracking and Erosion Tests on Silicone Rubber under AC and DC Voltages,” *Energies*, vol. 14, no. 19, p. 6051, Sep. 2021, doi: 10.3390/EN14196051.

[484] S. Huzaimah Kamal Hamadi, M. Isa, S. Nizam Md Arshad Hashim, and M. Othman, “Review on RTV Silicone Rubber Coatings Insulator for Transmission Lines,” *IOP Conf. Ser. Mater. Sci. Eng.*, vol. 864, no. 1, 2020, doi: 10.1088/1757-899X/864/1/012188.

[485] R. Sarathi and M. G. Danikas, “RTV Silicone Rubber Coatings for Outdoor Insulators: A Concise Review of Some Factors Affecting their Behavior and Some Comments,” *J. Eng. Sci. Technol. Rev.*, vol. 14, no. 1, pp. 163–169, 2021, doi: 10.25103/jestr.141.19.

[486] J. M. George *et al.*, “Field experience and laboratory investigation of glass insulators having a factory-applied silicone rubber coating,” *IEEE Trans. Dielectr. Electr. Insul.*, vol. 21, no. 6, pp. 2594–2601, 2014, doi: 10.1109/TDEI.2014.004600.

[487] T. Sorqvist, “Long-term field experience with RTV coated porcelain insulators,” 2000, doi: 10.1109/elinsl.2000.845489.

[488] H. Gao, Z. Jia, Z. Guan, L. Wang, and K. Zhu, “Investigation on field-aged RTV-coated insulators used in heavily contaminated areas,” *IEEE Trans. Power Deliv.*, vol. 22, no. 2, pp. 1117–1124, 2007, doi: 10.1109/TPWRD.2007.893432.

[489] H. Homma, C. L. Mirley, J. A. Ronzello, and S. A. Boggs, “Field and laboratory aging of RTV silicone insulator coatings,” *IEEE Trans. Power Deliv.*, vol. 15, no. 4, pp. 1298–1303, 2000, doi: 10.1109/61.891518.

[490] K. Maghsoudi, G. Momen, R. Jafari, and M. Farzaneh, “Rigorous testing to assess the self-cleaning properties of an ultra-water-repellent silicone rubber surface,” *Surf. Coatings Technol.*, vol. 374, pp. 557–568, Sep. 2019, doi: 10.1016/J.SURFCOAT.2019.05.073.

[491] G. Momen, M. Farzaneh, and R. Jafari, “Wettability behaviour of RTV silicone rubber coated on nanostructured aluminium surface,” *Appl. Surf. Sci.*, vol. 257, no. 15, pp. 6489–6493, May 2011, doi: 10.1016/J.APSUSC.2011.02.049.

[492] A. C. Baker *et al.*, “Insulator selection for AC overhead lines with respect to contamination,” *IEEE Trans. Power Deliv.*, vol. 24, no. 3, pp. 1633–1641, 2009, doi: 10.1109/TPWRD.2009.2024666.

[493] G. Momen and M. Farzaneh, “Survey of micro/nano filler use to improve silicone rubber for outdoor insulators Icing of transmission lines and structures View project Superhydrophobic and self-cleaning polymeric surfaces using injection molding systems View project,” *Rev. Adv. Mater. Sci.*, vol. 27, no. 1, pp. 1–13, 2011.

[494] M. Taghvaei, M. Sedighizadeh, N. NayebPashaee, and A. S. Fini, “Reliability assessment of RTV and nano-RTV-coated insulators concerning contamination severity,” *Electr. Power Syst. Res.*, vol. 191, p. 106892, Feb. 2021, doi: 10.1016/J.EPSR.2020.106892.

[495] X. Qiao, Z. Zhang, X. Jiang, R. Sundararajan, X. Ma, and X. Li, “AC failure voltage of iced and contaminated composite insulators in different natural environments,” *Int. J. Electr. Power Energy Syst.*, vol. 120, p. 105993, Sep. 2020, doi: 10.1016/J.IJEPES.2020.105993.

[496] Z. Zuo, J. Gao, R. Liao, X. Zhao, and Y. Yuan, “A novel and facile way to fabricate transparent superhydrophobic film on glass with self-cleaning and stability,” *Mater. Lett.*, vol. 239, pp. 48–51, 2019, doi: 10.1016/j.matlet.2018.12.059.

[497] A. Bake, N. Merah, A. Matin, M. Gondal, T. Qahtan, and N. Abu-dheir, “Preparation of transparent and robust superhydrophobic surfaces for self- cleaning applications,” *Prog. Org. Coatings*, vol. 122, no. May, pp. 170–179, 2018, doi: 10.1016/j.porgcoat.2018.05.018.

[498] A. Marmur, “From hygrophilic to superhygrophobic: Theoretical conditions for making high-contact-angle surfaces from low-contact-angle materials,” *Langmuir*, vol. 24, no. 14, pp. 7573–7579, 2008, doi: 10.1021/la800304r.

[499] J. Li, Y. Zhao, J. Hu, L. Shu, and X. Shi, “Anti-icing performance of a superhydrophobic PDMS/modified nano-silica hybrid coating for insulators,” *J. Adhes. Sci. Technol.*, vol. 26, no. 4–5, pp. 665–679, 2012, doi: 10.1163/016942411X574826.

[500] S. Xu, Q. Wang, and N. Wang, “Chemical Fabrication Strategies for Achieving Bioinspired Superhydrophobic Surfaces with Micro and Nanostructures: A Review,” *Adv. Eng. Mater.*, vol. 23, no. 3, p. 2001083, Mar. 2021, doi: 10.1002/ADEM.202001083.

[501] Q. Zeng, H. Zhou, J. Huang, and Z. Guo, “Review on the recent development of durable superhydrophobic materials for practical applications,” *Nanoscale*, vol. 13, no. 27, pp. 11734–11764, Jul. 2021, doi: 10.1039/D1NR01936H.

[502] K. Lu, D. Erb, and M. Liu, “Phase transformation, oxidation stability, and electrical conductivity of TiO2-polysiloxane derived ceramics,” *J. Mater. Sci.*, vol. 51, no. 22, pp. 10166–10177, 2016, doi: 10.1007/s10853-016-0244-6.

[503] S. A. Seyedmehdi and M. Ebrahimi, “Superhydrophobic modified-polyurethane coatings for bushing of power transformers: From material to fabrication, mechanical and electrical properties,” *Prog. Org. Coatings*, vol. 123, pp. 134–137, Oct. 2018, doi: 10.1016/J.PORGCOAT.2018.07.010.

[504] I. Ramalla, I. Ramalla, R. K. Gupta, and K. Bansal, “Effect on superhydrophobic surfaces on electrical porcelain insulator, improved technique at polluted areas for longer life and reliability,” *Int. J. Eng. Technol.*, vol. 4, no. 4, pp. 509–519, Oct. 2015, doi: 10.14419/ijet.v4i4.5405.

[505] J. Chen, J. Chen, L. Li, S. Wang, and Y. Xie, “Study on the self-cleaning phenomenon and anti-pollution flashover performance of micro-nanostructure superhydrophobic coating surface under a high humidity environment,” *Colloids Surfaces A Physicochem. Eng. Asp.*, vol. 630, no. September, p. 127552, 2021, doi: 10.1016/j.colsurfa.2021.127552.

[506] Z. Zhu, S. Fu, and A. H. Basta, “A cellulose nanoarchitectonic: Multifunctional and robust superhydrophobic coating toward rapid and intelligent water-removing purpose,” *Carbohydr. Polym.*, vol. 243, p. 116444, Sep. 2020, doi: 10.1016/J.CARBPOL.2020.116444.

[507] C. S. E. E. Willis, A.J. Phillips, F.F. Bologna, “Advanced Coatings for Insulators & Conductors: Overview of EPRI research opportunity for the power industry,” 2019.

[508] J. Wu and A. Schnettler, “Degradation assessment of nanostructured superhydrophobic insulating surfaces using multi-stress methods,” *IEEE Trans. Dielectr. Electr. Insul.*, vol. 15, no. 1, pp. 73–80, Feb. 2008, doi: 10.1109/T-DEI.2008.4446738.

[509] and M. T. N. Israr Ullah, Muhammad Amin, Haider Hussain, “Impact of Accelerated Ultraviolet Weathering on Polymeric Composite Insulators Under High Voltage DC Stress,” *CSEE J. POWER ENERGY Syst.*, vol. 8, no. 3, pp. 922–932, 2022, Accessed: Jun. 05, 2022. [Online]. Available: https://ieeexplore.ieee.org/stamp/stamp.jsp?arnumber=9215173.

[510] A. Y. Yassin, A. R. Mohamed, A. M. Abdelghany, and E. M. Abdelrazek, “Enhancement of dielectric properties and AC electrical conductivity of nanocomposite using poly (vinyl chloride-co-vinyl acetate-co-2-hydroxypropyl acrylate) filled with graphene oxide,” *J. Mater. Sci. Mater. Electron.*, vol. 29, no. 18, pp. 15931–15945, Sep. 2018, doi: 10.1007/S10854-018-9679-7/TABLES/3.

[511] I. Tantis, G. C. Psarras, and D. Tasis, “Functionalized graphene - poly(vinyl alcohol) nanocomposites: Physical and dielectric properties,” *Express Polym. Lett.*, vol. 6, no. 4, pp. 283–292, 2012, doi: 10.3144/expresspolymlett.2012.31.

[512] J. J. Park, J. Y. Lee, and Y. G. Hong, “Effects of vinylsilane-modified nanosilica particles on electrical and mechanical properties of silicone rubber nanocomposites,” *Polymer (Guildf).*, vol. 197, p. 122493, May 2020, doi: 10.1016/J.POLYMER.2020.122493.

[513] J. Chen, J. Chen, L. Li, S. Wang, and Y. Xie, “Study on the self-cleaning phenomenon and anti-pollution flashover

performance of micro-nanostructure superhydrophobic coating surface under a high humidity environment," *Colloids Surfaces A Physicochem. Eng. Asp.*, vol. 630, p. 127552, Dec. 2021, doi: 10.1016/J.COLSURFA.2021.127552.

[514] H. De Santos and M. A. Sanz Bobi, "A Cumulative Pollution Index for the Estimation of the Leakage Current on Insulator Strings," *IEEE Trans. Power Deliv.*, vol. 35, no. 5, pp. 2438–2446, Oct. 2020, doi: 10.1109/TPWRD.2020.2968556.

[515] D. Kone, R. A. Ghunem, L. Cisse, Y. Hadjadj, and A. H. El-Hag, "Effect of residue formed during the AC and DC dry-band arcing on silicone rubber filled with natural silica," *IEEE Trans. Dielectr. Electr. Insul.*, vol. 26, no. 5, pp. 1620–1626, Oct. 2019, doi: 10.1109/TDEI.2019.008203.

[516] R. A. Ghunem, S. H. Jayaram, and E. A. Cherney, "Suppression of silicone rubber erosion by alumina trihydrate and silica fillers from dry-band arcing under DC," *IEEE Trans. Dielectr. Electr. Insul.*, vol. 22, no. 1, pp. 14–20, Feb. 2015, doi: 10.1109/TDEI.2014.004484.

[517] U. B. Bagale *et al.*, "Multifunctional coatings based on smart nanocontainers," *Adv. Smart Coatings Thin Film. Futur. Ind. Biomed. Eng. Appl.*, pp. 135–162, Jan. 2020, doi: 10.1016/B978-0-12-849870-5.00014-8.

[518] A. Ouarga *et al.*, "Towards smart self-healing coatings: Advances in micro/nano-encapsulation processes as carriers for anti-corrosion coatings development," *J. Mol. Liq.*, vol. 354, p. 118862, May 2022, doi: 10.1016/J.MOLLIQ.2022.118862.

[519] S. Hatami Boura, M. Peikari, A. Ashrafi, and M. Samadzadeh, "Self-healing ability and adhesion strength of capsule embedded coatings—Micro and nano sized capsules containing linseed oil," *Prog. Org. Coatings*, vol. 75, no. 4, pp. 292–300, Dec. 2012, doi: 10.1016/J.PORGCOAT.2012.08.006.

[520] A. G. Cordeiro Neto, A. C. Pellanda, A. R. de Carvalho Jorge, J. B. Floriano, and M. A. Coelho Berton, "Preparation and evaluation of corrosion resistance of a self-healing alkyd coating based on microcapsules containing Tung oil," *Prog. Org. Coatings*, vol. 147, p. 105874, Oct. 2020, doi: 10.1016/J.PORGCOAT.2020.105874.

[521] T. Liu *et al.*, "Self-healing corrosion protective coatings based on micro/nanocarriers: A review," *Corros. Commun.*, vol. 1, pp. 18–25, Mar. 2021, doi: 10.1016/J.CORCOM.2021.05.004.

[522] C. I. Idumah, C. M. Obele, E. O. Emmanuel, and A. Hassan, "Recently Emerging Nanotechnological Advancements in Polymer Nanocomposite Coatings for Anti-corrosion, Anti-fouling and Self-healing," *Surfaces and Interfaces*, vol. 21, p. 100734, Dec. 2020, doi: 10.1016/J.SURFIN.2020.100734.

[523] N. J. Kanu, E. Gupta, U. K. Vates, and G. K. Singh, "Self-healing composites: A state-of-the-art review," *Compos. Part A Appl. Sci. Manuf.*, vol. 121, pp. 474–486, Jun. 2019, doi: 10.1016/j.compositesa.2019.04.012.

[524] S. Islam and G. Bhat, "Progress and challenges in self-healing composite materials," *Mater. Adv.*, vol. 2, no. 6, pp. 1896–1926, Mar. 2021, doi: 10.1039/D0MA00873G.

[525] B. Soo, H. Cho, H. M. Andersson, S. R. White, N. R. Sottos, and P. V Braun, "Polydimethylsiloxane-Based Self-Healing Materials **," pp. 997–1000, 2006, doi: 10.1002/adma.200501814.

[526] Y. Song *et al.*, "Antibacterial self-healing anticorrosion coatings from single capsule system," *J. Appl. Polym. Sci.*, vol. 138, no. 41, p. 51214, Nov. 2021, doi: 10.1002/APP.51214.

[527] C. M. Dry, "Smart Building Materials which Prevent Damage or Repair Themselves," *MRS Proc.*, 1992, doi: 10.1557/proc-276-311.

[528] X. Fu *et al.*, "Stimuli-responsive self-healing anticorrosion coatings: from single triggering behavior to synergetic multiple protections," *Mater. Today Chem.*, vol. 22, p. 100575, Dec. 2021, doi: 10.1016/J.MTCHEM.2021.100575.

[529] J. Ekeocha *et al.*, "Challenges and Opportunities of Self-Healing Polymers and Devices for Extreme and Hostile Environments," *Adv. Mater.*, vol. 33, no. 33, p. 2008052, Aug. 2021, doi: 10.1002/ADMA.202008052.

[530] E. Adibzadeh, S. M. Mirabedini, M. Behzadnasab, and R. R. Farnood, "A novel two-component self-healing coating comprising vinyl ester resin-filled microcapsules with prolonged anticorrosion performance," *Prog. Org. Coatings*, vol. 154, p. 106220, May 2021, doi: 10.1016/J.PORGCOAT.2021.106220.

[531] P. Poornima Vijayan and M. Al-Maadeed, "Self-Repairing Composites for Corrosion Protection: A Review on Recent Strategies and Evaluation Methods," *Mater. 2019, Vol. 12, Page 2754*, vol. 12, no. 17, p. 2754, Aug. 2019, doi: 10.3390/MA12172754.

[532] L. Qin, Y. Chu, X. Zhou, and Q. Pan, “Fast Healable Superhydrophobic Material,” *ACS Appl. Mater. Interfaces*, vol. 11, no. 32, pp. 29388–29395, Aug. 2019, doi: 10.1021/ACSAMI.9B07563/SUPPL_FILE/AM9B07563_SI_003.PDF.

[533] C. Xu, Z. Chen, C. Wang, and K. Chen, “Fabrication of Dual Self-Healing Multifunctional Coating Based on Multicompartment Microcapsules,” *ACS Appl. Mater. Interfaces*, vol. 13, no. 49, pp. 59298–59309, Dec. 2021, doi: 10.1021/ACSAMI.1C19304/SUPPL_FILE/AM1C19304_SI_001.PDF.

[534] M. S. Koochaki, R. E. Neisiany, S. N. Khorasani, A. Ashrafi, S. P. Trasatti, and M. Magni, “The influence of the healing agent characteristics on the healing performance of epoxy coatings: Assessment of the repair process by EIS technique,” *Prog. Org. Coatings*, vol. 159, p. 106431, Oct. 2021, doi: 10.1016/J.PORGCOAT.2021.106431.

[535] C. Zhang, H. Wang, and Q. Zhou, “Preparation and characterization of microcapsules based self-healing coatings containing epoxy ester as healing agent,” *Prog. Org. Coatings*, vol. 125, pp. 403–410, Dec. 2018, doi: 10.1016/J.PORGCOAT.2018.09.028.

[536] F. Mansfeld, “Electrochemical impedance spectroscopy (EIS) as a new tool for investigating methods of corrosion protection,” *Electrochim. Acta*, vol. 35, no. 10, pp. 1533–1544, Oct. 1990, doi: 10.1016/0013-4686(90)80007-B.

[537] C. Suryanarayana, K. C. Rao, and D. Kumar, “Preparation and characterization of microcapsules containing linseed oil and its use in self-healing coatings,” *Prog. Org. Coatings*, vol. 63, no. 1, pp. 72–78, Jul. 2008, doi: 10.1016/J.PORGCOAT.2008.04.008.

[538] M. Hasanzadeh, M. Shahidi, and M. Kazemipour, “Application of EIS and EN techniques to investigate the self-healing ability of coatings based on microcapsules filled with linseed oil and CeO2 nanoparticles,” *Prog. Org. Coatings*, vol. 80, pp. 106–119, Mar. 2015, doi: 10.1016/J.PORGCOAT.2014.12.002.

[539] S. Roshan and A. A. Sarabi, “Improved performance of Ti-based conversion coating in the presence of Ce/Co ions: Surface characterization, electrochemical and adhesion study,” *Surf. Coatings Technol.*, vol. 410, p. 126931, Mar. 2021, doi: 10.1016/J.SURFCOAT.2021.126931.

[540] A. C. Ramamurthy, W. I. Lorenzen, and S. J. Bless, “Stone impact damage to automotive paint finishes: An introduction to impact physics and impact induced corrosion,” *Prog. Org. Coatings*, vol. 25, no. 1, pp. 43–71, 1994, doi: 10.1016/0300-9440(94)00502-8.

PUBLICATIONS

JOURNAL ARTICLES

1) **"Performance of a nanotextured superhydrophobic coating developed for high-voltage outdoor porcelain insulators"**, Anahita Allahdini, Gelareh Momen, Frédérick Munger, Stephan Brettschneider, Issouf Fofana, Reza Jafari, *Colloids and Surfaces A: Physicochemical and Engineering Aspects,* 649, 129461, 2022.
2) **"Transparent non-fluorinated superhydrophobic coating with enhanced anti-icing performance"**, A. Allahdini, R. Jafari, G. Momen*, Progress in Organic Coating Journal*, 165, 106758, 2022.
3) **"Development of a dual capsule self-healing silicone composite using silicone chemistry and poly (melamine urea-formaldehyde) shells"**, A. Allahdini, R. Jafari, G. Momen, *Journal of Applied Polymer Science*, 139, 51670, 2022.
4) **"Potential anti-icing applications of encapsulated phase change material–embedded coatings; a review"**, AA. Yancheshme, A. Allahdini, K. Maghsoudi, R. Jafari, G. Momen, *Journal of Energy Storage*, 31, 101638, 2020.
5) **"Recent progress and challenges with 3D printing of patterned hydrophobic and superhydrophobic surfaces"**, R Jafari, C Cloutier, A Allahdini, G Momen, *The International Journal of Additive Manufacturing*, 103, 1225–1238, 2019.

MANUSCRIPT IN PREPARATION

6) **"Self-healing performance of all-silicone sprayable superhydrophobic coating at room temperature"**, Anahita Allahdini, Reza Jafari, Gelareh Momen.

CONFERENCES

1) **“Development of a dual capsule self-healing silicone composite using silicone chemistry within poly(melamine-urea-formaldehyde) shells”**, Anahita Allahdini, Reza Jafari, Gelareh Momen, 36th International Conference of Polymer Processing Society, Montreal, Quebec, Canada, September 2021.
2) **“Fabrication of a durable superhydrophobic coating for high voltage glass insulators”**, Anahita Allahdini, Reza Jafari, Gelareh Momen, CIGRE Conference, Montreal, Quebec, Canada, September 2019.